Author:
Kozyniak, Kathleen

Title:
Integrated mesoscale-hydrometeorological modelling for flood forecasting

INTEGRATED MESOSCALE-HYDROMETEOROLOGICAL MODELLING FOR FLOOD FORECASTING

by

Kathleen Kozyniak (M.Sc.)

Water and Environmental Management Research Centre (WEMRC)
Department of Civil Engineering, University of Bristol
United Kingdom

A thesis submitted to the University of Bristol in accordance with the requirements of the degree of Doctor of Philosophy in the Faculty of Engineering
September 2001

Approx. 73059 words

ABSTRACT

In an effort to improve upon rainfall forecasts produced by simple storm advection methods (nowcasts) and to broach the gap between them and the forecasts of complex Numerical Weather Prediction (NWP) models, in terms of the spatial detail and length of lead-time each provides, the research presented explores the possibility of combining elements of each into a physically-based algorithm for rainfall forecasting. It is an algorithm that uses as its foundation the rainfall prediction model of Mark French and Witold Krajewski, developed in 1994. Their model was designed to take advantage of the high resolution rainfall observations and tracking abilities provided by weather radar and to achieve a rainfall forecast by augmenting extrapolation techniques with a representation of storm dynamics in the form of "rising parcel" theory. The new algorithm/model retains those features but incorporates NWP data to assist with forecasting, using it as a means to enable an informed choice of algorithm pathways and, more specifically, to identify the ingredients of precipitation, namely ascending air of high moisture content.

A case study application of the new rainfall forecasting model to storms in Northern England shows its performance, at a lead-time of one hour, compares favourably with respect to extrapolation and persistence techniques and also NWP forecasts, and that it is able to provide more assured forecasts than persistence and nowcasts at longer lead-times. The robustness of the model is tested and confirmed by way of another case study, this time using Mediterranean storms and with predictions made in the context of urban hydrology. The case studies help to identify aspects of the model that need improvement, with representation of orographic forcing being a key one.

Both the model's encouraging performance and its pinpointed weaknesses provide impetus for further research in the area of integrated mesoscale-hydrometeorological modelling for flood forecasting.

WITH GRATEFUL THANKS TO THE HOLY TRINITY

ACKNOWLEDGEMENTS

My utmost gratitude goes to Professor Ian Cluckie, my thesis supervisor, for his constant enthusiasm and his undying belief in the research and confidence in me. Special thanks to Professor Cluckie for ensuring I was supported financially throughout the period of my studies and to the European Commission who, through funding the HYDROMET Project, financed the initial stages of the research.

Dr Ian Stewart was quite simply "my rock" when it came to working with data on the University of Bristol central computer server, never failing to help solve my computer and programming woes in impressively quick time. Thanks also to John Murphy for accommodating my data storage requirements and downloading data for me.

I wish to extend my appreciation to Dr Peter Panagi at JCMM for responding to and fulfilling all my requests for data and also for providing invaluable software. I would like to thank the UK Met Office for allowing the provision of its data through JCMM. Considerable thanks must go to Mr David Goulden who very kindly made timely retrievals of radar tapes from the Hameldon Hill radar whenever asked. I am grateful to Météo France for supplying ALADIN data and especially to Dr Hervé Andrieu for his generous assistance with obtaining the data.

My thanks to all past and present members of WEMRC in Lunsford House for their camaraderie and for tolerating my fashion sense and colourful language. I am most grateful for the help and pleasant company of Dr Dawei Han, Dr Richard Griffith, Dr Andy Lane, David Harvey, Miguel Rico-Ramirez, Gustavo Cerda-Villafana and Jun Qin, with special thanks to Efren Gonzalez-Ramirez, Gerald Rosenberg and Dr Zhiping Yang who all, at some stage, had the misfortune to share an office with me and my erratic temperament. Particularly appreciated were the female "presence" and companionship of Hongyan Jiang, Dr Wei Ping Kang, Lisa Collett, Dr Catherine Wilson, Marghi Peacock and Rebecca Christian.

I would like to make note of the kindness, terrific sense of humour and fabulous Christmas dinners of my friends Karen Morunga and Shirley Brown. Finally, a huge thanks to the whole Kozyniak clan for their constant support, presents and gossip updates. And biggest thanks of all to Mum and Dad for their prayers and love and particularly for raising me in warmth and sunshine.

TABLE OF CONTENTS

LIST OF FIGURES

LIST OF TABLES

ABBREVIATIONS

ABZ	Adjacent Baroclinic Zone
ALADIN	Aire Limitée Adaptation Dynamique développement International
ALADIN-C	ALADIN Convective rainfall
ALADIN-L	ALADIN Large scale rainfall
AMAP	As Much As Possible
ARPEGE	Action de Recherche Petite Grand Echelle
CAPE	Convective Available Potential Energy
CAPPI	Constant Altitude Plan Position Indicator
CBLWC	Cloud Base Liquid Water Content
cc	correlation coefficient
CIN	Convective Inhibition
CSI	Critical Success Index
DSD	Drop Size Distribution
EA	Environment Agency
ECWMF	European Centre for Medium-Range Forecasts
F&K	Mark French and Witold Krajewski
FAR	False Alarm Ratio
FTP	File Transfer Protocol
G&B	Konstantine Georgakakos and Rafael Bras
GANDOLF	Generating Advanced Nowcasts for Deployment in Operational Land-based flood Forecasts
GMT	Greenwich Mean Time
HIRE	Hydrological Integrated Radar Experiment
HRL	Hydrologic Research Laboratory
HYDROMET	development of active on-line HYDROlogical and METeorological models to minimise the impact of flooding
HYREX	HYdrological Radar Experiment
JCMM	Joint Centre for Mesoscale Modelling
LAM	Limited Area Model
LCL	Lifting Condensation Level
LFC	Level of Free Convection

LTHE	Laboratoire d'Etude des Transferts en Hydrologie et Environnement
MPA	Mesoscale Precipitation Area
MOPS	Moisture Observation Pre-Processing System
MPV	Moist Potential Vorticity
MRWF	Medium Range Weather Forecasting
NATO	North Atlantic Treaty Organization
NERC	UK Natural Environment Research Council
NEXRAD	NEXt generation RADars
NN	Nearest Neighbour
NWP	Numerical Weather Prediction
NWS	National Weather Service
QPF	Quantitative Precipitation Forecast
PFM	Precipitation Forecasting Model
POD	Probability of Detection
PV	Potential Vorticity
RAMS	Regional Atmospheric Model System
Rate_act	average actual rainfall rate
Rate_for	average forecast rainfall rate
RHI	Range Height Indicator
RMSE	Root Mean Square Error
RHI	Relative Humidity with respect to Ice
RHW	Relative Humidity with respect to Water
SRWF	Short Range Weather Forecasting
UK	United Kingdom
UKGM	United Kingdom Met Office's Unified Global Model
UKMM	United Kingdom Met Office's Unified Mesoscale Model
UKMMC	UKMM Convective rainfall
UKMML	UKMM Large scale rainfall
UKMO	United Kingdom Met Office
UoB	University of Bristol
USA	United States of America
USGS	United States Geological Survey
VIL	Vertically Integrated Liquid
VPR	Vertically Pointing Radar
VSRF	Very Short Range Forecasting
%cov_act	percentage actual rainfall coverage
%cov_for	percentage forecast rainfall coverage

CHAPTER ONE

INTRODUCTION

Gupta and Waymire (1981) grouped space-time rainfall simulation and forecasting models into three categories: numerical models based on atmospheric physics, empirical models based on perceived regularities in rainfall distributions, and stochastic models based on the treatment of rainfall's spatial structure as a random field. The development of quite different modelling approaches is unsurprising in light of Lorenz's theories on the chaotic nature of atmospheric processes. A chaotic system, as defined by Morrison (1991), is the transition between (near-) solvable and completely stochastic systems. Even though deterministic processes govern the evolution of rainfall generally, these processes interact in non-linear, complex and "sensitive-dependent" ways to produce an observed randomness (Lorenz, 1993).

Rainfall forecasting approaches such as ensemble predictions and dynamic-stochastic models have developed in response to this apparent randomness. Dynamic-stochastic models handle uncertainty by, for example, coupling a Kalman filter with a deterministic model to account for both model and observation errors and to optimally update the model state by merging forecasts and observations (Foufoula-Georgiou and Krajewski, 1995). But perhaps truer to Lorenz's concept of chaos, being sensitivity to initial conditions such that similar initial model states diverge increasingly with time to the extent they become uncorrelated (Berri *et al*, 1990), is ensemble forecasting. Ensemble forecasting renders multiple scenarios of rainfall manifestation and does so by introducing a series of perturbations to initial atmospheric conditions. The results are used to assign probabilities to scenarios or are combined by averaging to produce a forecast (Du *et al*, 1997). Approaches such as ensemble predictions and dynamic-stochastic models can give transparency to both model errors and the dangers of ignoring them.

Forecast errors that arise because of the chaotic nature of the system being modelled are compounded by simplifications necessarily employed in models in their representation of that system and the processes acting within it. Discretisation of space and time in prediction models simplifies scales of motion that exist as a continuum in the fluid atmosphere (Salby, 1992). Limits imposed on the spatial and temporal resolutions of the discretisation, as well as on the boundaries

of the model's domain, preclude full emulation of deterministic processes and complete representation of the initial state. The errors inevitably grow when entered into a cycle of non-linear interdependent equations, themselves based on simplified assumptions about the state of the atmosphere and atmospheric processes, so that, in time, progressively larger scales of motion are affected (Holton, 1992). Hence, success in point-predicting a meteorological variable depends on the proposed forecast lead-time, as well as the extent to which the domain plus the spatial and temporal scales of the forecasting model (and initialising observations) encompass and match those of the processes defining the variable being predicted. As an example, predicting the mid-latitude 500mb flow a week in advance necessitates knowing not only the initial state of the entire global atmosphere from the surface to the stratosphere but also the upper layers of the ocean (Holton, 1992).

A successful forecast is one that fulfils its purpose. The level of detail required to achieve that is variable. A decision may be based on information about a particular variable but an increasing level of precision in that information may not alter the certainty of the decision (Morrison, 1991), in other words there may be diminishing returns in providing extra detail in forecasts, such that the costs of doing so may be disproportionate to the benefits gained. Integral to the decision to issue a flood warning is the expected intensity and duration of an impending rainfall event. After flooding occurred in the south-west region of England during the Christmas holiday period of 2000, the residents affected criticised the Environment Agency (EA), responsible for issuing flood alerts, for lack of sufficient warning. The EA responded that flood forecasting "was not the exact science people think it is" and that it was "unable to forecast to the centimetre the rise in river levels" (BBC Radio Bristol, 2001). Aside from raising questions about the EA's quantification of uncertainty in its prediction of flood levels and the extent to which uncertainty influences its decision making, it also puts in doubt the level of precision needed in rainfall forecasts given that probably many factors contribute to the inherent forecasting uncertainty implied in the EA's comments.

To run hydrological models at all however, and especially to come anywhere close to assessing flood risk to the level of competency that the public demands, requires a quantitative precipitation forecast (QPF) on catchment and urban scales. This is by no means an easy task as rainfall formation, duration and intensity are influenced by synoptic, mesoscale, "local" and microphysical scale, as well as location-specific, processes and forcing (Sumner, 1988). For the likes of global or national Numerical Weather Prediction (NWP) models, the extent and duration of a flood-producing convective storm may lie within a fraction of both the forecast lead-time they provide and the spatial area represented by one of their model grid squares. Models with spatial

resolutions too coarse to resolve such storms explicitly, typically those with a grid length in excess of 5-10km, rely on subgrid parameterisations to produce rainfall (Dudek and Molinari, 1992). The level of detail and accuracy in rainfall forecasts achievable with NWP grid resolutions and parameterisations are not ideal for the purposes of flood forecasting and subgrid spatial heterogenity in rainfall is highly desirable (Barron, 1999). The development of weather radar has greatly advanced the ability to observe this subgrid spatial heterogenity over large areas and to observe it at frequent time intervals. Arguably the use of remote sensing in meteorological observing systems has been the source of the greatest improvements in weather forecasting, allowing "nowcasting" to evolve from the capability remote sensing provides to monitor and track weather phenomena (Morrison, 1991).

Nowcasting has become a method used in flood forecasting systems to quickly and efficiently provide very short-range (0-2 hours with possible extension up to 12 hours), high resolution rainfall predictions. "Nowcasts" are extrapolation forecasts based solely on translating a storm according to advection vectors derived from past storm movement (Browning, 1982). In some cases statistically determined trends in storm growth and decay may be included. The appropriateness of nowcasting depends very much on storm type and the lead-time it affords can be severely limited when a storm is highly dynamic and limited further by the need for a storm to be present before forecasting can begin. As a result of these drawbacks to nowcasting, it may seem that a high resolution model with a synoptic-scale or larger sized domain, employing complex and robust physics and assimilating a wealth of diverse observations, is the key to successful short range (up to 24 hours) rainfall forecasts for a catchment or urban area. This may be achievable in the long term but issues and problems still exist, such as:

- timeliness of model output given the demand of producing an array of forecast ranges,
- existence of a matching concentrated and extensive network of all requisite observations and minimisation of observation error to enable the model to realise and verify its potential,
- a constantly evolving understanding of atmospheric physics,
- the cost-effectiveness of any improvements in forecasting to be had over the combination of information from current NWP models and the simpler, resource-conservative nowcasting methods,
- handling the chaos element.

The main consequence of chaos in the atmosphere is that it limits predictability. The theoretical limit to predictability of synoptic-scale features ($10^4 km^2$) is 10-14 days (Daly, 1991). The realistic limit is 5-6 days (Holton, 1992) although errors in modelling the structure of features resolvable by global NWPs, such as jet streams, double in a period of two days (Lorenz, 1993). Even with an

appropriately fine resolution, chaos renders a three hour forecast of meso-γ scale (1-20km) features, such as an individual thunderstorm with its brevity in development and maturity, very unreliable (Foufoula-Georgiou and Krajewski, 1995). According to Lorenz (1993), increasingly fine model resolutions can only ever improve predictability by a matter of hours and improvements in computing technology are better channelled into the demands of ensemble forecasting.

A perceived need for accuracy in forecasting even at longer lead-times may ensure resources are directed into development of increasingly fine resolution NWP models. In the meantime (and probably a long time) flood forecasting systems are obliged to extract what they can from existing NWP models and nowcasting methods, given that the reliability of flood forecasts and the lead-time they afford in flood situations are critical to the presentation of a hazard. A flood only becomes a hazard when it threatens human life or property and a flood warning, and the preparedness it allows, is an obvious means of hazard mitigation. The contribution of various scales of motion and processes to rain formation suggests there might be varying degrees of predictability of a rainfall event at different forecast lead-times. The "eventual" progression of resolution-related errors to larger scales of motion provides, at least with respect to synoptic scale weather forecasting, a two to five day limit to predictability. A dependable 48 hour forecast, if only in terms of broadly delineating the rain area and relative rainfall intensity, would be useful for flood warning systems structured as graduated preparedness leading to rapid action as the level of flood risk becomes better defined. There are, however, few synoptic-scale rainfall events and often rainfall organisation bears no relation to the synoptic pattern (Rogers and Yau, 1989). Laprise *et al* (1994) found no correlation between the predictability of precipitation and various synoptic-scale meteorological parameters, and in general operational synoptic-scale models produce inadequate QPFs (Cortinas and Stensrud, 1995). Both pairings of Rogers and Yau and Cortinas and Stensrud identified the importance of mesoscale structures in the development of rainfall events. Mesoscale structures or organisation can have a spatial extent of 1-200km and a lifetime of up to one day (Browning, 1982). The implications of this for flood forecasting is that useful information may potentially be gained from mesoscale NWP models up to 24 hours but probably not beyond.

The United Kindgom Met Office's Unified Mesoscale Model (herein referred to as UKMM) is an example of a NWP model that is adept at predicting variables such as temperature, pressure and winds at the mesoscale but less so at predicting rainfall rates and rainfall coverage (Golding, 1998). Timeliness is also a problem and initial forecasts (1-3 hours) are not available to consumers in practice due to the time involved in assimilating data and generating the forecasts (Dicks and Panagi, 1997). The rainfall forecasts beyond the reliable range of nowcasting can

however still be useful for the purposes of flood forecasting in the manner mentioned previously, by intiating and progressing early stages of readiness. Recognising a need exists for higher resolution, more accurate and more timely forecast products than provided by the UKMM, the United Kingdom Meterological Office (UKMO) developed Nimrod. Nimrod is a sophisticated, automated, objective forecasting system focussing on lead-times of one to six hours and producing predictions of rainfall and other variables over areas 4-225km^2 in size (Golding, 1998). It features automated real-time retrieval, processing, correction, assimilation and objective interpretation of data combined with real-time objective assessment of different forecast and storm advection approaches, the latter leading to a weighting scheme favouring the best performing approach. Although much more elaborate than nowcasting and incorporating UKMM forecasts, Nimrod is not a physically-based model in the sense of being a series of differential equations based on atmospheric physics, modelling atmospheric processes. It is a complex algorithm of statistical tests and optimisation of established forecasting methods. It is also an example of how information from a mesoscale NWP model can be used in a statistical way to "fortify" nowcasting to improve its accuracy and extend its reliability at longer lead-times.

As an alternative, researchers such as Seo and Smith (1992) and French and Krajewski (1994) have attempted a physically-based approach to improving nowcasts. French and Krajewski augmented conventional storm advection methods with storm development and decay, achieved not by the extrapolation of trends or the merging of forecasts from different sources, but by a representation of convective processes. Model formulations were based on "rising parcel" theory and kept as simple as possible to facilitate speed in forecasting. The model was developed specifically to forecast rainfall associated with widespread, intense, convective storm systems but has since been applied by Wild (1996) and Andrieu (1996) in a variety of contexts, albeit in modified forms. The simplicity of the model's physics and the assumptions about the atmosphere on which it relies can expose it to criticism, particularly in attempts to use it regardless of storm type. The purpose of this thesis is to revisit the potential for general application of this rainfall forecasting approach, though less in the form of a physically-based representation of atmospheric processes than as a physically-based algorithm for rainfall forecasting. Like Nimrod, information from the UKMM is incorporated but, in this physically-based context, its role is to optimise the pathway through the algorithm in addition to the provision of base data. The algorithm represents a step toward integrated mesoscale-hydrometeorological modelling for flood forecasting in the sense that it is intended to produce quantitative precipitation forecasts at temporal and spatial resolutions appropriate for input to hydrological flow forecasting models operating on catchment and urban scales, whilst using mesoscale NWP data to guide those forecasts.

The following chapter explains in more detail the French and Krajewski model, including the history behind it and its continued development by researchers in both the United States and Europe, with brief mention also of complementary work undertaken in Japan. Model formulations used by the respective researchers are presented and the workings of the model critically reviewed, the latter to some extent achieved simply by tracing the timeline of modifications, as most addressed perceived shortcomings in the versions that evolved. The model adaptations have typically involved attempts to incorporate as much observational data as possible to limit the extent of parameterisation in the model and have also included endeavours to account for orographic enhancement of rainfall and to find alternative ways of determining the upward motion that is fundamental to "rising parcel theory". In this chapter the model is shown to be quite malleable, whilst still retaining its essence and functionality, and also well suited to incorporation of NWP data.

Chapter Three describes the new perspective needed to frame the French and Krajewski model as a simple algorithm constituting a methodology for rainfall forecasting, and the practical and conceptual modifications undertaken to achieve it. The resulting new form of the model focuses on the "ingredients" of rain formation and attempts to find them in remotely sensed data and UKMM forecasts. The UKMM forecasts are also used to define the mesoscale atmospheric conditions in which rainfall is forming so that the relative strength of forcing can be more appropriately assigned according to, and upon identifying, storm type. To achieve this, "signifiers" of convection and fronts are determined. Both these and the nature of the input data to the new algorithm are given further elaboration, with the latter shown to have significantly influenced the way the algorithm was constructed. The structure of the algorithm and the pathway decisions required to achieve a forecast are detailed.

Chapter Four presents a case study approach to the application of the algorithm and assessment of its performance. A number of storm events that occurred in Northern England during the period from December 1998 to October 1999 are used for that purpose. The assessment exercise is undertaken by means of a comparison to other forecasting techniques with respect to, firstly, one hour forecasts and then extended lead-times (2-6 hours), the main aim being to examine whether incorporation of UKMM forecasts enables the quality and range of the forecasts produced by the algorithm to better those of other simple forecasting techniques. Included is a comparison with UKMM rainfall forecasts, thereby providing a cursory examination of how the different forecasting methods might be placed (together) to meet the needs of a flood forecasting system. It is shown that, at the shorter lead-time, the new algorithm performs well compared to all the other forecasting techniques included in the comparison but at longer lead-times both the forecasts from

the algorithm and NWP forecasts have different attributes that do not clearly distinguish either as the more appropriate for use.

In Chapter Five, two important components of the algorithm and the way in which they contribute to its performance are looked at in more detail, specifically being the attempts to account for orographic forcing and the efforts made to shift away from reliance solely on a convective parameterisation for determination of vertical velocity. Deficiencies in the methodologies adopted for each are revealed and explanations for them proffered, so too are some ideas of changes that could be made to help the components realise their potential.

Chapter Six presents another case study application of the algorithm, but one that places it in a different geographical context, this time on the Mediterranean coastline of France, and also in the context of urban hydrology. The case study provides an opportunity to assess the performance of the algorithm, again compared to other forecasting techniques, given different source data and different types of storm events and at finer model resolutions. The algorithm is found to be relatively robust when exposed to alternative conditions but the exercise mainly serves to highlight the influence of the input data and the difficulties in trying to define fine-scale features using a mesoscale depiction of atmospheric conditions.

Overall, both the highlighted potential of the new algorithm and its deficiencies lay the basis for future work on an integrated mesoscale hydro-meteorological forecasting methodology that incorporates remotely sensed data and NWP forecast data in a physically-based rainfall rate prediction model. Suggestions are made in the concluding chapter regarding the direction such future work might take.

CHAPTER TWO

THE FRENCH AND KRAJEWSKI MODEL

The French and Krajewski (F&K) rainfall forecasting model, as detailed in their paper published in *Water Resources Research* in 1994, was the culmination of work undertaken by a number of researchers in the United States, beginning in the early 1980s (French and Krajewski, 1994). The lineage of its development can be easily traced and while the fundamental ideas were preserved throughout each stage, formulations were adapted in response to advances in meteorological observing systems and in order to simplify computation. Modification of the F&K model continued after its conception, mostly by European researchers but often in collaboration with either Mark French or Witold Krajewski whose original model consistently formed the bulk, not just skeletal framework, of newer versions.

2.1 Model foundation – Georgakakos and Bras

The F&K rainfall forecasting model had its seeds in the ideas of Konstantine Georgakakos and Rafael Bras (G&B) a decade earlier (French and Krajewski, 1994). Theirs was a hydrological approach to what was considered a hydrological problem; flood forecasting, of which rainfall forecasting was one element. The emphasis on hydrological solutions was consistent with the perspective of their sponsor, the Hydrologic Research Laboratory (HRL) of the US National Weather Service (NWS), and the duo's mandate to produce rainfall forecasts compatible in space and time with HRL's river basin models (Georgakakos and Bras, 1984a). It was also consistent with the alternative treatment of the problem seemingly sought by HRL when it engaged civil engineers to forecast rainfall.

The result was G&B's proposal to treat storm systems as clusters of independent unit area columns of the atmosphere, each column analogous to a water reservoir. A hydrologic system, such as a water reservoir, comprises three parts, namely water inflows, environmental response/water storage and water outflows, the latter typically an input to another hydrologic system (Yevjevich, 1972). G&B presented their model in precisely this way:

$$\frac{dX}{dt} = I - O_T - O_B \tag{2.1}$$

identifying inflows (I), outflows (O_T and O_B) and referring to the liquid water mass in the column (X) as the model state. Inflow comprised water vapour carried in air entering the base of the cloud column. Condensation of water vapour and the production of liquid water were the environmental response to the inflow. Outflows were either the removal of moisture from the top of the cloud (O_T) by strong updrafts or rainfall leaving the cloud base (O_B). Their assignment of rainfall as a system outflow meant estimation of future rainfall rate required concomitant prediction of the model state from whence it came. Thus G&B were clear in stating the prognostic variable of the model was not actually rainfall but was in fact the model state, and only from a prediction of liquid water mass could rainfall then be diagnosed.

2.1.1 Hydrologic vs meteorologic approach

Many of the theorems used in G&B's model were similar to those found in catchment-scale rainfall forecasting models of the day developed from a meteorological perspective. Collier (1975) and Bell (1978) each built a relatively simple, layered, physically-based, rainfall rate forecasting model within the context of the UKMO. All three models, Bell's, Collier's and G&B's, were premised on theories about rising air parcels, that as air rises it expands and cools, its capacity to hold water vapour reduces and the excess beyond saturation condenses to liquid water (Ahrens, 2000). They all used the rate of liquid-water-mass production from water vapour condensation as the predominant determinant of rainfall rate. All quantified the rate of condensation as the product of the vertical gradient in saturation water vapour density (or mixing ratio) and the strength of the updraft lifting saturated air through the gradient. Obvious differences between models lay in the way the velocity of the updraft was parameterised and in the atmospheric column versus multiple-layer methodology. Key but more subtle differences lay in how the conceptual approach and the forecast performance measures in use influenced how the respective models finally determined rainfall intensity.

Free from deliberate adherence to the conceptual framework of a hydrologic system, Collier and Bell could be less clear in distinguishing rainfall rate as a diagnosed variable of their models. Collier followed Bannon (1948) in likening the rate of condensation, or liquid water formation, within a layer of the atmosphere to the rate it was leaving it, effectively letting the rate of condensation automatically default as the rate of precipitation. Justification for this came from observations of liquid water in precipitating clouds, the concentration of which rarely exceeded

$0.5gm^{-3}$, although exceptions of $14gm^{-3}$ had been found (Klett and Pruppacher, 1997). As such, Bannon reasoned that cloud water content could be expected to vary little, between $0\text{-}1gm^{-3}$, and, in hydrologic terms, outflow could be considered the prime beneficiary of inflow. This all seemed to render G&B's conception of the model state, comprising both cloud water and rain water, superfluous to requirements given cloud water's relatively static and minor contribution to it. However Bannon's approach relied on an assumption of high precipitation efficiency. Precipitation efficiency can be defined in a number of ways, but typically as a comparison between the mass of rainfall reaching the ground and the mass of, either, water condensed in the cloud or water vapour entering the cloud. Observations indicated precipitation efficiencies for these two means of calculation were approximately 19% and 11% respectively, with evaporation losses at the sides and top of the cloud, as well as in downdrafts, being the main explanation for such a low level of conversion (Rogers & Yau, 1989). Notably, Collier's model had a tendency towards over-prediction, partial responsibility for which he attributed to his assumption that all condensate reached the ground.

Recognising that the rate of water vapour inflow did not match the rate of liquid water outflow, Bell slightly modified Bannon's approach in an attempt to resolve some of the discrepancies. Bell, like Collier, assumed a precipitation rate equivalent to the rate of condensation but only if an air parcel was saturated upon entering a layer of his model. If initially unsaturated but reaching saturation whilst ascending through the layer, the conversion of condensate to precipitation was tempered according to a 20 minute time scale for droplet growth, applied to the remaining time the saturated air parcel spent in the layer. In this latter situation Bell, like G&B, acknowledged the existence of cloud water and the model began to resemble more Yevjevich's idea of a hydrologic system, in this case a collection of hydrologic systems in series. In fact, the structure of Bell's model highlighted the importance of precipitation not only as outflow but also as inflow to consecutive systems, precipitation from one layer enhancing the washout of liquid water from the layer below. Such an effect was absent from G&B's unit column model but so was any provision for the orographic enhancement of rainfall, a component of which Bell was trying to emulate through the washout process and specifically the seeding of low level orographic clouds with particles from higher clouds.

Common to both Collier's and Bell's forecasted surface precipitation rate was its immunity to the forces of gravity and frictional drag. Neither of the two transformed the rate of precipitation formation in the cloud into a rainfall rate at the ground surface that explicitly accounted for the fall speed of the water mass. This was perhaps not particularly important because, although both presented their models as forecasting rainfall rates, performances were assessed using hourly, three hourly or daily rainfall accumulations, periods of time in which the majority of precipitation

formed might be expected to reach the ground. G&B's conceptual model and its analogy with a water reservoir both facilitated and demanded "proper" determination of rainfall rate: facilitated by the intermediate stage it provided between inflows and outflows, enabling precipitation rates to be calculated from the available water mass using generally accepted expressions for the distribution and terminal velocity of particle drop sizes; demanded by the depiction of the time evolution of the model state as a function of inflows and outflows, making the rate of precipitation integral to determining the future model state whilst also determined by the future model state (observations lend support to this idea of interdependency, suggesting a relationship exists between rainfall intensity and storm duration such that high rainfall intensities are associated with short duration storms (Sumner, 1988)); demanded also by G&B's choice to assess the model's performance in terms of instantaneous rainfall intensity, a useful measure with respect to flood forecasting given its link with storm duration, its indication of whether the storm is still continuing and its implications with respect to peaks in storm discharge (Sumner, 1988).

Fundamental to the success of all the models was the determination of the force of uplift carrying water vapour through the cloud. Collier's parameterisation of this vertical velocity was quite elaborate, featuring three components: boundary layer vertical velocity, large-scale baroclinic development and various scales of motion induced by orography. Bell's parameterisation had two components, a large-scale vertical velocity taken directly from a NWP model and an orographic component proportional to the product of the horizontal wind velocity and the gradient of the topographic slope. G&B chose a convective parameterisation, without additional orographic forcing, possibly in keeping with the type of landscape and storms they were most familiar with and which were, in their experience, the most synonymous with flood hazards. Whilst Collier was careful to qualify the appropriateness of his formulations to "moving baroclinic systems" and Bell's model was purposely assessed using storms in passing fronts and deep depressions, G&B did not limit application of their model to convective storms, noting that convective elements had been observed in frontal rainfall (Georgakakos and Bras, 1984a). They tested their model with a variety of storm types and concluded that there was little difference in the model's performance between them (Georgakakos and Bras, 1984b). Overall there was a tendency for the model to under-predict high precipitation rates but this aspect was seen to improve when the model was revised in a stochastic formulation compatible with use of a Kalman filter, the addition of the filter designed to enable best estimates of the model state to be made and subsequently used in state updating procedures.

2.2 Developments – Georgakakos and Lee

Georgakakos later dispensed with specific reference to the framework of a hydrologic system when he teamed with Lee in detailing the two-dimensional rainfall forecasting model they developed together (Georgakakos and Lee, 1990). One failing of G&B's conceptual model was that, in reality, the time evolution of the model state with respect to a fixed geographic location was not only dependent on inflow and outflow, but also on movement of the cloud column. The fact was storms, including cloud and the conditions producing rain, were not stationary, the hydrologic systems G&B described were in motion. Dynamic meteorologists had already discovered this and provided expressions for it in a set of partial differential equations governing the conservation of air mass, heat, momentum and water mass in the atmosphere (Pielke,1984). Abstracting only the latter equation for their purpose:

$$\frac{\partial q}{\partial t} = -\frac{\partial qu}{\partial x} - \frac{\partial qv}{\partial y} - \frac{\partial qw}{\partial z} + S \tag{2.2}$$

Georgakakos and Lee integrated it from the cloud base to the cloud top to give:

$$\frac{\partial Q}{\partial t} = -q_B \frac{\partial Z_B}{\partial t} - u\frac{\partial Q}{\partial x} - v\frac{\partial Q}{\partial y} - uq_B \frac{\partial Z_B}{\partial x} - vq_B \frac{\partial Z_B}{\partial y} + q_B w_B + S \tag{2.3}$$

They moulded G&B's formulations so as to satisfy the terms of equation (2.2) and included wind fields interpolated from an upper-air weather station to drive the local transport of liquid water mass. In the above equations the subscript B refers to cloud base values; q is the liquid water mass and Q denotes the vertically integrated value of q; t is time; u, v, w are transport velocities in the x, y and z directions respectively, and w is the vectorial sum of the updraft/downdraft and terminal velocity of water particles; S is a net source term for the sources and sinks of liquid water; Z is height measured from the land surface.

Georgakakos and Lee were encouraged by the results they achieved with their two-dimensional model, although this time a tendency for over-prediction was apparent but again corrected to some extent with the use of state updating. They envisaged performance would improve further with representation of the orographic enhancement of rainfall and with use of forecast meteorological input, volume scan radar data and satellite infrared cloud top observations.

2.3 The introduction of radar data – Georgakakos and Krajewski

Up until this point, rain gauges were the primary source of the rainfall measurements used either as inputs to, or for performance assessment of, all the models described above. Operational national weather radar networks had been established, or implementation well advanced, in many countries since the late 1970s (Browning & Collier, 1982, Hitsuma et al, 1982, Bodin, 1982, Collier, 1989). In the decade that followed, the storm tracking capabilities provided by remote sensing and the high space and time resolution of the measurements were becoming increasingly appreciated and "nowcasting" methods were being included in the armour of flood forecasting systems. The period between realisation of the G&B model and development of the Georgakakos and Lee model was one of protracted and incomplete revitalisation of the USA weather radar network, involving the progressive introduction of the NEXRAD (NEXt generation RADar) doppler radar system across the country. This perhaps inhibited Georgakakos's full commitment to running and assessing models with, and according to, radar data at that stage, however Georgakakos and Lee did tentatively test the potential for its use by calibrating their model first with data from rain gauges and then radar, discovering the results were similar. In the following year Georgakakos, with the assistance of Krajewski, looked more closely at including weather radar data as a direct measurement of the model state, i.e. the liquid water mass through the depth of the cloud. Together they reverted to the G&B model to demonstrate how using both radar measured rainfall and an average reflectivity value taken from volume scan radar data could and did work in that framework (Georgakakos and Krajewski, 1991). They consequently advocated using radar data in two-dimensional models such as that of Georgakakos and Lee.

2.4 The influence of remote sensing – Seo and Smith

So when Dong-Jun Seo and James Smith proposed incorporating volumetric radar data into a physically-based catchment-scale rainfall forecasting model, the idea was not entirely new (Seo and Smith, 1992). Seo had actually assisted Georgakakos and Krajewski with acquisition of radar data for their aforementioned research. The work of Seo and Smith was again a collaboration between HRL staff and civil engineers, with the latter supported by NEXRAD Joint System Program funding and no doubt with a view to maximising the utility of the new network. Seo and Smith, like Georogakakos and Lee, based their model on the dynamic meteorologists' governing equations but chose to eliminate the role of cloud water and focus solely on the time evolution of rain water. They did so using the same reasoning as Bannon, that the contribution of cloud water to total liquid water was small and relatively static, and their primary motivation for doing so was that cloud water particles were too small in size to be detected by conventional weather radar.

Estimates of liquid water from volume scan radar reflectivity values could not be truly representative of the model state if the latter included both cloud and rain water.

One of the duo's key innovations was how, by employing a Lagrangian frame of reference, they could translate their computational domain according to storm movement and omit the local transport terms from their time evolution equation. Therefore the Seo and Smith version of equation (2.2) took on the form:

$$\frac{\partial M}{\partial t} = -w\frac{\partial M}{\partial z} - \frac{\partial (MV)}{\partial z} - w\frac{\partial Q}{\partial z} \tag{2.4}$$

M (kgm^{-3}) being the rainwater content; Q (kgm^{-3}) the saturation vapour density; w (ms^{-1}) the velocity of air in the vertical z direction; V (ms^{-1}) the fall velocity of rainwater. The last two terms of equation (2.4) were, in effect, the components of S in equations (2.2) and (2.3). Seo and Smith integrated equation (2.4) from cloud base to cloud top and in the process introduced VIL into the nomenclature for this type of cloud column modelling, VIL being an acronym for "vertically integrated liquid". Figure 2.1 shows the typical vertical profile of liquid water content produced from full volume scan radar data and, from such profiles Seo and Smith calculated VIL (kgm^{-2}) as the summation of the rain water content through the depth of each of the different elevation scans of the radar:

$$VIL = \Sigma_{i=1}^{n} M_i \times \Delta h \tag{2.5}$$

Δh being the depth of the scan (in metres) and $i=1,....n$ referring to the number of scans of different elevation angle that comprise the full volume scan.

By assuming a vertically averaged updraft (w_m) within the cloud and negligible liquid water content at the top of the cloud, the time evolution of the model state, VIL, was again made analogous to a simple inflow/outflow hydrologic system and prediction once more a case of balancing mass through time:

$$\frac{dVIL}{dt} = \underbrace{(w_m - V_B)M_B}_{1} + \underbrace{w_m(Q_B - Q_T)}_{2} \tag{2.6}$$

with subscripts B and T indicating values at the cloud base and cloud top respectively. Term 1 represented an expression for the rate of rainfall from the cloud base (outflow) and term 2 the rate

of water vapour condensation (inflow). Whereas G&B assumed a constant cloud top pressure level of 200 mb, a level above which clouds were not expected to penetrate, Seo and Smith relied on zero reflectivity values in upper radar scans to indicate termination of the cloud top. There was a certain precariousness in adopting that approach given that weather radar could not determine "cloud" in the absence of rainfall and, as noted by Seo and Smith, upper beams were often missing. The level of the cloud base they would have similarly determined but for potential contamination of the lowest beam with ground clutter and potential for the cloud base to be below the sampling space of the lowest beam. Instead they assumed a fixed cloud base height of 2.5 km for the purpose of estimating VIL and calculating the rainfall rate at the cloud base. Therein lay a discrepancy in their definition of subscript B in equation (2.6) because 2.5 km was not necessarily equivalent to the level at which Q_B was determined. The lifting condensation level (LCL) defined the latter, being the level at which condensation of water vapour commences in air rising from the surface, and they determined the LCL in the manner of G&B, using measurable properties of an air parcel at the surface in conjunction with rising parcel theory.

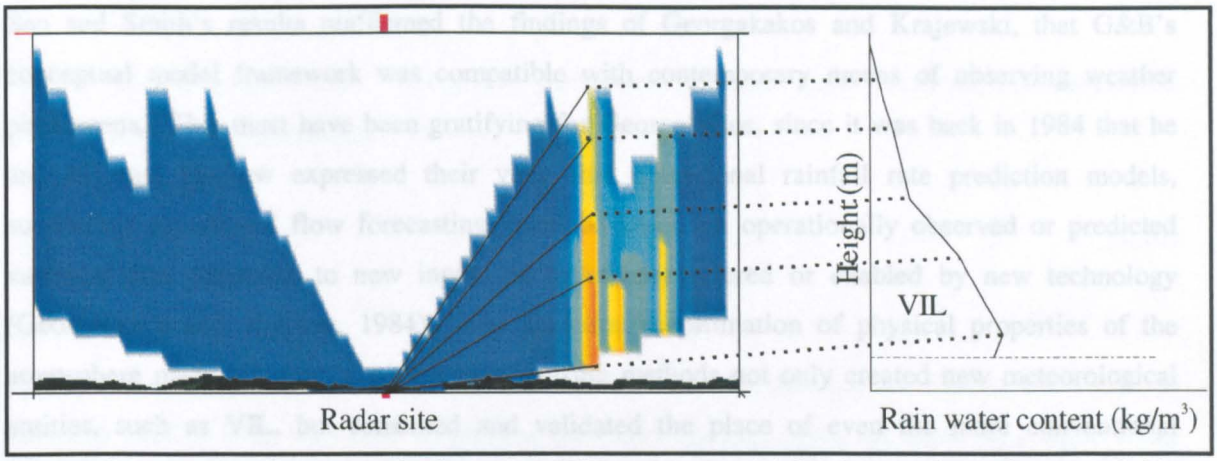

Figure 2.1: *One dimensional schematic of VIL estimation (right) from radar reflectivity (left). (adapted from Seo and Smith, 1992)*

Adding to the complexity, or confusion, Seo and Smith's estimation of M_B in each grid cell of their model was not simply a matter of obtaining the corresponding grid cell radar reflectivity value at a height of 2.5 km and converting it to a measurement of liquid water. Instead they maintained that M_B and VIL were linearly related in the form:

$$M_B = (a_1 VIL + b) / H \tag{2.7}$$

H (m) being the vertical extent of the cloud (2.5 km to echo top); a_1 and b the coefficients determined by linear regression of the whole initial field of ($M_B \times H$) on the whole initial field of VIL. The importance of this step became evident when trying to diagnose rainfall from predicted

VIL. Using equation (2.7) a value for M_B could be obtained upon making a forecast of VIL and by using empirically derived relationships between M, radar reflectivity values and rainfall rate, the latter could be calculated.

Like G&B, Seo and Smith used a convective parameterisation for the updraft velocity but, in contrast, acknowledged the limitations it implied, choosing only convective storms to calibrate the model and to verify it's performance with respect to extrapolation techniques. In terms of root mean square error (RMSE), their model outperformed nowcasts in all but one of the seven events used in their assessment exercise but had a tendency to under-predict mean rainfall. They saw scope for improving the model by incorporating dynamics to account for processes forming frontal rainfall and by using NWP forecasts of meteorological inputs instead of assuming values taken from radiosonde data persisted over the forecast lead time.

2.5 Final Progression – French and Krajewski

Seo and Smith's results reaffirmed the findings of Georgakakos and Krajewski, that G&B's conceptual model framework was compatible with contemporary means of observing weather phenomena. This must have been gratifying for Georgakakos, since it was back in 1984 that he and Michael Hudlow expressed their view that operational rainfall rate prediction models, supporting operational flow forecasting, must be based on operationally observed or predicted variables and adaptable to new inputs or techniques offered or enabled by new technology (Georgakakos and Hudlow, 1984). The quantitative estimation of physical properties of the atmosphere made achievable with remote sensing methods not only created new meteorological entities, such as VIL, but cemented and validated the place of even the more conventional variables, such as cloud top temperature and pressure, in Seo and Smith's model by reducing the number of assumptions otherwise made in their derivation. Furthermore, the images produced by remote sensing methods provided a means of measuring storm movement and the extrapolation of that movement forward in time offered an alternative to taking wind fields at a fairly standard, but still a little arbitrary, pressure level.

Witold Krajewski decided to take the inclusion of remotely sensed observations one step further with a PhD student called Mark French, together constructing the F&K model and legitimising many of its components by the measurability of the meteorological variables used (French and Krajewski, 1994). Core aspects of the F&K model drew directly from the formulations of Seo and Smith, VIL was the model state, its value obtained by solving equation (2.5), its relationship with M_B defined by equation (2.7) and its time evolution determined in accordance with equation (2.6). The means to calculate the other variables making up equation (2.6), namely V_B, w_m, Q_B and Q_T,

were also sourced from Seo and Smith's model or otherwise that of G&B, all of whom had relied heavily on empirically derived relations when developing their parameterisations for each.

2.5.1 Terminal velocity (V_B)

F&K's calculation of the terminal velocity of the cloud base liquid water mass (V_B) was based on Gunn and Kinzer's relation between terminal velocity and drop diameter:

$$V(D) = -\alpha D^{\beta} \tag{2.8}$$

D (m) being the drop diameter; α ($m^{1-\beta}s^{-1}$) and β (dimensionless) empirical parameters taken to have values 386.6 and 0.67 respectively. Use of the above relation required characterisation of M_B in terms of drop sizes, for which the Marshall-Palmer drop size distribution (DSD) was chosen:

$$N(D) = N_0 e^{-\Lambda D} \tag{2.9}$$

with N_0 ($m^{-3}mm^{-1}$) and Λ (mm^{-1}) being DSD parameters, the latter largely dependent on the rainfall rate and the former determined from:

$$N_0 = \frac{Z\Lambda^7}{720} \tag{2.10}$$

Z (mm^6m^{-3}) being the radar reflectivity. Using the Marshall-Palmer DSD, Doviak and Zrnić, as noted by F&K (1994), were able to produce the following expression for cloud base liquid water content:

$$M_B = \frac{\pi}{6}\rho\int_0^{\infty} D^3 N(D)dD = \pi\rho N_0\Lambda^{-4} \tag{2.11}$$

ρ (kgm^{-3}) being the density of water.

They also provided the formulation for the terminal velocity of the liquid water mass based on equations (2.8) to (2.11):

$$V_B = M_B{}^{\gamma}\frac{\alpha}{6}(\pi\rho N_0)^{-\gamma}\Gamma(4+\beta) \tag{2.12}$$

Γ being the gamma function and where $\gamma = \beta/4$.

2.5.2 Updraft velocity (w_m)

F&K kept the updraft velocity convective in its parameterisation but the formulation of G&B, below, was taken in preference to a more complicated version adopted by Seo and Smith:

$$w_m = \varepsilon(C_p \Delta T)^{1/2} \tag{2.13}$$

C_p ($Jkg^{-1}K^{-1}$) being the specific heat of dry air at constant pressure; ε a dimensionless parameter requiring estimation and theoretically proportional to the ratio of kinetic energy to thermal energy per unit mass of air at pressure level p_w (mb); T (K) being temperature and with:

$$\Delta T = T_m - T_w \tag{2.14}$$

Equation (2.14) was an expression for the difference between the in-cloud temperature (T_m) and that of ambient air (T_w), assuming temperature followed a constant pseudoadiabat and adiabat respectively. The two temperatures were derived as follows:

$$T_w = \frac{T_0}{p_0^{0.286}} (3/4\, p_B + 1/4\, p_T)^{0.286} \tag{2.15}$$

$$T_m = \theta_e \left(\frac{p_w}{p_n} \right)^{0.286} \exp\left(- \frac{L(T_m) r_s(T_m, p_w)}{C_p T_m} \right) \tag{2.16}$$

subscript *0* representing surface level variables; r_s ($kgkg^{-1}$) being the saturation mixing ratio; L (Jkg^{-1}) the latent heat of condensation; θ_e (K) the equivalent potential temperature; the exponent 0.286 being R_d/C_p; R_d ($Jkg^{-1}K^{-1}$) being the dry air gas constant; p (mb) pressure with p_n a nominal pressure of 1000 mb and p_w defined as:

$$p_w = p_B - \frac{p_B - p_T}{4} \tag{2.17}$$

p_w represented the pressure level at which, with reference to an idealised parabolic vertical profile of updraft velocity in a convective cloud, it was thought the rate of updraft approximated the vertically averaged updraft velocity within the cloud.

2.5.3 Saturation water vapour density (Q)

Saturation water vapour density (Q) at the cloud base and cloud top were calculated in the manner of Seo and Smith,

$$Q = \frac{r_s(T,p)p}{R_d T} \tag{2.18}$$

which required the temperature and pressure at the cloud base and cloud top to be specified. G&B had already showed how cloud base values of Q could be calculated using surface level observations of pressure, temperature and dew point temperature (T_d):

$$p_B = \frac{1}{\left(\frac{T_0 - T_d}{223.15} + 1\right)^{3.5}} p_0 \tag{2.19}$$

$$T_B = \frac{1}{\left(\frac{T_0 - T_d}{223.15} + 1\right)} T_0 \tag{2.20}$$

F&K also borrowed from G&B their method of calculating the temperature and pressure at the cloud top, which they based on the principle that equivalent potential temperature in an air parcel is conserved as it rises, thereby allowing the Poisson equation for θ_e:

$$\theta_e = T\left(\frac{p_n}{p}\right)^{R_d/C_p} \exp\left(\frac{L(T)r_s(T,p)}{C_p T}\right) \tag{2.21}$$

to be used to determine either temperature or pressure at the cloud top provided that one of the two was already known. Whereas G&B had chosen a uniform cloud top pressure and Seo and Smith had estimated the height of the cloud top from volume scan radar data and converted it to pressure using the hydrostatic approximation for moist air and radiosonde profiles of the environmental mixing ratio, F&K employed a different way again of dealing with the problem and in the process furthered the use of remotely sensed observations in their model. Unlike G&B and Seo and Smith they estimated the cloud top temperature first rather than pressure and did so using satellite infrared brightness temperature as previously suggested by Georgakakos and Lee (Georgakakos and Lee, 1990).

2.5.4 Making the forecast

F&K had therefore managed to formulate the bulk of the model in terms of empirical formulae and measurable variables but still had two parameters, namely the DSD parameter, Λ, and the updraft velocity parameter, ε, which remained undefined but fundamental to the model's performance. Being related to the mean diameter of the rain drops in a unit volume, the DSD parameter Λ was integral to the determination of VIL. Parameter ε modulated the strength of convection and its magnitude influenced both the rate of condensation and the rainfall rate.

The presence of "free" parameters had also featured in the modelling of Seo and Smith and G&B, each of their models having at least two "unknowns" needing estimation through parameter search procedures involving calibration of the models using storm events. The inclusion of progressively more observational data, as the model developed from G&B's initial model framework to the F&K version, had failed to eliminate the need for free parameters or even diminish their importance and the dependence of good model performance on the skill of their estimation. Neither had increasing use of observational data helped reduce the number of assumptions needed to maintain the desired model attributes of simplicity and efficiency. F&K's appropriation of Seo and Smith's theoretical framework and many of their parameter derivations implied acceptance of the set of assumptions they had employed when implementing their model, such as:

- there was no mixing of air between cloud columns - the vertical flux was thought to dominate lateral mixing over an area the size of a model grid square (in Seo and Smith's case 12km × 12km, 32km × 32km for F&K)
- condensation was immediately converted to rainwater without first passing through the cloud water/ice phase - requiring the qualification that the model represented warm rain processes only, as well as evocation of Bannon's reasoning that cloud water had a steady state uniform profile.
- negligible (effectively zero) rainwater content was present at the cloud top - based on the low temperatures observed at the tops of convective clouds and the associated low specific humidity.
- the vertical variation of the updraft velocity was adequately represented by a vertically averaged value - premised on Kessler's (1969) quadratic profile of updraft velocity and considered appropriate given that a model grid square was larger than the spatial area associated with an individual cloud column updraft.
- the fall velocity of raindrops in quiet air did not vary with atmospheric pressure and could be parameterised in terms of raindrop diameter - based upon the empirical work of Gunn and Kinzer.

- microphysical processes of coalescence, collision, evaporation were inconsequential - made so by the assumed instantaneous conversion of condensation to rainwater.
- a linear relationship existed between VIL and water content at the base of the cloud and that the coefficients of the equation, obtained through linear regression of the two variables, varied in time but not space - as concluded from the work undertaken by Seo and Smith.

Additionally, over the period of the forecast lead-time:

- atmospheric pressure and the spatially averaged water vapour field were considered invariant.
- density of air was constant and adequately represented by a vertically averaged value.
- cloud base and cloud top elevations remained constant.

Given that a number of the above were premised on observed characteristics of convective clouds, F&K followed Seo and Smith in testing their model with respect to convective storms only, which they undertook with the assistance of a Frenchman called Hervé Andrieu, who joined them under a NATO Scientific Exchange Program (Andrieu et al, 1994). Aware of the improvements in forecasting that G&B achieved by implementing state updating procedures, F&K appeared keen to do likewise and also keen to similarly use a Kalman filter for that purpose. In order to use a Kalman filter, F&K had to present the model dynamics as a linear system. As a first step towards this they combined equations (2.6) and (2.7) to arrive at a version of the former which, by replacing reference to M_B with VIL, confirmed the status of VIL as the model state and showed the dependence of its time evolution on its current value:

$$\frac{dVIL}{dt} = \underbrace{AVIL}_{1} + \underbrace{B\left[aVIL + b\right]^{1+\gamma}}_{2} + \underbrace{S}_{3} \tag{2.22}$$

where:

$$A = \frac{aw_m}{H} \tag{2.23}$$

$$B = \frac{-C}{H^{1+\gamma}} \tag{2.24}$$

$$C = \frac{\alpha}{6}\left[\pi\rho N_0\right]^{-\gamma}\Gamma(4+\beta) \tag{2.25}$$

$$S = \frac{bw_m}{H} + w_m\left[Q_B - Q_T\right] \tag{2.26}$$

Unhappy with the unwieldy nature of term 2 in equation (2.22), F&K achieved its simplification by rearranging equation (2.7) and giving ($M_B \times H$) the guise of VIL' as below:

$$VIL' = aVIL + b \tag{2.27}$$

then took the time derivative of that equation:

$$\frac{dVIL'}{dt} = a\frac{dVIL}{dt} \tag{2.28}$$

and proceeded to replace VIL in equation (2.22) with VIL' to produce a non-linear expression for the model dynamics:

$$\frac{dVIL'}{dt} = AVIL' + B'VIL'^{1+\gamma} + S' \tag{2.29}$$

making:

$$B' = aB \tag{2.30}$$

$$S' = aw_m\left[Q_B - Q_T\right] \tag{2.31}$$

A linear approximation to equation (2.29) was subsequently derived to produce the linear differential equation of the model dynamics they were seeking:

$$\frac{dVIL'}{dt} = \left[AN_{1\mu} + B'N_{2\mu}\right]\mu_{VIL} + \left[AN_{1r} + B'N_{2r}\right]r_{VIL} + S' \tag{2.32}$$

μ_{VIL} and r_{VIL} being the mean and residual of VIL' respectively and $N_{1\mu}$, $N_{2\mu}$, N_{1r}, N_{2r} all being linearisation coefficients requiring optimisation through model calibration procedures. Space and time dependence in all foregoing equations being implicit.

Presentation of equation (2.32) suggested F&K, whether consciously or inadvertently, had moved away from explicitly modelling the time evolution of "observable" liquid water content, averaged over the area of a discretised column of the atmosphere, to modelling the mathematical construct ($M_B \times H$). F&K derived a solution to equation (2.32) by separating out the mean and variance components and integrating each in terms of expected values:

$$E\left[VIL'(t)\right] = \phi E\left[VIL'(t_0)\right] - \frac{E\left[\mu_S(t)\right]}{A(t)N_{1\mu}(t) + B'(t)N_{2\mu}(t)}\left[1-\phi\right] \tag{2.33}$$

$$Var\left[VIL'(t)\right] = E\left[VIL'(t)^2\right] - E^2\left[VIL'(t)\right] \tag{2.34}$$

$E[\mu_s]$ being the mean of S', E[VIL'] equivalent to μ_{VIL} of equation (2.32) and where:

$$\phi = \exp\left[\left(AN_{1\mu} + B'N_{2\mu}\right)\left(t - t_0\right)\right] \tag{2.35}$$

t-t_0 being the forecast lead-time.

In making a prediction of rainfall rate using equations (2.5) to (2.35), F&K employed the following steps (French and Krajewski, 1992):

1. Measurements of the input variables (surface temperature and pressure, dew point temperature and satellite cloud top temperature) were obtained for time $t=0$ and interpolated to the model grid.
2. An estimate of VIL and H for time $t=0$ was made from radar data, with the condition that VIL×H could not exceed 0.003 kgm^{-3} and M_B (for the purposes of determining linear regression coefficients a and b) could not exceed 0.015kgm^{-3}.
3. The previous forecast of VIL was updated using the latest observation of VIL.
4. The "properties" of the rain field, including cloud top temperature and the variables determined from radar reflectivity, i.e. VIL, the radar measured depth of the cloud (H) and the DSD parameter N_0, were translated according to a velocity vector determined from cross correlating radar images for a period immediately prior to the time of making the forecast.
5. The VIL field and radar base beam data were linearly regressed to find the coefficients a and b, later used for all grid points of the domain.
6. Dew point temperature and surface temperature and pressure were assumed to remain constant at each grid point for the duration of the forecast lead-time and these variables, in combination with the translated cloud top temperature field, were used to determine the values of the updraft velocity and saturation vapour densities at the cloud base and cloud top for each grid point.

This step was conditional on clouds being present. Clouds were identified using three criteria: a difference of at least 25K between dew point temperature and infrared brightness temperature, an infrared brightness temperature less than 270K and a value of VIL greater than zero.

7. The main prediction step was undertaken, whereby VIL was converted to VIL' and solutions to equation (2.33) and (2.34) obtained, with the implication being that the "instantaneous" rainfall and condensation rates obtained for time $t+\Delta t$ had persisted for the duration of the forecast lead-time. Two predictions were undertaken, one using a time step equivalent to the time resolution of the observations for the purpose of state updating and the other at the desired lead-time of the forecast ($t+\Delta t$). Although the VIL source and sink rates were calculated using seconds as the unit of time, Δt was kept as minutes. The forecasted value of VIL' obtained was then converted to VIL.
8. M_B was calculated from the forecast value of VIL using equation (2.7), then converted to a radar reflectivity value from which a rainfall rate was subsequently determined.

The relationship F&K used to obtain rainfall rate from radar reflectivity took the widely accepted form (Collier, 1989):

$$Z = XR^Y \tag{2.36}$$

R being rainfall rate in mm/hr and X and Y empirically derived parameters. Various combinations of values for X and Y have been suggested (Battan, 1973), each qualified in terms of storm type and/or precipitation type. The Z-R relation for stratiform rain is typically taken as $Z=200R^{1.6}$, whereas convective thunderstorms tend towards higher values of X and as such F&K opted for $Z=300R^{1.4}$. In terms of assessing the model's performance, the transformation of reflectivity to rainfall rate was not going to be critical provided the observations against which the forecasts were measured were rainfall rates estimated from radar reflectivity using the same Z-R relation.

F&K gauged the efficacy of the model's forecasts, both with and without state updating, in terms of a comparison of the model's performance with two other forecasting methods, namely simple advection of the current rain field and assumed persistence of the current rain field (Andrieu *et al*, 1994). Performance measures were mean error, RMSE and the correlation between observed and forecasted rainfall rates averaged over an area of 32 km by 32 km. Three storms only were used for assessment purposes and for all three both the stochastic (state updating) and the purely deterministic versions of the model outperformed the persistence and advection forecasts. F&K heralded the stochastic formulation as the most successful of the two model versions and although it did reduce mean error and RMSE, it also reduced the degree of correlation that had been

achieved without its inclusion. What was not clear was the influence the restrictions on the values of VIL×H and M_B in point 2 above, equating to a radar reflectivity of approximately 31dBZ and 38 dBZ respectively, had on the results and it was not specified why they were employed. Using F&K's chosen Z-R relation, the imposed maximum reflectivity values approximated rainfall rates of 2.8 mm/hr and 8.8 mm/hr respectively. Figure 2.2 shows that the observed lower beam radar reflectivity exceeded the constrained value of M_B and whereas the stochastic model could allow the estimates of the current state of VIL to be increased, not so the version of the model without state updating. It can be seen from Figure 2.2 that inclusion of the state updating procedure resulted in a tendency to produce higher rainfall rates. Irrespective of whether or not state updating was included, F&K saw potential for improving results through incorporating NWP forecast data and they recognised adaptations to the model would be required when applying it in areas of mountainous terrain where orographic enhancement of rainfall was likely to occur.

2.6 Crossing the Atlantic

Soon after these results, researchers in England and France took up the framework of F&K's model, each tweaking the formulations in different ways, trying to make it theoretically malleable to the variety of storm types observed across the United Kingdom and Europe.

2.6.1 The French Connection – Andrieu *et al*

The collaboration between Andrieu and F&K that began in Iowa continued during the reciprocal part of the NATO Scientific Exchange Program in which they were partaking, when Andrieu returned to France accompanied by French. In France they sought to trial the model using rainfall events recorded during a meteorological experiment held in the Cevennes region for a period from 1986 to 1988 (Andrieu *et al*, 1996).

Autumn storms in the Cevennes region were often associated with the passage of moist air masses and fronts from the direction of the Mediterranean Sea, and intensification of rainfall was commonly observed within the vicinity of the area's mountainous terrain. These conditions were quite different to the types of storms previously used to run the model, bringing into question the appropriateness of having just a convective parameterisation for the updraft velocity and resulting in a decision to devise a new one. This presented an opportunity to include in the new parameterisation some account of the uplift of moist air over mountain barriers and the consequent orographic enhancement of rainfall.

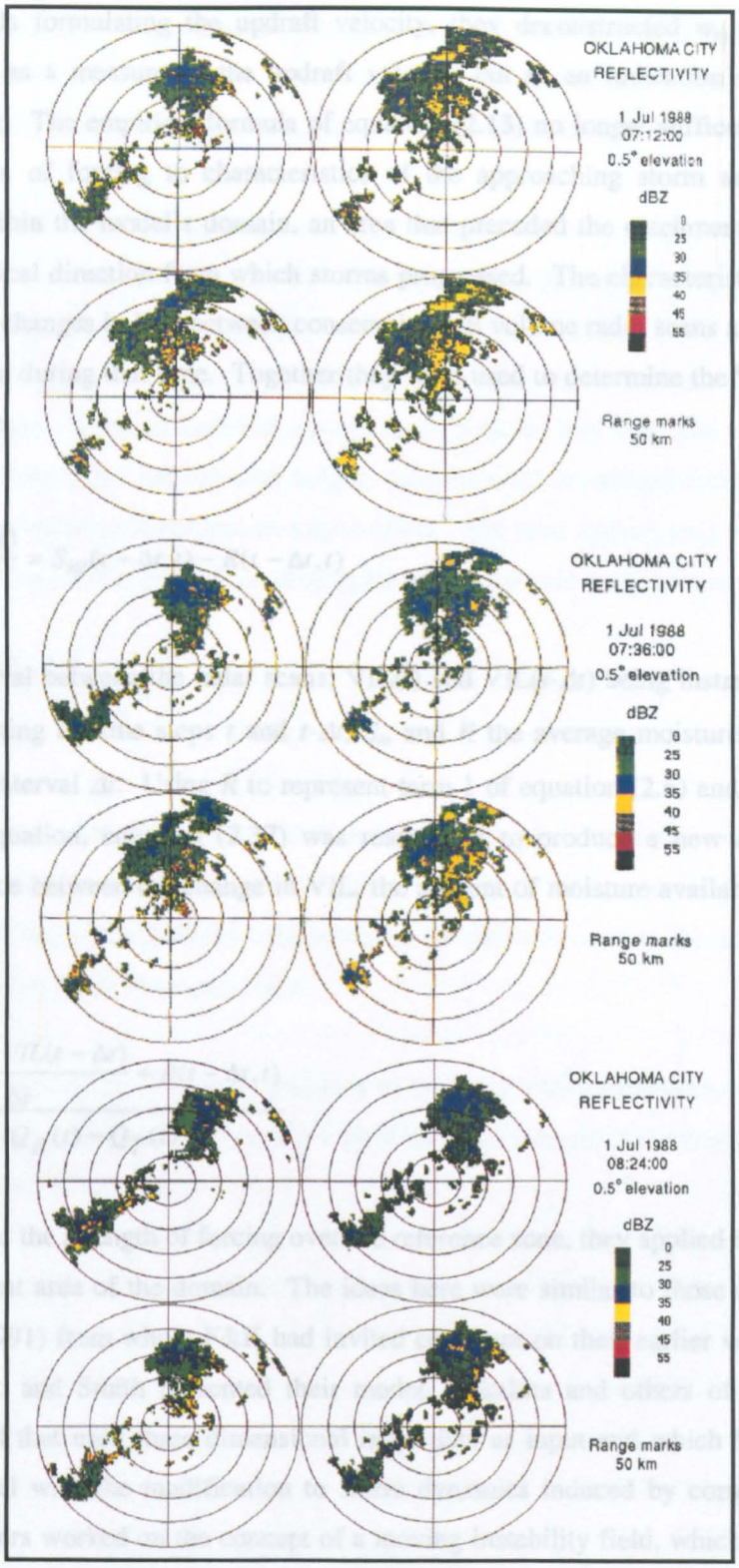

Figure 2.2: *Performance of the F&K model. Three examples are provided, relating to the dates and times indicated. Each example shows four rain fields: (upper left) the current time radar observation, (lower left) the previous hour observation, (upper right) the current time forecast with updating, and (lower right) the current time forecast without updating. (adapted from French and Krajewski, 1994)*

As a step towards formulating the updraft velocity, they deconstructed w_m of F&K's model, presenting it not as a measure of the updraft velocity but as an indication of the strength of mesoscale forcing. The empirical formula of equation (2.13) no longer sufficed and instead they related the degree of forcing to characteristics of the approaching storm as observed over a reference area within the model's domain, an area that preceded the catchments of concern with respect to the typical direction from which storms progressed. The characteristics under scrutiny were quantitative changes in VIL between consecutive full volume radar scans and the rainfall rate and moisture input during that time. Together they were used to determine the "VIL budget" over the reference zone:

$$\frac{VIL(t) - VIL(t - \Delta t)}{\Delta t} = S_m(t - \Delta t, t) - R(t - \Delta t, t) \tag{2.37}$$

Δt being the interval between the radar scans; VIL(t) and VIL(t-Δt) being instantaneous values of VIL at the beginning of time steps t and t-Δt; S_m and R the average moisture input and rate of rainfall over the interval Δt. Using R to represent term 1 of equation (2.6) and replacing S_m with term 2 of that equation, equation (2.37) was rearranged to produce a new expression for w_m involving a balance between the change in VIL, the amount of moisture available and the rainfall rate:

$$w_m(t) = \frac{\dfrac{VIL(t) - VIL(t - \Delta t)}{\Delta t} + R(t - \Delta t, t)}{Q_B(t) - Q_T(t)} \tag{2.38}$$

Having determined the strength of forcing over the reference zone, they applied its value uniformly over the assessment area of the domain. The ideas here were similar to those of Eiichi Nakakita (Ikebuchi *et al*, 1991) from whom F&K had invited comment on their earlier work. At about the same time as Seo and Smith presented their model, Nakakita and others of Kyoto University presented a model that used three dimensional radar data as input and which had been designed specifically to deal with the modification to storm dynamics induced by complex terrain. The Japanese researchers worked on the concept of a moving instability field, which they described as having a high rate of water vapour to liquid water conversion and which they identified by modelling storm characteristics during a period prior to commencing rainfall predictions. Identification of the instability field involved estimating the rate of water vapour to liquid water conversion from a combination of three-dimensional wind and moisture fields, extracted from the radar data, in conjunction with ground-level meteorological station data. The resulting instability field was translated across the model's domain at the estimated speed of the storm and made to

interact with the existing water vapour field as it did so. They dealt with orography by filtering it out, undertaking all calculations on a terrain-following coordinate system and with input meteorological fields interpolated to the computational grid accordingly.

Andrieu *et al* chose to remain with a standard representation of orography on a cartesian grid and attempted to incorporate orographic influences by augmenting the rate of updraft obtained through equation (2.38) with an orographic updraft determined in the much the same way as Bell (1978), being the product of surface horizontal wind velocity and the windward mean slope of the catchment of interest. Whereas Bell had a multi-layered model and was able to linearly decrease the magnitude of orographic forcing with height, Andrieu *et al* introduced a calibration parameter in an attempt to approximate a column-averaged effect. The total updraft (w_z) within a grid cell of their model was therefore the sum of the orographic and mesoscale components:

$$w_z(t) = \underbrace{\alpha_0 \bar{v}_0(t)\nabla\bar{z}_0}_{1} + \underbrace{\alpha_m w_m(t)}_{2} \tag{2.39}$$

with v_0 the horizontal wind velocity at ground level, ∇z_0 the gradient of the windward facing land surface of the catchments and the over-score referring to their mean values. Calibration parameters, α_0 and α_m, modulated the orographic contribution (term 1 in the above equation) and the mesoscale forcing (term 2) respectively.

Perhaps realising expression of model dynamics in terms of VIL' rather than VIL was somewhat abstract, French no longer pursued that path with Andrieu in France, managing instead to replicate equation (2.29) using VIL:

$$\frac{dVIL}{dt} = AVIL + BVIL^{1+\gamma} + S \tag{2.40}$$

by dropping the intercept term of equation (2.7) to give:

$$VIL = \frac{H}{a} M_B \tag{2.41}$$

Apart from all references to w_m having been replaced with w_z, the coefficients A and B in equation (2.40) remained essentially unchanged from their previous definitions (equations (2.23)-(2.25)). However coefficient B had the addition of one new calibration parameter, X:

$$B = -\frac{1}{X}\left[\frac{a}{H}\right]^{1+\beta/4} \frac{\alpha}{6} \frac{\Gamma(4+\beta)}{\left(\pi\rho N_0\right)^{\beta/4}} \tag{2.42}$$

which effectively modulated the downward velocity of the water mass. Andrieu *et al* interpreted the function of X as governing the response of the hydrologic system and in doing so resurrected once again G&B's water reservoir analogy.

Despite eliminating one of the parameters needing calibration in F&K's model, namely A, by using the Marshall-Palmer empirical relation:

$$\Lambda = 4.1R^{-0.21} \tag{2.43}$$

(R being the rainfall rate in $mmhr^{-1}$), the use of two parameters instead of one in the formulation of the updraft velocity and the introduction of parameter X brought the number of free parameters to three, one more than the original F&K model.

When it came to implementing the model, they used a storm of 36 hours duration to calibrate the three parameters and another storm of 35 hours to validate the model. As the Cevennes experiment had not been designed with implementation of the F&K model in mind, radar scans had been taken at only two elevations and satellite data had not been archived. In the absence of infrared brightness temperatures, cloud top temperatures were determined by assuming a pseudo-adiabatic lapse rate of $5Kkm^{-1}$ from cloud base to cloud top. The model was again formulated to be compatible with a Kalman filter and a system of state updating employed. Assessment of the model's forecasts consisted of taking the same performance criteria used to evaluate the original F&K model, namely RMSE and correlation coefficients, and the model's forecasts were similarly compared with those from advection and persistence prediction methods. The calibrated model produced a higher RMSE than either of the two other forecasting techniques and the degree of correlation was lower than achieved by the persistence method. The results were however affected by one anomalous hour for which the model over-predicted the actual rainfall rate by approximately 400%. Andrieu *et al* attributed the large error to their blanket application of the mesoscale updraft calculated in the reference zone to the rest of the model's domain, when for that particular hour the conditions producing strong mesoscale updrafts in the reference zone did not translate to the catchment areas. Removal of this hour raised the performance of the model relative to the other two approaches, whereby the model produced the best correlation statistic and its RMSE came a close second to persistence. The occurrence of the anomaly highlighted to Andrieu

et al the importance of correctly estimating the updraft velocity and exposed a weakness in their approach.

2.6.2 UK - HYREX

Whilst Andrieu *et al* made use of data from a past experiment, Moore, Pedder and Thorpe took advantage of an existing and ongoing experiment in the United Kingdom to make the model's implementation one of its six core tasks (Moore et al, 1995). The Hydrological Radar Experiment (HYREX), conducted from 1993 to 1997, was funded by the UK Natural Environment Research Council (NERC) and involved collaboration between the Institute of Hydrology, the Rutherford Appleton Laboratory and universities of London, Newcastle, Reading and Salford. The principal focus of HYREX was on the use of weather radar to observe the variability of rainfall in storms crossing southwest England. Key projects included assessing how variability in rainfall affected river flow and determining how that variability could be better measured, modelled and forecasted (BADC, 2001, Cluckie *et al*, 2000). Moore, from the Institute of Hydrology, together with Pedder and Thorpe, both from the University of Reading, headed investigations into precipitation forecasting using radar data.

When first implementing the model, Moore *et al* kept largely true to the original formulations of the F&K model but decided not to employ F&K's statistical linearisation and state updating procedures. Results produced from solving the non-linear form of the model's dynamics were compared with persistence and advection forecasts with respect to six storms recorded during HYREX. The conclusions Moore *et al* drew from this exercise was that the model had reasonable success in predicting frontal events but less skill in matching the dynamics of convective storms. Reasons for the contrary results were not fully explored but may have been, in part, contained in the reasons why Seo and Smith had earlier recommended including a representation of frontal dynamics in the model. The recommendation came from having recognised cross-correlation storm advection techniques, which they had used and which the likes of Wild (1996) and Moore *et al* had used after them, were well suited to the often coherent movement of frontal storms, more so than the comparatively erratic movement of convective cells (Seo and Smith, 1992).

On the basis of their results, Moore *et al* proposed changes to the model. They replaced the linear fit between VIL and $M_B \times H$ with a relational fit determined algebraically and allowed it to vary across the domain. They employed a different advection scheme and added a calibration shell to optimise the free parameters. The results achieved with the model upon introducing the changes have yet to be published.

Working toward a PhD at the University of Salford during the initial years of HYREX, Adrian Wild realised the F&K model, with its emphasis on the use of remotely sensed data, complemented his PhD research into estimation of precipitation using remote sensing techniques and the practical applications of those estimates (Wild, 1996). A case study presentation in his thesis of the model's implementation over an area of northwest England provided a means of illustrating the potential for using remotely sensed products in rainfall forecasting. Like Moore *et al* he persevered with expressing model dynamics in terms of VIL' but linearised equation (2.29) very simply by giving the exponent the value of one:

$$\frac{dVIL'}{dt} = AVIL' + B'VIL' + S' \tag{2.44}$$

Whilst Wild acknowledged linearisation in this way could lead to divergence, he justified it with reference to the shortness of the forecast lead-time (maximum of one hour), the heavy reliance throughout the model on empirical formulations and the theoretically small value of γ (approximately 0.167).

Similar to Andrieu *et al* (1996), Wild's total updraft velocity included an orographic component (term 2 below) that he likewise formulated in the manner of Bell (1978):

$$w_m = \underbrace{\varepsilon\left(C_p \Delta T\right)^{1/2}}_{1} + \underbrace{\bar{v}_0 \nabla \bar{z}_0}_{2} \tag{2.45}$$

Lacking surface wind data he instead generated the updraft by applying the same velocity vector that he used to advect the storm and which he obtained from cross-correlating consecutive radar images of rainfall. For the sake of simplicity he ignored possible vertical variation in the orographically induced updraft and his parameterisation lacked the calibration parameter that Andrieu *et al* had introduced. The other component of the updraft was F&K's and G&B's convective parameterisation (equation (2.13)) but in comparison to his predecessors Wild used a higher value for the free parameter ε (0.035 compared to 0.002 used by both F&K and G&B), finding it produced better and more consistent results with respect to the storms included in his case study. No other calibration parameters needed estimation as he, like Andrei *et al*, calculated parameter A using equation (2.43).

Wild decided not to assess the model in terms of instantaneous rainfall rates, choosing instead to use values of VIL, thereby managing to avoid any errors associated with the back transformation of VIL to rainfall rate. His stated intention in undertaking assessment in this way was to more clearly

show, through the larger range of magnitudes that VIL could attain, the differences between actual and forecasted rain fields. The model's forecasts of VIL at lead-times of half an hour and one hour were compared against those of persistence and advection methods using measures of error, RMSE, correlation with respect to spatial averages over an area of 20 km by 20 km as well as the percentage coverage and average value of VIL. Six events, mostly frontal storms, were used for assessment purposes with two events each from early autumn, winter and spring periods. The model failed to better advection and persistence forecasts of average VIL and percentage coverage of VIL at the half-hour lead-time, faring only marginally better over one hour. However, it did produce the higher correlation coefficients at both lead-times and often scored the lower error and RMSE. Wild's conclusion was much the same as that of Moore *et al* (1995), that the model was competent at handling frontal storms. Like Moore *et al*, he questioned the presumed linear relationship between VIL and M_B and also commented on the problems inherent to estimating VIL from volumetric radar data, the latter he made with reference to measurement errors associated with beam overshooting and the occurrence of bright band, amongst others. Wild considered the quality of the model's performance to be highly sensitive to the accuracy of the chosen storm advection method and estimation of the updraft velocity. He suggested trialling use of NWP wind fields to improve the former and augmenting the latter with a component representing air mass convergence.

While Wild had been completing his PhD, Moore had continued working with the model and in 1998 published, in conjunction with Bell, the results of a sensitivity study on the model's response to different input fields of temperature and pressure (Bell and Moore, 1998). This involved running the model first with a combination of infrared brightness temperatures and data from meteorological stations and then solely with data from a mesoscale NWP model, namely the UKMO Unified Model. In this project Moore and Bell respected the convective parameterisations used by F&K and were careful to select two convective storms from HYREX data for their research. By this time they were aware of the work of Andrieu *et al* (1996) and decided to adopt their revised equations and new method of calculating the updraft velocity. They had also discovered that the likes of Wild's linearised version of the model, whereby a value of zero was assumed for parameter γ, could perform just as well as, if not better than, the non-linear version and had the benefit of greater computational efficiency. They conducted their sensitivity study using the linearised form of the model as well as a steady state form in which VIL remained unchanged throughout the forecast lead-time. Moore and Bell proposed an alternative method of calculating the rainfall rate, which they applied to both forms of the model:

$$R = -\frac{(A+B)VIL}{\rho_0} \tag{2.46}$$

A and B being the coefficients in equation (2.40). With respect to the steady state version of the model, this method of calculating rainfall rate still resulted in forecasted rainfall rates that varied from initial rainfall rates because the value of A depended on the value of the updraft velocity. At the completion of the sensitivity study, Moore and Bell concluded that both versions were relatively insensitive to input fields of temperature and pressure and postulated that a single average field value might suffice.

2.6.3 Recent developments

In the same year that Bell and Moore published the results of their sensitivity study, Andrieu presented further model development work that he and Leslie Dolcine had undertaken at the Laboratoire Central des Ponts et Chaussées in France (Andrieu *et al*, 1998). They again teamed with Mark French and together refined the equation for the time evolution of VIL, producing a formulation that more clearly depicted the simplicity of the concepts behind it. In doing so they gave greater prominence to their idea that rainfall rates and VIL were related through the response time of the system. The response time, up to this point, had being represented by parameter X in equation (2.42). The new form of the model dynamics became:

$$\frac{dVIL}{dt} = S - \underbrace{hVIL}_{R} \tag{2.47}$$

h being synonymous with $1/X$ and defined as the inverse of the time required to transform VIL into rainfall rate R. Parameter h was easily derived from radar observations at the beginning of each forecast time step:

$$h = \frac{R}{VIL} \tag{2.48}$$

and assumed to remain constant over the forecast lead-time.

They no longer operated the model in a Lagrangian frame of reference and instead employed a Eulerian system, which required them to take explicit account of advective components:

$$\frac{\partial VIL}{\partial t} = -u\frac{\partial VIL}{\partial x} - v\frac{\partial VIL}{\partial y} - hVIL + S \tag{2.49}$$

They handled this in practice by applying uniform values of u and v across the model's domain and determining the values of u and v by cross correlation of consecutive radar images, in the same way as the Lagrangian system velocities had been estimated.

There was a certain familiarity about equation (2.49) as it closely resembled a formulation of Georgakakos and Lee, who had all the while continued working on the physically-based rainfall forecasting model that they had developed at the Institute of Hydraulic Research, University of Iowa (Georgakakos and Lee, 1996). With reference to condensed liquid water equivalent, Q, rather than VIL, their equation, in discrete form, for the time evolution of the model state was:

$$\frac{\partial Q}{\partial t} = -\frac{\Delta}{\Delta x}\left\{\overline{QU}\right\} - \frac{\Delta}{\Delta y}\left\{\overline{QV}\right\} - hQ + S\varepsilon \tag{2.50}$$

with $\overline{U}$ and $\overline{V}$ being the weighted, average, horizontal wind velocities in the x and y directions respectively; parameter ε having the same meaning as in equation (2.13) and the same function of controlling the strength of updraft. In contrast to the derivation of parameter h presented by Dolcine *et al*, Georgakakos and Lee employed a more complex determination:

$$h = \frac{4c\varepsilon_2}{Z_T - Z_B}\left[\frac{1 + 3/4N_v + 1/4N_v^{\,2} + 1/24N_v^{\,3}}{e^{N_v}}\right] \tag{2.51}$$

ε_2 being the inverse of the drop size distribution parameter Λ; c (s^{-1}) having a value of 3500 and taken from the empirical equation for terminal velocity adopted by Georgakakos and Lee:

$$V(D) = cD \tag{2.52}$$

and N_v determined by:

$$N_v = \frac{w_m}{c\varepsilon_2} \tag{2.53}$$

with w_m the vertical velocity of the air mass as stated previously.

In equations (2.49) and (2.50) parameter h was intended as the quantification of the microphysical processes acting to produce rainfall from the condensed liquid water present in the atmosphere. Whereas G&B, Seo and Smith, F&K and Georgakakos and Lee had all attempted to formulate

these processes in terms of terminal and updraft velocities and drop size distributions, the approach of Dolcine *et al* allowed the French team to account for all microphysical processes without having to be explicit about what they were or dependent on empirical relations to calculate them.

Dolcine *et al* applied an equally radical approach to the calculation of the source term S in equation (2.49). Gone again was any explicit reference to physical processes, no longer was S to be determined in terms of the gradient in saturation water vapour densities and strength of updraft, nor reliant on the assumptions associated with that method. In fact, the significant achievement that Dolcine *et al* made in formulating their model was that, apart from ground slope data, they managed to dispense with all inputs to the model other than those derived from volumetric weather radar data. Therefore, initial values of S were based on using consecutive radar images to follow the path of rain cells and to observe the variation of VIL over the time between the two volumetric radar scans. The observed rate of change of VIL was taken to be the rate of liquid water formation at the beginning of the forecast lead-time. The initial value of S attributed to a grid cell of the model was allowed to evolve through:

$$\frac{\partial S(x,y,t)}{\partial t} = -u\frac{\partial S(x,y,t)}{\partial x} - v\frac{\partial S(x,y,t)}{\partial y} + G_S(x,y,t) \tag{2.54}$$

with G_s included to account for growth and decay in storm dynamics. Having limited themselves to the use of radar data, the only modifying influence on rainfall rate that Dolcine *et al* could represent was that of orographic forcing:

$$G_S(x,y,t) = \alpha_0 V_0(t)\nabla z_0(x,y) \tag{2.55}$$

with the above parameterisation essentially being term 1 of equation (2.39). Calibration of α_0 was still required but the calibration exercise had been simplified by reduction of the model's free parameters from three to one.

By completely eliminating almost all expressions of meteorological processes from the model's formulations Dolcine *et al* very nearly perfectly realised G&B's original concept of using applied hydrology to forecast rainfall. Imposed on a column of the atmosphere was a hydrologic model that they likened to a linear reservoir model of the form:

$$VIL(t+\Delta t) = e^{-k(t)\Delta t}VIL(t) + (1-e^{-k(t)\Delta t})S(t) \tag{2.56}$$

and in its construction they employed the phenomenological or "black box" approach commonly taken in hydrological modelling, whereby complex physical processes are subsumed into a "system response", with modelling of that system response replacing faithful and painstaking reproduction of the processes themselves (Han, 1991).

Dolcine *et al* found this method of forecasting to work well at a lead-time of one hour when using the same case studies from the Cevennes Radar Experiment that Andrieu *et al* had used previously, in addition to two events recorded latterly with the Monte Grande radar in Italy. In all cases the model performed better than the persistence method, and likewise with respect to the advection method in all but one. Performance criteria consisted of RMSE, the coefficient of correlation and the coefficient of efficiency, the latter relating the variance between model forecasts and actual observations to the variance of actual observations from the mean of the observations (Nash and Sutcliffe, 1970). For this assessment different values of the calibration parameter α_m were used for each storm and optimised separately for each storm. A subsequent sensitivity study showed that interchanging the value of the parameter between storms actually had little impact on the results. A sensitivity study was also undertaken to determine the benefit obtained from employing state updating procedures using a Kalman filter. The marginal improvement in forecasting was considered insufficient to warrant its inclusion.

Evaluation of the model also included testing it with three simulated storm events of different temporal variability. It was shown that the model's performance decreased as the temporal variability increased, which Dolcine *et al* explained in terms of equation (2.56). Noting that the source term in equation (2.56) became the predominant determinant of forecasted VIL when the lead-time exceeded the response time, Dolcine *et al* acknowledged that improved forecasting on those occasions would require a parameterisation of S that was more reflective of microphysical processes and atmospheric dynamics. Failure to account for microphysical processes resulted in the model's system response time being shorter than the natural response time of the atmospheric column.

In subsequent work, the trio of Dolcine, Andrieu and French went to the opposite extreme in formulating microphysical processes in almost intricate detail (Andrieu *et al*, 2000). This time they were joined by another Frenchman, Jean-Dominique Creutin from the Laboratoire des Transferts en Hydrologie et Environnement CNRS in Grenoble. Together they not only embellished the source term with microphysical parameterisations but also reverted to F&K's "microphysically" based method of determining R, the rainfall output. Having decided that neglect of cloud water was the key reason for the discrepancy between the previous model's system response time and

that of "nature", they proposed a two-reservoir model that explicitly accounted for the time evolution of both cloud water and rain water:

$$\frac{\overline{dm}}{dt} = w_m[Q_B - Q_T] - \overline{S}_{mM} \tag{2.57}$$

$$\frac{\overline{dM}}{dt} = [w_m - V_B]M_B + \overline{S}_{mM} \tag{2.58}$$

with $\overline{S}_{mM}$ representing vertically integrated (indicated by the overbar) processes controlling the conversion of cloud water to rain water. Three such processes were explicitly determined, namely autoconversion (AC), accretion (CC) and evaporation (Ev):

$$\overline{S}_{mM} = \int_{Z_B}^{Z_T} S_{mM} = \overline{AC} + \overline{CC} - \overline{Ev} \tag{2.59}$$

Each of the three mechanisms were parameterised using previously published empirical relations. For initialisation of cloud water values and the provision of other meteorological inputs they envisaged use of NWP model data. They compared the performance of this new model with that of extrapolation methods and also the original version of the F&K model and did so in relation to three rain events, of increasing temporal variability, that were simulated using a meteorological microphysical mono-dimensional model. The performance measures were again the correlation of efficiency, RMSE and coefficient of correlation and assessment undertaken using a lead-time of 30 minutes. For all simulated events and for all performance criteria, the two-reservoir model outperformed the advection and F&K models. However the group went on to show that the improvements gained by incorporating the cloud water component were dependent on the degree of uncertainty in the accuracy of cloud water observations, an uncertainty of 20% or more rendered the two-reservoir model equivalent to the F&K model.

Dolcine, Andrieu and Creutin later joined with Daniel Sempere-Torres from the Universitat Politècnica de Catalunya, Spain, to couple the rainfall forecasts with a rainfall-runoff model (Andrieu *et al*, 2001). The continual broadening of nationalities involved in developing the rainfall forecasting model was to some extent due to much of the research in Europe being undertaken as part of the HYDROMET Project, funded by the European Commission. The core objective of the HYDROMET Project was the "development of active on-line hydrological and meteorological models to minimise the impact of flooding" (Cluckie *et al*, 2000), for which the principle co-ordinator was the University of Bristol who were partnered by tertiary institutions from France,

Italy, Greece, Spain and Slovenia. In this coupling work, Andrieu *et al* showed a preference for using the "black box" hydrologic model for lead-times up to 2 hours and the microphysical model for longer lead-times. They again found that both models produced better forecasts compared to the persistence method of forecasting, the performance measures this time being RMSE and the coefficient of efficiency. However, they also found that better rainfall forecasts did not necessarily produce a commensurate improvement in flow forecasting. Persistence forecasts were equally effective when the response time of the catchment was long in comparison to the lead-time of the forecasts.

2.7 Summary and discussion

Figure 2.3 traces the timeline of the F&K model (in yellow), showing the main protagonists and their respective expressions for the time evolution of the model state. The F&K model was the culmination of ideas and research undertaken in the USA (in green), and was subsequently taken up by researchers in the UK (in pink) and France (in blue) with a view to adapting it to suit their particular storm conditions. Missing from the schematic is the parallel work of the Japanese group, Nakakita *et al* (1991), who similarly developed a catchment scale, physically-based rainfall forecasting model incorporating three dimensional radar data and developed specifically for mountainous areas. Their ideas, particularly their modelling of a perceived instability field, featured in the more recent work of Georgakakos and Lee (1996), which is similarly not shown in the schematic as it is considered an extension of their own research rather than that of F&K. Some of the methodologies of the Japanese group were strongly evident in the French team's work on the F&K model, as were the formulations of Georgakakos and Lee, their expression for model dynamics virtually replicated in Andrieu *et al*'s "black box" model.

The purpose of detailing the history behind the F&K model, and how others have since adopted it and experimented with it, is to provide an overview of all the research that informs and inspires the work presented in the following chapters. It highlights the adaptability of the framework first proposed by G&B, how the methodologies and formulations were as dynamic as the processes being modelled. Theirs was a framework that appeared to successfully marry meteorological theories with hydrological approaches, a combination proving superior to short period rainfall forecasting methods of persistence and advection in virtually all examples of its implementation. A key feature of the framework was its simplicity and computational efficiency, allowing models to run operationally in real-time. However, Georgakakos in his later work recommended looking more closely at the assumptions required to maintain simplicity and saw a need for improvement of the physics employed (Georgakakos and Lee, 1996). Andrieu *et al* (1996) also expressed doubt about taking too literally the solutions to parameterisations as actual quantification of the processes

they were purported to emulate, particularly with respect to the updraft velocity. This scepticism was supported to some extent by examples of wholly convective parameterisations producing reasonable results in situations of frontal storms (G&B, 1984; Moore *et al*, 1996; Wild 1996). The merit of the parameterisations became more evident though in later work by the French, in which elimination of meteorological theory was shown to diminish the value of forecasts, particularly at longer lead times. Borrowing Andrieu *et al*'s hydrologic system concept, it might be concluded that while the simple parameterisations have limited ability to fully emulate actual real-life processes, they are sufficient to reasonably approximate the response of the system.

Each model version represented in Figure 2.3 often constituted an attempt to act on recommendations arising from preceding work. The establishment of advanced observing systems and the increased availability of data enabled the inclusion of remotely sensed estimates in the model and thereby allowed the early suggestions of Georgakakos and Lee (1990) to come to fruition. Anticipated advances in technology and computing resources led a number of researchers, notably Seo and Smith (1992), F&K (1992), Wild (1996) and Andrieu *et al* (2000) to recommend replacing meteorological input from observing stations with finer scale NWP model forecasts. Georgakakos and Lee (1996) experimented with using forecasted wind fields from a NWP model to drive the local transport of liquid water mass in their model and found them to be no more effective than assuming persistence of observed wind fields. The Japanese team utilised NWP model forecast data in more recent work on their rainfall forecasting model (Ikebuchi *et al*, 2001), but qualified their confidence in doing so with employment of a stochastic framework for state updating which they believed would help ameliorate forecast errors associated with NWP data inaccuracies. Moore and Bell suggested such errors may not matter due to insensitivity of the model to the meteorological inputs (Bell and Moore, 1998).

The following chapter will detail the development of a new version of the F&K model which extends the use of NWP model data beyond the provision of meteorological input values to construction of a forecasting algorithm based on identification of variables that act as ingredients of rainfall production.

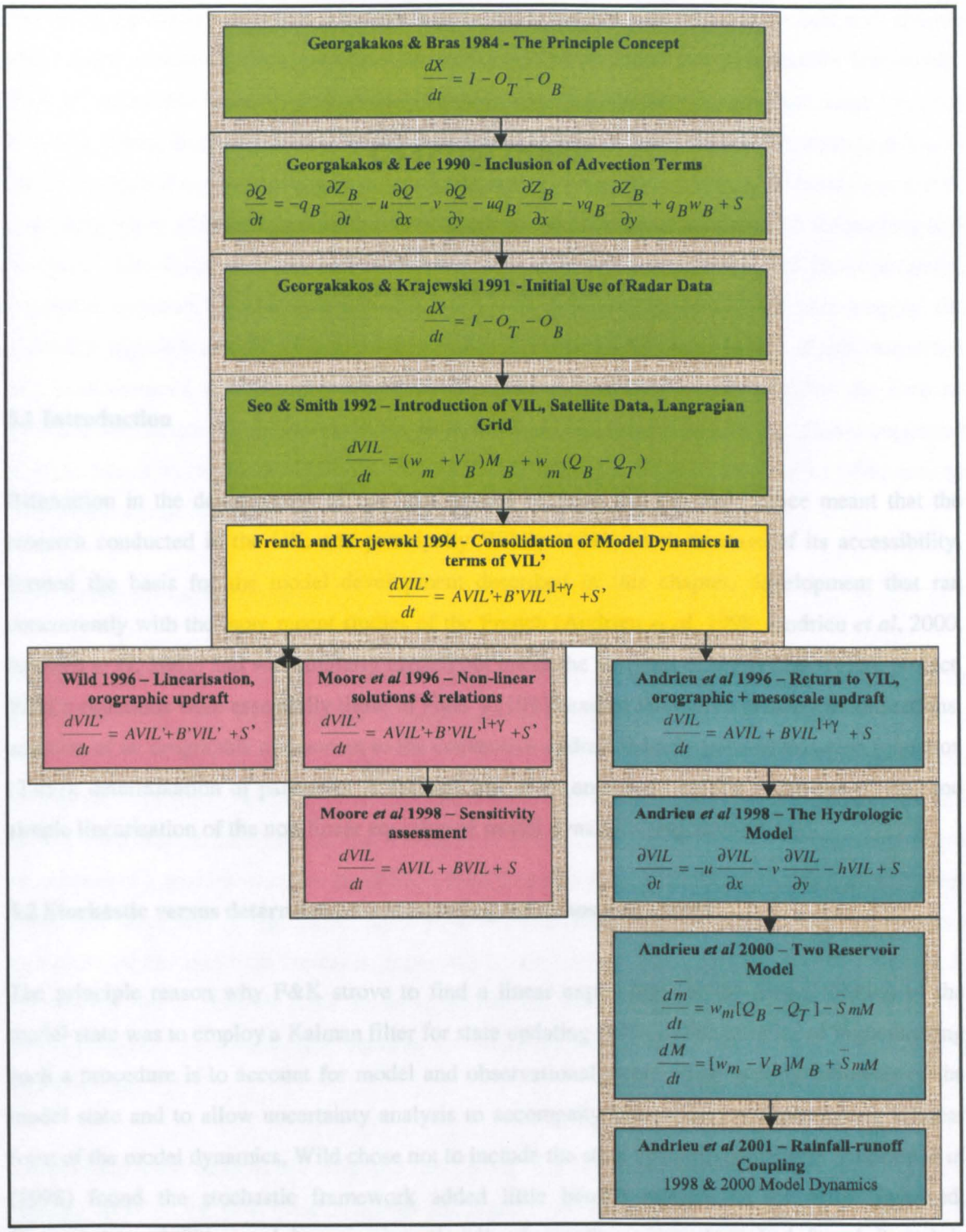

Figure 2.3: *Schematic of the development of the F&K model. It traces development from its conceptualisation in the USA (green boxes) to its culmination in 1994 (yellow box) and its subsequent utilisation and adaptation in the UK (pink boxes) and France (blue boxes). Shown are the principal researchers, their respective equations for the time evolution of the model state and the date of publication.*

CHAPTER THREE

MODEL DEVELOPMENT

3.1 Introduction

Bifurcation in the development of the F&K model between the UK and France meant that the research conducted in the UK, and principally Wild's (1996) work because of its accessibility, formed the basis for the model development described in this chapter, development that ran concurrently with the more recent studies of the French (Andrieu *et al*, 1998; Andrieu *et al*, 2000, Andrieu *et al*, 2001) and was similarly carried out under the auspices of the HYDROMET project. Wild's equations were essentially those of F&K's (1992) except with three primary modifications: addition of an orographic component to the convective updraft velocity parameterisation (equation (2.45)), determination of parameter Λ through use of an empirical relation (equation (2.43)) and simple linearisation of the non-linear equation of model dynamics (equation (2.44)).

3.2 Stochastic versus deterministic – accounting for chaos and errors

The principle reason why F&K strove to find a linear expression for the time evolution of the model state was to employ a Kalman filter for state updating (1994). The purpose of implementing such a procedure is to account for model and observational errors when making estimates of the model state and to allow uncertainty analysis to accompany forecasting. Despite taking a linear form of the model dynamics, Wild chose not to include the state updating procedure. Andrieu *et al* (1998) found the stochastic framework added little benefit relative to the effort involved. Georgakakos (2000) noted how computationally demanding researchers had found it and is currently continuing research into diminishing the computational load. Although it is accepted that real-time updating of the model state would probably improve the performance of the precipitation forecasting model proposed here (herein referred to as the PFM), derivation of a stochastic form of the model dynamics has not been attempted, as the purpose of the research was to gauge the deterministic capabilities of the PFM and not to devise an efficient state estimator.

Incorporating stochastic elements in a forecasting model is one way of trying to deal with chaotic atmospheric processes whilst another, as mentioned in Chapter One, is ensemble forecasting. Typically ensemble forecasting in an operational context is undertaken for medium range forecasts (UKMO, 2001a; Barkmeijer *et al*, 2000). At the short lead-times looked at in this study (1-6 hours) and at the spatial resolutions employed (1-5km), ensemble forecasting was considered impractical, especially when working towards real-time applications for which timeliness in forecasting is a concern. Also it is important, before implementing a model in a resource- and time-consuming ensemble framework, to establish it has some skill in forecasting. Rather than employ the ensemble approach and take the mean of a series of forecasts, for the purposes of this research it has been assumed that output from the PFM tends towards the mean such that the forecast produced can be considered representative of the average of a possible ensemble. This is supported to some extent by the work of Bell and Moore (1998) who showed Andrieu *et al*'s (1996) version of the model to be relatively insensitive to perturbations in initial conditions.

3.3 Ingredients based approach

An often mentioned, but as yet not fully implemented, recommendation made by those who have worked with the F&K model and its variants was the incorporation of forecasts from a fine-scale NWP model. In making that recommendation, proponents largely foresaw the input being limited to the meteorological variables otherwise taken from meteorological stations. Reliance on data from meteorological stations has disadvantages in that stations are typically sparsely located and the measured variables must be assumed to remain constant over the period of the forecast lead-time. The latter may be reasonable under some circumstances and limited lead-times but becomes untenable as the lead-time increases, especially in the vicinity of fast moving fronts (French & Krajewski, 1994). Use of NWP forecasts avoids the need to assume persistence in values of meteorological inputs but in turn replaces it with a tenuous assumption that the forecasts can be taken as truth.

Large-scale NWP models, for example the UKMO's General Circulation Model (UKGM), are receptacles of global data from numerous and hugely varied sources. Assimilation of data in the models leads to an analysed state of the atmosphere which acts as boundary conditions to smaller scale models, such as the UKMO's Mesoscale Model (UKMM), which themselves assimilate local data and provide a more detailed picture of atmospheric conditions over a limited area. The two aforementioned UKMO models are brought together and embedded in a Unified Model framework that also includes coupled ocean modeling (Hardaker, 2001). It stands to reason that there must be information that can be extracted from this wealth of data and, as such, the smaller-scale NWP models must have something to offer, particularly at long lead-times, over and above, for example,

one meteorological station covering the forecast domain (Haile *et al*, 1997). Use of mesoscale NWP output offers a context in which to place a fine-scale rainfall forecasting model, an opportunity to determine if the broader conditions are favourable to storm initiation, development or decay and constitutes acknowledgement that processes of precipitation formation operate over continuous spatial and temporal scales (Sumner, 1988). Given that small-scale precipitation patterns can emerge within synoptic scale systems as manifestations of mesoscale or locally forced responses to larger-scale meteorology (Carpenter, 1982), performance of a fine resolution, localised model may be compromised if it cannot account for the larger-scale meteorological processes to which local weather is responding. This Browning (1982) saw as the problem with using nowcasting techniques to predict rainfall associated with frontal storms. The errors in those cases, he surmised, arose from a failure to predict growth and decay on the synoptic scale and hence recommended subjective modification of nowcasts based upon prevailing mesoscale and synoptic conditions.

The UKMO's Nimrod system is one example of an attempt to tackle some of the problems identified by Browning and does so by merging remotely sensed data with UKMM forecasted meteorological fields. Rainfall predicted by Nimrod is the optimised, weighted sum of the rainfall prediction produced by the UKMM and that produced from a nowcasting technique using radar images which have undergone automated correction procedures. The advection velocities used in the nowcasting technique are themselves an optimised, weighted sum of the UKMM wind fields and the storm velocity estimated by using the method of maximising the cross correlation between radar images (Golding, 1998). In a sense, the Nimrod system contains the three components Golding (1998) proposed as necessary for optimal short range forecasting, these being extrapolation, local climatology and large-scale development - that is, if UKMM forecasted rain fields are taken as explicitly representing culmination of the latter. Notably the approach does not greatly exploit the array of data and information contained within the UKMM. It discards standard variables that the UKMM predicts fairly reliably, such as pressure and temperature, in preference for the precipitation field which it fails to adequately resolve (Golding 1998) and the estimation of which is primarily undertaken so as to account for its cumulative impact on larger scale dynamics (Pierce *et al*, 2000).

At present the F&K model and its derivatives remain simple representations of local-scale physical processes, which operate in the absence of synoptic context but provide a suitable framework for combining Golding's three recommended components of a forecasting model and particularly for use of UKMM data in a more analytical way than described above. The F&K model already incorporates extrapolation techniques, has local climatology representation through its use of high

resolution, remotely sensed data combined with topographic data and the model formulations are conducive to assimilating UKMM fields.

To date the ability of the F&K model to make reasonable predictions at fine spatial resolutions ($\leq$25km^2) has largely relied on employing short forecast lead-times, for which nowcasting techniques are known to perform well. The F&K model can be likened to nowcasting in its assimilation of weather radar data and satellite data combined with extrapolation of trends in movement achieved through feature tracking. However, a representation of dynamics in the form of simple rising parcel theory has been shown to elevate its performance with respect to simple advection methods that translate existing rainfields across catchments unmodified. Application of simple rising parcel theory enabled F&K to parameterise convectively-driven vertical accelerations of air parcels in terms of the difference between in-cloud and environmental temperatures. Knowing not all convective potential energy generated by this temperature difference converts to kinetic energy (Georgakakos & Lee, 1996), they used a parameter to control the extent of the conversion, the value of which they determined through optimisation procedures. They realised rising parcel theory and thermally induced vertical motion are not explanations for the vertical accelerations associated with dynamic uplift, such as the vertical forcing of air over mountains and at frontal boundaries, which are typically weaker than those of convection (Sumner,1988). However the indiscriminate use of the model for a range of synoptic conditions, as undertaken by Wild (1996), was not unjustified given that there exist observations of mixed widespread and convective rainfall (Rogers & Yau, 1989) and also spatial and temporal inhomogenities in vertically pointing radar data during the passage of frontal storms (Wild, 1996). Theories supporting those observations include the triggering of convection by forced uplift associated with fronts and orography, or from the instability produced by terrain-induced retardation of surface front movement combined with differential advection aloft (Smith 1982). In applying the model to situations where dynamic lifting predominates there is a need for caution, particularly when optimising the parameter described above using a set of such storms. The value of the parameter obtained will effectively suppress the thermal updraught created by the model so the speed of uplift approximates, for example, slow frontal lifting in localities where frontal systems are common. Use of the parameter in this way detracts from what was intended to be a physically based model with local optimisation and shifts it towards simply being a framework for exercising skill in parameter estimation.

In order to avoid misrepresentation of the rainfall process, the information contained in UKMM data can be absorbed into the framework of the F&K model, not just in terms of direct inputs but in a way that differentiates between the types of forcing producing the rain. Such an approach encompasses the concept behind the UKMO's proposed Nimrod-GANDOLF integrated system

(Collier *et al*, 2000). GANDOLF (Generating Advanced Nowcasts for Deployment in Operational Land-based flood Forecasts) merges remotely sensed data and NWP predictions whilst also employing ideas of Zipser (1982) in the form of an operational conceptual model of the life cycle of a convective cell, with the appropriate stage of development identified in real-time through an object oriented approach (ERSWRC, 1999). The triggering of this convective component in the model is achieved by identifying air-mass type through a neural network classification of satellite images (Pankiewicz, 1997) and matching it with convective potential as indicated in UKMM data (Collier *et al*, 2000). When no convection is evident Nimrod, rather than GANDOLF, is used to generate predictions. The UKMM data therefore assists in determining the appropriate forecast approach with respect to the prevailing conditions.

Such a sophisticated identification of air-mass type has not been copied for the PFM, rather the ideas for incorporating UKMM data followed those of Brooks *et al* (1996), an ingredients based approach founded simply on the tendency of heavy rain to be associated with particular conditions, that certain factors need to be present for it to eventuate. This may be as rudimentary as the presence of high relative humidity to more complex phenomena such as symmetric instability. The ingredients for precipitation production identified by Brooks *et al* are exactly those upon which the framework of the G&B (1984b) and subsequently F&K (1994) models were based, the lifting of moist air to condensation, with the speed of uplift, water vapour content and precipitation efficiency together dictating the rate of rainfall. The amount of rain that falls at any fixed geographic location depends also upon the size and speed of the precipitating system. According to Brooks *et al*, the key to forecasting rain lies in identifying areas in which air of high moisture content is ascending. Fundamental to locating areas of ascent is determination of the nature of the vertical motion, whether it derives from buoyant (convective) or forced (non-convective) mechanisms.

This formed the principle behind the proposed extended use of mesoscale NWP data in the PFM, being for the identification of areas of high water vapour content combined with mechanisms of uplift as well as for differentiation of the strength of forcing involved. The aim was to maintain a high degree of simplicity and make tentative first steps into determining potential for the use of NWP data in an ingredients-based approach to rainfall forecasting.

3.4 Methodology

Having established a rationale for including NWP data and its mode of use, a methodology had to be constructed to first determine what constitutes high water vapour content and how areas of uplift can be identified, differentiated and the rate of uplift parameterized. A literature search and an

examination of rainfall events were principal components of the methodology, the literature search directed towards collating a set of signifiers of upward motion and of saturation of the atmosphere, and the examination of storms towards verifying their potential and relevance. Ultimately, the ideas gained through that process had to be moulded into an algorithm for model implementation and then the performance of the new model tested. Satisfying both development and testing phases necessitated making core decisions regarding the geographic location of the model's domain, its size, the horizontal resolution of the grid, data sources and the rainfall events to be used. The accessibility of data and availability of computing and other resources were key determinants of how signifiers were assembled, data examined, the algorithm constructed and the model tested.

3.4.1 The domain

The area chosen to constitute the PFM's domain was an artefact of inheriting Wild's coding for the model, the datasets he used to run his model and his topographic elevation data. The domain is shown in Figure 3.1, extending from North Wales to northern England and including the Cambrian Mountains and the Pennines, regions known to exhibit orographic influences on rain formation (Acker *et al*, 1997; Browning and Hill, 1979). The area corresponds to the coverage of the weather radar located at Hameldon Hill from which Wild sourced his full-scan radar data. Following Wild, the domain was divided into a square grid of 84×84 square cells, each of dimensions 5km by 5km. This matched the spatial resolution of the UK single-site and network radar data and gave a computational grid of 7056 points upon which to calculate forecasts. All data were mapped onto the grid and the result obtained for each computational point was considered averaged over the 25km^2 cell it represented. In common with F&K (1994) and Wild (1996), not all of the domain was included in performance tests, instead an assessment grid of magnitude 42 by 42 grid cells was nested in its centre and the outer domain served as boundary conditions.

3.4.2 The data

Inputs needed to develop and test the model were NWP, radar and satellite data. Visualisation of the data was imperative for model development and files were processed and formatted with this in mind. Out of the visualisation software packages freely available, Vis5d proved the most compatible with the UNIX system used to run the model. It is a software package that has been developed within the Space Science and Engineering Centre of the University of Wisconsin and is provided free via the internet (http://www.ssec.wisc.edu/pub/vis5d-5.2). It is ideally suited to examining NWP data and has been largely designed for that purpose, allowing presentation of three dimensional graphics and featuring time animation capabilities. It also has facilities to determine air parcel trajectories, construct vertical soundings and calculate additional variables from those in

the original data set. Of particular use is the "import" utility which allows multiple data files of varying resolution and co-ordinate systems to be combined and resampled to the specified grid of choice, the horizontal resampling being based on weighted averages of the closest neighbouring values to each grid point of the model domain. Errors associated with various interpolation schemes have been examined by Kromp-Kolb *et al* (1995), particularly in reference to wind fields, who found that higher-order horizontal schemes, such as bicubic interpolation, produced fewer errors than linear schemes. In any future development of the model the interpolation options should be looked at in more detail. Vis5d was used to manage all data, with each data type (NWP, satellite and radar) processed into separate ".v5d" files which were then amalgamated, using the import utility, into one file that conformed in resolution and geographic location to the domain grid described above. Due to a heavy demand on available computer space and the considerable size of some of the NWP data files, the default compression employed by Vis5d, namely scaling down to one byte integers, was left unaltered. The influence of this compression was evident in the results at times, with slight variations occurring in values at the fourth decimal place.

Figure 3.1: *The domain used for PFM development. The approximate site of the Hameldon Hill weather radar is indicated. The topography shown is at a horizontal resolution of 500m.*

3.4.2.1. Mesoscale NWP data

All NWP data used in the model development phase of this research came from archived runs of the UKMM which, upon request, is supplied free to members of the Universities' Weather

Research Network (UWERN) via the Joint Centre for Mesoscale Modelling (JCMM) at the University of Reading. The JCMM is supported by both the UKMO and the Natural Environment Research Council (NERC).

Throughout the history of the UKMM, attempts have been made to increase and improve its system of data assimilation, to improve the physics employed and particularly its representation of land surface processes and their influence on dynamics, as well as to operate the model on increasingly fine resolutions. Currently the horizontal resolution of the operational UKMM stands at 0.11° by 0.11° (approximately 11km by 11km), enabling representation of topographic detail except where peaks and valleys extend less than 22km (Hand *et al*, 1995). Uniform grid lengths are achieved by operating the model on a rotated grid and locating the UKMM's North Pole at 37°N 177.5°E so that the "equator" effectively runs through it centre (UKMO, 1998a; UKMO, 2001b). It has 38 vertical levels for which a hybrid system is employed, the closely spaced lower levels being on terrain-following numerical coordinates that are based on the ratio of pressure to surface pressure and grading to wider, higher levels defined by pressure only.

The UKMM nests within the UKGM (Figure 3.2), upon which it depends for boundary conditions that evolve from the assimilation of wind, pressure, temperature and humidity measurements from global sources. Local surface observations are not included in the UKGM but are assimilated at the mesoscale, as are higher resolution radiosonde data. Also exclusive to the UKMM is a moisture preprocessing system in which a three dimensional cloud analysis is produced from a combination of relative humidity measurements, surface cloud reports, cloud top temperatures (derived from infrared satellite imagery) and radar measured rainfall. The latter does not itself constitute the analysed UKMM rain field but is instead assimilated in terms of the "latent heat nudging" associated with the condensation processes it represents.

Cortinas and Stensrud (1995) stressed the need to understand the workings of NWP models when using their output for weather forecasting, to know what physical processes are represented explicitly (grid-scale) or implicitly (subgrid scale) and the parameterizations used. The two configurations of the Unified Model (UKGM and UKMM) rely on a balance between gravitational and pressure gradient forces known as hydrostatic equilibrium (Rogers and Yau, 1989), which prevents the generation of vertical instabilities which might be found in heavy showers and thunderstorms (Byron-Scott et al, 1998). Both use parameterizations for microphysical processes occurring in frontal cloud leading to precipitation formation, for development of convective cloud and precipitation, for radiation and for surface and sub-surface processes. One of the principal implications of the parameterizations with respect to convective processes is that the resolved model vertical winds will not be representative of sub-grid scale "within-cloud" convective

updrafts and therefore can not be used directly to drive the PFM's rate of convective condensation. The UKMM is known to be most reliable with respect to its predicted fields of primary variables such as temperature and pressure but has less success in predicting precipitation fields, a shortcoming attributed to the coarseness of the resolution (Golding 1998) and also to the generally poor observation of water substance in the atmosphere (UKMO, 1998b).

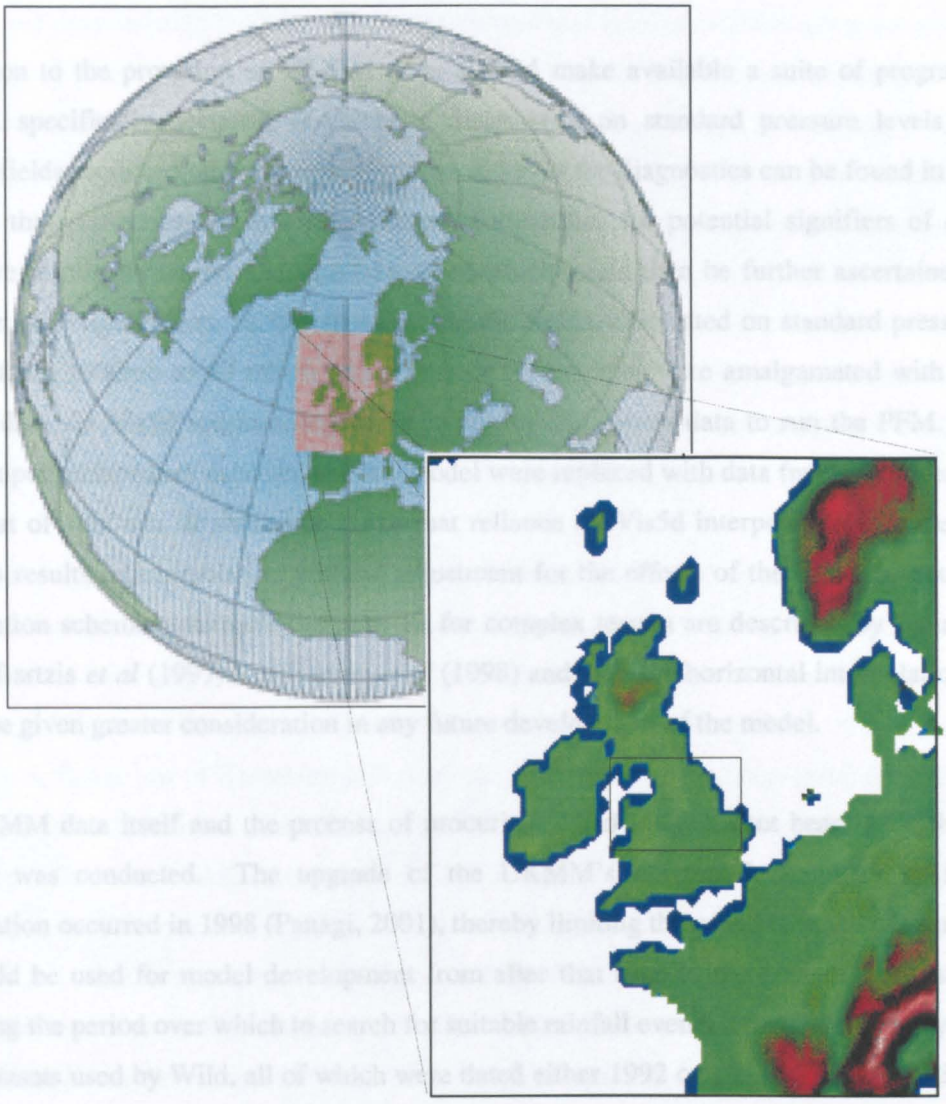

Figure 3.2: *The area covered by the UKMO's two operational configurations of the Unified Model. The top left diagram (taken from http://www.meto.gov.uk/cgi-bin/printpage.cgi) depicts both the Global Model and the UKMM (coloured red). The lower right diagram shows the UKMM in more detail (produced using UKMM topography fields supplied by JCMM and Vis5d) with the inner box indicating the area of the PFM's domain.*

The UKMM operates on a cycle of assimilation, analysis and forecasting, employing continuous assimilation, 3-hourly validation of assimilated data and 6-hourly generation of hourly forecasts for a period of up to 48 hours (T+48) from the corresponding time of validation (T=0: 0000Z, 0600Z,

1200Z, 1800Z). The products (T=0 to T+48) are available to end users approximately three hours after each of the four validation times listed, largely due to forecasting not being initiated until two hours after the time of validation. The fields predicted on hybrid coordinates are: temperature, horizontal and vertical winds, pressure, specific humidity, cloud liquid water and cloud ice. A large number of other diagnostics are provided on standard pressure levels as detailed in Appendix I (Dicks and Panagi, 1997).

In addition to the provision of UKMM data, JCMM make available a suite of programs called MDIAG, specifically designed to calculate diagnostics on standard pressure levels from the UKMM fields produced on hybrid coordinates. A list of the diagnostics can be found in Appendix II, a list that proved useful as a comprehensive reference for potential signifiers of conditions conducive to rain formation, the significance of which could then be further ascertained through literature and visualisation. It was these diagnostic fields, calculated on standard pressure levels ranging from 1000mb to 50 mb in increments of 50 mb, that were amalgamated with radar and satellite data via Vis5d routines, together comprising the source data to run the PFM. As such, routine input surface data used in the F&K model were replaced with data from the lowest pressure level, that of 1000mb. It should be noted that reliance on Vis5d interpolation of meteorological variables results in interpolation without adjustment for the effects of the finer-scale topography. Interpolation schemes attempting to account for complex terrain are described by Baumann *et al* (1997), Bartzis *et al* (1997) and Hanaki *et al* (1998) and, like the horizontal interpolation scheme, should be given greater consideration in any future development of the model.

The UKMM data itself and the process of procuring it had a significant bearing on the way the research was conducted. The upgrade of the UKMM's horizontal resolution to its current specification occurred in 1998 (Panagi, 2001), thereby limiting the possible range of rainfall events that could be used for model development from after that time to the present. Whilst helpfully narrowing the period over which to search for suitable rainfall events it precluded simply taking the same datasets used by Wild, all of which were dated either 1992 or 1993. The size of the primary data files (approximately 0.6 Gigabytes per 24 hour forecast run), relative to the total computing resources available (less than 20 Gigabytes), placed a restriction on the number of events that could be examined. It became obvious there would not be enough events to constitute a representative sample of different rainfall types or enough hours of rainfall to allow determination of statistical significance in the relationships between diagnostics and rainfall patterns. Thus identifying a set of signifiers relied merely on selecting diagnostics cited in the literature and viewing the data to gauge whether, at least for the events obtained, the diagnostics were well resolved by the UKMM.

3.4.2.2 Radar data

Initially it was thought that both network radar data and full volume single-site radar data, comprising four elevation scans, could be obtained from JCMM. It was only after receiving data supplied in response to the first request that it was realised only the lowest beam from single-site data was available. The product of on-site processing of radar reflectivity values is the rainfall estimate and despite being integral to determination of that estimate all four scans are not archived, rather only the final product is retained. However, the data for each elevation is temporarily stored on tape at the site until the tape is overwritten with new data, meaning full volume radar data can be obtained provided the tape is retrieved within a day or two of the rainfall event occurring. Thus again, like the UKMM data, the nature of the available data and the process of procuring it had a bearing on the events chosen for model development. The lack of archived multiple elevation radar data precluded any retrospective identification of storms and in deciding the number of events to be obtained, consideration had to be given to the period of time available to undertake the research and also the remoteness of the site, the latter with respect to limitations on the goodwill extended by a volunteer who attempted a timely retrieval of the tape upon request.

Viewing the data using Vis5d revealed that all events were plagued by a considerable number of missing elevation scans, to the extent that it raised concern over the quality of the data and whether it was fit to be used (Figure 3.3). The radar at Hameldon Hill has not been without its problems (Edwards, 1996) and it is uncertain to what extent these had been rectified. A reluctant decision was made to forego use of Hameldon Hill radar data, leaving network radar rainfall estimates as the only alternative. A decision made all the more difficult because full volume radar data had filled a prominent role in the F&K model and thus necessitated considerable reworking of the model formulations to accommodate single level data. The modifications made will be explained in a later section. The network radar data provided by JCMM undergoes on-site processing only, namely removal of permanent clutter, conversion to precipitation rate using the Z-R relationship of $Z=200R^{1.6}$ and some correction for attenuation, range effects and occultation. The resolution of the network radar data is 5km by 5km and images are produced every 15 minutes as a composite of data from the total of 15 C-band radars the UKMO has situated throughout the UK, the Republic of Ireland and Jersey (Driscoll *et al*, 2000).

3.4.2.3 Satellite data

Half-hourly satellite data were obtained from JCMM as well as a program to interpolate the Meteosat data from its polar stereographic projection to a Cartesian grid, making a potentially difficult task very easy given that each image covers a large expanse that includes northeastern

Canada, northern Africa and western Europe, and being an area not uniform in latitude and longitude (Dicks and Panagi, 1997). Generally areas of precipitation are associated with colder cloud tops, an example of which is given in Figure 3.4.

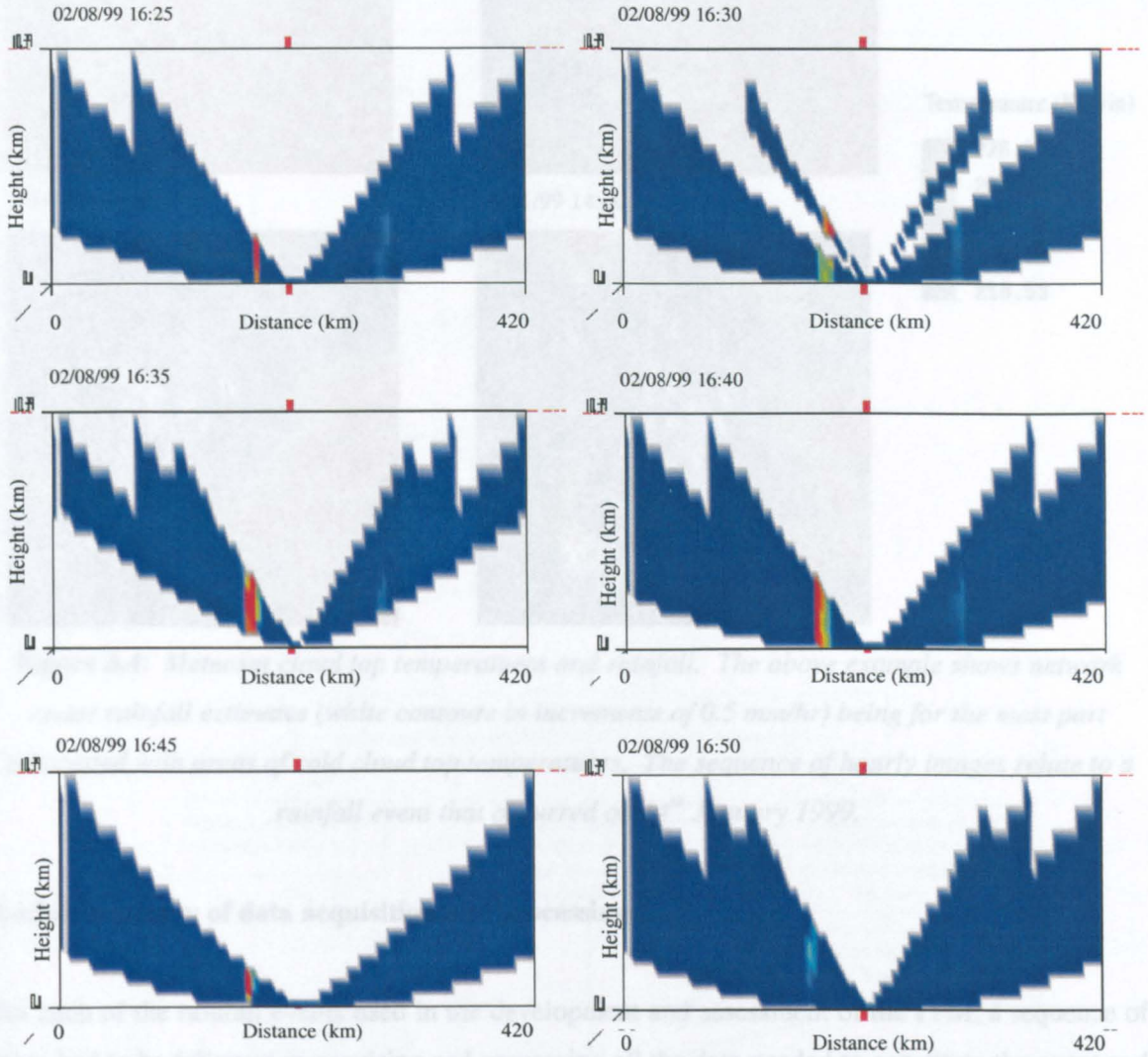

Figure 3.3: *Full volume radar data from the Hameldon Hill weather radar. A full scan comprises 4 different elevations and is completed every 5 minutes. A sequence of 6 consecutive full scans is shown above (dark blue representing the volume of the scan, bright colours are observed rain cells), the date and time indicated above each. The first is missing the top beam, the second is missing the third highest beam, the third is missing the lowest beam, the fourth is missing the top beam, the fifth is missing the two highest beams whilst the sixth comprises all four beams.*

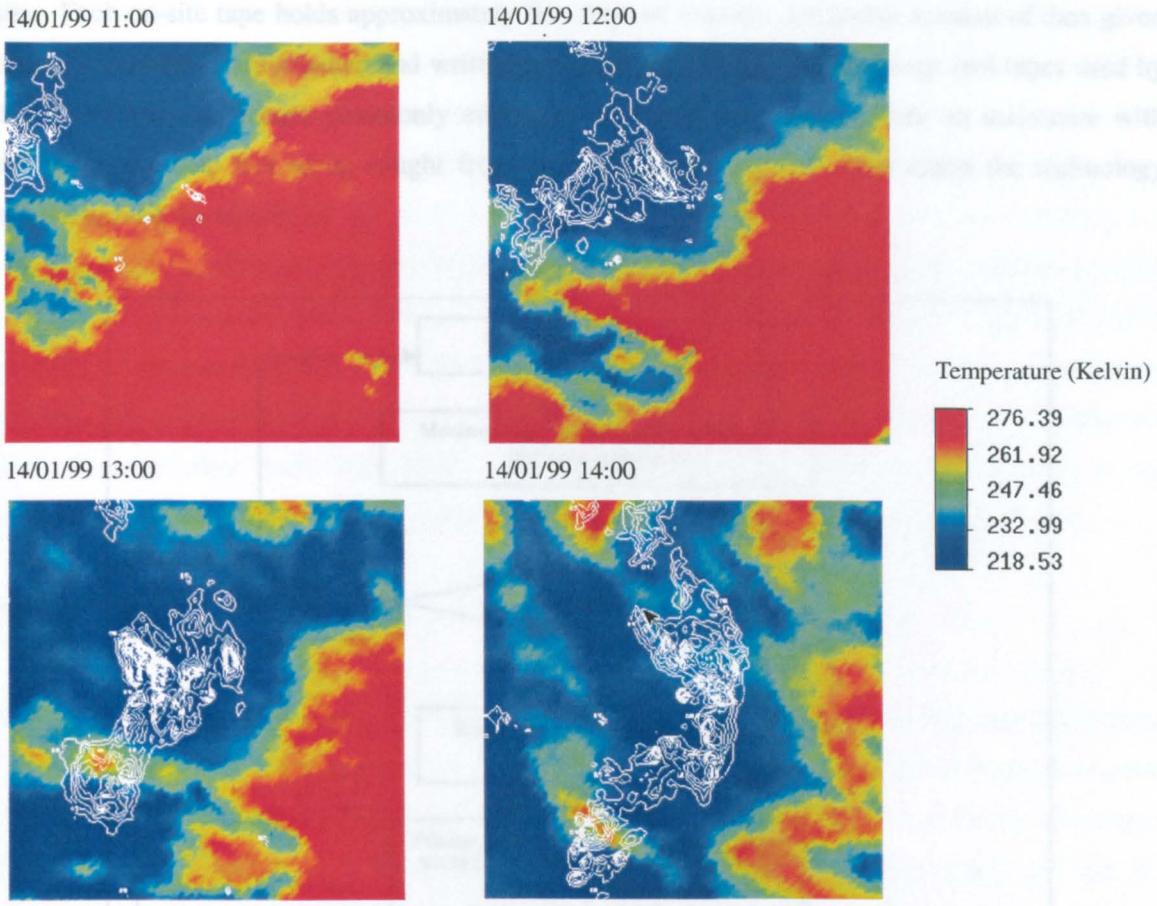

Figure 3.4: *Meteosat cloud top temperatures and rainfall. The above example shows network radar rainfall estimates (white contours in increments of 0.5 mm/hr) being for the most part associated with areas of cold cloud top temperatures. The sequence of hourly images relate to a rainfall event that occurred on 14th January 1999.*

3.4.2.4 Summary of data acquisition and processing

For each of the rainfall events used in the development and assessment of the PFM, a sequence of steps had to be followed in acquiring and processing all the data needed to constitute the event and to run the PFM. Those steps are displayed in Figure 3.5 and, as can be seen, were initiated by the onset of rain.

Once rainfall had commenced over the area of the chosen domain, its duration and intensity were then monitored to gauge whether the storm might be suitable for use in the research exercise. The surveillance of storms was enabled by real-time transmission of network radar images to the Water and Environmental Management Research Centre (WEMRC) at the University of Bristol (UoB), courtesy of the Environment Agency, and their display on a computer workstation dedicated for that purpose. Immediately following a rainfall event, and having decided to obtain records of it, a request was made for retrieval of the tape containing the Hameldon Hill radar data from the radar

site. Each on-site tape holds approximately five days of records, a sizeable amount of data given that four elevations are scanned and written to tape every 5-minutes. The large reel tapes used by the UKMO are no longer commonly employed as a means of storing data so assistance with extracting the data had to be sought from UoB Computer Services who retain the technology needed to read the tapes.

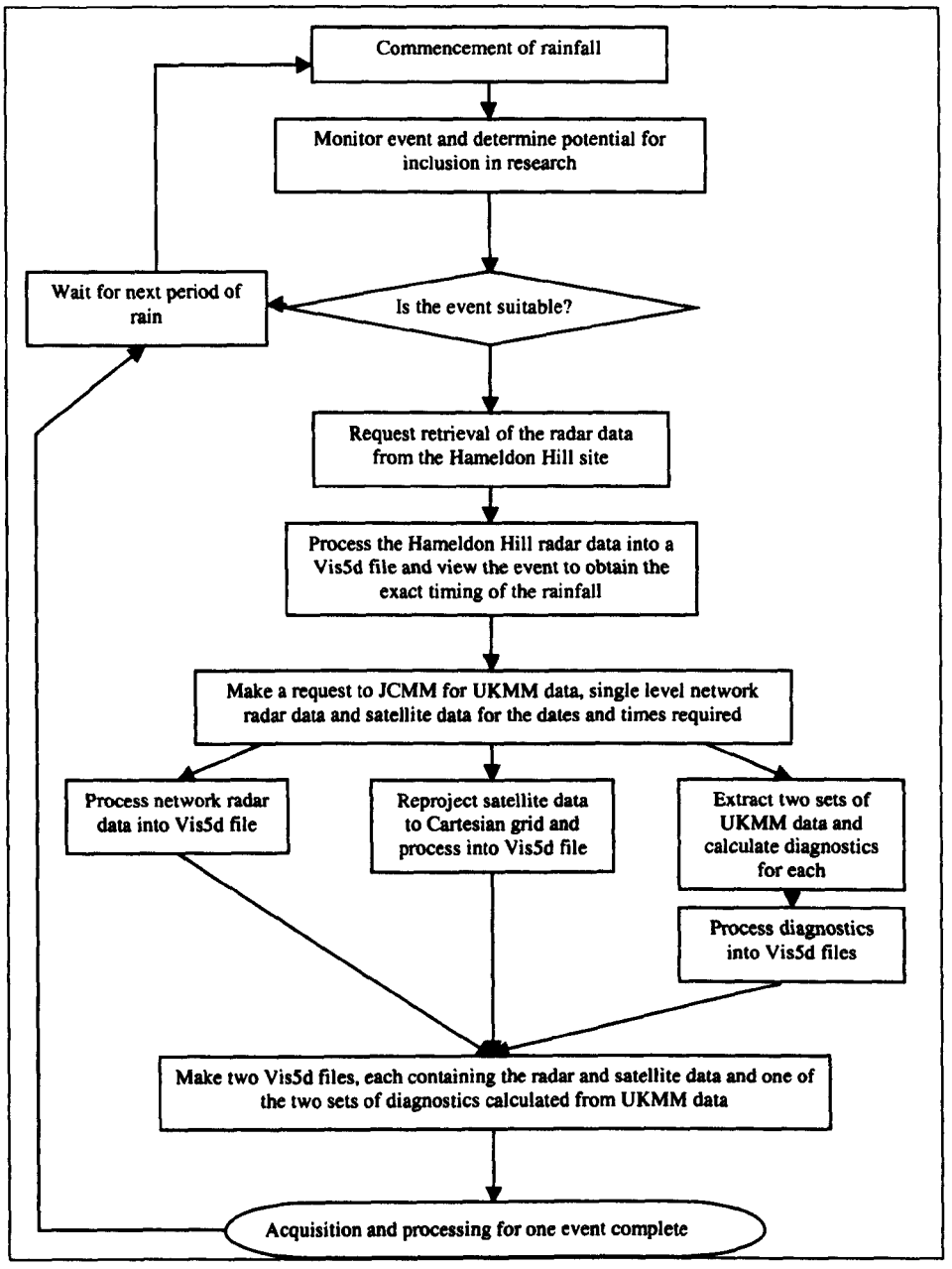

Figure 3.5: *The steps taken to acquire and process data for each of the events used for development and assessment of the PFM.*

Upon receipt of the tape, all records on it were downloaded to the UNIX system being used to undertake the work on the PFM and then processed into Vis5d files for visualization. Through viewing the files, the date of the event could be confirmed and the start and end times of the event

pinpointed. With the exact timing of rainfall established, a request was made to JCMM for the corresponding UKMM data, single level network radar data and the satellite data. The radar and satellite data were processed into separate Vis5d files, the latter requiring the additional step of reprojection onto a Cartesian grid. For reasons to be explained later, two sets of UKMM forecasts covering the time of interest had to be prepared. Preparation of each set involved extracting the relevant hours from the 24 UKMM hourly forecasts generated from each model analysis that fell immediately prior to and within the time of the event. Diagnostics were then calculated from the primary data using MDIAG, after which they were processed into Vis5d files and subsequently merged with those containing the radar and satellite data. The end result was two Vis5d files per event that were then ready to be used to run the PFM, both files containing UKMM, radar and satellite data corresponding to the area of the domain and conforming to the same resolution.

3.5 The rainfall events

The events will be presented in detail in the following chapter, suffice it to say that only four events were obtained, together extending over a period of twelve days and totalling 138 hours of rainfall. Two of the events were recorded during winter conditions and featured frontal rainfall. The first of these spanned Christmas 1998, being 3 days of unsettled stormy weather on the 24th, 25th and 26th December, each day having approximately 9 hours of rainfall. The second of these frontal events occurred in the following month and again spanned three days, namely the 14th, 15th and 16th January 1999, together totalling 33 hours of rainfall. The third event was a summertime event and was distinctly convective in nature, with the associated synoptic conditions prevailing through the early part of August 1999 giving rise to 5 days, from the 1st to 5th August inclusive, of showery weather comprising 51 hours of rainfall. The last event, concentrated predominantly within one day, was an autumnal storm that occurred mainly on the 24th October and brought with it a mixture of convective and widespread rainfall over a 27 hour period.

Similar to F&K (Andrieu *et al*, 1994), the limited nature of data resources led to the same set of storms being used for both model development and performance assessment. However the former was not in terms of calibrating the model's free parameters, for in this case there were none as the value of ε in the convective updraft parameterisation was taken to be the same value used by both F&K (Andrieu *et al*, 1994) and G&B (1984b) and remained fixed throughout. It was more with respect to visualising signifiers extracted from literature and seeing how well these tended to correspond with actual rain fields. The decision to adopt the same value of ε as used by F&K and G&B was made after experimenting with other values and discovering that their value of 0.002 produced the best results. Furthermore, the strong similarity of the formulations and methodologies used in the PFM with those in the models of G&B and F&K, and also that G&B in

particular found this value of ε to be optimal when testing their model with a variety of storm types, suggests the same value might be transferable to the PFM.

3.6 Signifiers

The signifiers underpin the algorithm governing the PFM's implementation and are intended to reasonably, and ideally reliably, indicate the presence of the basic ingredients needed for precipitation formation - saturation of the atmosphere coupled with vertical uplift. A measure of wariness guided the selection and so influenced the design of the algorithm, a wariness that acknowledged the key role of the signifiers in the PFM and also the nature of the source data from which they come. Use of NWP forecasts requires the exercise of some caution, the forecasts being products subject to both degradation by chaos in the atmosphere and NWP model deficiencies, and which are initialised not from observations alone but an analysed state of the atmosphere constructed through merging observations with previous model forecasts. Consideration had to be given therefore not only to ingredients in nature that culminate in precipitation but also UKMM fields that appear to link particularly well with precipitation. The potential for inaccuracies in forecast data means that where possible the algorithm needs to compensate for or ameliorate these largely indeterminate errors in ways that, if practicable, diminishes complete reliance on the data for rainfall production and exhibits a preference towards trends and general profiles as opposed to dependence on literal values. The signifiers chosen, justification for their inclusion and their function in the algorithm are detailed below.

3.6.1 Saturation

Evidence of a high percentage of relative humidity is a standard condition used to delineate saturated areas of the atmosphere, and taking values of less than 100% is a common and acceptable way of accounting for possible errors in the estimation of moisture in the atmosphere (Schultz and Schumacher, 1999). Saturation in conjunction with uplift typically leads to cloud development but not necessarily precipitation. The likelihood of precipitation from a cloud is related to its age, temperature and particularly to its thickness (Rogers and Yau, 1989). Rogers and Yau (1989) found the typical thickness of rain-producing clouds to vary geographically, continental clouds having to attain greater vertical extension than those of maritime origin before rain is initiated. Case studies suggest that a thickness of between 2 and 4.5 km provides a 20% chance of precipitation being produced from a cloud, an observation reflected in the methodology by which precipitation is initiated in the UKMM's cloud model of convective precipitation. The triggering of convective precipitation in the UKMM requires both cloud liquid/ice and cloud depth to exceed specified values, cloud depth usually taken as 1.5km over sea and 4km over land but subject to

adjustment dependent on cloud top temperatures. The dependence of rainfall on high water content and cloud thickness might explain the visual correspondence between radar measured rainfall and UKMM forecasts of high relative humidity at the pressure level of 600mb (approximately 4km above sea level). This correspondence appears independent of storm type as shown in Figure 3.6, which features an example for each of the four different storm events that have been examined in this study. Furthermore the rain area appears better defined where high relative humidity with respect to ice is concurrently present at 700mb. This last point is not surprising given that the presence of ice facilitates precipitation development, with the lower equilibrium vapour pressure over ice compared to water allowing ice crystals to grow through the diffusion of water vapour at the expense of supercooled water droplets. The larger crystals fall, collide with and collect other ice crystals or water droplets and eventually exist the cloud base as rain, hail, snow or graupel depending on whether the cloud base is below the 0°C melting level (Rogers & Yau, 1989).

On the basis of the perceived relationships described above the choice of the PFM's principal signifier of probable rainfall areas favours expediency and is taken to be relative humidity with respect to water exceeding 90% at a single pressure level, that of 600mb, partnered with 100% or more relative humidity with respect to ice also at a single pressure level, that of 700mb. The former is slightly greater than the value of 85% used in the UKMM Moisture Observation Pre-Processing System (MOPS) as the critical threshold for cloud formation (Hand *et al*, 1995). The reference to relative humidity with respect to ice recognises the importance of phase changes in rainfall development within mid-latitude regions and tries to compensate a little for the fact that cold rainfall processes, more so than warm rainfall processes, are likely to occur over the UK. Cloud depth is necessarily determined as part of the PFM's formulations and so easily provides further qualification to the identification of probable rain areas. The minimum cloud depth required is set to a value of 2 km. Clearly the appropriateness of the three criteria, particularly the relative humidity specifications, could be better determined with examination of many rainfall events and a more involved delineation of rain area may well prove warranted.

Placing the signifier in the context of the algorithm for the PFM's implementation, determination of rainfall rate at any given point in the domain requires either the presence of pre-existing rain or for all of the following conditions to be satisfied: greater than 90% relative humidity with respect to water at 600mb, 100% or greater relative humidity with respect to ice at 700 mb, and cloud depth to be greater than or equal to 2 km. The relaxation of the criteria with respect to existing rain areas accounts to some extent for the fact that neither the technique for delineating rain areas by the chosen relative humidity distribution and cloud depth nor the UKMM forecasts of moisture, or even its analysis of moisture, are infallible. The assumption here is that grid cells delineated by this method are synonymous with a saturated column of the atmosphere and with cloud

development. The nature of the forcing operating within the column still has to be determined, whether the vertical motion is such that precipitation will develop and if so the relative intensity of that precipitation.

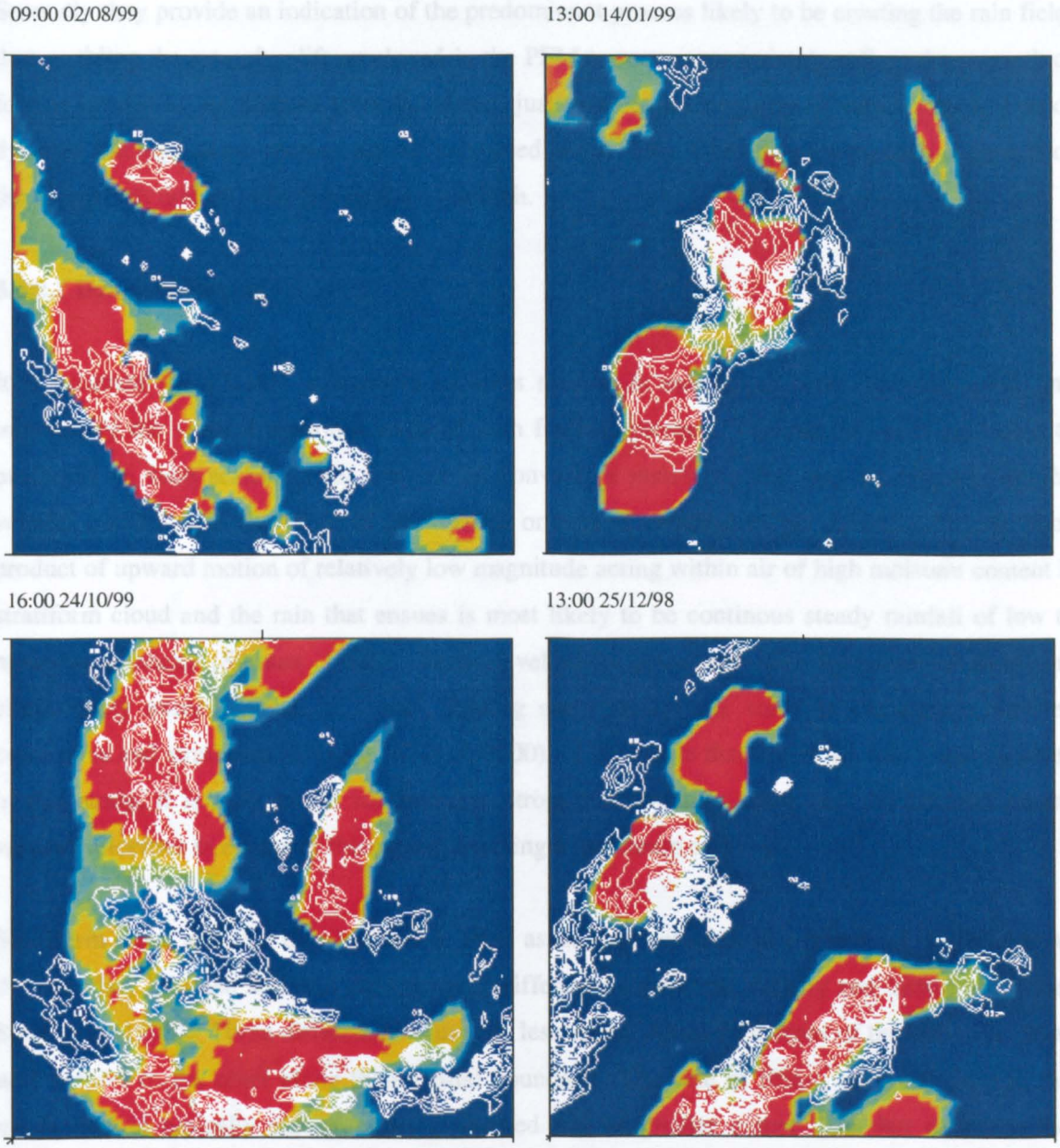

Figure 3.6: *Visual correspondence between the saturation signifier and rainfall. Above are examples of instances in each of the four "events" when the signifier for saturation (>90% humidity at 600mb, areas in red) shows a reasonable approximation to the observed rainfall area (white contours in increments of 0.5 mm/hr). The date and time are indicated above each.*

3.6.2 Uplift

Within the PFM algorithm the role of uplift signifiers is twofold. Primarily they identify where uplift exists and as such where, within the "saturated" areas, precipitation might be occurring. Secondly they provide an indication of the predominant process likely to be creating the rain field, thus enabling the rate of uplift employed in the PFM to more appropriately reflect the strength of forcing involved. As decided from the outset, just two broad categories of vertical uplift, that of dynamic forcing and convection, are differentiated in the PFM. Considered separately is the role of the orographic updraft, which contributes to both.

3.6.2.1 Dynamic forcing

It is assumed the UKMM adequately resolves mesoscale and larger scale dynamic uplift and importantly the vertical motion associated with frontal systems. The rate of uplift attributed to processes on such scales, in the absence of convective instability that may be triggered by the vertical motion, is in the order of centimetres or tens of centimetres per second. The common product of upward motion of relatively low magnitude acting within air of high moisture content is stratiform cloud and the rain that ensues is most likely to be continous steady rainfall of low to moderate intensity (Sumner, 1988). Vertical velocities associated with formation of stratiform cloud rarely exceed a rate of 1 ms^{-1}, leading some to use the value to distinguish between convective and stratiform rain (Amitai *et al*, 2000). It is notable that out of the four events utilized in this study, it is only in the summertime, strongly convective event that the UKMM attains vertical velocities in excess of this figure, reaching a maximum of 3 ms^{-1}.

Stratiform cloud and rain development is often associated with frontal systems. A front refers to the boundary between adjacent air-masses of different temperature, density and humidity (Byron-Scott *et al*, 1998). These differences cause the less dense, warmer air-mass of the two to be lifted with respect to the other along their shared boundary. The rate of lifting achieved through this mechanism is typically slower, more prolonged and of greater extent than that of convective buoyancy (Sumner, 1988). This is frontal theory at its utmost basic and fails to allude to the different types of fronts that have been identified and the conceptual models constructed to explain them, each type having implications for the location of clouds and precipitation with respect to the front. However, of primary concern in this study is that fronts represent a mechanism of lifting of sufficient magnitude to result in precipitation.

The methods of identifying fronts and assessing their significance in the PFM are taken from Tim Hewson (1998). Hewson developed an objective means of locating fronts, entailing the use of a

thermal front parameter and based on the observation that relatively dramatic changes in the magnitude of thermal gradients occur across a front. Figure 3.7 provides an idealised example of the cross-front variation expected in a series of scalar differentials of a thermodynamic variable (τ). It can be seen from this that within the boundaries of the frontal zone (lines A and B) the thermodynamic variable changes ($\partial\tau/\partial x$) most rapidly. Near the boundaries the rate of that change ($\partial^2\tau/\partial x^2$) is also rapidly changing and at the boundaries it peaks so that the line of the front corresponds to where the gradient of $\partial^2\tau/\partial x^2$ is equal to zero ($\partial^3\tau/\partial x^3=0$).

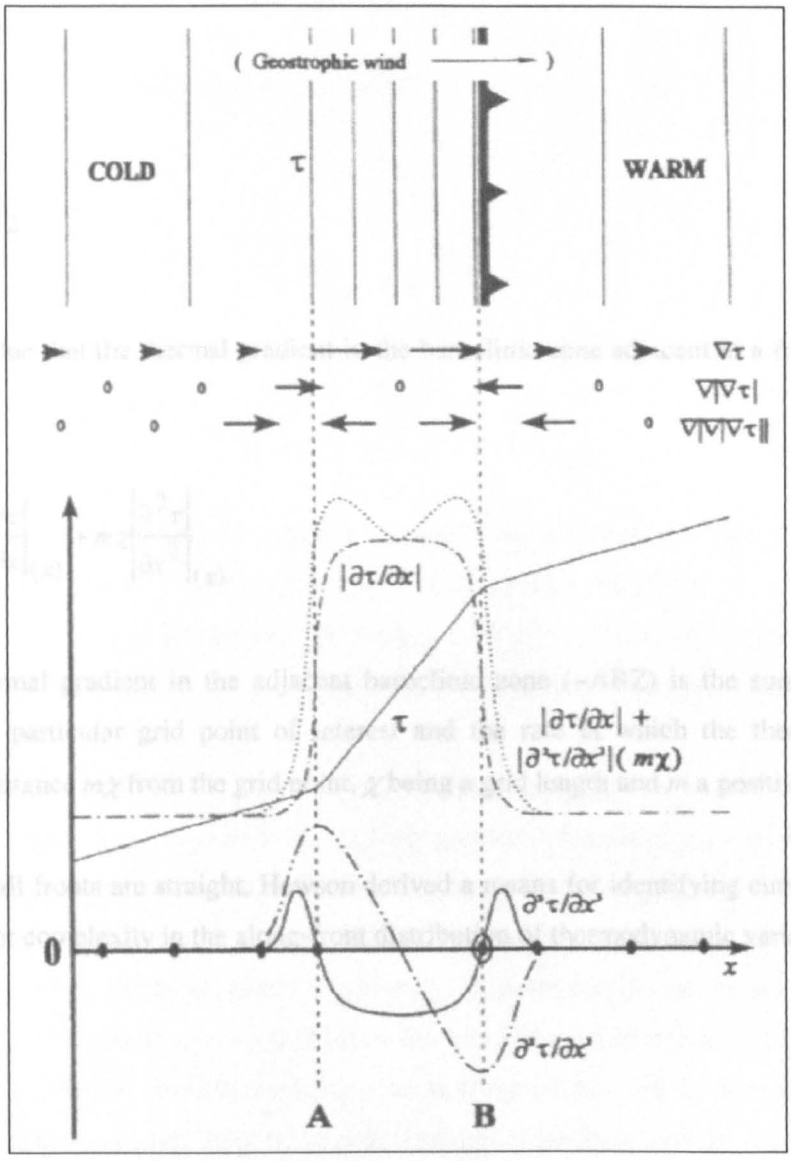

Figure 3.7: *Thermal characteristics of frontal zones. At the top of the diagram is a plan view of an idealised cold front and below it is a graph depicting the behaviour of scalar differentials of a thermodynamic variable within the vicinity of the frontal zone (area between lines A and B). The ringed dot on the graph shows the location of the front and other dots on the x axis indicating where $\partial^3\tau/\partial x^3=0$. The idealised front in this case is straight and without an along-front gradient in the thermodynamic variable (Taken from Hewson, 1998).*

As can be seen in Figure 3.7, and as noted by Hewson, not all locations of $\partial^3\tau/\partial x^3=0$ denote a front and so he proposed a criteria, comprising two "masking" variables, by which to eliminate spurious fronts. The first of these is defined by:

$$\left[-\frac{\partial^2\tau}{\partial x^2}\right] > K_1 \tag{3.1}$$

K_1 being the value that the rate of change of thermal gradient across a front, in the direction of cold air, must exceed.

The second is:

$$\left|\frac{\partial\tau}{\partial x}\right|_{(\sim ABZ)} > K_2 \tag{3.2}$$

K_2 being the value that the thermal gradient in the baroclinic zone adjacent to a front must exceed and where:

$$\left|\frac{\partial\tau}{\partial x}\right|_{(\sim ABZ)} = \left|\frac{\partial\tau}{\partial x}\right|_{(x)} + m\chi\left|\frac{\partial^2\tau}{\partial x^2}\right|_{(x)} \tag{3.3}$$

so that the thermal gradient in the adjacent baroclinic zone (~ABZ) is the sum of the thermal gradient at the particular grid point of interest and the rate at which the thermal gradient is changing at a distance $m\chi$ from the grid point, χ being a grid length and m a positive fraction.

Given that not all fronts are straight, Hewson derived a means for identifying curved fronts which also accounts for complexity in the along-front distribution of thermodynamic variables:

$$\frac{\partial\left(\nabla|\nabla\tau|\right)_s}{\partial s} = 0 \tag{3.4}$$

and with:

$$\hat{s} = \pm\nabla|\nabla\tau|/\|\nabla|\nabla\tau|\| \tag{3.5}$$

where unit vector $\hat{s}$ can be shown to be a unit axis having an orientation at each grid point parallel to the vector field of $\nabla|\nabla\tau|$ through it (i.e. the streamline of $\nabla|\nabla\tau|$ having a cross front orientation). Hewson advises that an estimate of $\hat{s}$ at any one grid point is best made by taking an average of its values at the five most immediate grid points. Also adapted were the formulae for the masking variables, such that equation (3.1) becomes:

$$-\nabla|\nabla\tau|\cdot\left(\frac{\nabla\tau}{|\nabla\tau|}\right) > K_1 \tag{3.6}$$

and equations (3.2) and (3.3) become respectively:

$$|\nabla\tau|_{(\sim ABZ)} > K_2 \tag{3.7}$$

and

$$|\nabla\tau|_{(\sim ABZ)} = |\nabla\tau|_{(x,y)} + m\chi|\nabla|\nabla\tau||_{(x,y)} \tag{3.8}$$

Hewson's preferred choice of thermodynamic variable is wet bulb potential temperature, a property that is conserved in pseudo-adiabatic processes. He provides values for K_1 and K_2, which for surface fronts are 0.3 °C per 100 km per 100 km and 1.35 °C per 100 km respectively at a height of 900 mb. All three, the front locator and two masking variables, are calculable using MDIAG.

One of the primary motivations Hewson had in developing his methodology for objectively identifying significant fronts was to facilitate their graphical presentation. The merit of the front locator is most apparent in this respect and easily visualised through contouring in a graphics display. It is less amenable to calculations on discrete grid points, where to get an exact value of zero for equation (3.4) can be considered fortunate. In preference to laboriously searching for a zero value within the vicinity of each grid point, the identification of significant fronts in the PFM is dependent soley on the masking variables. As is expected and can be seen in Figure 3.8, the areas where the criteria are met shadow the zero contours of the front locator. Furthermore a visual comparison of the masking criteria with respect to the location of rain bands in the selected rainfall events, an example of which is given in Figure 3.9, raises confidence in this proposed methodology and in the predictive ability of the UKMM with respect to frontal systems.

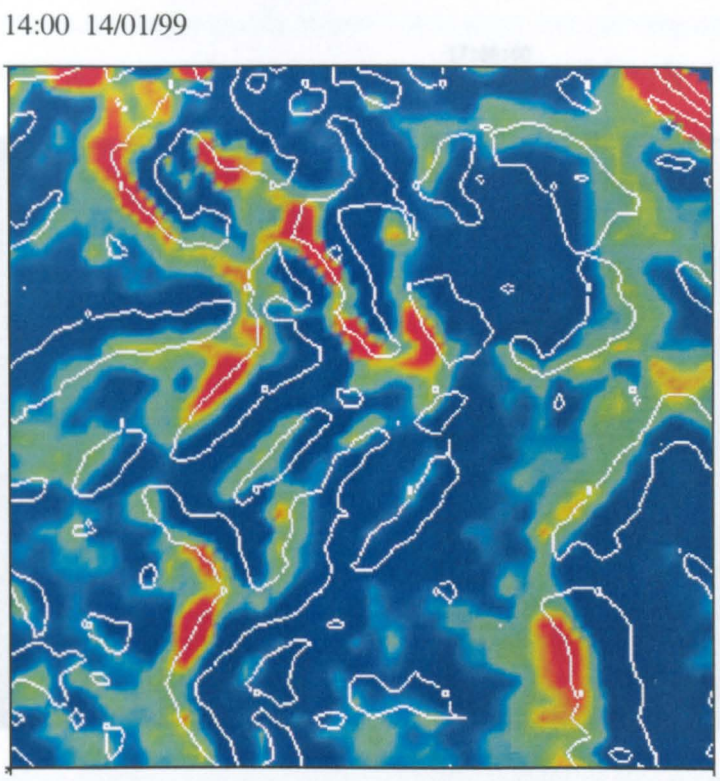

Figure 3.8: *Coincidence of zero values in the front locator (white contours) with areas where the masking variable, defined by equation (3.6), exceeds the critical value (shown in red).*

It is acknowledged not all fronts exhibit continous rising motion, a fact which has led to categorisation of ana and kata fronts, the former associated with rising air in the warm sector and the latter with the ascent of warm air inhibited by subsiding drier air (Barry & Chorley, 1992). Both are associated with precipitation but with the overlying subsiding motion of kata fronts resulting in lighter rain and eventual dissolution of clouds. The two are not unrelated and kata fronts are thought to evolve from ana fronts (Carlson, 1991 & Winkler *et al*, 2001). It is possible to distinguish between the two by application of quasi-geostrophic theory and employing the assumption that quasi-geostrophic forcing is primarily responsible for the vertical motion around fronts (Hewson, 1998). The method involves calculating Q vectors:

$$\mathbf{Q} \equiv (Q_1, Q_2) = \left(-\frac{R}{p}\frac{\partial \mathbf{V}_g}{\partial x} \cdot \nabla T, -\frac{R}{p}\frac{\partial \mathbf{V}_g}{\partial y} \nabla T \right) \tag{3.9}$$

which are proportional to the rate of change of horizontal temperature gradient forced by geostrophic motion alone (Holton, 1992). In equation (3.9) R is the gas constant for dry air, p is pressure, T is temperature and $\mathbf{V}_g = i u_g + j v_g$, with $\boldsymbol{i}$ and $\boldsymbol{j}$ being eastward and northward unit vectors respectively and likewise u_g and v_g the eastward and northward components of the geostrophic wind.

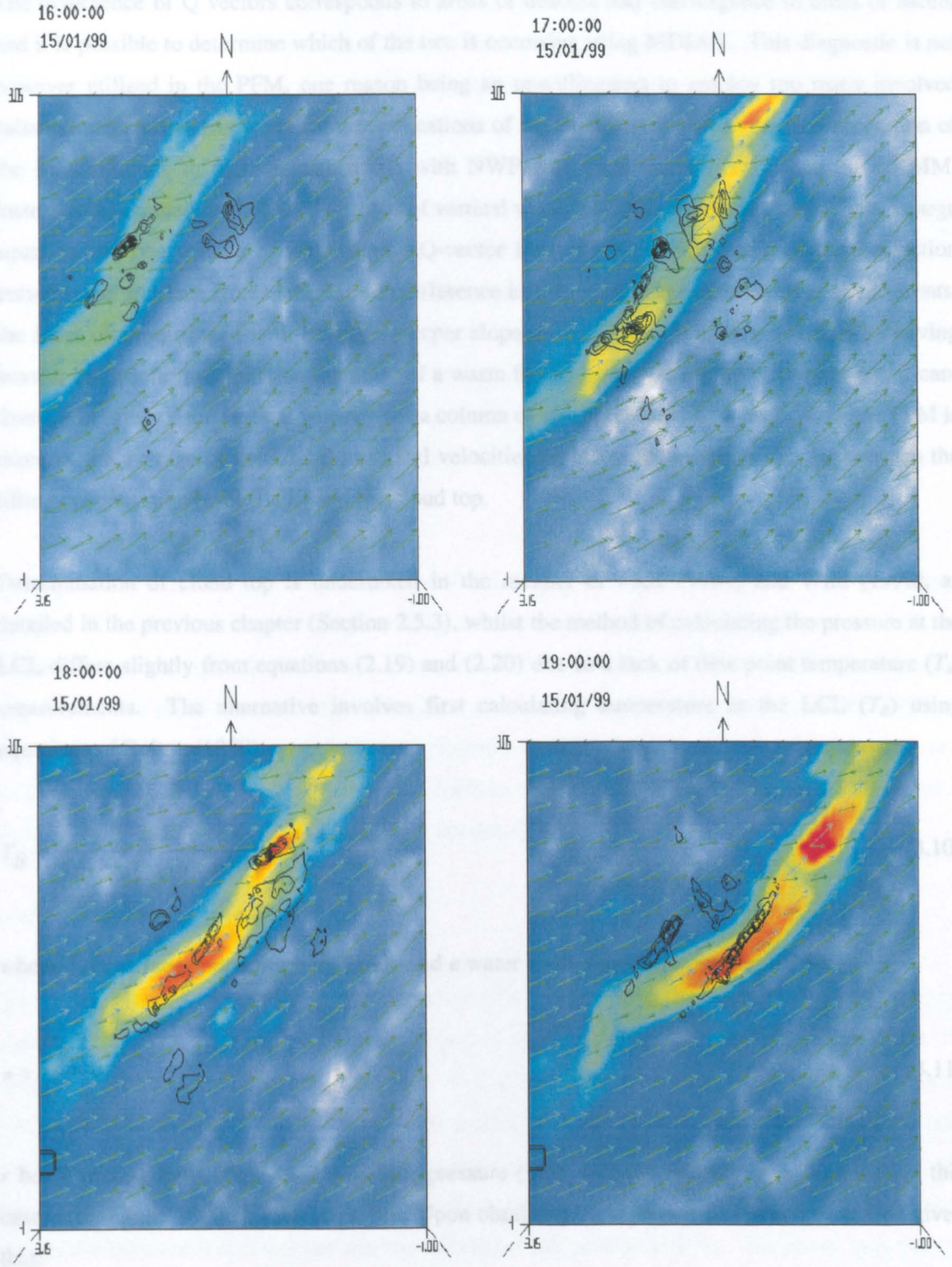

Figure 3.9: *Visual correspondence between the front masking criteria and rainfall. The sequence of images shows the movement of a surface front (masking criteria in bright colours), the corresponding 700 mb wind field (blue arrows) and 850 mb wind field (green arrows) and black contours of rainfall rates determined from radar reflectivity (intervals of 5 mm/hr) for the times and date shown.*

The divergence of Q vectors corresponds to areas of descent and convergence to areas of ascent and it is possible to determine which of the two is occurring using MDIAG. This diagnostic is not however utilized in the PFM, one reason being an unwillingness to employ too many involved calculations, particularly when future applications of the model are likely to require adaptation of the MDIAG code to make it compatible with NWP data from models other than the UKMM. Instead it is assumed the UKMM's profile of vertical wind, which is determined through the omega equation and one version of which is the Q-vector form (Holton, 1992), reflects the distinction between ana and kata fronts and also the difference in lifting rates between warm and cold fronts, the latter often attributed with having a steeper slope to the frontal boundary and so with having heavier but briefer precipitation than that of a warm front. Thus, within the vicinity of significant fronts, the value of the vertical velocity for a column of air represented by a grid cell in the PFM is taken as the average of the UKMM vertical velocities on the pressure levels that lie between the lifting condensation level (LCL) and the cloud top.

Determination of cloud top is undertaken in the manner of F&K (1994) and Wild (1996), as detailed in the previous chapter (Section 2.5.3), whilst the method of calculating the pressure at the LCL differs slightly from equations (2.19) and (2.20) due to a lack of dew point temperature (T_d) measurements. The alternative involves first calculating temperature at the LCL (T_B) using equations of Bolton (1980):

$$T_B = \frac{2840}{3.5 \ln T_0 - \ln e - 4.805} + 55 \tag{3.10}$$

where T_0 is surface temperature in Kelvin and e water vapour pressure determined by:

$$e = \frac{p_0 r}{622 + r} \tag{3.11}$$

r being mixing ratio (gkg^{-1})and p_0 surface pressure (mb), with all references to "surface" in this case meaning the 1000mb pressure level. Upon obtaining T_B, equation (2.19) can be solved given that:

$$\frac{T_0}{T_B} = \frac{T_0 - T_d}{223.15} + 1 \tag{3.12}$$

In widespread stratiform rain the distribution of vertical velocity with height tends to change continually but is thought to average to a parabolic form, at least during heavy rain (Atlas and

Wexler, 1958), whereby maximum velocities occur at approximately the 600 mb level and decrease above and below to zero at 1000mb and 200mb (Houghton, 1985). Whilst calculating the average of this profile is considered appropriate with respect to frontal rain, general application of the approach within "saturated" areas otherwise not characterised by the presence of a significant objective front or convection tends to result in an over-estimation of the rain area and under-estimation if disregarded. As a seemingly effective compromise the vertical wind speed at the LCL forms the default option in the PFM algorithm which, if the parabolic profile holds true, is quite likely to represent weaker forcing than is actually present in the profile. The identification of a significant front overrides the default option for the grid point and it is replaced, as already mentioned, by an average of the UKMM vertical profile of dynamic uplift between the LCL and the top of the cloud. Where dynamic uplift and convection co-exist, the latter dominates and the parameterisation of convective updraft is always implemented in preference to taking the UKMM vertical wind.

The ingredients for convective rainfall require not only moisture and uplift but also instability (Doswell III *et al*, 2000). As such, the pathway to the convective parameterisation relies on indices of gravitational (upright) or slantwise convection, or rather indices of potential or conditional instabilities, that could result in convection given additional factors that first enable the instabilities to be realised and then released. All must therefore be qualified on the need for air in the column to be deemed "saturated" by the PFM and on uplift to be present in the column to effect the release of the instability. Each will be discussed in more detail below.

3.6.2.2 Convection - upright

The F&K method of determining the rate of uplift within a convective cloud (refer Section 2.5.2) is retained for grid cells in which free convection is deemed to be operating and parameter ε of equation (2.13) remains fixed at a value of 0.002 throughout, with both F&K (1992) and G&B (1984b) finding that particular value to be optimal. Free convection refers to an upward acceleration of an air parcel due to its buoyancy (Bridger and Riegel, 1992), from the conversion of potential energy to kinetic energy (Rogers and Yau, 1989). An air parcel will become buoyant and be displaced upward if it is warmer and less dense than the surrounding air. The parcel may rise or be raised to its LCL whereupon the amount of water vapour in the parcel will reach saturation and begin to condense. Condensation leads to the release of latent heat, making it possible that the rising parcel will cool at a slower rate (pseudoadiabatic lapse rate) than the rate at which ambient air temperature decreases with increasing altitude (environmental lapse rate). If above the LCL the pseudoadiabatic lapse rate is less than the lapse rate of the ambient air, the saturated parcel's

movement in the direction of displacement will be accelerated (Rogers and Yau, 1989) and likely to give rise to high rates of precipitation.

There are a number of ways of defining a state of instability in the atmosphere, sometimes differentiated as available energy and lapse rate definitions (Doswell III *et al*, 2000), although the placement of the different methods into either category and the perceived validity of different methods both appear to vary amongst researchers. Assessment of moist static stability and CAPE (Convective Available Potential Energy) are commonly used to determine air parcel stability and are invariably described as lapse rate and available energy methods respectively. One method often cited as a determinate of convective instability involves analysing the vertical distribution of a thermodynamic variable conserved under pseudoadiabatic processes, an approach that tends to be placed alternately in each camp (Curry and Webster, 1999 and Doswell III *et al*, 2000).

American researchers in particular seem to favour the use of CAPE as a measure of a parcel's buoyancy and therefore as a measure of convective instability (Blanchard, 1998 and Sherwood, 2000). More specifically, CAPE is the maximum kinetic energy per unit mass (units of Jkg^{-1}) a parcel could obtain in moving from its level of free convection (LFC) to its level of neutral buoyancy (or equilibrium level) and is determined in terms of the temperature difference between the parcel and the environment. The equation typically given for its evaluation is:

$$CAPE = g \int_{z_{LFC}}^{z_{EL}} \left(\frac{T_{vp} - T_{ve}}{T_{ve}} \right) dz \tag{3.13}$$

where T_{vp} is the virtual temperature of the parcel, T_{ve} is the virtual temperature of the environment, and z_{EL} and z_{LFC} are the heights of the equilibrium level and level of free convection respectively (Blanchard, 1998). Its assessment with respect to pressure co-ordinates is usually expressed as:

$$CAPE = \int_{p_{EL}}^{p_{LFC}} (T_{vp} - T_{ve}) R_d \, d \ln p \tag{3.14}$$

where R_d is the gas constant for dry air and p is pressure (Emanuel, 1997).

The definition and calculation of CAPE is not entirely uniform amongst researchers. Positive CAPE is associated with convective instability but some choose to qualify the instability by convective inhibition (CIN) (Doswell III *et al*, 2000), effectively being the work needed to lift the parcel to its LFC and which must be overcome for the instability to be released (Smith, 1997):

$$CAPE = CAPE - CIN \tag{3.15}$$

with

$$CIN = g \int_{z_{SFC}}^{z_{LFC}} \left(\frac{T_{vp} - T_{ve}}{T_{ve}} \right) dz \tag{3.16}$$

where z_{SFC} refers to the ground surface (Blanchard, 1998). Furthermore, whilst some researchers calculate the temperature of the parcel assuming it follows a pseudo-adiabat others use a reversible saturated adiabat, obtaining sizeable differences in the value of CAPE as a result (Smith, 1997). Blanchard (1998) suggested both CIN and CAPE should be normalised by the depth over which they are integrated. Smith (1997) commented on how various methodologies have been constructed to deal with significant differences that occur between values of CAPE calculated with respect to surface parcels and those 100-500m above the surface, noting how the calculation of CAPE exhibits sensitivity to small temperature and moisture changes. The variations in defining, determining and utilising CAPE has created some uncertainty over how it is best calculated and/or interpreted (Sherwood, 2000). These uncertainties and CAPE's apparent sensitivity to inputs, the latter particularly important when relying on forecast NWP data, in addition to the availability in MDIAG of alternative methods of determining instability involving variables already utilised in the PFM, means the alternative methods are employed as signifiers of instability in this particular application rather than calculation of CAPE.

The predominant signifier of convective instability in the PFM is the vertical distribution of equivalent potential temperature (θ_e). It is a property that is conserved in air rising pseudo-adiabatically, and a vertical profile that shows a decrease with height (z):

$$\frac{\partial \theta_e}{\partial z} < 0 \tag{3.17}$$

indicates potential for convective instability exists (Schultz and Schumacher, 1999). When calculating the vertical gradient in θ_e with respect to standard pressure levels ($\partial\theta e/\partial p$), as in MDIAG, positive values indicate instability (Figure 3.10). It must be noted that this index is viewed as indicating potential instability with respect to lifting a layer (or column), rather than a parcel, of air to saturation (Rogers and Yau, 1989). Lifting a layer that has a vertical profile of decreasing θ_e with height will result in the lower, warmer, moister air of the layer reaching saturation more quickly than drier air above it, causing it to cool more slowly and thereby steepening the lapse rate within the layer. Lifting therefore destabilizes the layer (Anthes and

Cotton, 1989) and bringing the layer to saturation renders it unstable to convective-scale perturbations (Sherwood, 2000). As Schultz and Schumacher (1999) point out, where the value of equation (3.17) suggests instability is present, it is not in fact created unless there is sufficient uplift to bring air to saturation and its release is dependent on further ascent, hence the reference to *potential* instability. In a saturated atmosphere the criterion can be interpreted with respect to parcel instability in the manner of Holton (1992):

$$\frac{\partial \theta_e^*}{\partial z} < 0 \tag{3.18}$$

where θ_e^* is the equivalent potential temperature of a hypothetically saturated atmosphere that has the thermal structure of the actual atmosphere. Notably θ_e^* and θ_e are the same in a saturated atmosphere, and within the PFM's delineated probable rainfall area the atmospheric column represented by a grid cell is assumed to be saturated and to have the thermal structure as presented by the UKMM. Under the criterion of equation (3.18) instability of a parcel exists because a parcel of air will be warmer than the air into which it moves (Holton, 1992) or, as an alternative explanation, instability exists because such a distribution of θ_e shows the environmental lapse rate in saturated air to be greater than the pseudo-adiabatic lapse rate (Peppler, 1988).

When implementing the PFM algorithm a check is made to determine if the condition for convective instability holds true at any pressure level above the LCL for the areas satisfying the humidity and cloud depth criteria. If so, and the UKMM wind fields suggest there is upward movement in the column or orographic uplift is calculated for the grid cell or there is existing rain present suggesting the instability is quite possibly being released, then the convective parameterisation is selected to determine the updraft velocity for that cell. This index of instability is not evaluated in areas that fall outside the zone of high relative humidity and requisite cloud depth, even if they appear to have rainfall as estimated from radar reflectivity. In these areas there is less confidence in the UKMM profile of moisture and as such an index more dependent on temperature than moisture is adopted, namely moist static stability, in preference to one based on θ_e which is more sensitive to moisture than it is to temperature (NWS Louisville, 2001).

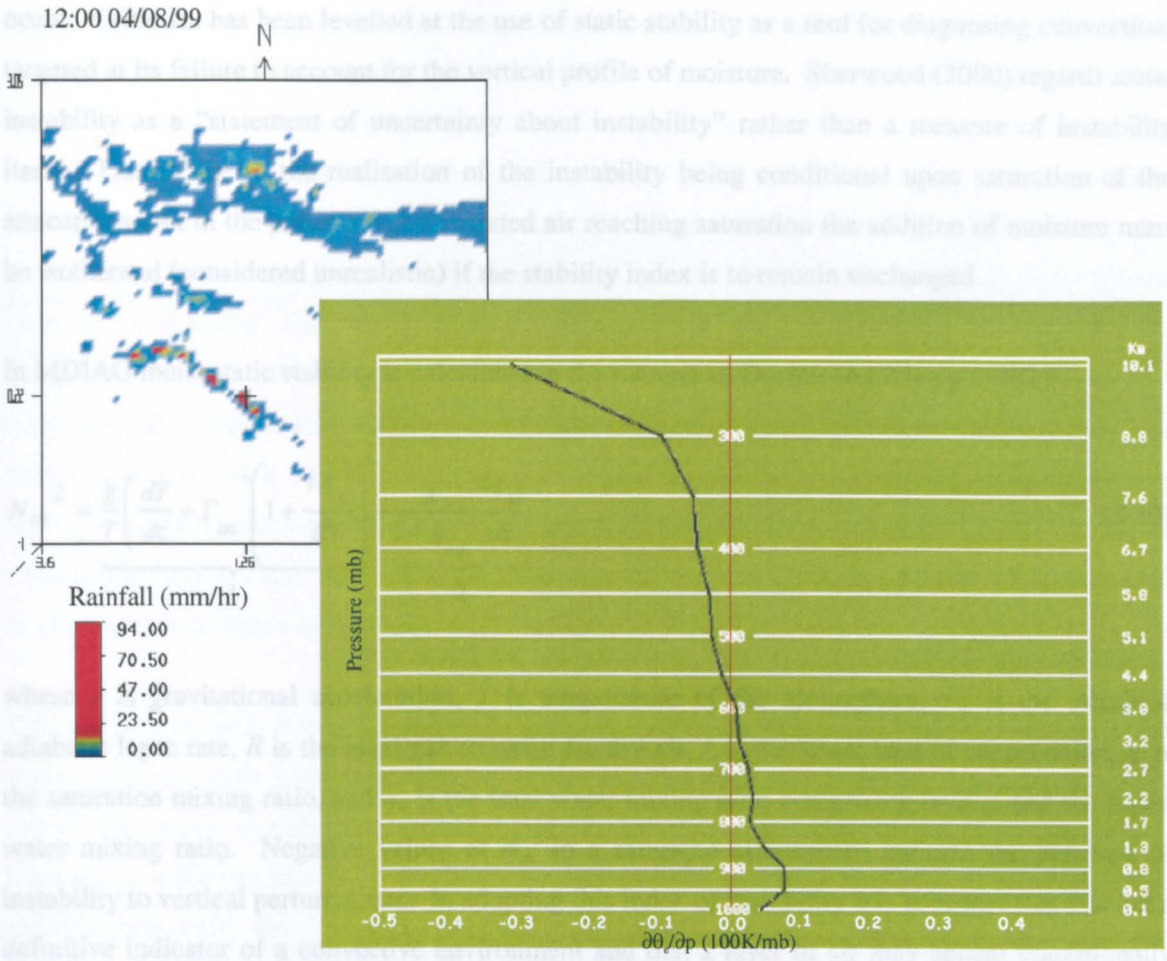

Figure 3.10: *Potential convective instability as indicated by a decrease of θ_e with height. The vertical sounding (bottom left) of values for $\partial\theta_e/\partial p$ is for the location indicated by the black cross in the top left display, which is positioned amongst showers that occurred at 1200 GMT on 4th August 1999. Positive values of $\partial\theta_e/\partial p$, extending from 1000mb up to 600mb, suggest the showers were probably of convective origin.*

Calculation of moist static stability (N_m^2) is the traditional lapse rate method of determining conditional instability (Doswell III *et al*, 2000) and is a means of comparing the lapse rate of ambient air to the pseudoadiabatic lapse rate and thus, conditional upon the air being saturated, acts as a measure of the stability of a parcel of air with respect to vertical perturbations. If the atmosphere is statically stable a parcel that is vertically displaced from its equilibrium level will tend to return to its equilibrium level. In a statically unstable environment the parcel will be accelerated in the direction of displacement (Holton, 1992). Collier *et al* (2000) noted the value of measuring static instability in relation to their work on the UKMO Convection Diagnosis Project. They found that values of tropospheric static stability, calculated using UKMM fields and at the resolution of the UKMM, together with knowledge of topography and surface landuse provide suitable indication of where localised (subgrid with respect to the UKMM) convection is likely to

occur. Criticism has been levelled at the use of static stability as a tool for diagnosing convection, targeted at its failure to account for the vertical profile of moisture. Sherwood (2000) regards static instability as a "statement of uncertainty about instability" rather than a measure of instability itself. This is due to the realisation of the instability being conditional upon saturation of the atmosphere but in the process of unsaturated air reaching saturation the addition of moisture must be isothermal (considered unrealistic) if the stability index is to remain unchanged.

In MDIAG moist static stability is calculated in the manner of Durran and Klemp (1982):

$$N_m^2 = \underbrace{\frac{g}{T}\left(\frac{dT}{dz} + \Gamma_m\right)\left(1 + \frac{Lq_s}{RT}\right)}_{1} - \underbrace{\frac{g}{1+q_w}\frac{dq_w}{dz}}_{2} \tag{3.19}$$

where g is gravitational acceleration, T is temperature of the atmosphere, Γ_m is the saturated adiabatic lapse rate, R is the ideal gas constant for dry air, L is the latent heat of vaporisation, q_s is the saturation mixing ratio, and q_w is the total water mixing ratio comprising both q_s and the liquid water mixing ratio. Negative values of N_m^2 in a saturated atmosphere indicate the presence of instability to vertical perturbations. In adopting this index of instability it is accepted that it is not a definitive indicator of a convective environment and that a layer of air may appear conditionally stable and yet be convectively unstable (Anthes and Cotton, 1989). Furthermore, in implementing evaluation of this index it is assumed the condition of saturation is already met and that the UKMM temperature profile still holds.

The second term of Durran and Klemp's formulation (equation 3.19) attempts to counter specious instability by qualifying it with respect to the vertical distribution of moisture, and in its derivation the duo showed how formulae lacking its inclusion could present a stable, saturated atmosphere as unstable. The total water mixing ratio is a conserved property in a saturated air parcel (Rogers and Yau, 1989) therefore, because the saturation mixing ratio is a function of temperature and pressure only and decreases with height, sustaining the magnitude of a parcel's buoyancy achieved from lapse rate differences alone, relies on a liquid water mixing ratio that increases with height (Smith, 1997). Use of formulae that neglect term 2 requires the assumption that this increase of the liquid water mixing ratio with height is commensurate with the decrease in saturation mixing ratio, which applies when following a parcel's trajectory but not in an Eulerian co-ordinate system where conservation of total water, as taken from Durran and Klemp (1982), is given by:

$$\frac{\partial q'_w}{\partial t} + \bar{u}\frac{\partial q'_w}{\partial x} + w'\frac{d\bar{q}_w}{dz} = 0 \tag{3.20}$$

where the prime and overbar denote perturbation and mean state variables respectively. The liquid water mixing ratio is not a readily observed variable and not one provided in UKMM data. The MDIAG routine for calculating moist static stability therefore replaces it with the value of specific humidity. In saturated conditions the vertical gradient of the specific humidity will approximate that of the saturation mixing ratio, and thus adoption of specific humidity only will inevitably give a positive value for term 2 when it might otherwise be near neutral, were the liquid water mixing ratio to be included, and thus it places a stringent test on any instability indicated by the comparison of lapse rates. Durran and Klemp (1982) adopted such a moisture profile, which they considered to be reasonably realistic, when illustrating the differences between their formula and others against which it was being compared. Despite uncertainty regarding the UKMM moisture profile in areas equation (3.19) is to be implemented, the second term is retained with the aim of eliminating marginal and weak instability, however the result is disregarded if the moisture profile renders otherwise stable air unstable.

The presence of static instability combined with saturation means that convective precipitation can evolve with very little large scale vertical velocity (Anthes and Cotton, 1989). Again, as mentioned above with respect to evaluation of the release of convective instability, the presence of rainfall is regarded as sufficient indication that static stability is being released. As this index is assessed in rainfall areas only, any instability deemed to be present is considered the forcing mechanism producing the rainfall and the convective parameterisation of updraft velocity is implemented.

3.6.2.3 Slantwise convection

Acceleration of a parcel in a slantwise direction can occur when an air parcel is convectively stable with respect to vertical (convective stability) and horizontal (inertial stability) displacements but unstable with respect to slantwise movement. It is a situation referred to as symmetric instability, which when released gives rise to slantwise convection. Slantwise convection often manifests as banded precipitation, occurs on a larger scale than gravitational convection and can be triggered by synoptic scale ascent or orographic forcing (Schultz and Schumacher, 1999).

Symmetric instability is most easily examined in two dimensions and explained with reference to surfaces of constant potential temperature (isentropic surfaces). If a parcel undergoes slantwise displacement with respect to sloping isentropic surfaces, then its motion in the direction of displacement is determined by (Rogers and Yau, 1989):

$$\frac{d^2\Delta}{dt^2} = f\delta y \cos\beta \frac{\partial u_g}{\partial z}\left[\frac{\delta z}{\delta y} - \frac{\left(f - \frac{\partial u_g}{\partial y}\right)}{\left(\frac{\partial u_g}{\partial z}\right)}\right] \tag{3.21}$$

Δ being distance, u_g the westerly component of the geostrophic wind (geostrophic wind being the flow of air generally parallel to isobars resulting from a balance between pressure gradient and Coriolis forces), β the angle of displacement with respect to a horizontal surface, $\delta z/\delta y$ the slope of the isentropic surface and f the Coriolis parameter.

The crucial part of equation (3.21) is the factor in square brackets, which if positive indicates symmetric instability exists. The left hand side of this factor is the slope of the isentropic surface whilst the right hand side can be considered the slope of the absolute vorticity vector of the air parcel. The absolute vorticity of an air parcel (or its rotational characteristics) comprises two components, the vertically directed planetary vorticity (f) and relative vorticity. The former is induced by rotation of the earth and its magnitude at a location is dependent on latitude, whilst the latter is an air parcel's rotational characteristics relative to the earth, such as movement within a cyclone or anticyclone (Barry and Chorley, 1992). The slope of the absolute vorticity vector is expressed as the ratio of the horizontal to vertical components of absolute vorticity, and symmetric instability exists when the slope of the isentropic surface is greater than that of the absolute vorticity vector (Rogers and Yau, 1989).

Symmetric instability is more complicated to objectively determine than convective instability. Analysing the potential vorticity (PV) of air-masses is one means of identifying when conditions in the atmosphere could accelerate an air parcel's slantwise displacement (Weismueller and Zubrick, 1998). Potential vorticity refers to angular momentum within constant isentropic surfaces, moist potential vorticity (MPV) being with reference to a saturated atmosphere. MPV can be calculated on isobaric surfaces from UKMM data as below (Panagi, 1997; Bedrick *et al*, 1997):

$$MPV = -g\left(-\frac{\partial v}{\partial p}\frac{\partial \theta_e}{\partial x} + \frac{\partial u}{\partial p}\frac{\partial \theta_e}{\partial y} + \frac{\partial \theta_e}{\partial p} AV\right) \tag{3.22}$$

where AV stands for absolute vorticity. In either the saturated or unsaturated cases it is a measure of the ratio of absolute vorticity to the depth of the vortex (Byron-Scott *et al*, 1998). Negative values of MPV are associated with areas of moist symmetric instability, which if released lead to cloud and precipitation formation. It should be noted that if negative values arise because the

vertical gradient of θ_e is suggestive of convective instability this will already have been detected in the PFM when checking for upright convection and the determination of a convective updraft will have already been implemented. Figure 3.11 shows an example where there is reasonable coincidence between areas of negative MPV, as determined from UKMM forecast data, and observed rainfall. When trying to view how well this signifier matched observed rainfall it was found that very weak negative values can be reasonably widespread. A better visual correspondence can be obtained by making the signifier of symmetric instability a value of MPV less than –1.0 PV unit ($10^{-6}m^2s^{-1}Kkg^{-1}$). As with the assessment of convective instability, a check for symmetric instability is confined to the zone defined by high humidity and requisite depth of cloud and release of the instability is similarly determined in terms of existing rain or evidence of upward vertical motion. Due to uncertainty regarding the UKMM moisture profile outside this zone, no evaluation of symmetric instability is attempted in those areas even in the presence of observed rainfall.

In this study the same parameterisation of updraft applies to both upright and slantwise convection due to similarities in the magnitude of the accelerations achieved in both (Schultz and Schumacher, 1999). Thus a grid cell in which slantwise convection is deemed to be operating is treated as having upright convection. This is not entirely appropriate or satisfactory and does not account for the possibility that some of the condensation arising from slantwise movement that originates inside a grid cell may occur outside the cell. The simple approach of employing the same parameterisation for all modes of convection is merely an attempt to differentiate between the contrasting upward velocities typically observed between convective processes and dynamic lifting, being metres per second versus centimetres per second respectively (Anthes and Cotton, 1989). The F&K determination of convective updraft (equations 2.13-2.16) is still possible for slantwise convection given that it is derived from comparing the temperature of a parcel when following a pseudo-adiabatic ascent against its temperature when following a dry adiabatic ascent, and not against the ambient temperature profile. Slantwise and upright convection do, however, evolve at different rates and so distinguishing between these processes is particularly important when their presence influences the dynamics of the forecasting model (Wiesmueller and Zubrick, 1998). This is not the case here, wherein each timestep of the PFM is initialised with new inputs of temperature, pressure, wind and humidity that are all taken directly from the UKMM and therefore remain independent of the evolution of the PFM's rain field.

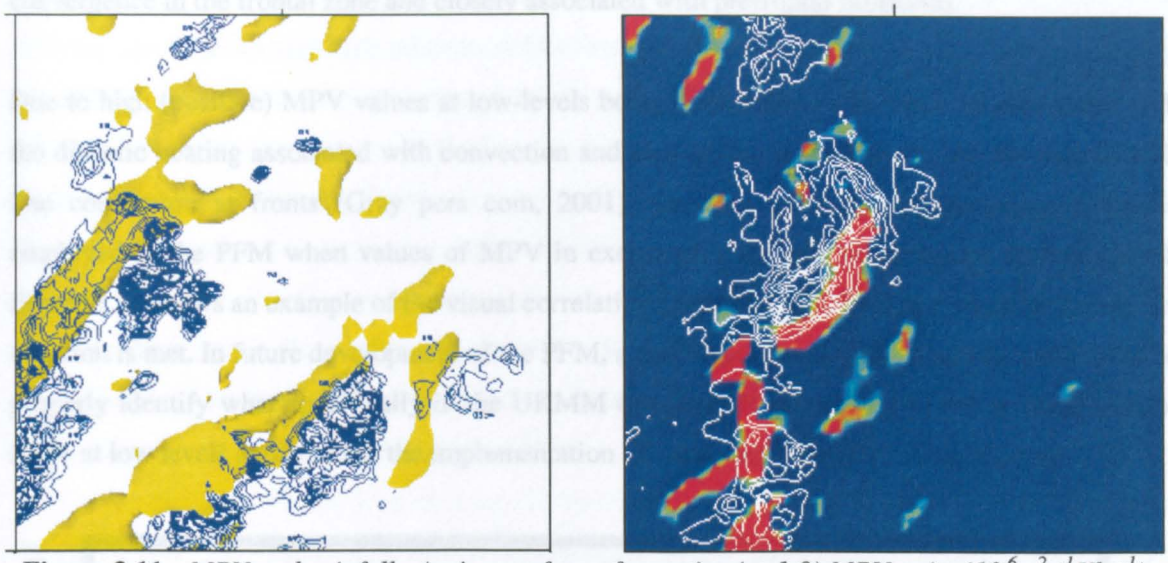

Figure 3.11: *MPV and rainfall. An iso-surface of negative (<-1.0) MPV units ($10^{-6}m^2s^{-1}Kkg^{-1}$), indicating areas of potential symmetric instability, is shown left for 13:00 25th December 1998 together with the rain field for that time (blue contours in increments of 0.5mm/hr). The graphic to the right shows the rain field for 09:00 15th January 1999 (white contours in increments of 2.0 mm/hr) against areas having in excess of 1 MPV unit (red) at the 1000 mb level.*

Although not indicative of symmetric instability, it is worthwhile noting that positive values of potential vorticity are also implicated in precipitation forming processes and serve as a diagnostic tool with respect to the cloud development observed in satellite imagery (Debi *et al*, 2001). Typically PV is positive and increases with height from the surface to the stratosphere, Figure 3.12 showing the vertical distribution of potential vorticity as a function of latitude. A value of 1 PV unit is considered indicative of tropospheric air and a value of 4 stratospheric air. The distinction between the two is a value of 1.5 PV units and the height of its contour delineates the height of the dynamical tropopause (Hoskins *et al*, 1985). Tropospheric values in excess of 1.5-2 PV units suggest an intrusion of stratospheric air and the resulting steep PV gradients are linked to strong dynamic development in the atmosphere, such as rapid cyclogenesis (Carlson 1991; Bedrick *et al*, 1997) and convective destabilization (Browning *et al*, 2000; Bedrick *et al*, 1997). Billingsley (2001) discusses the dynamics associated with an upper-level PV anomaly moving over a tropospheric front, whereby low-level cyclonic circulation can result and can create a warm advection area of positive PV, associated with which is upward vertical motion. Potential vorticity is a property conserved in adiabatic (no transfer of heat between the system and the environment) frictionless flow (Holton, 1992) but in the presence of friction and/or diabatic heating, such as from the latent heat of condensation, potential vorticity is not conserved and positive anomalies of MPV can evolve (Gray pers com, 2001). Bénard *et al* (1992), in simulating frontogenesis induced by

shear in a moist atmosphere, found that positive MPV anomalies were produced by frictional convergence in the frontal zone and closely associated with prefrontal rainbands.

Due to high (positive) MPV values at low-levels being often linked with areas of ascent and with the diabatic heating associated with convection and also having been observed to correspond with line convection at fronts (Gray pers com, 2001), the convective updraft parameterisation is employed in the PFM when values of MPV in excess of 1 PV unit occur at the 1000 mb level. Figure 3.11 shows an example of the visual correlation between a rain field and areas for which this criterion is met. In future development of the PFM, a more rigorous analysis could be undertaken to properly identify what specifically in the UKMM dynamics is giving rise to the accumulation of MPV at low levels and whether the implementation of a convective updraft is appropriate.

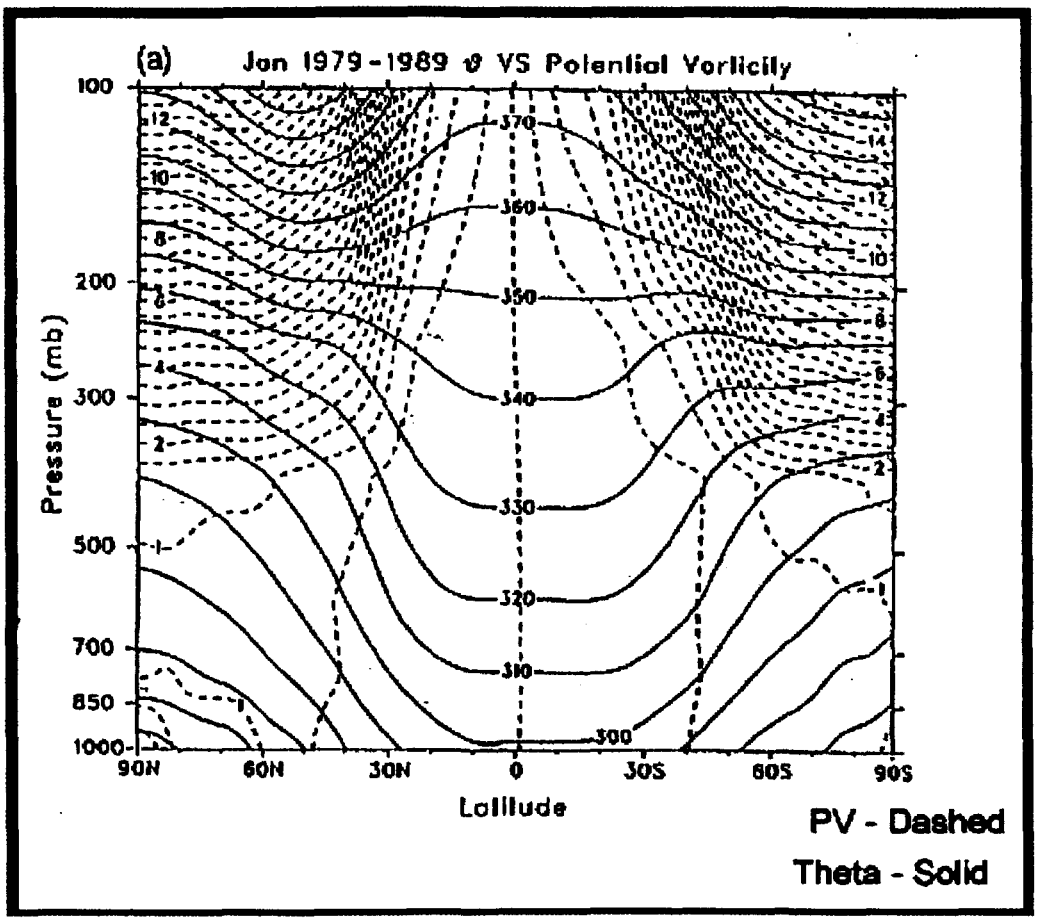

Figure 3.12: *Vertical cross-section of the zonal mean of PV (dashed lines) for the month of January (taken Billingsley, 2001).*

3.6.2.4. Orographic uplift

Both types of vertical motion, dynamic and convective, have the addition of orographic forcing where appropriate. Orographic uplift is determined through term 2 of equation (2.45) in the same

way as Wild (1996) but with the UKMM 1000mb wind field replacing his use of the vector of storm velocity. The addition of orographic forcing is deemed "appropriate" in the presence of an existing rain field, an approach taken to reflect research implicating it more in the enhancement of precipitation rates than in the initiation of precipitation (Barros and Lettenmaier, 1994). In the UK this enhancement is associated with the "seeder-feeder" mechanism, whereby rain from upper-level seeder clouds falls through lower, orographically-induced feeder clouds, the drops enlarging through coalescence thus producing higher rainfall rates (Carruthers and Choularton, 1983). The orographic feeder clouds occur when moist air is raised to saturation by the upward motion resulting from winds flowing over topographic barriers. In isolation these clouds tend not to precipitate because droplets spend insufficient time within the cloud to allow rain formation before being carried over the barrier (Browning, 1979).

Browning *et al* (1974) noted that while the main effect of hills is to intensify precipitation, they can also increase the extent of rain by providing enough uplift to release potential instability. The dual role of orographic forcing is acknowledged in the PFM algorithm, whereby it not only augments vertical velocity in the presence of existing rain but it also enables generation of new areas of rainfall by contributing to the release of any instability attributed to the grid cell.

F&K (1994) and Wild (1996) produced hourly forecasts with their models, each translating the existing rain field across the model domain in one timestep before calculating liquid water changes and so did not account for modification that, in reality, is likely to occur with its passage over varied terrain. By introducing twelve, five minute time-steps into a one hour forecast, the PFM allows the rain field to evolve under the influence of orographic forcing, enabling any new areas of rainfall that are generated from orographically-induced release of instability to be treated in the next time step as an existing rain field, having the opportunity for enhancement through seeder-feeder mechanisms. The length of the time-step (5 minutes/300 seconds) means that any storm velocity in excess of 60 km/hr may result in the rain field passing over more than one grid cell in a time-step (in terms of the Beaufort scale, winds of this strength approach gale force but fall short of the speed of winds associated with a storm, violent storm or hurricane (Strangeways, 2001)). However, too small a time step may be inconsistent with the likelihood of the column producing a response to the forcing. As it is, the length of the time-step just matches the lowest limit Bell (1978), when constructing his rainfall forecasting model, considered feasible for droplet growth from condensation.

3.7 Advection scheme

Access to UKMM data makes available various options for the manner in which the rain field is translated across the domain. Precipitation nowcasts rely on extrapolating the past storm movement forward in time, the velocity vector for which is typically determined by using some form of pattern matching between consecutive radar images. Both F&K (1994) and Wild (1996) implemented such a procedure to place their computational domains in a Lagrangian frame of reference. Whereas F&K maximised the correlation between whole radar images, Wild focused on tracking raincell maxima within the image. In Wild's methodology, upon locating in the first radar frame the area of greatest total rainfall, which is calculated with respect to a predetermined number of pixels, a search is conducted in the second frame around that location for the same sized area that best matches, in terms of producing the best correlation, the cluster of pixels containing the rainfall maximum of the first frame. The x and y components of the velocity vector are obtained from the differences in the x and y locations of the paired rain areas and the entire rain field is moved uniformly across the domain according to the derived velocity vector. This same approach is retained in the PFM, however it is not the only method of advection that can be employed.

Mid-level winds are thought to steer the movement of storms, with "mid-level" commonly taken to mean 700mb but varying anywhere between 850mb and 500mb (Byron-Scott *et al*, 1998). Forecasted UKMM wind fields at these levels offer an alternative to extrapolating past movement forward in time and also offer an alternative to uniform advection. In the PFM, the x and y components of the steering level winds within each grid cell can be used to displace the associated rain field from its current position to another cell. If, as a result, the rain from two different cells move into one cell, the approach taken is to attribute the destination cell with the higher rainfall rate of the two.

Given that the PFM algorithm offers an option of different advection schemes, there has to be a means to select the most appropriate. Therefore, prior to commencing the one hour forecast proper, a series of nowcasts are made, whereby the preceding hour's rain field is translated according to velocity vectors determined by the cross correlation method described above, as well as according to the 700mb and 850mb winds and results from all three, in addition to assumed persistence of the rain field, are correlated with the most current rain field. The method that appears to give the best correlation is selected as the advection technique for the next forecast. Yet to be properly investigated is the possibility of incorporating the movement of fronts or other fields such as MPV in determining the displacement of the storm over the forecast lead time.

3.8 Adaptation for missing VIL

The F&K model achieves a rainfall prediction by modeling the time evolution of VIL, with initial values of VIL being estimated from volume scan radar reflectivity. An assumed linear relationship between VIL and the cloud base liquid water content (CBLWC) enables the latter to be calculated from forecasted VIL, which can then be converted to a reflectivity value and rainfall rate. As experienced in this research and in the research of others (Georgakakos & Krajewski 1991, Andrieu *et al*, 1996), the quality of volume scan radar data is not always satisfactory, nor necessarily available or limited in depth or in detail of the volume scanned. Options in these cases may be to simply not use the model or possibilities may exist to construct a vertical profile of liquid water content, as shown by Andrieu *et al*, when more than one elevation scan is available and under the assumption of homogeneity in the vertical profile of reflectivity (VPR) over the area concerned (Andrieu *et al*, 1999). An alternative being explored here is to employ the framework for rainfall prediction established by F&K whilst relying on single-level network radar data.

In making use of network radar data it is assumed that an estimate of CBLWC, in units of kgm^{-3}, can be derived from it (using equations (2.10), (2.11) and (2.43)). In the absence of any further information regarding the vertical profile of liquid water, the CBLWC in effect replaces VIL as the model state, the time evolution of which is still simply a function of inflows and outflows of liquid water (equation (2.6)). Following F&K, the net gain/loss to the system is still calculated with respect to a cloud column but, given that the distribution of it through the depth of the cloud is unknown, an estimation of the contribution to the CBLWC is required and ideally one that inherently accounts for the eventual filtering of contributions at higher levels to the cloud base. As a first guess the cloud column gain/loss, as calculated over a 5 minute time-step, is averaged over the depth of the cloud to obtain a concentration per cubic metre, which is added to the grid cell CBLWC as a tentative estimation of the CBLWC at the end of the time-step. A rudimentary estimate of the depth of the cloud is made from the difference in geopotential height of the standard UKMM pressure levels that are closest to that of the LCL and cloud top. A final estimation of the CBLWC is derived by multiplying the first estimate by a factor that varies across the domain and is determined prior to commencing the 12 time-steps required to make the one hour forecast. This factor is simply the ratio of the initial CBLWC, as calculated from the most current network radar image, to a PFM estimate of CBLWC produced using a preliminary "calibration" time-step and based on initial conditions. Essentially the factor is vaguely analogous to the precipitation efficiency (E) of the system which Brooks *et al* (1996) defined as $E=m_p/m_i$, m_p being the mass of water falling as precipitation and m_i the influx of water vapour into the cloud. Brooks *et al* considered the instantaneous rainfall rate to be proportional to the vertical moisture flux into the system with E being the coefficient of proportionality. The efficiency of a precipitating system

varies spatially and over time and while the first can be accounted for by allowing the uniquely determined factors to be advected with the rainfield at the beginning of each time-step, dealing with the second is more difficult and in this case the factors are assumed to be temporally invariant over the forecast lead-time. Additionally, the CBLWCs and forecasts are linearly regressed and the derived relationship used to adjust first estimates of CBLWC in grid cells lacking an initial observed CBLWC and/or a non-zero estimate of CBLWC at the start of the forecast. The inclusion of this "efficiency" factor provides another means, in addition to having consideration for the relative humidity of ice as discussed in Section 3.6.1, of ameliorating the implications of assuming that warm rain processes only are operating. Through this factor higher efficiencies, such as might be achieved in the presence of ice and graupel (Barros & Lettenmaier, 1994), can be allowed to evolve in the PFM without explicit determination of the water phase.

The forecasted rainfall rate can be determined from CBLWC in the manner of F&K (1992), beginning with conversion to a reflectivity value using:

$$Z = \frac{720 M_B}{\pi \rho \Lambda^3} \tag{3.23}$$

from which a rainfall rate is calculated using the same Z_R relation employed by the UKMO to construct the rain field, being $Z=200R^{1.6}$.

3.9 The PFM algorithm - summary

The flow diagram of Figure 3.13 maps the sequence of key tasks, the order of core decisions and the routes of alternative pathways contained within the gamut of applying the PFM. This includes acquiring and preparing data before entering into the algorithm proper, which then starts with an objective selection of advection scheme prior to commencing the thirteen 5 minute time-steps of the forecast. The orographic updraft is calculated first due to its influence on both the magnitude of the updraft velocity and the triggering of instability, after which a mode of forcing is assigned to each grid cell according to the criteria discussed above and the appropriate updraft velocity determined.

Upon having the updraft velocity, the rates of inflow to and outflow from the system can be calculated and compared to give the net gain/loss over the length of the time-step and the first guess evolution of the CBLWC is made by averaging the gain/loss over the cloud column. Depending on how many time-steps have passed, the index used to adjust the first guess is either calculated or employed, leading to a confirmed 5 minute forecast in the case of the latter.

Properties of the rain field are advected and the next time-step begins until all are completed to give the final one hour forecast.

The significant changes that have been made to the original form of the model adopted from Wild can be summarised as follows:

- Timesteps have been reduced from one hour to 5 minutes to allow for modification of the rainfield as it traverses areas of complex orography, this also facilitates calculation of rainfall accumulations for flow forecasting purposes.
- Due to the unreliability of the Hameldon Hill radar, network radar data and not volume scan radar data is used. A preliminary 5 minute time-step is used to gauge the relationship between cloud column evolution and CBLWC, whereby the net gain/loss of water to the column calculated from initial conditions is averaged over the depth of the cloud to obtain an estimate of CBLWC, which is then related to the observed CBLWC. The index obtained and the regression coefficients produced from linearly regressing the two fields are used in subsequent timesteps to adjust first-guess forecasts of CBLWC.
- For every forecast, different ways of representing the storm's velocity are considered for rainfield advection. These include UKMM winds at 700mb and 850mb, persistence and nowcasting. Whichever representation produces the best correlation for the preceding hour is selected for the forecast.
- Low-level wind speed is used to calculate orographic uplift as opposed to the speed of storm movement.
- The predicted rainfall area is delineated by the advected rainfall area and any other areas where the relative humidity with respect to water at 600 mb exceeds 90%, the relative humidity with respect to ice at 700 mb is greater than or equal to 100% and the cloud depth is at least 2km.
- Within the delineated rainfall area, a convective updraft is calculated if convective instability exists in the column, as determined by the vertical profile of θ_e in areas of high humidity and sufficient cloud depth or by moist static stability in existing rainfall areas outside these zones. A convective updraft is also calculated if symmetric instability is thought to exist as indicated by MPV values of less than -1 PV unit. Additionally a convective updraft is calculated if at 1000 mb MPV exceeds a value of 1 PV unit. Within the delineated rainfall area the atmosphere is assumed to be saturated, which itself implies that any identified instabilities are realised but that uplift is still required for the release of the instability. Where there is pre-existing rain this instability is assumed to be released, otherwise there must be positive UKMM updraft in the column or an orographic updraft. In the absence of convection, a test is undertaken to determine if a significant front is present. If so, the average of the vertical updraft between the LCL and cloud top is taken as the vertical velocity. The default option in the PFM is the UKMM vertical velocity at the LCL.

- The predicted CBLWC is converted to a rainfall rate by reversing the steps made to convert the radar estimated rainfall into cloud liquid water, ie a reflectivity value is determined from the CBLWC and a rainfall rate is calculated using a standard Z-R relationship, in this case being $Z=200R^{1.6}$.

The next chapter details the implementation of the model, its performance over lead-times of one hour to six hours, and shows a comparison of its performance with other forecasting techniques, namely, persistence, nowcasting and UKMM forecasts.

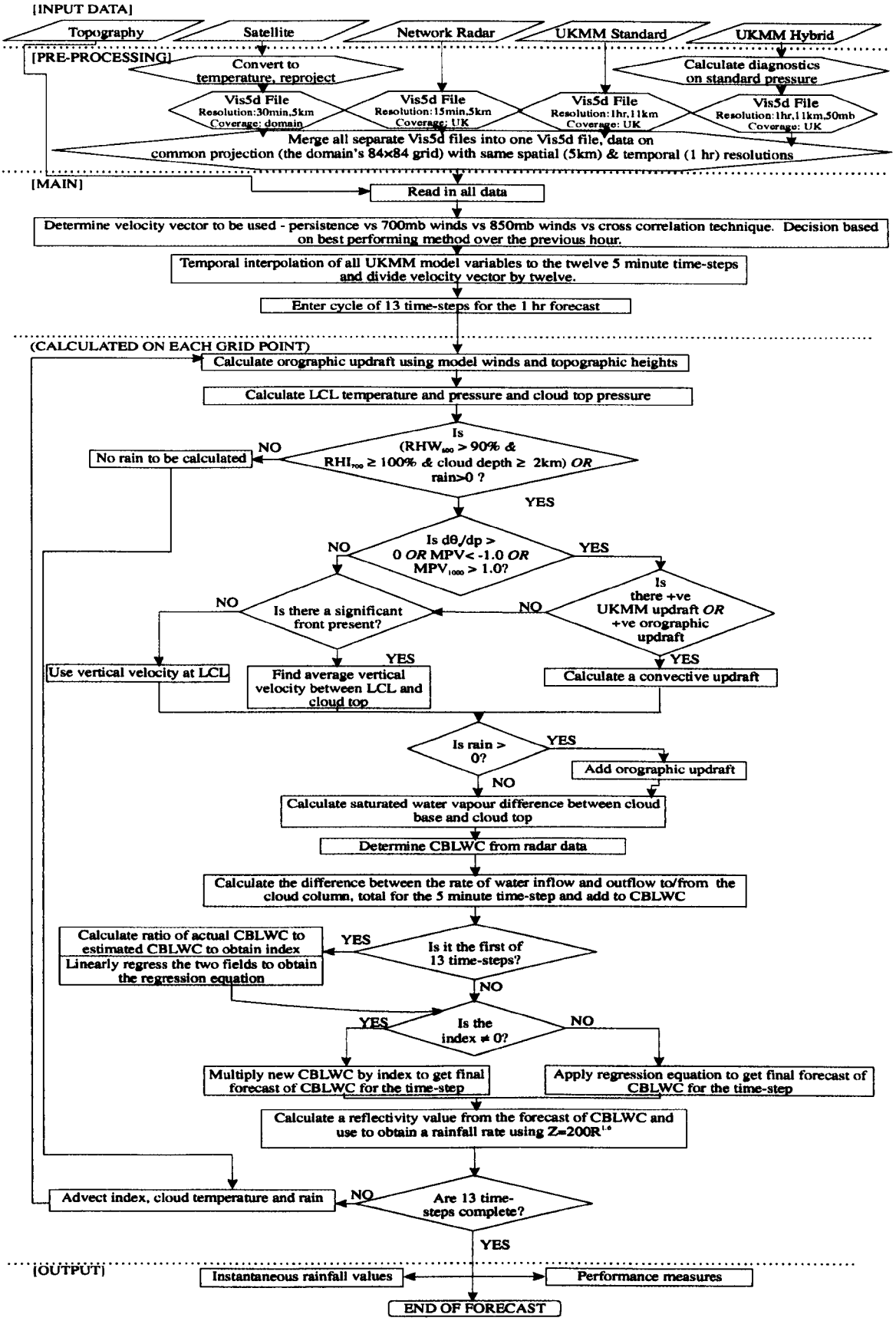

Figure 3.13: *Flow diagram of the steps involved in implementing the PFM. RHW and RHI are the relative humidity with respect to water and ice respectively, all other abbreviations are as stated in the text. Numerical subscripts refer to the pressure level to which the variable pertains.*

CHAPTER FOUR

PFM PERFORMANCE – UK CASE STUDY

4.1 Real-time application

In formulating a rainfall forecasting model, the aim must surely be to place it in an operational context, whereupon input data arrives in real-time and time constraints demand nominal delay between data receipt and forecast output. It is an issue that has to be addressed at some point and preferably prior to embarking on model development so that any new ideas can be grounded in the practicalities of their implementation. The method of PFM data acquisition and preparation, described in the preceding chapter, is perhaps suggestive of a relatively cumbersome process, hindered to some extent by extensive pre-processing which entails not only re-sampling to appropriate resolutions and co-ordinate systems but often calculation of secondary products from the primary source data.

All three input data types (satellite, radar, UKMM) can be, and generally are to various paying organisations, made routinely available in operational real-time environments by the UKMO via email or file transfer protocol (FTP) (UKMO, 2001c). Radar data is updated every 15 minutes, satellite data every 30 minutes, whilst each set of 48 hourly UKMM forecasts are generated four times daily. Automated retrieval and pre-processing of data is a standard feature of today's flood forecasting systems, the detail of which is not delved into here but the feasibility of which, in relation to the data required to operate the PFM, is undoubted. For the purposes of this research, all data manipulation and PFM runs were undertaken on the University of Bristol's central computer server, being a Sun Enterprise 450 consisting of 4×400MHZ UltraSPARC-II processors and having a total of 4 Gigabytes of memory (University of Bristol, 2001). On this system the conversion of one radar image into a usable format compatible with the PFM's computational framework and domain is achieved in seconds, likewise the satellite data. The conversion of UKMM data from hybrid co-ordinates to standard pressure levels and the calculation of diagnostics, all using MDIAG, is onerous in comparison, needing a minimum of 100 Megabytes of computer memory and approximately two minutes of computer time to produce one set of the sixteen diagnostics

necessary to run the PFM. This output from MDIAG covers the entire UKMM domain (Figure 3.2) and includes twenty pressure levels, overall constituting 146×182×20 computational points. Hence the two-minute time frame could be further shortened by reducing the spatial extent of the source data and adapting the MDIAG code appropriately, as opposed to the current order of calculating diagnostics and then extracting the area corresponding to the PFM's domain. In a real-time environment the preparation of data would be greatly facilitated by use of multiple processors and potential for time-saving exists through processing forecast products in advance of receiving the corresponding remotely-sensed data. The one-hour PFM forecast itself, using the prepared data, takes approximately 80 seconds including calculation of performance measures at the end of the forecast and also monitoring statistics as it progresses, the latter being a means of checking whether the PFM is yielding sensible results for model variables in the course of producing a forecast.

Data accessibility and timeliness in forecasting may not be problematic with respect to the operational implementation of the PFM, accessibility difficulties avoided to some extent by use of network rather than volume scan radar data and timeliness dependent on the computer resources in use, but a potential issue is the gap between the time of validity of each data product supplied by the UKMO and its time of receipt, which ranges from 15 minutes with respect to radar data to 3 hours for UKMM data. Accepting that UKMM forecast products are not available until three hours after the analysis upon which they are based, the PFM has been run in two modes, one with data that would be available in real-time (herein referred to as "real-time") and the other with the forecasts generated from the most recent analysis prior to the time in question (herein referred to as "perfect"). For example, with respect to a lead-time of one hour, if a PFM forecast was being made for a time of 0600 then the real-time run of the model would involve using only the forecasts generated from the analysis at 0000, i.e. T=0000+5 and T=0000+6, while the perfect run would use the same T=000+5 products but replace T=0000+6 data with that from the analysis at 0600, i.e. T=0600+0. This was intended to help gauge whether significant degradation in the PFM's performance occurs when using forecast data that is quite distanced from an analysed state of the atmosphere. In reality it is unlikely the gap between the time of validity and time of receipt will ever be significantly narrowed, as the analysed state of the atmosphere is based on the assimilation of data 90 minutes before and after the time it represents, and as such a gap of a little less than two hours is the minimum that might be expected.

4.2 Performance assessment and measures

Having constructed the PFM algorithm, it remained to be seen how it would perform and particularly how its performance compared with other rainfall forecasting techniques. Evaluation

of the PFM's success was undertaken for both the real-time and perfect PFM runs and focused on the results obtained within the inner assessment grid of the domain, being the central 42 by 42 grid cells referred to in Section 3.4.1. The majority of performance measures were calculated with respect to instantaneous rainfall rates, with rates below 0.125 $mmhr^{-1}$ excluded. Lead-times of one hour to six hours, in hourly increments, were appraised. It should be noted that for lead-times longer than one hour it appeared necessary to remove the requirement for a "dry" grid cell to have a minimum depth of cloud before it was allowed to produce rain, a criteria found to become progressively too limiting. The likely reason for this is that the cloud top temperatures of the forecasted rain field are dependent on the clouds present at the beginning of the forecast, which have undergone translation across the domain by extrapolation of the storm movement that occurred during the hour prior to the time of initiating the forecast. At longer lead-times it becomes increasingly likely that significant cloud development and/or changes in storm motion occur during the interim period between the start time of velocity vector determination and the time for which the forecast is being made.

Forecasts from four other rainfall prediction techniques provided standards against which the PFM's results were compared, these being:

1. the *UKMM large scale rainfall* (UKMML), which is explicitly resolved by the UKMM.
2. the *UKMM convective rainfall* (UKMMC), which is parameterised on the sub-grid scale by the UKMM.
3. a *nowcast*, which refers to simple advection of the rain field without modification and so without account for storm growth and decay, with advection achieved using velocity vectors determined by the same technique as in the PFM (Section 3.7), i.e. maximizing the correlation between radar images based on identifying the area of maximum total rainfall in one image and searching for the closest match in the following image.
4. *persistence*, which means the forecasted rain field is exactly as it was at the start of the forecast, the rain field persists in location, size and intensity for the duration of the forecast lead-time.

Unfortunately neither the UKMO's Nimrod nor GANDOLF forecasts were available for comparison.

The 6-hourly generation of UKMM products rendered direct comparison of all forecasting techniques difficult because the UKMML/C forecasts rarely had a length of lead-time consistent with the lead-time being assessed. However, the main purpose in conducting the comparison was not to assess the ability of each model when given the same lead-time but to evaluate the PFM's predictions with respect to other forecasts that might be available operationally. Therefore, when making the real-time comparison of the different forecasts, the UKMML/C forecast was always

that which corresponded to the actual rain field under consideration and was produced closest to the time of the actual while theoretically still being available in real-time. As a result the lead-time of the UKMML/C forecasts ranged from three hours to nine hours even though the lead-time under consideration remained fixed and initially less than 3 hours. When making the perfect comparison, the UKMML/C forecast was simply always the one produced closest to the time of the actual, and so ranged from being the analysis itself to a forecast with five hours lead-time. It must also be remembered that the UKMML/C forecasts were made at a spatial resolution of 11km by 11km, greater than the other forecast methods, and required interpolation to the 5km by 5km grid cells of the domain.

A variety of performance measures were used to ascertain the accuracy of the model.

- Root Mean Square Error (RMSE):

$$RMSE = \left[1/N \sum_{j=1}^{N} \left(\hat{y}_j - y_j \right)^2 \right]^{0.5} \tag{4.1}$$

where N is the number of points in the domain, $\hat{y}$ is the forecast value at grid point j and y is the actual value at the same point.

- Average forecast rainfall rate (rate_for) versus average actual rainfall rate (rate_act)
- Percentage forecast rainfall coverage (%cov_for) versus percentage actual rainfall coverage (%cov_act)
- Critical Success Index (CSI), Probability of Detection (POD) and False Alarm Ratio (FAR), all of which were assessed on a grid cell by grid cell basis. These three indices help to gauge the degree of similarity in the spatial distribution of the two rain fields being compared, CSI being the most testing of the three because it is the only one that accounts for the error in predicting rain when it does not occur and also the error of predicting no rain when it does occur (Collier *et al*, 2000). Each index is best understood with the aid of a diagram (Wild, 1996):

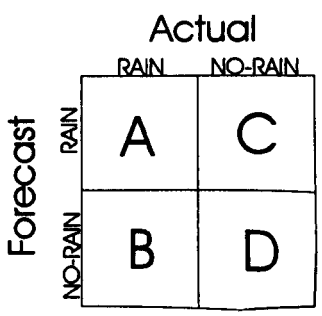

where:

$$CSI = \frac{A}{A + B + C} \tag{4.2}$$

$$POD = \frac{A}{A + B} \tag{4.3}$$

$$FAR = \frac{C}{A + C} \tag{4.4}$$

A perfect score for each of CSI and POD is a value of 1 and a perfect score for FAR is a value of 0.

- Correlation coefficient between actual and forecasted rainfall rates. The correlation coefficient statistics were calculated on a grid cell by grid cell basis (resolution of 5km) (cc5km) and also over spatial averages of 10km×10km (cc10km), 15km×15km (cc15km), 20km×20km (cc20km) and 25km×25km (cc25km). Additionally, "nearest neighbour" correlation coefficients (ccNN) were calculated, "nearest neighbour" being the best coefficient obtained when correlating the grid cell actual rainfall rate with, separately, the forecasted rainfall rate in the same grid cell and in each of the immediately adjacent grid cells.

4.3 The case study events

Assessment of the PFM's performance was undertaken on a case study basis using the four events described in the previous chapter, namely the three-day wintertime event in December 1998, the two-day wintertime event in January 1999, the five-day summertime event in August 1999 and the 1-day autumnal event in October 1999.

4.3.1 December 1998

A low pressure system dominated synoptic conditions over the UK in the last week of December, giving rise to unsettled weather that was generally mild in temperature but notably windy and with periods of heavy rain. The three days of the event, the 24th, 25th and 26th, each had rainfall associated with passing fronts and shared similarities in the timing of rainfall, wind velocities and the direction of storm movement. A sample of the rain field pattern on each day, in the form of four consecutive network radar images at hourly intervals, is given in Figure 4.1. Weather maps of

the synoptic conditions at 1200 GMT (Greenwich Mean Time) on each of the three days are displayed in Figure 4.2.

The morning of the 24th dawned fine and dry before a warm front brought wet weather to the UK later that morning, mainly in the form of an eastward moving north-south oriented rain band that approached from over the Irish Sea, but also through another narrow band of less intense rainfall on the eastern side of the Pennines that developed as the front began to push across the country. Rainfall within the area of the PFM domain was largely confined to the hours between 0900 GMT and 1800 GMT, during which rainfall rates peaked at 27.5 $mmhr^{-1}$. As the front passed over the sea and then land, the cooler land surface compared to sea surface temperatures (Figure 4.3) caused the front, and the associated precipitation, to intensify at the coastline and particularly over coastal hills where progress of the front slowed. Similarly, the temperature contrast between land and sea on the eastern flank of the UK assisted in the development of rainfall there. Surface winds were south-westerly throughout the day, though sheared to the right with height, resulting in winds at 700mb that were more steadily westerly to north-westerly. The UKMM representation of the wind field reached a maximum wind speed just short of gale force at approximately 57 $kmhr^{-1}$.

A cold front was primarily responsible for the rain that fell on the 25th, which occurred within the same period, 0900 GMT to 1800 GMT, as the day before. On that occasion the rain was clearly structured into two, closely spaced, southwest-northeast oriented bands, both moving towards the northeast within a storm system that was incrementing eastward. Again the rain appeared to intensify at coasts, and this time to a greater extent over inland ranges, and once more the progress of the front slowed overland. Surface winds remained south-westerly for the duration of the event and, if UKMM forecasted wind fields were accurate, the winds were lighter than the day before, not exceeding 45 $kmhr^{-1}$, with evidence of slight shearing to the right with height. The 25th was the wettest day of the month and the maximum rainfall rate registered by the radar network on that day, 77$mmhr^{-1}$, was considerably greater than the previous day and greater than the maximum value of 20 $mmhr^{-1}$ attained the following day. Although cold fronts are expected to have higher rainfall intensities than warm fronts (Barry and Chorley, 1992), it is uncertain to what extent incidences of bright band influenced the network radar estimates. The freezing level, according to UKMM data, could be found at a height of 800 metres on the 25th, a figure relatively high compared to a level of 450 metres on the 24th and 320 metres on the 26th.

The freezing level height on the 26th increased however with the passage of a warm front that brought a wide band of rain from the south-west, again between the hours of 0900 GMT and 1800 GMT, that despite lacking some coherency in form had fairly uniform movement towards an east to north-easterly direction. Orographic enhancement of rainfall was apparent, particularly over the

Cambrian Mountains, and rainfall tended to persist over the higher ground. Winds on the 26th were stronger than during the previous two days with UKMM surface wind speeds reaching over 70 $kmhr^{-1}$. Surface wind direction was at first predominantly southerly, then briefly turned southeasterly before ending the event decidedly southwesterly. Wind shear was towards the right with increasing height so that at 700mb the winds were southwesterly throughout the event.

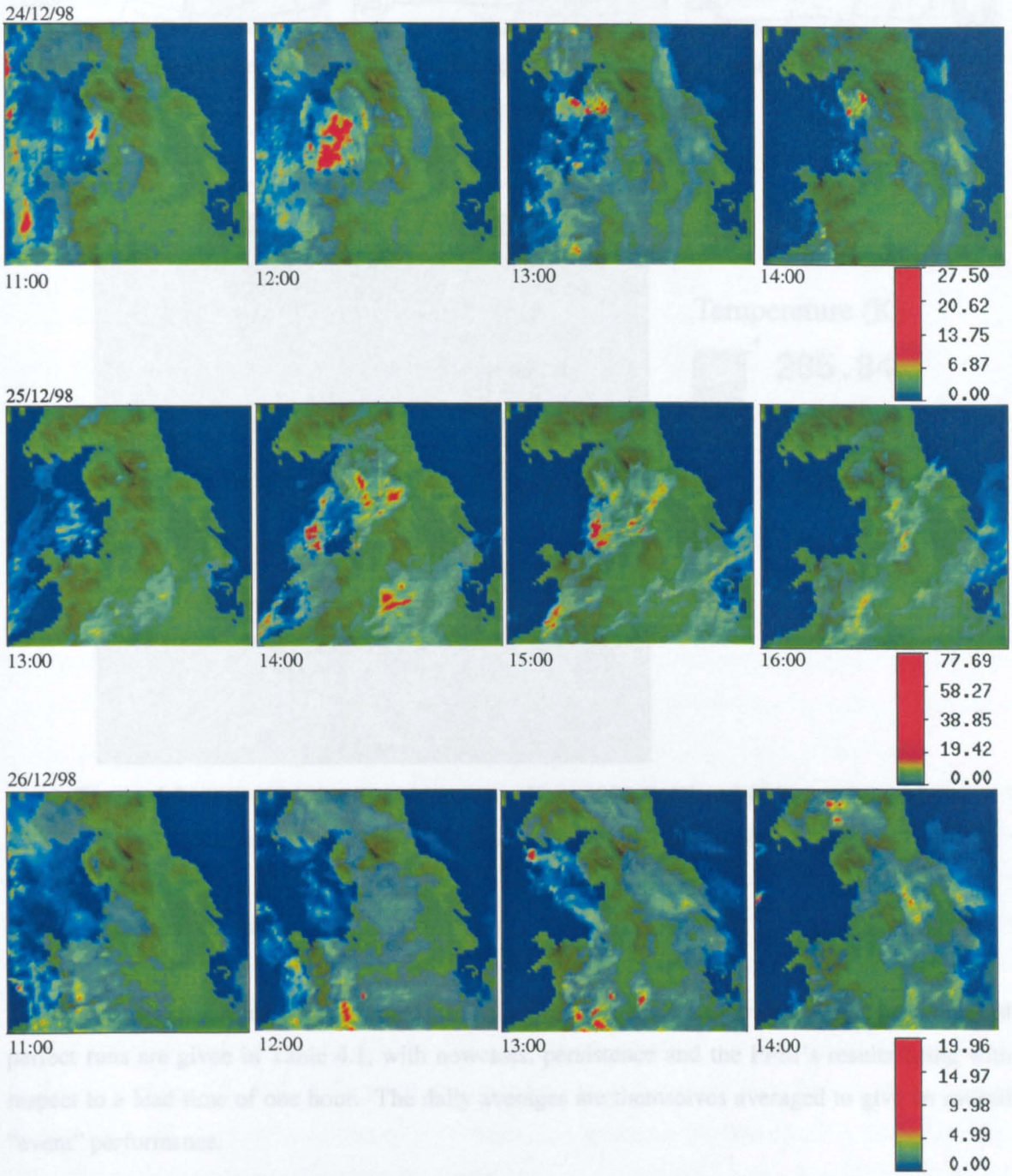

Figure 4.1: *Four consecutive hourly images of rainfall for each day of the wintertime event: 24th (top), 25th (middle) and 26th (bottom). Below right of each set of images is the legend showing rainfall rates in $mmhr^{-1}$ and below left of each individual image is the time to which it corresponds.*

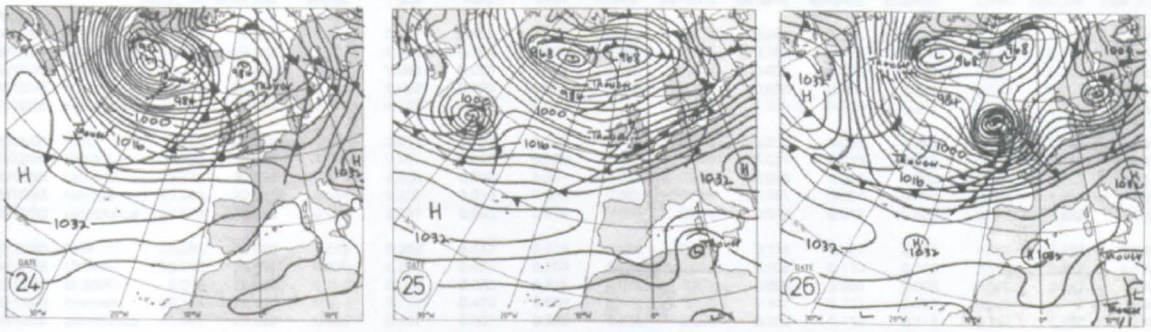

Figure 4.2: *Synoptic conditions at 1200 GMT on the 24th (left), 25th (middle) and 26th (right) of December 1998. (Eden, 1999a))*

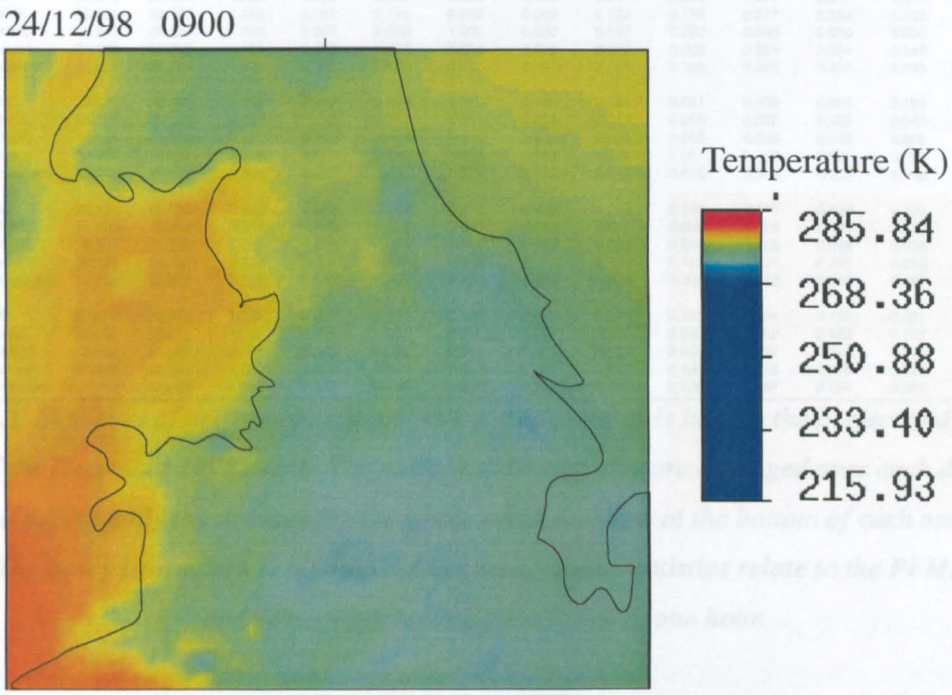

Figure 4.3: *UKMM 1000mb temperatures (K) at 0900 GMT on 24th December 1998. Temperatures appear cooler over land than over the surrounding sea areas.*

4.3.1.1 One hour lead-time

The daily average performance statistics for each of the five models and for both the real-time and perfect runs are given in Table 4.1, with nowcasts, persistence and the PFM's results being with respect to a lead-time of one hour. The daily averages are themselves averaged to give an overall "event" performance.

		%cov_for	%cov_act	RMSE	CSI	POD	FAR	cc5km	cc10km	cc15km	cc20km	cc25km	ccNN	rate_for	rate_act
Perfect															
24/12/98	PFM	23.980	28.326	1.231	0.257	0.452	0.505	0.190	0.214	0.247	0.276	0.322	0.417	1.265	1.146
24/12/98	UKMML	55.342	28.326	1.177	0.294	0.739	0.650	0.084	0.127	0.168	0.211	0.249	0.148	0.781	1.146
24/12/98	UKMMC	0.227	28.326	1.088	0.003	0.003	0.902	0.000	0.001	0.001	0.001	0.002	0.001	0.042	1.146
24/12/98	nowcast	34.442	28.326	1.503	0.262	0.426	0.621	0.018	0.027	0.038	0.051	0.064	0.147	1.231	1.146
24/12/98	persistence	28.319	28.326	1.376	0.295	0.585	0.495	0.201	0.224	0.260	0.289	0.335	0.509	1.185	1.146
25/12/98	PFM	19.488	23.520	1.563	0.254	0.393	0.543	0.055	0.066	0.074	0.082	0.088	0.224	1.544	1.930
25/12/98	UKMML	39.733	23.520	1.590	0.307	0.656	0.583	0.026	0.029	0.031	0.033	0.035	0.055	0.810	1.930
25/12/98	UKMMC	3.773	23.520	0.622	0.008	0.090	0.991	0.000	0.000	0.000	0.000	0.000	0.005	0.063	1.930
25/12/98	nowcast	22.203	23.520	2.034	0.203	0.313	0.635	0.045	0.068	0.081	0.087	0.091	0.203	1.938	1.930
25/12/98	persistence	22.928	23.520	2.035	0.227	0.383	0.579	0.016	0.014	0.015	0.019	0.023	0.146	1.882	1.930
26/12/98	PFM	25.384	25.699	0.579	0.202	0.317	0.575	0.078	0.101	0.114	0.127	0.138	0.257	0.783	0.740
26/12/98	UKMML	56.702	25.699	0.826	0.280	0.660	0.703	0.089	0.098	0.105	0.110	0.115	0.116	0.848	0.740
26/12/98	UKMMC	6.015	25.699	0.486	0.019	0.032	0.818	0.002	0.002	0.003	0.004	0.006	0.010	0.159	0.740
26/12/98	nowcast	28.124	25.699	0.614	0.290	0.476	0.609	0.112	0.153	0.187	0.211	0.230	0.234	0.758	0.740
26/12/98	persistence	25.605	25.699	0.620	0.187	0.307	0.582	0.080	0.094	0.103	0.112	0.118	0.197	0.688	0.740
	PFM	*22.951*	*25.848*	*1.124*	*0.238*	*0.387*	*0.541*	*0.108*	*0.127*	*0.145*	*0.162*	*0.183*	*0.299*	*1.197*	*1.272*
	UKMML	*50.592*	*25.848*	*1.198*	*0.293*	*0.685*	*0.645*	*0.066*	*0.085*	*0.101*	*0.118*	*0.133*	*0.106*	*0.813*	*1.272*
	UKMMC	*3.338*	*25.848*	*0.732*	*0.010*	*0.042*	*0.904*	*0.001*	*0.001*	*0.001*	*0.002*	*0.003*	*0.005*	*0.088*	*1.272*
	nowcast	*28.257*	*25.848*	*1.384*	*0.252*	*0.405*	*0.622*	*0.058*	*0.083*	*0.102*	*0.116*	*0.128*	*0.194*	*1.309*	*1.272*
	persistence	*25.617*	*25.848*	*1.344*	*0.237*	*0.425*	*0.552*	*0.099*	*0.111*	*0.126*	*0.140*	*0.159*	*0.284*	*1.252*	*1.272*
Real-time															
24/12/98	PFM	24.616	28.326	1.239	0.266	0.463	0.503	0.188	0.211	0.243	0.271	0.317	0.411	1.273	1.146
24/12/98	UKMML	55.461	28.326	1.184	0.297	0.745	0.648	0.089	0.133	0.174	0.217	0.254	0.152	0.801	1.146
24/12/98	UKMMC	0.013	28.326	1.088	0.000	0.000	1.000	0.000	0.000	0.000	0.000	0.000	0.000	0.010	1.146
24/12/98	nowcast	34.442	28.326	1.504	0.262	0.426	0.621	0.018	0.027	0.038	0.051	0.064	0.147	1.231	1.146
24/12/98	persistence	28.319	28.326	1.376	0.295	0.585	0.495	0.201	0.224	0.260	0.289	0.335	0.509	1.185	1.146
25/12/98	PFM	20.326	23.520	1.831	0.249	0.398	0.570	0.040	0.045	0.051	0.058	0.065	0.183	1.566	1.930
25/12/98	UKMML	48.551	23.520	1.630	0.273	0.706	0.657	0.014	0.017	0.018	0.020	0.022	0.044	0.858	1.930
25/12/98	UKMMC	8.434	23.520	0.626	0.048	0.144	0.768	0.005	0.007	0.012	0.020	0.030	0.020	0.188	1.930
25/12/98	nowcast	22.203	23.520	2.034	0.203	0.313	0.635	0.045	0.068	0.081	0.087	0.091	0.203	1.938	1.930
25/12/98	persistence	22.928	23.520	2.035	0.227	0.383	0.579	0.016	0.014	0.015	0.019	0.023	0.146	1.882	1.930
26/12/98	PFM	26.134	25.699	0.599	0.205	0.322	0.577	0.073	0.094	0.105	0.117	0.127	0.248	0.786	0.740
26/12/98	UKMML	54.680	25.699	0.845	0.285	0.652	0.694	0.083	0.091	0.096	0.099	0.101	0.108	0.893	0.740
26/12/98	UKMMC	8.503	25.699	0.487	0.032	0.051	0.816	0.003	0.004	0.005	0.008	0.008	0.009	0.175	0.740
26/12/98	nowcast	28.124	25.699	0.614	0.290	0.476	0.609	0.112	0.153	0.187	0.211	0.230	0.234	0.758	0.740
26/12/98	persistence	25.605	25.699	0.620	0.187	0.307	0.582	0.080	0.094	0.103	0.112	0.118	0.197	0.688	0.740
	PFM	*23.692*	*25.848*	*1.223*	*0.240*	*0.394*	*0.550*	*0.100*	*0.117*	*0.133*	*0.149*	*0.170*	*0.281*	*1.208*	*1.272*
	UKMML	*52.698*	*25.848*	*1.220*	*0.285*	*0.701*	*0.666*	*0.062*	*0.080*	*0.096*	*0.112*	*0.126*	*0.102*	*0.851*	*1.272*
	UKMMC	*5.650*	*25.848*	*0.734*	*0.026*	*0.065*	*0.861*	*0.003*	*0.004*	*0.006*	*0.009*	*0.013*	*0.010*	*0.124*	*1.272*
	nowcast	*28.257*	*25.848*	*1.384*	*0.252*	*0.405*	*0.622*	*0.058*	*0.083*	*0.102*	*0.116*	*0.128*	*0.194*	*1.309*	*1.272*
	persistence	*25.617*	*25.848*	*1.344*	*0.237*	*0.425*	*0.552*	*0.099*	*0.111*	*0.126*	*0.140*	*0.159*	*0.284*	*1.252*	*1.272*

Table 4.1 *Summary of performance statistics for the five models in both the perfect and real-time runs of the December 1998 event. The performance statistics are averaged over each day of the event and additionally the average for the whole event is shown at the bottom of each model run in italics. The best performance is highlighted in green. These statistics relate to the PFM, nowcasts and persistence having a lead-time of one hour.*

The PFM made an inauspicious start to this wintertime event with its results for the 24th showing a tendency to under-predict rainfall coverage and over-predict rainfall rate. Contributing to this under-prediction of rainfall area was the UKMM's lack of upper-level high relative humidity at the leading edge of the main rain band and within the vicinity of the narrower band of lighter rain to the east of it. Additionally the UKMM vertical winds in these same areas often showed profiles of predominantly downward motion. The persistence method had the best average rainfall rate, rainfall coverage and perfect-run CSI for that day, which attests to the front's retardation at the land-sea interface. The CSI of the real-time UKMML interestingly exceeded that produced by the perfect UKMML data and also that of persistence, but managed the latter mainly through a high POD that came from predicting virtually double the observed rainfall area. The UKMMC scored the lowest RMSE and this trend was found to continue through all events, a pattern that seemed particularly related to the prediction of low rainfall rates and also probably related to the generally high FAR registered by all models in all events, together suggesting that in terms of RMSE it was

better to predict no rain at all rather than to produce forecasts of the calibre shown by the other models. It is debatable whether such an outcome from a performance measure is desirable when it is intended to differentiate the value offered by models in flood forecasting applications, but it at least highlights the merit in considering a range of performance measures if trying to select between models. Of all the forecasting techniques recording similar rainfall rates, the PFM produced the best RMSE.

Spatial and temporal consistency in the location of rainfall intensification assisted the persistence method in achieving the highest average correlation coefficient at all scales, with the PFM closely following and actually exceeding persistence for the majority of the nine hours of forecasting on the 24th. One of the principal reasons for developing the PFM was to try to incorporate elements of storm development and decay which might otherwise be missed using simple advection or persistence forecasting techniques, so it is of interest to look at the evolution of rain field size and rainfall intensity as the storm progressed (Figure 4.4). The stationary nature of the rain band and comparatively good correlation of the rain field from hour to hour meant that the main advection procedure implemented by the PFM was that of persistence. The absence of storm movement in the PFM, resulting in a failure to introduce more rain into the assessment domain during the initial stages of the event, combined with a lack of forecasted upper-level high relative humidity in the advancing sections of the front, meant that nowcasting was better positioned to achieve the perceived "growth" in the storm, or rather the arrival of rain into the domain, and better able to emulate the associated trends in rainfall intensities. The UKMML showed skill in predicting the increase in rainfall coverage but was slow to introduce decay, as were all the models. The PFM's rainfall coverage came generally closest to the observed coverage during the storm's declining phase but at the same time tended toward a higher rainfall rate than any of the other models.

The PFM was again inclined to under-predict rainfall coverage on the 25th but this time under-predicted rainfall rate as well. However, as can be seen from Figure 4.5, the under-prediction of rainfall coverage is only significant for one out of the nine forecasts, at five hours after commencement of predictions. It can also be seen from Figure 4.5 that the PFM managed to forecast the initial growth in rainfall at hour four but failed to emulate the even greater increase in the following hour. This occurred for much the same reasons given in explanation for the failure to predict growth on the 24th, a lack of UKMM upper-level high relative humidity in the top half of the more northern rain band and the PFM's stagnation of the rain field. At hour seven, the PFM fairly successfully predicted the downward turn in the extent and intensity of the storm, the predicted rain field for that hour shown in Figure 4.6. The positioning of the rain field needed slight improvement however, likewise the definition and location of the areas of more intense rainfall, but the discrepancies did not prevent the PFM from achieving the highest correlation

coefficient for that hour (Figure 4.7). Overall, correlation for the real-time PFM forecasts on the 25th came second to nowcasting, although given perfect data, the PFM scored highest at the 5km range and also nearest neighbours and, as can be seen in Figure 4.7, even with real-time forecasts the PFM had the higher correlation at the 5km scale for all but two hours. Apart from UKMMC and UKMML (except not the latter for the perfect run), the PFM scored the lowest RMSE for the day, registered the lowest FAR of all models and was second only to UKMML with respect to CSI and POD. The UKMML again, as on the 24th, over-predicted rainfall coverage by almost 100% and under-predicted rainfall rate similarly.

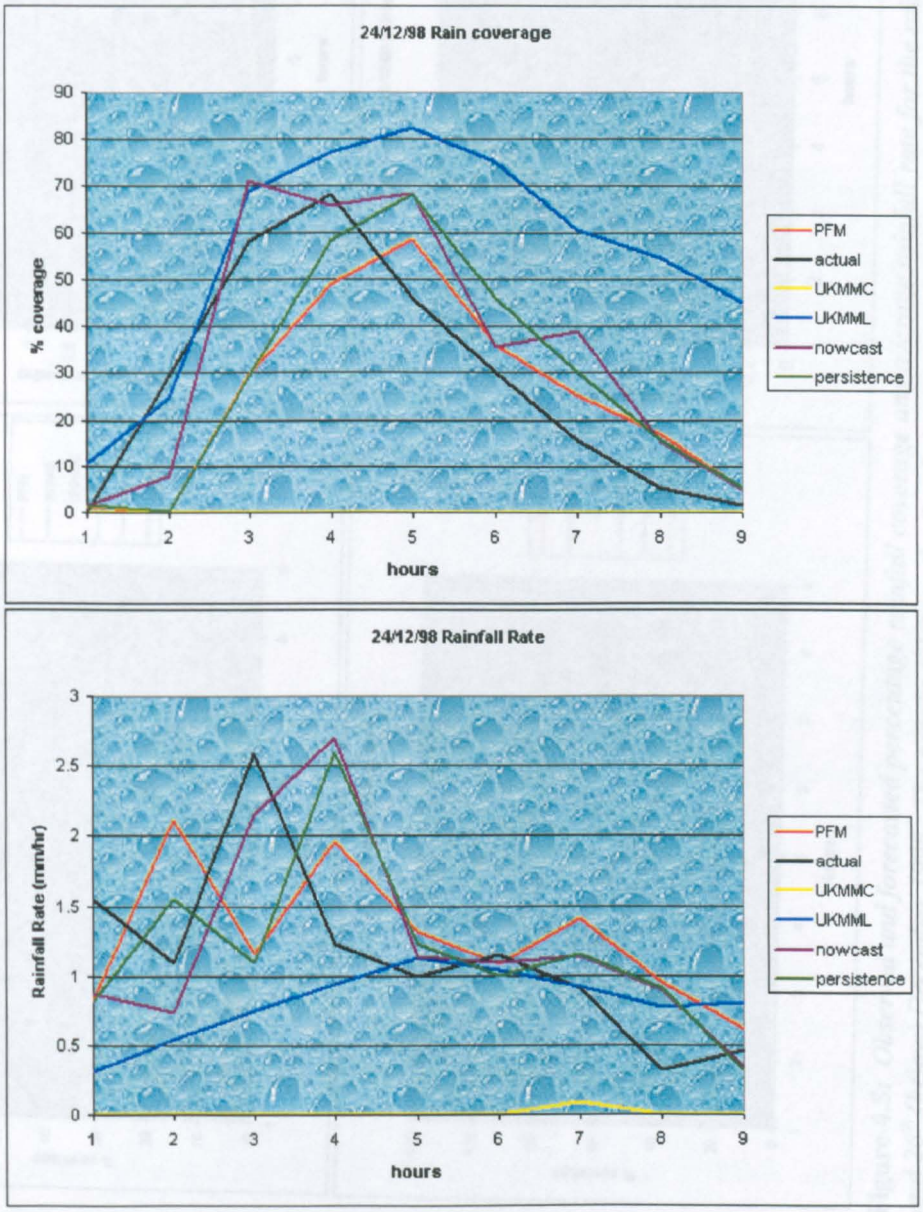

Figure 4.4: *Observed and forecasted percentage rainfall coverage and average rainfall rate for the rainfall event on the 24th December 1998. The graphs relate to the "real-time" run and a one-hour forecast lead-time, with "hours" on the horizontal axis referring to the number of hours (or the number of the forecast) since the event began.*

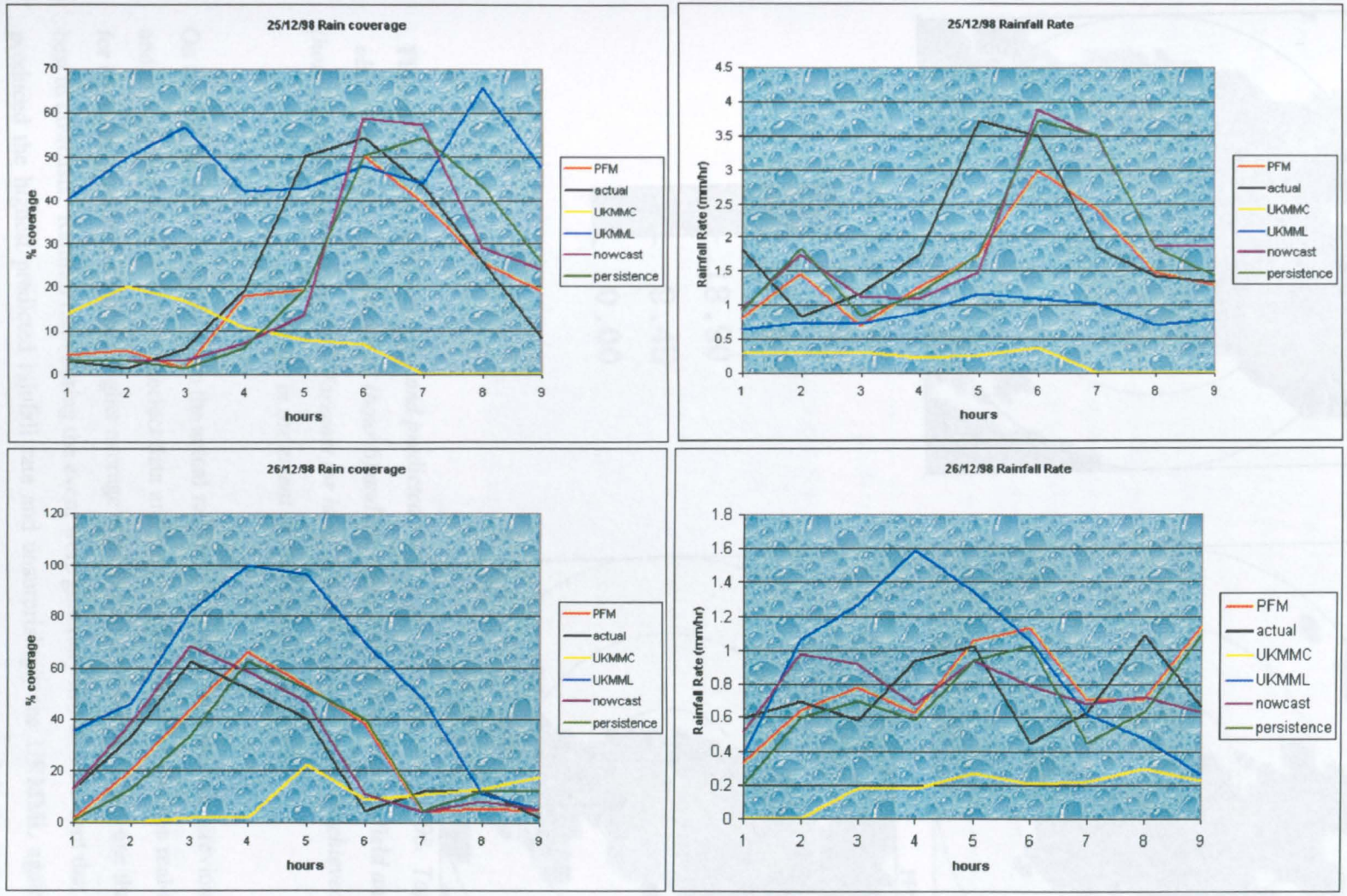

Figure 4.5: *Observed and forecasted percentage rainfall coverage and average rainfall rate for the rainfall events on the 25th (top) and 26th (below) December 1998. The graphs relate to the "real-time" run and a one-hour forecast lead-time, with "hours" on the horizontal axis referring to the number of hours (or the number of the forecast) since the event began.*

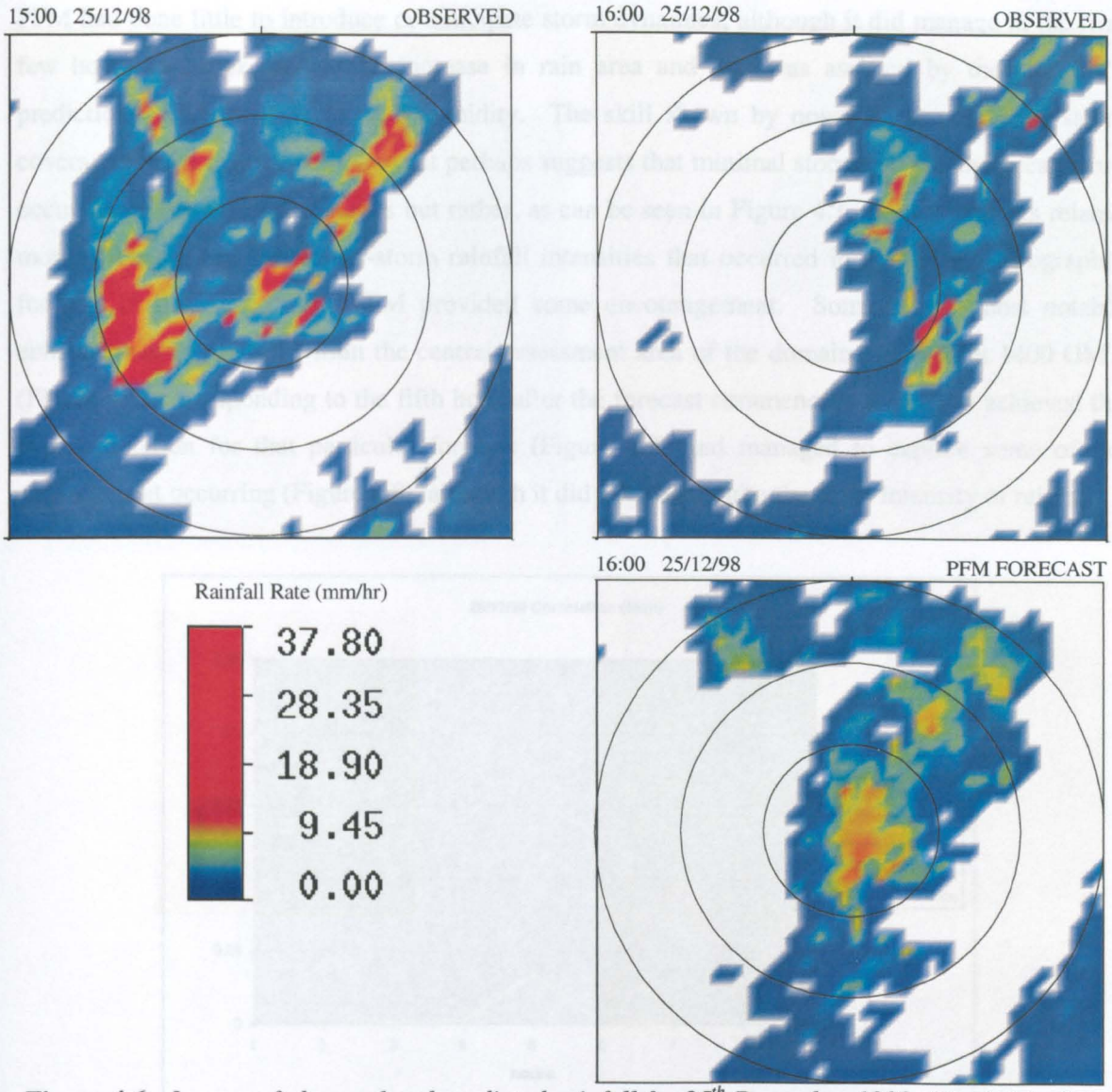

Figure 4.6: *Images of observed and predicted rainfall for 25th December 1998. Top left is the observed rain field at 1500 GMT (hour 6) and top right is the observed rain field an hour later (hour 7). Below right is the PFM forecast for hour 7, which appears to have achieved some of the decrease in the extent of the original rain field.*

On the 26th the PFM came closer to the actual rainfall coverage than it had the previous two days, it under-predicted slightly with the perfect data and over-predicted slightly for the real-time data, but for both sets produced a slightly higher average rainfall rate than observed and one that was second best to nowcasts. Rainfall rates during the event were generally low to the extent that the UKMML produced the highest predicted rainfall rate and unsurprisingly the UKMML again doubled the observed rainfall coverage. The best CSI and area-averaged correlations were achieved by nowcasts, followed by the PFM (except 5km correlations), but the PFM attained the greater nearest neighbour correlation suggesting the forecasts were "thereabouts" in terms of relative performance. The results of the PFM largely mirrored persistence throughout the event (Figure 4.5) and thus the

PFM had done little to introduce or anticipate storm dynamics, although it did manage in the first few hours to better predict the increase in rain area and this was assisted by the UKMM's predictions of upper-level relative humidity. The skill shown by nowcasts in emulating storm coverage for the majority of the event perhaps suggests that minimal storm growth and decay were occurring at the storm peripheries but rather, as can be seen in Figure 4.1, storm dynamics related more to changes of the within-storm rainfall intensities that occurred in response to orographic forcing. In that respect the PFM provided some encouragement. Some of the most notable enhancement of rainfall within the central assessment area of the domain occurred at 1400 GMT (Figure 4.1) corresponding to the fifth hour after the forecast commenced. The PFM achieved the best correlation for that particular forecast (Figure 4.7) and managed to capture some of the enhancement occurring (Figure 4.8), although it did not attain quite the same intensity of rainfall.

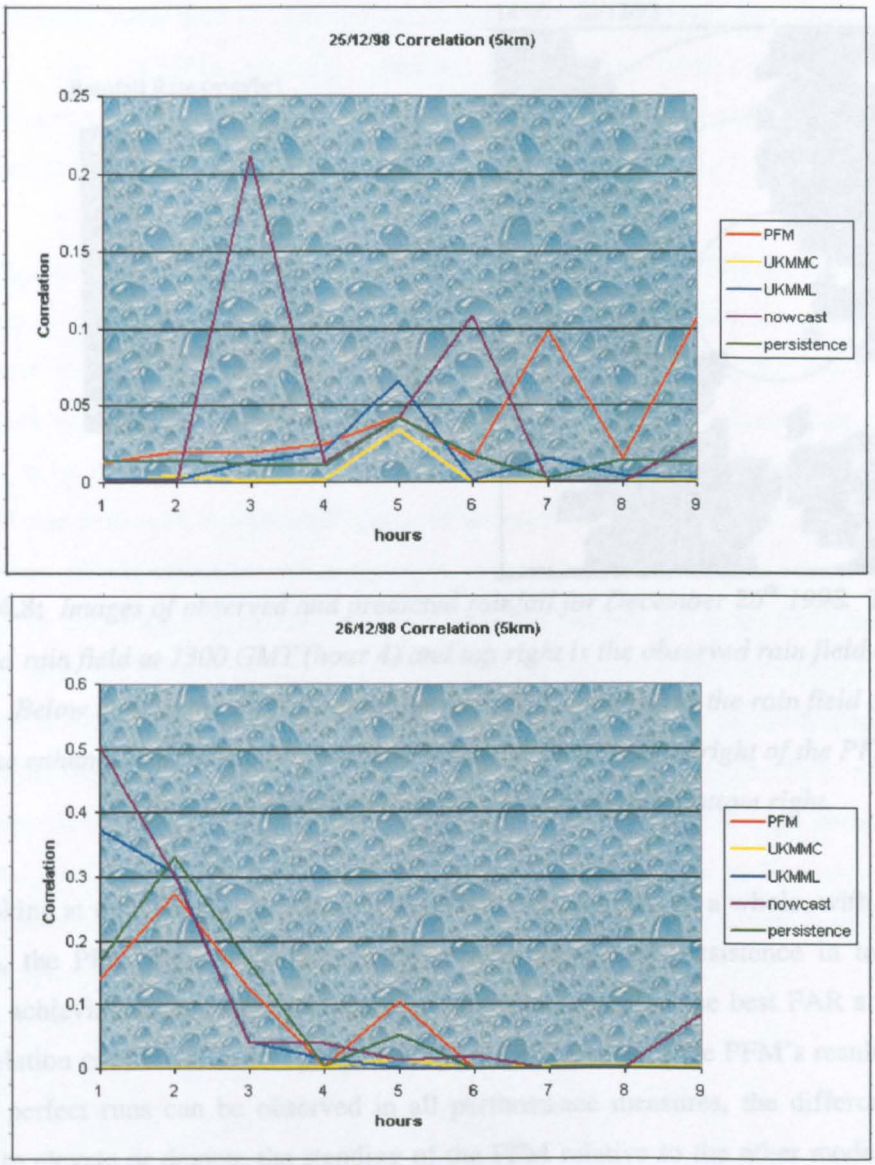

Figure 4.7: *The correlation between forecasts and observed rainfall at the 5km scale for 25th December 1998 (top) and 26th December 1998 (bottom), using real-time data.*

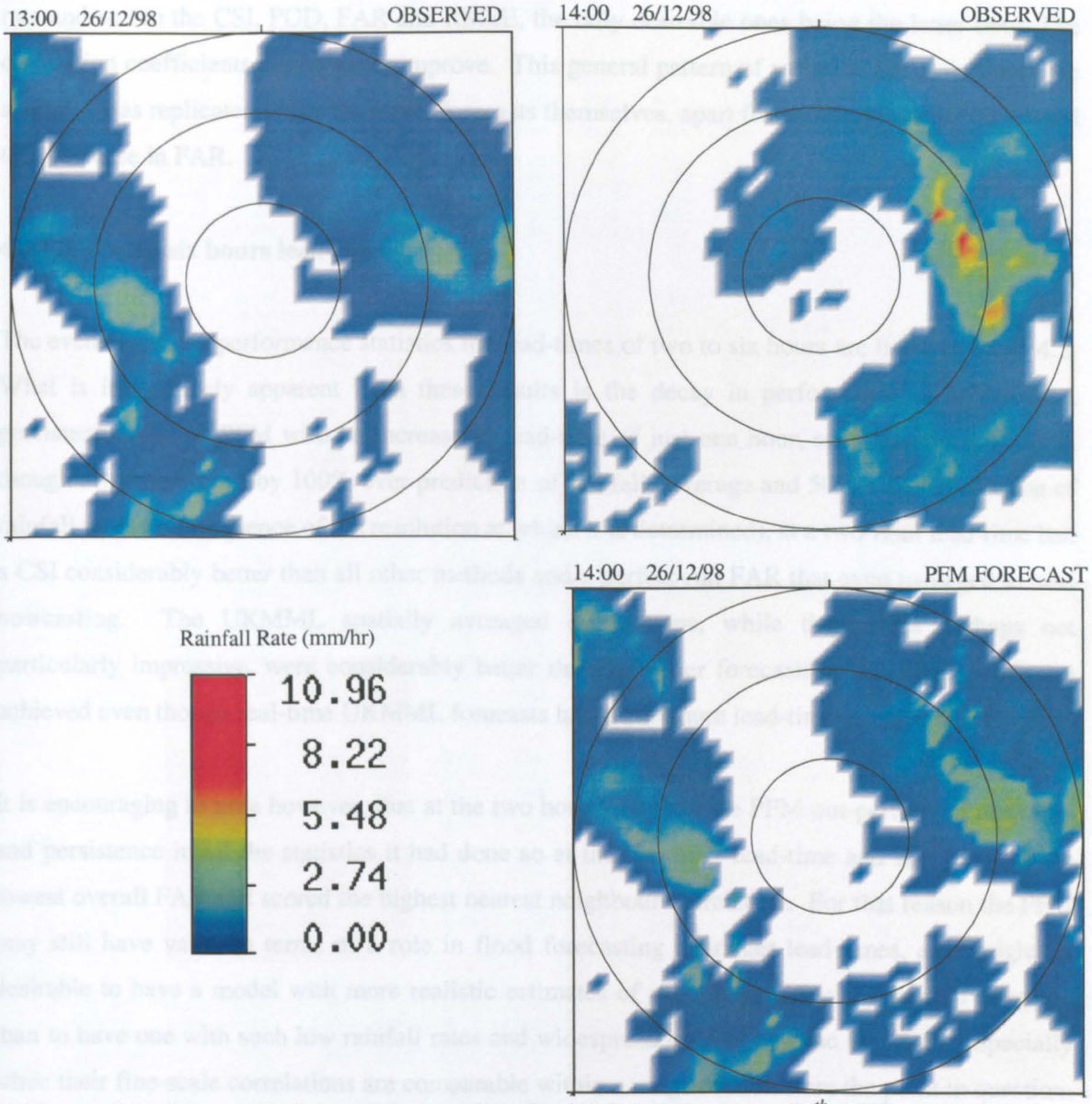

Figure 4.8: *Images of observed and predicted rainfall for December 26th 1998. Top left is the observed rain field at 1300 GMT (hour 4) and top right is the observed rain field an hour later (hour 5). Below right is the PFM forecast for hour 5. Compared to the rain field of the previous hour, some enhancement of rainfall intensity occurs towards middle right of the PFM forecast and there is also some development of the rain cells bottom right.*

When looking at the average performance statistics for the event as a whole, with respect to real-time data, the PFM fares reasonably well, coming second to persistence in terms of rainfall coverage, achieving a better RMSE than persistence or nowcasts, the best FAR and generally the best correlation coefficient at all spatial averages. Differences in the PFM's results between real-time and perfect runs can be observed in all performance measures, the differences having the potential to elevate or demote the standing of the PFM relative to the other models. With use of perfect data, the forecast of rainfall coverage had a tendency to decrease, as did the average rainfall

rate and so too the CSI, POD, FAR and RMSE, the only desirable ones being the latter two. The correlation coefficients did however improve. This general pattern of variation in the performance statistics was replicated in the UKMML forecasts themselves, apart from an increase in CSI related to a decrease in FAR.

4.3.1.2 Two to six hours lead-time

The event averaged performance statistics for lead-times of two to six hours are listed in Table 4.2. What is immediately apparent from these results is the decay in performance of nowcasting, persistence and the PFM with an increase in lead-time of just one hour, such that the UKMML, though always plagued by 100% over-prediction of rainfall coverage and 50% under-prediction of rainfall rate (a consequence of the resolution at which it is determined), at a two-hour lead-time had a CSI considerably better than all other methods and a perfect-run FAR that even managed to beat nowcasting. The UKMML spatially averaged correlations, while themselves perhaps not particularly impressive, were considerably better than the other forecasting techniques and were achieved even though real-time UKMML forecasts had a minimum lead-time of three hours.

It is encouraging to note however, that at the two hour lead-time the PFM out-performed nowcasts and persistence in all the statistics it had done so at the one hour lead-time and still retained the lowest overall FAR and scored the highest nearest neighbour correlation. For that reason the PFM may still have value in terms of a role in flood forecasting at longer lead-times, as it might be desirable to have a model with more realistic estimates of rainfall intensity and rainfall coverage than to have one with such low rainfall rates and widespread coverage as the UKMML, especially when their fine-scale correlations are comparable within a range of 5km from the point in question. The pattern in correlation statistics continued over all lead-times apart from that of 5 hours. Beyond two hours the PFM consistently had a higher CSI than nowcasting and persistence and also became more competitive in estimating average rainfall rate and rainfall coverage, nowcasting in particular dropping dramatically in that respect and with it its RMSE. The PFM still managed to attain a better RMSE than persistence, the latter being the only method with comparable rainfall coverage and rainfall rate as the lead-time increased. The respectable performance of persistence throughout, relative to nowcasting and the PFM, owed much to the retardation of the front at the land-sea interface and over hills.

		%cov_for	%cov_act	RMSE	CSI	POD	FAR	cc5km	cc10km	cc15km	cc20km	cc25km	ccNN	rate_for	rate_act
2 hour															
Perfect															
	PFM	23.415	28.385	1.469	0.169	0.326	0.587	0.025	0.035	0.048	0.061	0.074	0.147	1.226	1.266
	UKMML	53.324	28.385	1.303	0.314	0.694	0.618	0.059	0.078	0.096	0.116	0.133	0.098	0.860	1.266
	UKMMC	3.179	28.385	0.804	0.010	0.040	0.893	0.001	0.001	0.001	0.002	0.003	0.005	0.087	1.266
	nowcast	26.545	28.385	1.681	0.181	0.300	0.620	0.019	0.026	0.031	0.034	0.039	0.088	1.260	1.266
	persistence	27.008	28.385	1.698	0.145	0.347	0.589	0.015	0.019	0.027	0.037	0.048	0.111	1.290	1.266
Real-time															
	PFM	24.495	28.385	1.492	0.174	0.336	0.597	0.025	0.034	0.047	0.059	0.072	0.152	1.256	1.266
	UKMML	55.917	28.385	1.328	0.305	0.712	0.641	0.054	0.073	0.091	0.109	0.125	0.093	0.902	1.266
	UKMMC	5.780	28.385	0.806	0.028	0.087	0.846	0.003	0.004	0.006	0.010	0.014	0.010	0.128	1.266
	nowcast	26.545	28.385	1.681	0.181	0.300	0.620	0.019	0.026	0.031	0.034	0.039	0.088	1.260	1.266
	persistence	27.008	28.385	1.698	0.145	0.347	0.589	0.015	0.019	0.027	0.037	0.048	0.111	1.290	1.266
3 hour															
Perfect															
	PFM	26.396	29.384	1.667	0.127	0.306	0.642	0.021	0.032	0.044	0.057	0.070	0.081	1.257	1.322
	UKMML	55.188	29.384	1.383	0.317	0.696	0.620	0.052	0.073	0.093	0.114	0.132	0.092	0.871	1.322
	UKMMC	2.675	29.384	0.845	0.010	0.015	0.880	0.001	0.001	0.002	0.002	0.003	0.005	0.086	1.322
	nowcast	22.908	29.384	1.720	0.124	0.248	0.708	0.005	0.006	0.008	0.010	0.013	0.028	1.089	1.322
	persistence	27.494	29.384	1.901	0.087	0.299	0.677	0.010	0.017	0.025	0.035	0.045	0.056	1.314	1.322
Real-time															
	PFM	28.636	29.384	1.691	0.150	0.353	0.631	0.020	0.032	0.044	0.056	0.072	0.095	1.243	1.322
	UKMML	58.153	29.384	1.411	0.306	0.717	0.646	0.047	0.067	0.086	0.106	0.123	0.086	0.919	1.322
	UKMMC	6.606	29.044	0.845	0.032	0.076	0.823	0.003	0.005	0.007	0.011	0.016	0.012	0.146	1.298
	nowcast	22.908	29.384	1.720	0.124	0.248	0.708	0.005	0.006	0.008	0.010	0.013	0.028	1.089	1.322
	persistence	27.494	29.384	1.901	0.087	0.299	0.677	0.010	0.017	0.025	0.035	0.045	0.056	1.314	1.322
4 hour															
Perfect															
	PFM	25.032	27.227	1.573	0.122	0.327	0.632	0.025	0.037	0.049	0.062	0.073	0.096	1.180	1.301
	UKMML	54.759	27.227	1.346	0.289	0.691	0.654	0.052	0.076	0.097	0.120	0.141	0.091	0.896	1.301
	UKMMC	3.011	27.227	0.760	0.011	0.017	0.878	0.001	0.001	0.002	0.002	0.003	0.005	0.091	1.301
	nowcast	16.969	27.227	1.519	0.087	0.188	0.743	0.005	0.008	0.011	0.015	0.020	0.031	0.905	1.301
	persistence	27.138	27.227	1.803	0.070	0.323	0.653	0.009	0.009	0.011	0.013	0.016	0.048	1.249	1.301
Real-time															
	PFM	27.979	27.227	1.662	0.128	0.356	0.650	0.021	0.028	0.038	0.046	0.056	0.090	1.234	1.301
	UKMML	56.352	27.227	1.372	0.284	0.695	0.668	0.046	0.068	0.089	0.110	0.128	0.083	0.921	1.301
	UKMMC	5.556	27.227	0.760	0.033	0.045	0.817	0.004	0.005	0.008	0.013	0.018	0.012	0.129	1.301
	nowcast	16.969	27.227	1.520	0.087	0.188	0.743	0.005	0.008	0.011	0.015	0.020	0.031	0.905	1.301
	persistence	27.138	27.227	1.804	0.070	0.323	0.653	0.009	0.009	0.011	0.013	0.016	0.048	1.249	1.301
5 hour															
Perfect															
	PFM	22.079	23.420	1.599	0.094	0.262	0.634	0.007	0.009	0.010	0.013	0.016	0.059	1.187	1.301
	UKMML	53.005	23.420	1.334	0.256	0.687	0.696	0.041	0.064	0.084	0.106	0.125	0.081	0.854	1.301
	UKMMC	3.485	23.420	0.710	0.011	0.018	0.906	0.001	0.002	0.002	0.003	0.004	0.005	0.097	1.301
	nowcast	14.184	23.420	1.412	0.047	0.133	0.890	0.001	0.002	0.004	0.006	0.009	0.009	0.629	1.301
	persistence	23.484	23.420	1.646	0.058	0.255	0.621	0.004	0.004	0.005	0.007	0.010	0.039	1.118	1.301
Real-time															
	PFM	23.084	23.420	1.589	0.109	0.287	0.622	0.010	0.014	0.018	0.025	0.032	0.069	1.177	1.301
	UKMML	53.012	23.420	1.355	0.259	0.691	0.694	0.043	0.066	0.087	0.108	0.126	0.079	0.878	1.301
	UKMMC	5.824	23.420	0.709	0.033	0.045	0.846	0.004	0.006	0.010	0.015	0.022	0.013	0.129	1.301
	nowcast	14.184	23.420	1.412	0.047	0.133	0.890	0.001	0.002	0.004	0.006	0.009	0.009	0.629	1.301
	persistence	23.484	23.420	1.647	0.058	0.255	0.621	0.004	0.004	0.005	0.007	0.010	0.039	1.118	1.301
6 hour															
Perfect															
	PFM	16.742	17.923	1.268	0.067	0.193	0.702	0.014	0.020	0.027	0.037	0.049	0.069	1.051	1.149
	UKMML	47.813	17.923	1.156	0.196	0.648	0.764	0.035	0.058	0.079	0.100	0.118	0.082	0.796	1.149
	UKMMC	3.808	17.923	0.543	0.008	0.017	0.971	0.001	0.001	0.001	0.002	0.002	0.006	0.095	1.149
	nowcast	9.751	17.923	1.171	0.017	0.099	0.950	0.000	0.001	0.001	0.002	0.002	0.007	0.454	1.149
	persistence	17.791	17.923	1.330	0.039	0.180	0.678	0.008	0.009	0.013	0.019	0.026	0.026	1.072	1.149
Real-time															
	PFM	16.556	17.923	1.317	0.073	0.207	0.691	0.015	0.022	0.031	0.043	0.058	0.074	1.107	1.149
	UKMML	47.813	17.923	1.156	0.196	0.648	0.764	0.035	0.058	0.079	0.100	0.118	0.082	0.796	1.149
	UKMMC	4.790	17.923	0.543	0.018	0.028	0.910	0.001	0.001	0.002	0.002	0.002	0.006	0.118	1.149
	nowcast	9.751	17.923	1.171	0.017	0.099	0.950	0.000	0.001	0.001	0.002	0.002	0.007	0.454	1.149
	persistence	17.791	17.923	1.330	0.039	0.180	0.678	0.008	0.009	0.013	0.019	0.026	0.026	1.072	1.149

Table 4.2: *Summary of the average performance statistics for the December 1998 event for both the perfect and real-time runs and from two hours to six hours lead-time. The best performance for each particular statistic is highlighted in green.*

4.3.2 January 1999

Conditions on the 14th and 15th January were fairly typical of the unsettled weather that affected much of the UK at various times between the 13th and 20th January, conditions not unlike those experienced during the December 1998 event. The dominant feature throughout the two days was a low-pressure system centred to the northwest of the UK, which progressively deepened and, as it did, an increasing number of fronts evolved within it bringing periods of heavy rain over much of

the country. The general synoptic conditions at 1200 GMT on the 14th and 15th of January are shown in Figure 4.9 and examples of the rainfall on each day are given in Figure 4.10.

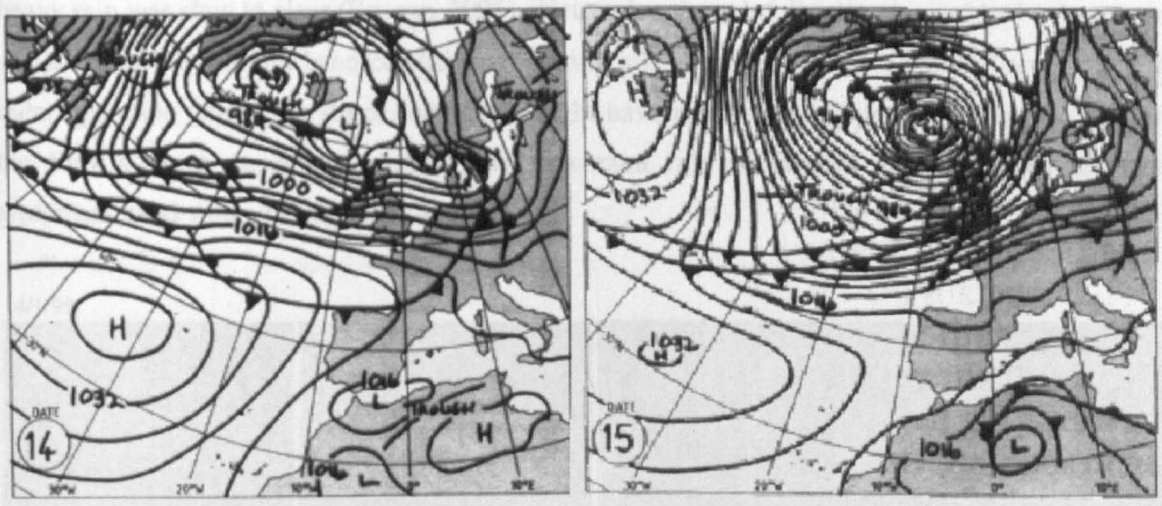

Figure 4.9: *Synoptic conditions at 1200 GMT for the 14th and 15th January 1999 (Eden, 1999b).*

Following a bright start to the morning of the 14th, cloud and rain swept into western England as an occluded front moved eastward across the country and by 0900 GMT rain had started falling within the area of the PFM domain. The band of rain moved across the region during the seven hours that followed but by 1800 GMT it had largely dissipated, although it was not until the storm's latter stages, when the rain cells began to disband, that the day's peak rainfall rate of 22 $mmhr^{-1}$ was recorded. In Scotland temperatures were cold enough for the rain to fall as snow and over northern areas of the PFM's domain the UKMM's estimates of the freezing level fell to 320m during the initial hours of the event. Winds were strong, UKMM surface winds reaching up to gale force and, along western coasts, were directed mainly from the southwest while inland they turned from westerly to southwesterly as the front neared. They changed again as the front passed, the wind field across the whole domain becoming westerly by the event's end. Upper-level winds veered to the right and were for the most part northwesterly, a direction more in keeping with the south-eastward movement of the rain field. As in the December event, the role of topography was to slow movement of the rain field and to expand and intensify rainfall, with isolated showers lingering over high ground after the main band of rain had cleared.

Rainfall started earlier in the day on the 15th and lasted longer, commencing at approximately 0600 GMT and continuing until 0600 GMT the following day as consecutive fronts with accompanying rain bands crossed the UK. Winds were gale force and mostly southwesterly, but turned westerly to northwesterly within the vicinity of fronts. Upper-level winds, in contrast, remained mostly southwesterly throughout and exhibited variable shear as surface winds shifted direction. Similar to the previous day, rain bands approached from the west or northwest and pushed across and down

the country towards the southeast. Also similar was the effect of elevated terrain on rainfall rates and frontal movement, the result of which was between 50 and 70 mm of rain falling over the mountains of North Wales on the 15th and flooding in the Midlands and Southern Wales where heavy rain was slow to clear (Brugge, 2001). Network radar rainfall estimates reached a maximum of 126 $mmhr^{-1}$ but bright band conditions (freezing level possibly as low as 220m) or vagaries in radar operation during the storm conditions might have produced the high measurement. Within the PFM's inner assessment domain the maximum rate of rainfall was less than half the aforementioned value, peaking at 50$mmhr^{-1}$.

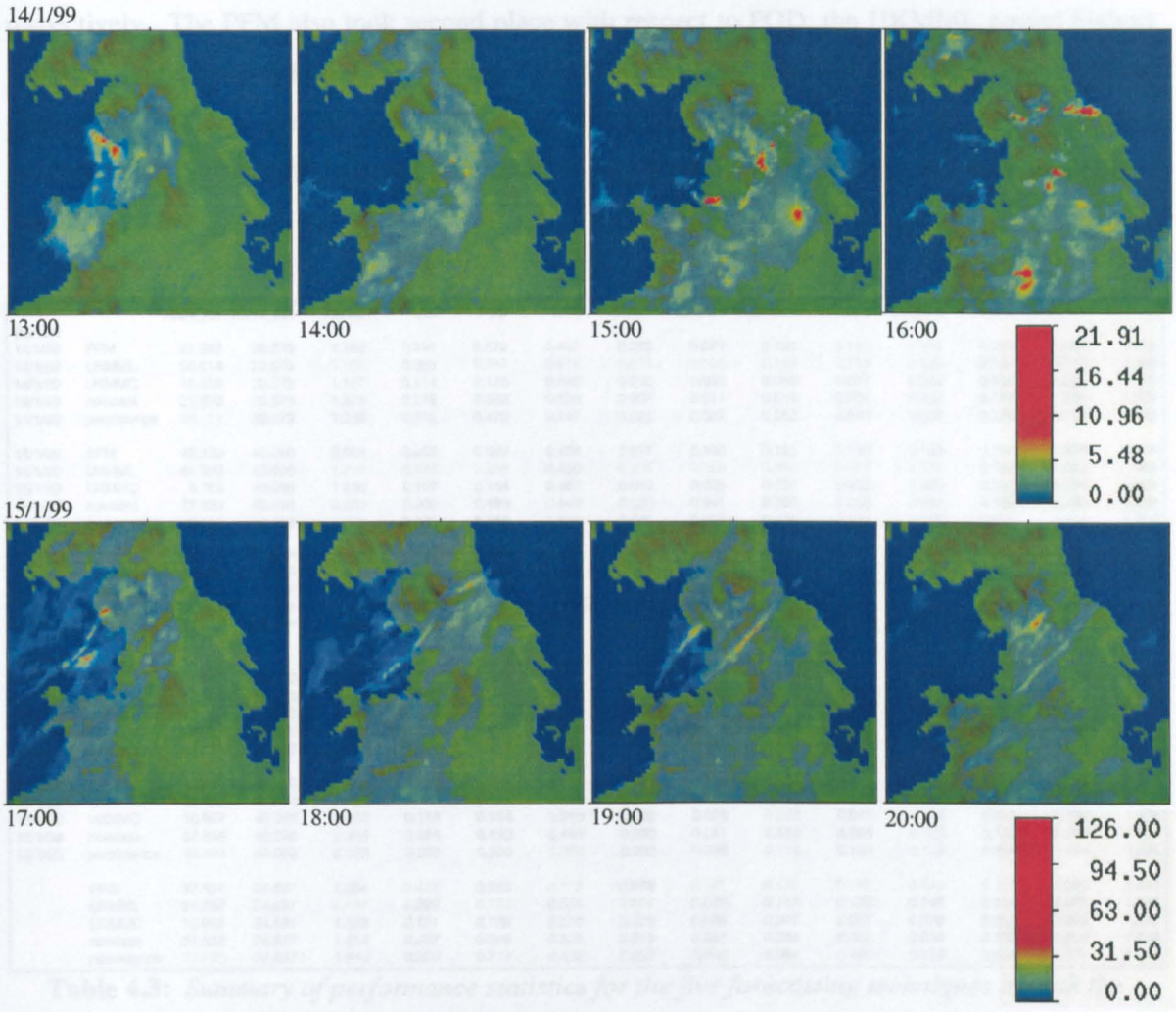

Figure 4.10: *Four consecutive hourly images of rainall for each day of the January 1999 event: 14th (top) and 15th (bottom). Below right of each set of images is the legend showing rainfall rates in $mmhr^{-1}$ and below left of each individual image is the time to which it corresponds.*

4.3.2.1 One hour lead-time

Results from each of the five forecasting techniques with respect to a lead-time of one hour (UKMML and UKMMC of variable lead-time) are presented in Table 4.3 as daily averages and overall event averages. The PFM performed comparatively well on the 14th, more so with real-time data as opposed to perfect data. With use of the former it achieved the best CSI, FAR and correlation coefficient on all scales. It produced the second best average rainfall coverage, behind persistence, but over-estimated it by almost 8%, a figure reduced using perfect data but seemingly at the expense of correctly identified rain cells, as CSI and FAR decreased and increased respectively. The PFM also took second place with respect to POD, the UKMML scored highest with double the observed rainfall coverage. UKMMC forecasts had the lowest RMSE, continuing the pattern that arose in the December case study, whilst the PFM had a lower RMSE than persistence and nowcasting, a result unfortunately tarnished by its comparatively low estimation of rainfall rate.

		%cov_for	%cov_act	RMSE	CSI	POD	FAR	cc5km	cc10km	cc15km	cc20km	cc25km	ccNN	rate_for	rate_act
Perfect															
14/1/99	PFM	31.822	29.579	1.182	0.396	0.572	0.407	0.055	0.079	0.101	0.132	0.168	0.289	1.093	1.388
14/1/99	UKMML	56.614	29.579	1.104	0.359	0.752	0.614	0.074	0.089	0.103	0.116	0.130	0.137	0.719	1.388
14/1/99	UKMMC	15.319	29.579	1.117	0.114	0.176	0.640	0.030	0.043	0.058	0.077	0.099	0.058	0.207	1.388
14/1/99	nowcast	25.529	29.579	1.325	0.219	0.302	0.606	0.007	0.011	0.016	0.024	0.033	0.116	1.205	1.388
14/1/99	persistence	27.721	29.579	1.355	0.312	0.472	0.447	0.025	0.037	0.052	0.076	0.107	0.229	1.251	1.388
15/1/99	PFM	42.139	40.096	2.004	0.405	0.589	0.438	0.077	0.100	0.121	0.142	0.163	0.329	1.628	1.904
15/1/99	UKMML	64.399	40.096	1.779	0.476	0.846	0.480	0.105	0.129	0.151	0.173	0.195	0.195	1.085	1.904
15/1/99	UKMMC	9.765	40.096	1.936	0.107	0.144	0.467	0.019	0.025	0.031	0.038	0.045	0.038	0.194	1.904
15/1/99	nowcast	37.535	40.096	2.383	0.356	0.493	0.449	0.030	0.041	0.053	0.068	0.083	0.189	1.795	1.904
15/1/99	persistence	39.883	40.096	2.333	0.388	0.550	0.398	0.080	0.098	0.116	0.134	0.152	0.299	1.894	1.904
	PFM	*36.980*	*34.837*	*1.593*	*0.401*	*0.580*	*0.423*	*0.066*	*0.089*	*0.111*	*0.137*	*0.166*	*0.309*	*1.360*	*1.646*
	UKMML	*60.506*	*34.837*	*1.442*	*0.417*	*0.799*	*0.547*	*0.089*	*0.109*	*0.127*	*0.145*	*0.162*	*0.166*	*0.902*	*1.646*
	UKMMC	*12.542*	*34.837*	*1.526*	*0.110*	*0.160*	*0.554*	*0.025*	*0.034*	*0.044*	*0.058*	*0.072*	*0.048*	*0.201*	*1.646*
	nowcast	*31.532*	*34.837*	*1.854*	*0.287*	*0.398*	*0.528*	*0.019*	*0.026*	*0.035*	*0.046*	*0.058*	*0.152*	*1.500*	*1.646*
	persistence	*33.802*	*34.837*	*1.844*	*0.350*	*0.511*	*0.422*	*0.052*	*0.068*	*0.084*	*0.105*	*0.129*	*0.264*	*1.572*	*1.646*
Real-time															
14/1/99	PFM	31.897	29.579	1.163	0.403	0.579	0.401	0.061	0.087	0.111	0.144	0.182	0.314	1.085	1.388
14/1/99	UKMML	61.206	29.579	1.115	0.335	0.770	0.645	0.059	0.072	0.084	0.097	0.112	0.126	0.729	1.388
14/1/99	UKMMC	20.962	29.579	1.113	0.147	0.225	0.640	0.032	0.045	0.061	0.080	0.103	0.059	0.211	1.388
14/1/99	nowcast	25.529	29.579	1.325	0.219	0.302	0.606	0.007	0.011	0.016	0.024	0.033	0.116	1.205	1.388
14/1/99	persistence	27.721	29.579	1.355	0.312	0.472	0.447	0.025	0.037	0.052	0.076	0.107	0.229	1.251	1.388
15/1/99	PFM	43.204	40.096	2.005	0.421	0.597	0.426	0.091	0.114	0.134	0.156	0.178	0.349	1.634	1.904
15/1/99	UKMML	62.757	40.096	1.799	0.457	0.815	0.482	0.097	0.120	0.141	0.164	0.183	0.181	1.063	1.904
15/1/99	UKMMC	10.967	40.096	1.932	0.116	0.154	0.516	0.020	0.026	0.033	0.041	0.048	0.041	0.196	1.904
15/1/99	nowcast	37.535	40.096	2.383	0.356	0.493	0.449	0.030	0.041	0.053	0.068	0.083	0.189	1.795	1.904
15/1/99	persistence	39.883	40.096	2.333	0.388	0.550	0.398	0.080	0.098	0.116	0.134	0.152	0.299	1.894	1.904
	PFM	*37.551*	*34.837*	*1.584*	*0.412*	*0.588*	*0.413*	*0.076*	*0.101*	*0.123*	*0.150*	*0.180*	*0.332*	*1.360*	*1.646*
	UKMML	*61.982*	*34.837*	*1.457*	*0.396*	*0.793*	*0.564*	*0.078*	*0.096*	*0.113*	*0.130*	*0.148*	*0.154*	*0.896*	*1.646*
	UKMMC	*15.965*	*34.837*	*1.523*	*0.131*	*0.189*	*0.578*	*0.026*	*0.036*	*0.047*	*0.061*	*0.075*	*0.050*	*0.203*	*1.646*
	nowcast	*31.532*	*34.837*	*1.854*	*0.287*	*0.398*	*0.528*	*0.019*	*0.026*	*0.035*	*0.046*	*0.058*	*0.152*	*1.500*	*1.646*
	persistence	*33.802*	*34.837*	*1.844*	*0.350*	*0.511*	*0.422*	*0.052*	*0.068*	*0.084*	*0.105*	*0.129*	*0.264*	*1.572*	*1.646*

Table 4.3: *Summary of performance statistics for the five forecasting techniques in both the perfect and real-time runs of the January 1999 event. The performance statistics are averaged over each day of the event and additionally the average for the whole event is shown at the bottom of each run in italics. The best performance is highlighted in green. These statistics relate to the PFM, nowcasts and persistence having a lead-time of one hour.*

When focussing on the temporal changes in the size of the rain field within the assessment domain, it can be seen from the graph of rainfall coverage in Figure 4.11 that the PFM was marginally

better than the other techniques in anticipating the initial growth in the rain field between hours two and three, although its forecast at hour three fell well short of the actual increase observed. CSI values (Figure 4.11) for hours three and four suggested the PFM's predicted expansion of the rain area was well located and this is supported by the apparent visual correspondence between the actual and predicted fields displayed in Figure 4.12. Beyond hour four however the PFM appeared to lack any rain field development, seeming to shadow nowcasts until persistence became the preferred advection option, so that in the final hours of the event the PFM not only showed little evidence of detecting storm decay but also missed the movement of rain cells out of the assessment domain. The PFM's overestimation of rainfall coverage, which exceeded the forecasts of all other methods except UKMML, occurred only in the final three hours. A visual inspection of the UKMM's 600mb relative humidity fields revealed that, up to the fifth hour, these areas coincided well with the observed rain field. Beyond that time the ≥90% humidity areas tended to lag behind the main rain band and the PFM responded by producing an amount of rain in those areas in addition to within the existing rain field. The PFM rainfall rate mostly tracked persistence and nowcasts throughout but still failed to attain the observed peaks in rainfall intensity.

Similar to the results of the 14th, the PFM performed better on the 15th using real-time rather than perfect data. Similar too was the tendency to over-predict rainfall coverage and under-predict rainfall rate for both runs. With respect to the real-time run, persistence achieved the best rainfall coverage and the best average rainfall rate, with the PFM this time trailing third behind nowcasts for both performance measures. The UKMML scored the best CSI and POD and the best correlation coefficients at all scales. The PFM had a better CSI and POD than nowcasts and persistence and also better correlation coefficients, as well as having the greatest nearest neighbour correlation of all methods. While the PFM's statistical performance, relative to the other methods, was not as good as it was the previous day there were still encouraging signs that it was able to better predict some of the early expansion in rain area. This can be discerned from the graph of rainfall coverage (Figure 4.13), where on the rising limbs of the curve representing observed rain coverage the PFM often gave the closer approximation, particularly at hours two, three, ten, eleven, seventeen and nineteen, a pattern mostly reflected in the graph of CSI (Figure 4.13). It was not so skilled however in forecasting decreases in storm extent nor in emulating the observed rainfall rates. With respect to the former, this was generally not through a failure by the UKMM to reduce the extent of the upper-level high relative humidity, but more often due to these areas being, at times, slightly offset from the observed rain field.

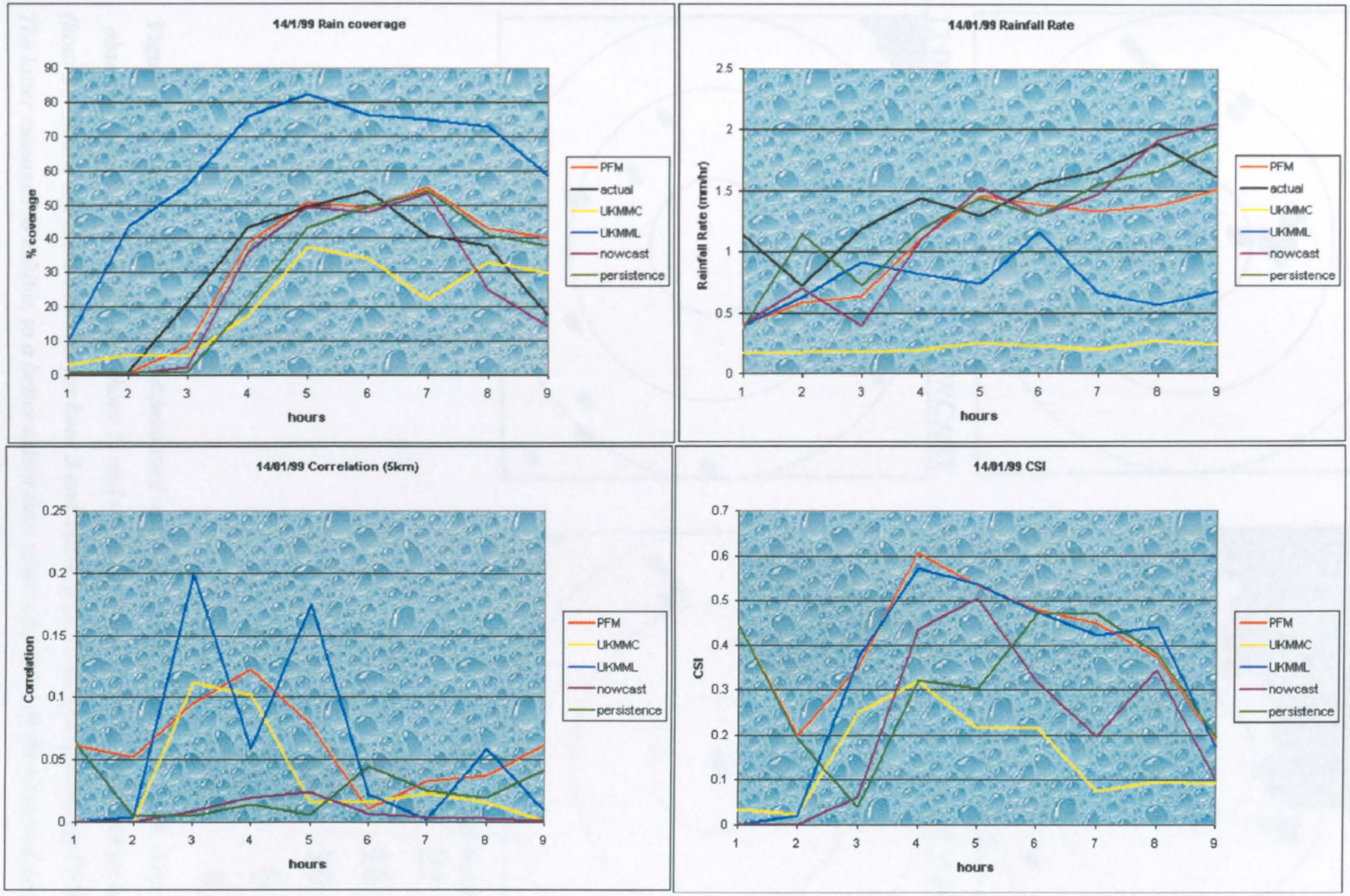

Figure 4.11: *Observed and forecasted percentage rainfall coverage (top left) and rainfall rate (top right), correlation coefficient at the 5 km scale (bottom left) and the CSI (bottom right) for the 14th January 1999 event. All graphs relate to the real-time run and a lead-time of one hour for persistence, nowcasts and the PFM. Labelled along the horizontal axis are the number of hours (or the number of the forecast) after the event*

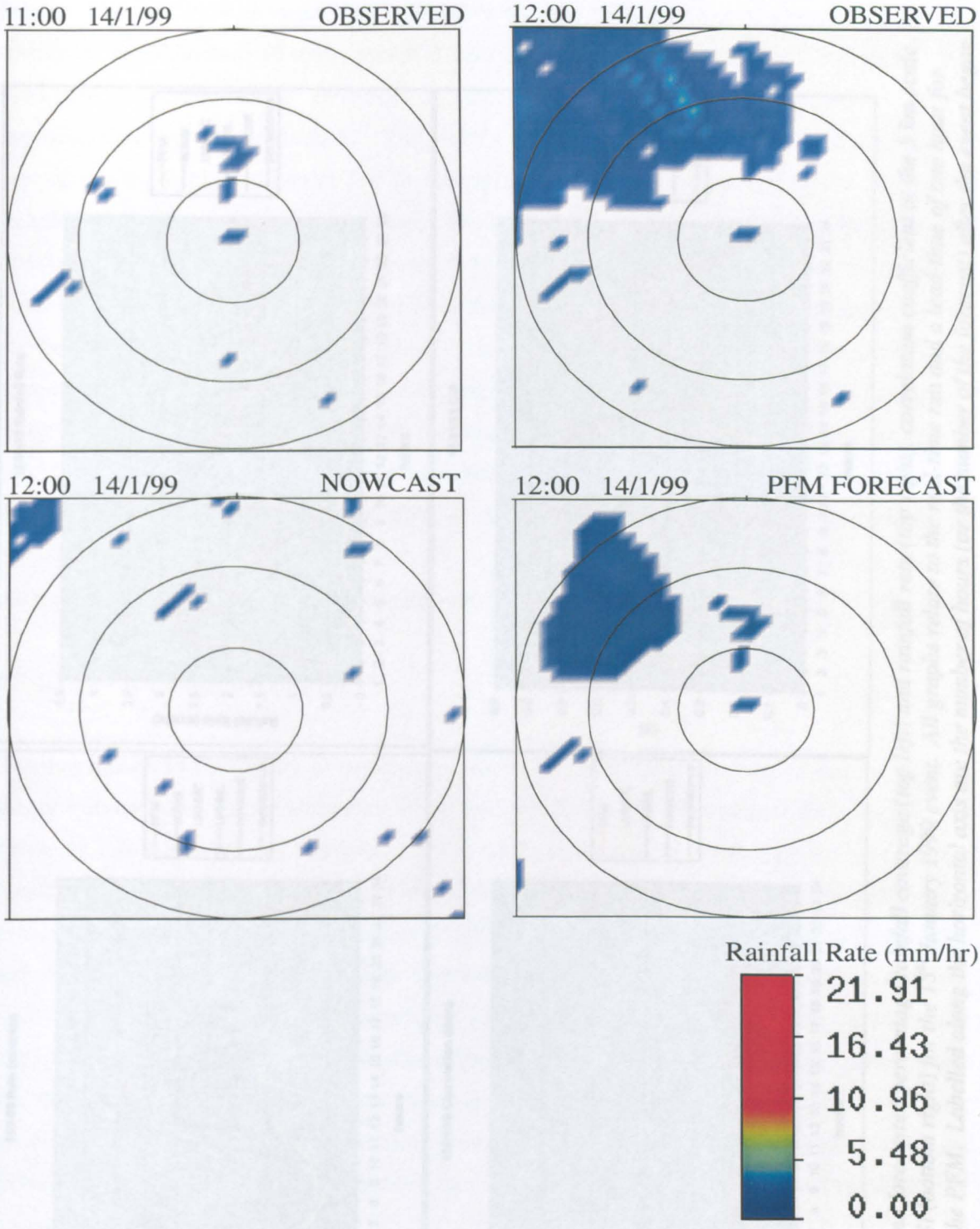

Figure 4.12: *Images of observed and predicted rainfall for the 14th January 1999. Top left is the observed rain field at 11:00 GMT (hour 2) and top right is the observed rain field an hour later (hour 3). Below left is the nowcast for hour 3 and below right is the corresponding PFM forecast. The latter managed to exhibit, to a better extent than nowcasts, some of the observed growth in the rain field that occurred over the hour*

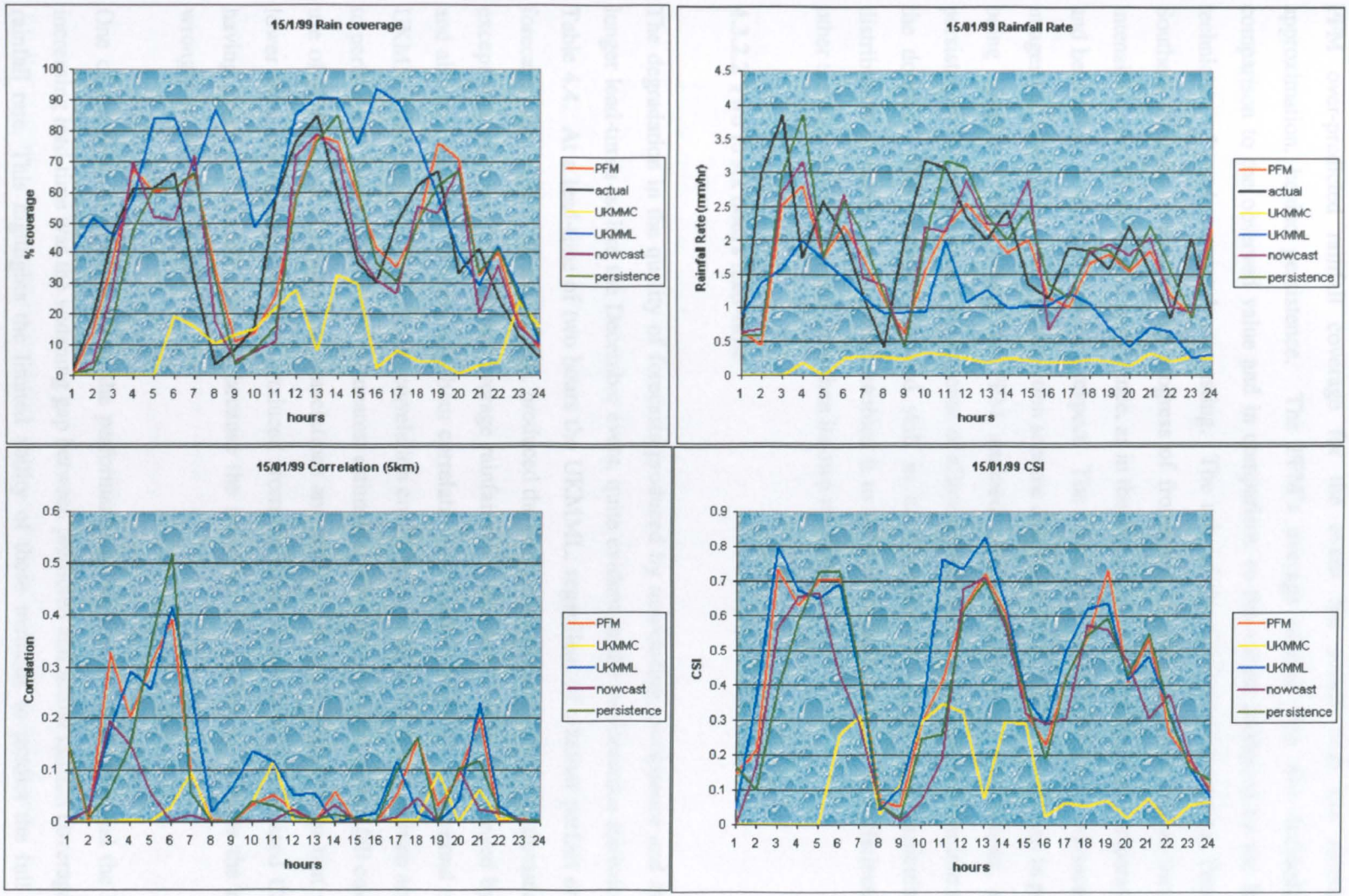

Figure 4.13: *Observed and forecasted percentage rainfall coverage (top left) and rainfall rate (top right), correlation coefficient at the 5 km scale (bottom left) and the CSI (bottom right) for the 15th January 1999 event. All graphs relate to the real-time run and a lead-time of one hour for persistence, nowcasts and the PFM. Labelled along the horizontal axis are the number of hours (or the number of the forecast) after the event began.*

For the event overall, with respect to the real-time run, the PFM produced the best CSI, FAR and correlation coefficients at all scales except at 5km where it was superseded by the UKMML. The PFM over-predicted rainfall coverage for the event but ended with the second closest approximation, behind persistence. The PFM's average rainfall rate was decidedly low in comparison to the observed value and in comparison to the values produced by the forecasting techniques of persistence and nowcasting. The role of the Cambrian Mountains, Pennines and Southern Uplands in slowing the progress of fronts and in acting as focal points for lingering, intensified rainfall meant that persistence, as in the December event, performed comparatively well and better than nowcasting in every respect. The correlation achieved between consecutive radar images had implications for the advection scheme chosen in the PFM, often resulting in persistence being adopted. This meant the PFM attained comparatively good correlations, similar to persistence, but sometimes at the expense of allowing movement of peripheral rain into and out of the domain. The UKMML showed skill in its forecasts of frontal rain, particularly in its distribution of rainfall rates, which enabled it to achieve higher correlation coefficients than the other techniques even at scales finer than its own resolution.

4.3.2.2 Two to six hours lead-time

The degradation in the quality of forecasts produced by nowcasting, persistence and the PFM at longer lead-times is, like the December event, quite evident in the performance statistics listed in Table 4.4. At a lead-time of two hours the UKMML, regardless of whether perfect or real-time forecasts were used in the assessment, produced the best performance statistics in almost all aspects except rainfall coverage, FAR and average rainfall rate. The best FAR was achieved by the PFM and also the equal-best nearest neighbour correlation coefficient, while it came second only to the UKMML in terms of CSI, POD and correlation coefficients at all other scales. Given accessibility to perfect data the PFM provided the nearest estimate to the observed average rainfall coverage and use of perfect data also improved correlations and RMSE, but gave rainfall rates that were even lower than the already low rates produced from real-time data. It also decreased CSI despite having improved rainfall coverage because the latter served mainly to increase the number of wrongly appointed rain cells.

One of the most obvious trends in the performance of nowcasts, persistence and the PFM with increasing lead-time was the widening gap between predicted and actual rainfall coverage, likewise rainfall rate. This highlights the limited ability of these methods to predict the full onset and intensity of a storm without the presence of an existing rain field. The PFM faired marginally better than the others, however, in predicting rainfall coverage but was comparable to the others with respect to rainfall rate, whilst nowcasts showed the most steady decline in values, as they did

for the December event. The PFM's better estimation of rainfall area typically translated into CSI, POD and FAR statistics that were better than those of persistence and nowcasts.

		%cov_for	%cov_act	RMSE	CSI	POD	FAR	cc5km	cc10km	cc15km	cc20km	cc25km	ccNN	rate_for	rate_act
2 hour															
Perfect															
	PFM	33.957	37.468	1.808	0.269	0.412	0.494	0.032	0.045	0.058	0.075	0.093	0.165	1.303	1.690
	UKMML	64.252	37.468	1.529	0.449	0.850	0.513	0.096	0.117	0.136	0.156	0.175	0.178	0.936	1.690
	UKMMC	13.527	37.468	1.624	0.118	0.162	0.522	0.027	0.037	0.049	0.063	0.079	0.053	0.207	1.690
	nowcast	26.079	37.468	1.903	0.186	0.270	0.641	0.009	0.013	0.018	0.024	0.031	0.087	1.298	1.690
	persistence	33.766	37.468	2.077	0.224	0.386	0.510	0.021	0.027	0.033	0.040	0.048	0.144	1.530	1.690
Real-time															
	PFM	33.708	37.468	1.812	0.271	0.411	0.490	0.029	0.041	0.052	0.066	0.083	0.165	1.323	1.690
	UKMML	65.664	37.468	1.537	0.425	0.840	0.531	0.083	0.103	0.121	0.140	0.159	0.165	0.921	1.690
	UKMMC	17.329	37.468	1.620	0.141	0.195	0.547	0.028	0.039	0.051	0.067	0.083	0.055	0.210	1.690
	nowcast	26.079	37.468	1.903	0.186	0.270	0.641	0.009	0.013	0.018	0.024	0.031	0.087	1.298	1.690
	persistence	33.766	37.468	2.077	0.224	0.386	0.510	0.021	0.027	0.033	0.040	0.048	0.144	1.530	1.690
3 hour															
Perfect															
	PFM	36.446	40.270	1.962	0.238	0.407	0.504	0.042	0.063	0.085	0.110	0.137	0.160	1.284	1.716
	UKMML	66.161	40.270	1.583	0.477	0.846	0.482	0.102	0.124	0.144	0.164	0.183	0.188	0.946	1.716
	UKMMC	14.521	40.270	1.706	0.127	0.167	0.500	0.030	0.041	0.053	0.068	0.084	0.054	0.211	1.716
	nowcast	19.958	40.270	1.969	0.119	0.192	0.684	0.006	0.010	0.014	0.020	0.026	0.042	1.084	1.716
	persistence	33.084	40.270	2.245	0.158	0.342	0.553	0.021	0.032	0.045	0.059	0.073	0.120	1.519	1.716
Real-time															
	PFM	36.508	40.270	1.939	0.244	0.426	0.487	0.035	0.053	0.072	0.094	0.118	0.167	1.276	1.716
	UKMML	67.635	40.270	1.588	0.453	0.837	0.500	0.090	0.110	0.129	0.148	0.167	0.177	0.924	1.716
	UKMMC	18.810	40.270	1.702	0.154	0.205	0.509	0.031	0.043	0.056	0.072	0.088	0.056	0.217	1.716
	nowcast	19.958	40.270	1.969	0.119	0.192	0.684	0.006	0.010	0.014	0.020	0.026	0.042	1.084	1.716
	persistence	33.084	40.270	2.245	0.158	0.342	0.553	0.021	0.032	0.045	0.059	0.073	0.120	1.519	1.716
4 hour															
Perfect															
	PFM	33.978	41.561	2.084	0.180	0.330	0.573	0.035	0.051	0.066	0.082	0.099	0.081	1.301	1.698
	UKMML	68.861	41.561	1.619	0.465	0.835	0.493	0.079	0.097	0.114	0.132	0.149	0.158	0.957	1.698
	UKMMC	15.826	41.561	1.727	0.121	0.165	0.527	0.024	0.033	0.042	0.055	0.067	0.039	0.219	1.698
	nowcast	13.718	41.561	1.973	0.071	0.119	0.715	0.009	0.013	0.018	0.023	0.030	0.027	0.964	1.698
	persistence	30.602	41.561	2.247	0.119	0.283	0.586	0.016	0.025	0.034	0.043	0.053	0.072	1.491	1.698
Real-time															
	PFM	33.960	41.561	2.056	0.185	0.341	0.545	0.027	0.040	0.053	0.066	0.080	0.089	1.276	1.698
	UKMML	69.335	41.561	1.608	0.450	0.825	0.502	0.078	0.096	0.113	0.131	0.148	0.158	0.901	1.698
	UKMMC	20.751	41.561	1.722	0.151	0.207	0.536	0.026	0.035	0.046	0.058	0.072	0.042	0.226	1.698
	nowcast	13.718	41.561	1.973	0.071	0.119	0.715	0.009	0.013	0.018	0.023	0.030	0.027	0.964	1.698
	persistence	30.602	41.561	2.299	0.119	0.283	0.586	0.016	0.025	0.034	0.043	0.053	0.072	1.491	1.698
5 hour															
Perfect															
	PFM	29.576	40.799	2.094	0.149	0.292	0.620	0.010	0.016	0.022	0.029	0.037	0.064	1.243	1.713
	UKMML	70.306	40.799	1.658	0.437	0.825	0.523	0.072	0.089	0.105	0.122	0.138	0.146	0.938	1.713
	UKMMC	16.423	40.799	1.755	0.104	0.151	0.586	0.017	0.023	0.030	0.038	0.046	0.026	0.223	1.713
	nowcast	8.319	40.799	1.942	0.036	0.064	0.832	0.002	0.003	0.005	0.006	0.008	0.009	0.768	1.713
	persistence	27.813	40.799	2.306	0.128	0.289	0.562	0.012	0.018	0.025	0.033	0.042	0.077	1.458	1.713
Real-time															
	PFM	29.273	40.799	2.054	0.156	0.295	0.592	0.008	0.013	0.019	0.024	0.030	0.073	1.227	1.713
	UKMML	69.293	40.799	1.644	0.431	0.811	0.521	0.073	0.090	0.106	0.124	0.141	0.150	0.873	1.713
	UKMMC	22.229	40.799	1.749	0.139	0.202	0.595	0.019	0.026	0.034	0.042	0.051	0.029	0.231	1.713
	nowcast	8.319	40.799	1.942	0.036	0.064	0.832	0.002	0.003	0.005	0.006	0.008	0.009	0.768	1.713
	persistence	27.813	40.799	2.306	0.128	0.289	0.562	0.012	0.018	0.025	0.033	0.042	0.077	1.458	1.713
6 hour															
Perfect															
	PFM	24.031	39.104	1.967	0.162	0.268	0.603	0.014	0.021	0.027	0.034	0.041	0.087	1.104	1.732
	UKMML	69.355	39.104	1.700	0.420	0.817	0.541	0.056	0.072	0.087	0.103	0.121	0.120	0.889	1.732
	UKMMC	17.369	39.104	1.771	0.105	0.158	0.580	0.018	0.024	0.031	0.039	0.047	0.028	0.222	1.732
	nowcast	3.910	39.104	1.833	0.021	0.033	0.842	0.001	0.002	0.003	0.004	0.005	0.008	0.412	1.732
	persistence	23.394	39.104	2.256	0.149	0.281	0.475	0.010	0.014	0.018	0.023	0.029	0.072	1.409	1.732
Real-time															
	PFM	25.179	39.104	1.944	0.174	0.282	0.599	0.015	0.022	0.029	0.036	0.044	0.091	1.110	1.732
	UKMML	67.644	39.104	1.698	0.410	0.793	0.539	0.053	0.068	0.083	0.099	0.116	0.116	0.857	1.732
	UKMMC	21.819	39.104	1.766	0.133	0.195	0.598	0.019	0.027	0.035	0.044	0.053	0.030	0.235	1.732
	nowcast	3.910	39.104	1.833	0.021	0.033	0.842	0.001	0.002	0.003	0.004	0.005	0.008	0.412	1.732
	persistence	23.394	39.104	2.256	0.149	0.281	0.475	0.010	0.014	0.018	0.023	0.029	0.072	1.409	1.732

Table 4.4: *Summary of the average performance statistics for the January 1999 event for both the perfect and real-time runs and from two to six hours lead-time (with respect to nowcasts, persistence and the PFM). The best performance for each particular statistic is highlighted in green.*

Similar to the December event, the PFM's correlation coefficients at a lead-time of five hours were worse than those at six hours to the extent they fell below persistence. Interestingly, even the UKMMC produced better correlation coefficients than either the PFM or persistence at lead-times of five and six hours and also made comparable estimations of rainfall coverage. Although fronts

were the dominant feature and controlling influence on overall rainfall development and distribution, convective elements were embedded in the storm system. The UKMM predicted convective lines within the primary rain bands (Figure 4.14), particularly in its latter stages, and some of the sharp showers over the Pennines (Figure 4.10) were likely to have resulted from the triggering of this instability through orographic lifting. It is possible that the very high maximum rainfall rate observed during this event was the product of convection.

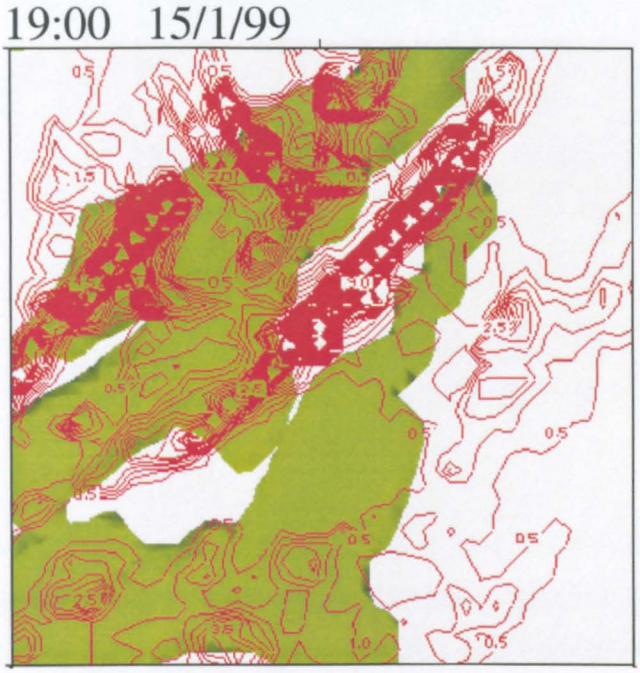

Figure 4.14: *UKMM predicted potential instability (dOe/dp>0, green areas) and rainfall rates (red contours at intervals of 0.5 mmhr^{-1}) at 1900 GMT on the 15th January 1999.*

4.3.3 August 1999

August 1999 was a very wet month in England, with many places recording 50% more rainfall than average (Hulme, 2001). Temperatures were hot to start with, up to 30°C in southern England, and thunderstorms were common in the afternoons and evenings, having made their way up to the UK from France in a hot and humid southeasterly airflow. The general synoptic conditions for the first five days of August are shown in Figure 4.15, the prevailing feature in each image is the fairly stationary area of low pressure centred to the southeast of the UK. Over the course of the five days there were three distinct periods of rainfall associated with these conditions and examples of the nature of the rainfall during each are shown in Figure 4.16, by way of a sample of four consecutive network radar images.

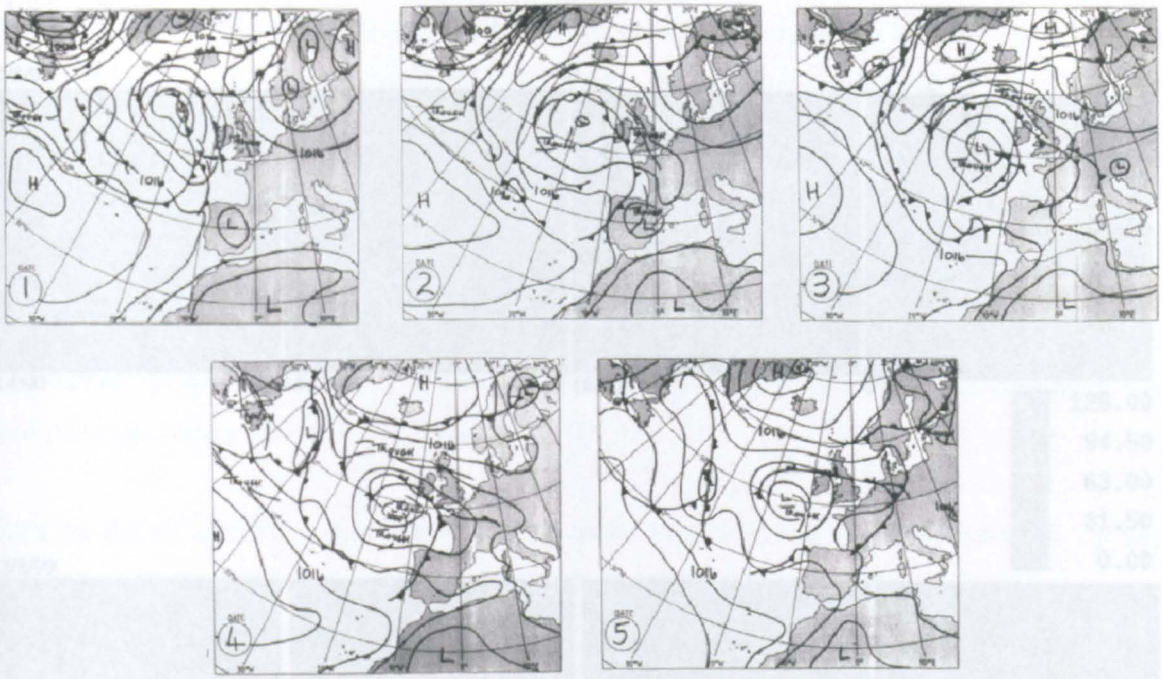

Figure 4.15: *General synoptic conditions at 1200 GMT for 1st to the 5th August 1999 (Eden, 1999c).*

The first period of rainfall occurred between the hours of 1200 GMT and 1800 GMT on the 1st August, when thunderstorms tracked northwards from the south coast of England along a trough of low pressure that channelled them along a fairly narrow line over the Midlands and between Wales and the Pennines. The high rainfall rates achieved, up to 126 $mmhr^{-1}$, and the relatively fixed nature of their path resulted in flash flooding in the Midlands during the six hours of thunderstorm activity (Brugge, 2001). Surface winds were light, amounting to a gentle breeze at 18 $kmhr^{-1}$, and variable in direction across the domain, though mostly directed toward the line of rain cell movement, which meant that southeasterlies in the south converged with an easterly flow over the Pennines and with northerly winds that flowed down the west coast of Northern England. This distribution set up a local clockwise circulation north of the Welsh Hills, which migrated very slowly northwards. Upper-level winds maintained a southerly component throughout and were generally in keeping with the direction of rain cell movement.

Conditions were much the same the following day with a similar path taken by the thunderstorms that appeared around 1500 GMT in the afternoon. The rain cells were less organised than the day before but were no less troublesome, giving heavy falls in places and disrupting power supplies (Brugge, 2001). Rain continued overnight and until midday on the 3rd August.

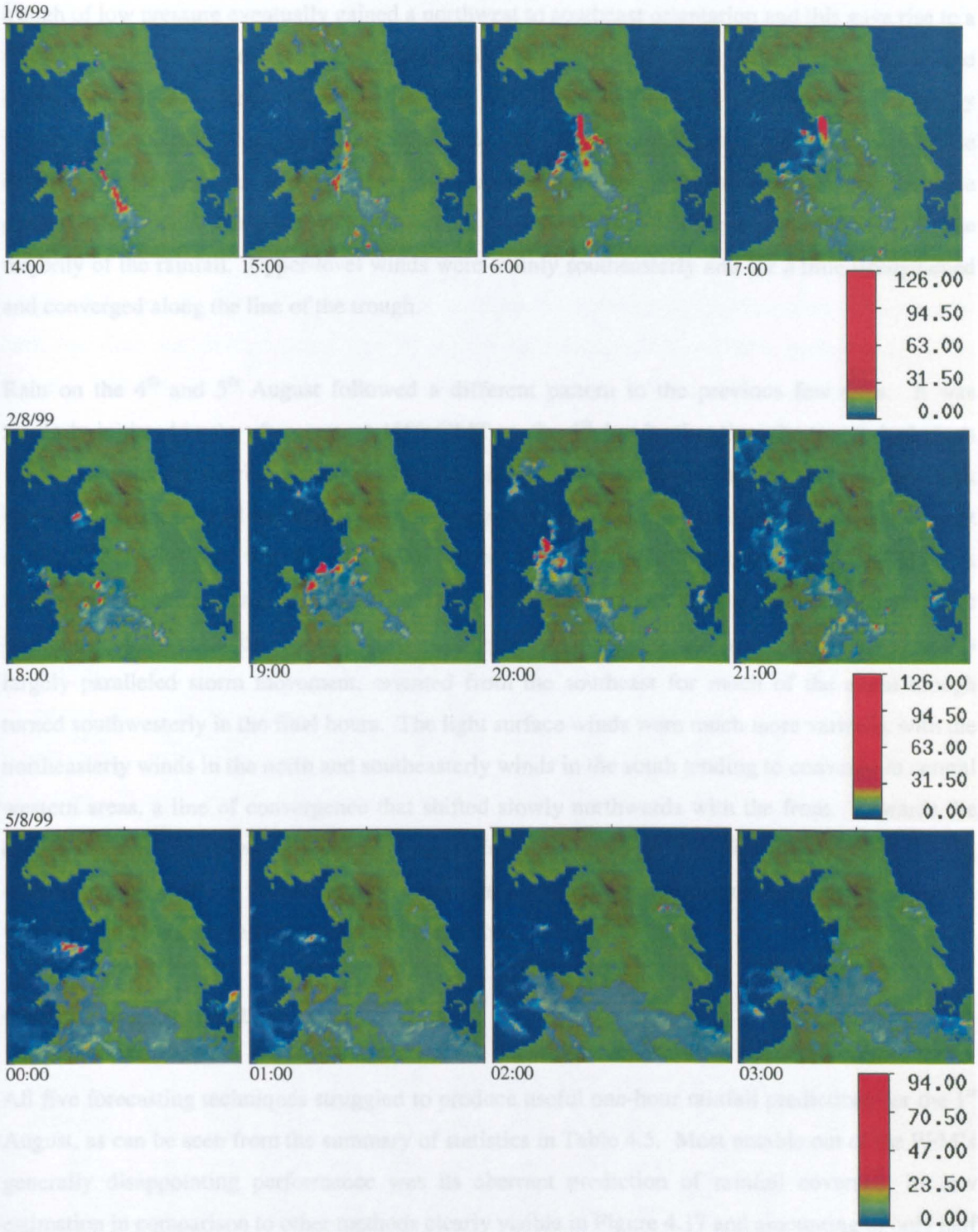

Figure 4.16: *Four consecutive hourly images of rainfall for the three distinct periods of rainfall constituting the August 1999 event (ie. 1st, 2nd/3rd, 4th/5th). The date is displayed at the top of each set of images and at the bottom of each image is the time to which it corresponds. Below right is the legend showing rainfall rates in mmhr^{-1}.*

Wind direction on the 2nd and 3rd August was variable both spatially and temporally but wind speed was consistently light. Initially the wind field was much the way it had been on the 1st but the trough of low pressure eventually gained a northwest to southeast orientation and this gave rise to a three-way split in wind direction over the domain. Northern and central areas of the western side of the region had northerly winds, the northern and central areas of the eastern side had easterly winds while southern areas had southerly winds. As time progressed, wind directions across the domain kept shifting and, as a result, various localised areas of divergence and convergence were created, and as much of this activity was centred over the Welsh Hills it became the locality for the majority of the rainfall. Upper-level winds were mainly southeasterly and for a time strengthened and converged along the line of the trough.

Rain on the 4th and 5th August followed a different pattern to the previous few days. It was similarly initiated in the afternoon, at 1500 GMT on the 4th, but by that time the trough had given way to a northward moving occluded front that straddled the country. Rain cell organisation took on frontal alignment and had coherency in movement towards the north. Rain continued overnight and was heavy at times, with the maximum rainfall rate of 94mmhr^{-1} recorded before midnight. A line of thunderstorms trailed behind the main rain band and these contributed to the surface flooding that occurred by the end of the event (1500 GMT) the next day. Upper-level winds largely paralleled storm movement, oriented from the southeast for much of the event though turned southwesterly in the final hours. The light surface winds were much more variable, with the northeasterly winds in the north and southeasterly winds in the south tending to converge in central western areas, a line of convergence that shifted slowly northwards with the front. Towards the end of the event southwesterly winds emerged from the south and had the effect of fragmenting wind direction over the whole domain, such that a central area of divergence developed within what was an almost hyperbolic pattern of wind flow.

4.3.3.1. One hour lead-time

All five forecasting techniques struggled to produce useful one-hour rainfall predictions for the 1st August, as can be seen from the summary of statistics in Table 4.5. Most notable out of the PFM's generally disappointing performance was its aberrant prediction of rainfall coverage, its low estimation in comparison to other methods clearly visible in Figure 4.17 and amounting to only half the observed. Understandably this led to a low POD but also culminated in a low CSI because of an apparent lack of success in correctly positioning the diminutive rain field, as evidenced by a value of FAR that failed to better that of persistence despite the rainfall coverage of the PFM's forecasts being considerably less. A significant contributor to the PFM's problems was that the UKMM's profiles of relative humidity tended towards low values and did not exceed 90% at the

600mb level at any time during the six hours of rainfall. With such high intensity rainfall rates and, in some areas, low moisture inputs, a number of the PFM's cells were depleted of liquid water by the end of the forecast lead-time. The UKMMC was the only method to over-predict the rainfall coverage but grossly under-predicted rainfall rate and produced the worst correlations. The PFM on the other hand consistently overestimated the rainfall rate (Figure 4.17), a product of the method used to determine CBLWC and, more specifically, the application of linearly-regressed coefficients that were on this occasion biased towards high values. Perhaps surprisingly for a convective event, persistence won in most categories of statistical performance but a result possibly explained by convective activity being sustained by a fairly focussed and well-defined line of uplift along the length of the trough. The PFM managed to produce the second best correlation coefficients with both real-time and perfect data. Use of perfect data enhanced the PFM's performance in all respects, allowing it to benefit from an improved, though still inadequate, representation of moisture.

	%cov_for	%cov_act	RMSE	CSI	POD	FAR	cc5km	cc10km	cc15km	cc20km	cc25km	ccNN	rate_for	rate_act
Perfect														
1/8/99 PFM	7.757	15.665	7.728	0.135	0.175	0.573	0.097	0.117	0.129	0.138	0.153	0.218	8.424	7.577
1/8/99 UKMML	0.000	15.665	6.510	0.000	0.000	1.000	0.000	0.000	0.000	0.000	0.000	0.000	0.000	7.577
1/8/99 UKMMC	24.613	15.665	6.500	0.103	0.286	0.840	0.004	0.008	0.014	0.023	0.033	0.025	0.468	7.577
1/8/99 nowcast	12.680	15.665	9.476	0.159	0.241	0.692	0.002	0.009	0.024	0.040	0.053	0.081	6.870	7.577
1/8/99 persistence	12.122	15.665	8.065	0.235	0.322	0.477	0.099	0.124	0.144	0.161	0.186	0.260	7.362	7.577
2/8/99 PFM	16.335	15.363	1.923	0.306	0.491	0.546	0.110	0.138	0.167	0.197	0.237	0.312	1.969	2.370
2/8/99 UKMML	14.232	15.363	1.769	0.257	0.409	0.566	0.040	0.062	0.079	0.094	0.110	0.071	0.884	2.370
2/8/99 UKMMC	17.050	15.363	1.746	0.130	0.244	0.754	0.028	0.040	0.052	0.066	0.079	0.047	0.434	2.370
2/8/99 nowcast	15.014	15.363	2.331	0.243	0.403	0.602	0.031	0.054	0.081	0.110	0.147	0.175	2.371	2.370
2/8/99 persistence	14.704	15.363	2.312	0.293	0.457	0.539	0.112	0.131	0.156	0.182	0.217	0.279	2.448	2.370
4/8/99 PFM	19.383	19.326	1.593	0.317	0.456	0.520	0.061	0.096	0.126	0.154	0.185	0.256	1.562	1.935
4/8/99 UKMML	19.770	19.326	1.457	0.253	0.375	0.631	0.035	0.050	0.065	0.078	0.092	0.063	0.586	1.935
4/8/99 UKMMC	17.337	19.326	1.442	0.145	0.240	0.712	0.009	0.016	0.026	0.038	0.050	0.063	0.551	1.935
4/8/99 nowcast	20.675	19.326	1.819	0.328	0.478	0.513	0.063	0.112	0.158	0.202	0.239	0.286	1.782	1.935
4/8/99 persistence	18.979	19.326	1.781	0.315	0.452	0.504	0.063	0.088	0.109	0.125	0.145	0.208	1.748	1.935
PFM	*14.491*	*16.785*	*3.748*	*0.253*	*0.374*	*0.547*	*0.090*	*0.117*	*0.141*	*0.163*	*0.192*	*0.262*	*3.985*	*3.961*
UKMML	*11.334*	*16.785*	*3.245*	*0.170*	*0.261*	*0.732*	*0.025*	*0.037*	*0.048*	*0.057*	*0.067*	*0.045*	*0.490*	*3.961*
UKMMC	*19.667*	*16.785*	*3.229*	*0.126*	*0.257*	*0.768*	*0.014*	*0.021*	*0.031*	*0.042*	*0.054*	*0.045*	*0.484*	*3.961*
nowcast	*16.123*	*16.785*	*4.542*	*0.244*	*0.374*	*0.602*	*0.032*	*0.058*	*0.088*	*0.117*	*0.146*	*0.181*	*3.674*	*3.961*
persistence	*15.268*	*16.785*	*4.053*	*0.281*	*0.411*	*0.506*	*0.091*	*0.114*	*0.136*	*0.156*	*0.183*	*0.249*	*3.853*	*3.961*
Real-time														
1/8/99 PFM	7.644	15.665	7.835	0.126	0.165	0.525	0.094	0.110	0.116	0.116	0.123	0.202	9.582	7.577
1/8/99 UKMML	0.000	15.665	6.501	0.000	0.000	1.000	0.000	0.000	0.000	0.000	0.000	0.000	0.000	7.577
1/8/99 UKMMC	20.588	15.665	6.491	0.123	0.284	0.812	0.010	0.018	0.028	0.037	0.046	0.038	0.402	7.577
1/8/99 nowcast	12.680	15.665	9.476	0.159	0.241	0.692	0.002	0.009	0.024	0.040	0.053	0.081	6.870	7.577
1/8/99 persistence	12.122	15.665	8.065	0.235	0.322	0.477	0.099	0.124	0.144	0.161	0.186	0.260	7.362	7.577
2/8/99 PFM	15.514	15.363	1.941	0.306	0.479	0.538	0.110	0.138	0.165	0.193	0.231	0.310	2.030	2.370
2/8/99 UKMML	18.257	15.363	1.784	0.195	0.382	0.680	0.031	0.047	0.060	0.073	0.086	0.059	0.786	2.370
2/8/99 UKMMC	18.386	15.363	1.765	0.130	0.248	0.760	0.028	0.039	0.052	0.066	0.079	0.045	0.440	2.370
2/8/99 nowcast	15.014	15.363	2.331	0.243	0.403	0.602	0.031	0.054	0.081	0.110	0.147	0.175	2.371	2.370
2/8/99 persistence	14.704	15.363	2.312	0.293	0.457	0.539	0.112	0.131	0.156	0.182	0.217	0.279	2.448	2.370
4/8/99 PFM	19.203	19.326	1.590	0.319	0.456	0.515	0.061	0.095	0.124	0.152	0.182	0.253	1.569	1.935
4/8/99 UKMML	20.557	19.326	1.475	0.240	0.363	0.642	0.031	0.045	0.059	0.073	0.087	0.058	0.652	1.935
4/8/99 UKMMC	13.818	19.326	1.449	0.110	0.173	0.752	0.004	0.008	0.013	0.017	0.023	0.034	0.485	1.935
4/8/99 nowcast	20.675	19.326	1.819	0.328	0.478	0.513	0.063	0.112	0.158	0.202	0.239	0.286	1.782	1.935
4/8/99 persistence	18.979	19.326	1.781	0.315	0.452	0.504	0.063	0.088	0.109	0.125	0.145	0.208	1.748	1.935
PFM	*14.120*	*16.785*	*3.789*	*0.250*	*0.367*	*0.526*	*0.088*	*0.114*	*0.135*	*0.154*	*0.179*	*0.255*	*4.394*	*3.961*
UKMML	*12.938*	*16.785*	*3.253*	*0.145*	*0.248*	*0.774*	*0.021*	*0.031*	*0.040*	*0.048*	*0.058*	*0.039*	*0.479*	*3.961*
UKMMC	*17.597*	*16.785*	*3.235*	*0.121*	*0.235*	*0.775*	*0.014*	*0.022*	*0.031*	*0.040*	*0.049*	*0.039*	*0.442*	*3.961*
nowcast	*16.123*	*16.785*	*4.542*	*0.244*	*0.374*	*0.602*	*0.032*	*0.058*	*0.088*	*0.117*	*0.146*	*0.181*	*3.674*	*3.961*
persistence	*15.268*	*16.785*	*4.053*	*0.281*	*0.411*	*0.506*	*0.091*	*0.114*	*0.136*	*0.156*	*0.183*	*0.249*	*3.853*	*3.961*

Table 4.5: *Summary of performance statistics for the five forecasting techniques in both the perfect and real-time runs of the August 1999 event. The performance statistics are averaged over each distinct rainfall period and additionally the average for the whole event is shown, in italics, at the bottom of each run. The best performance is highlighted in green.*

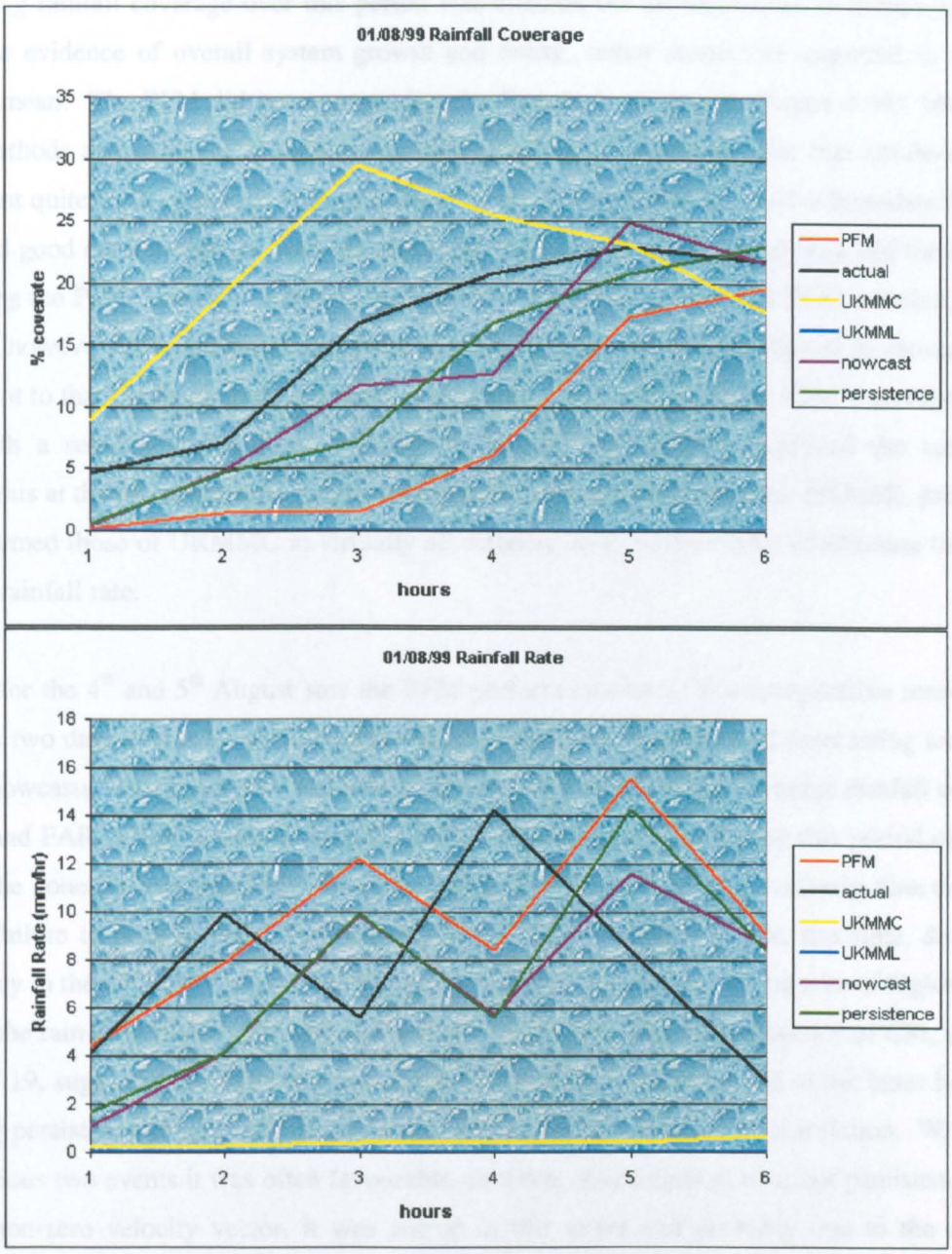

Figure 4.17: *Observed and forecasted percentage rainfall coverage and average rainfall rate for rainfall event on the 1st August 1999. The graphs relate to the real-time run and a one-hour forecast lead-time, with "hours" on the horizontal axis referring to the number of hours (or the number of the forecast) since the event began.*

The PFM elevated its performance for the next period of rainfall, which began with afternoon thunderstorms on the 2nd August and lasted for a total of 21 hours. In contrast to its estimation of average rainfall coverage for the previous day, the PFM produced a value closest to the actual with use of real-time data. It achieved a better RMSE than nowcasting and persistence but also tended to lower the average rainfall rate. It scored the highest CSI, POD and FAR and also the highest correlation coefficients, except at the 5km scale where it was narrowly beaten by persistence. The

fluctuating rainfall coverage over this period was difficult for all techniques to handle and there was little evidence of overall system growth and decay, rather storm size appeared to oscillate about a mean. The PFM did however predict the first peak, at hour 4 (Figure 4.18), better than other methods and achieved it through implementing an advection scheme that emulated storm movement quite well, combined with assistance by an upper-level 90% relative humidity field that exhibited good correspondence with the observed rain field. Use of perfect data had the effect of increasing the PFM's rainfall coverage, with an associated improvement in POD but also increase in FAR, however these successes and failures in positioning rain cells balanced to provide a CSI equivalent to that obtained using real-time data. Perfect data decreased the PFM's average rainfall rate, with a seemingly associated decrease in RMSE, and slightly improved the correlation coefficients at the broader scales. Interestingly, in the convective conditions, UKMML predictions outperformed those of UKMMC in virtually all respects, even to the extent of attaining the higher average rainfall rate.

Results for the 4th and 5th August saw the PFM perform similarly, in a comparative sense, to the previous two days across all performance measures and with respect to all forecasting techniques except nowcasts. Nowcasts gave the best results in every aspect except average rainfall coverage, RMSE and FAR, which attests to the influence of the occluded front during this period of rainfall and to the cohesive and relatively slow movement of the rain field in a northerly direction. The PFM's failure to provide better forecasts than simple nowcasting was not, this time, due to any deficiency in the UKMM's prediction of upper-level relative humidity, as the area of high humidity tracked the rain field reasonably well and was of comparable size. The sequence of CSI, shown in Figure 4.19, suggested the PFM was penalised, particularly at hour ten and in the latter hours, for adopting persistence as its advection option, a choice that also affected its correlation. Whereas in the previous two events it was often favourable, in terms of correlation, to adopt persistence rather than a non-zero velocity vector, it was not so in this event and probably due to the overland approach of the storm. This produced less variation in the characteristics of the moving rain field than had been evident when the direction of approach was from across the Irish Sea, whereupon the rain field changed considerably upon encountering land and for which the Pennines and Welsh Hills extended parallel to, rather than normal to, the leading edge of the rain band. It was encouraging to see that for any single hour the PFM often produced a better correlated forecast, if only very marginally, than the advection scheme it had adopted for that hour.

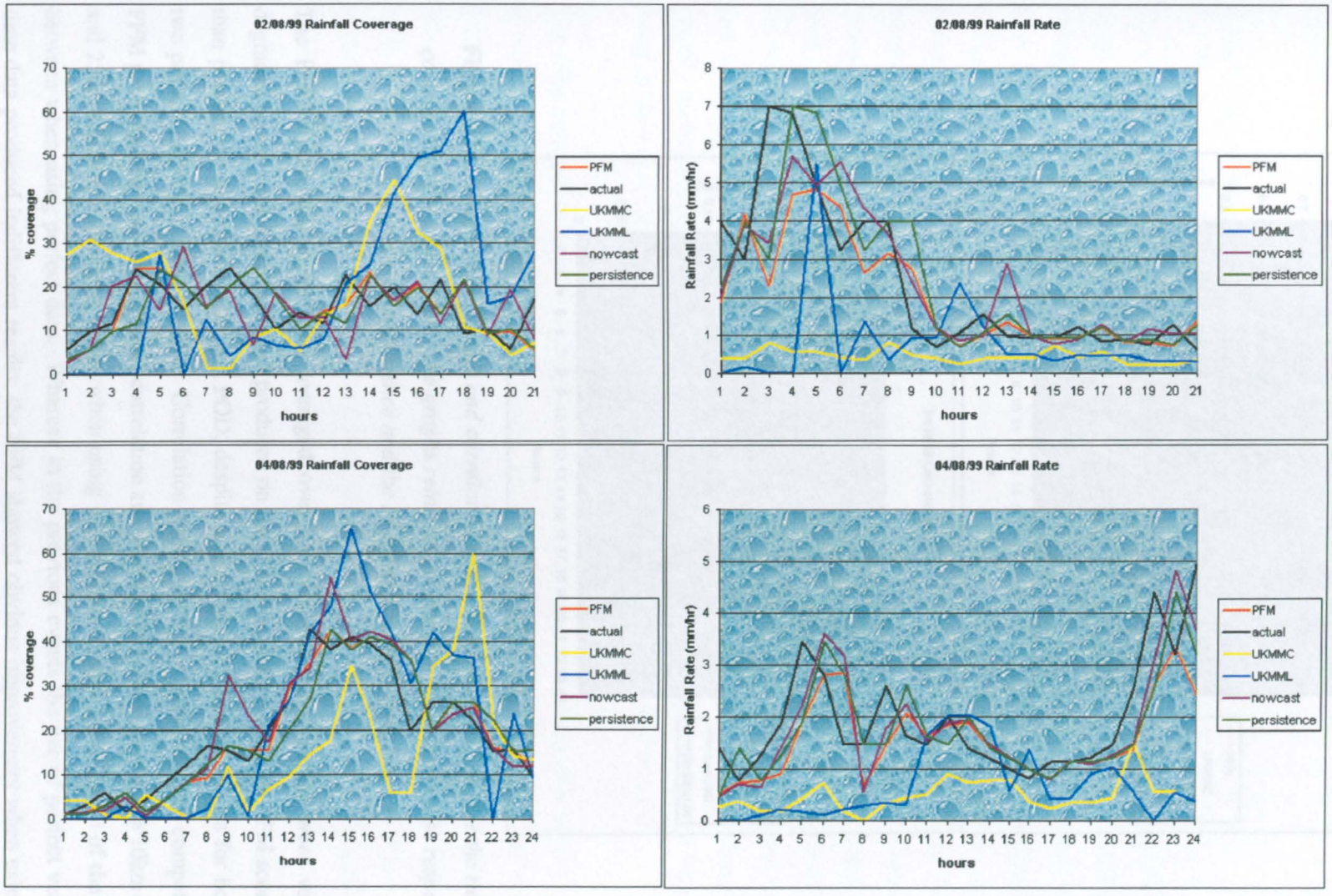

Figure 4.18: *Observed and forecasted percentage rainfall coverage and average rainfall rate for the rainfall events commencing on the 2nd (top) and 4th (bottom) August 1999. The graphs relate to the real-time run and a one-hour forecast lead-time, with "hours" on the horizontal axis referring to the number of hours (or the number of the forecast) since the event began.*

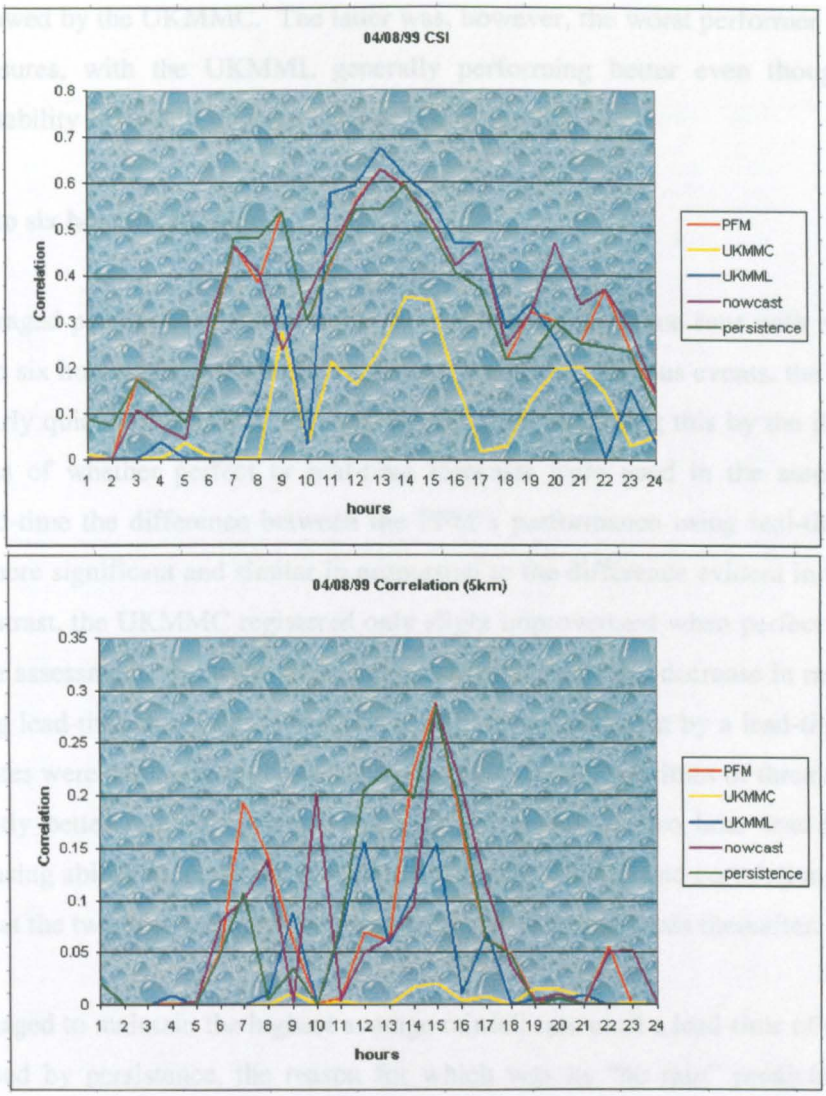

Figure 4.19: *Graphs of CSI (top) and correlation at the 5km scale (bottom) for the rainfall commencing 4th August 1999. The graphs relate to the one-hour lead-time (with respect to nowcasts, persistence and the PFM) and the real-time run.*

The PFM's performance statistics averaged over the whole five-day period were very much degraded by the poor forecasts it had produced on the first day. As a result, the PFM scored lower than persistence in terms of CSI and POD, despite having produced better values for both in the two periods of rainfall that followed. Correlation coefficients were however still competitive, the PFM gave the best nearest neighbour correlation and also the best correlation at the 10km ($100km^2$) and 25km ($625km^2$) averaging scales when using real-time data, with the addition of the scales in between when using perfect data. Whereas in the previous events the use of perfect versus real-time data produced indifferent results, the PFM showed obvious improvement when using perfect data. This highlights the difficulty that NWP models, not necessarily just the UKMM, have in trying to accurately predict the dynamics of a convective environment at longer lead-times. Out of all the forecasting techniques, nowcasts provided the best estimation of the event-averaged rainfall

coverage, followed by the UKMMC. The latter was, however, the worst performer with respect to all other measures, with the UKMML generally performing better even though broad-scale convective instability existed throughout each period of rainfall.

4.3.3.2. Two to six hours lead-time

The event-averaged performance statistics for the perfect and real-time runs with respect to lead-times of two to six hours are presented in Table 4.6. As in the previous events, the UKMML took precedence fairly quickly in terms of CSI and correlations, achieving this by the three-hour lead-time regardless of whether perfect or real-time forecasts were used in the assessment. With increasing lead-time the difference between the PFM's performance using real-time and perfect data became more significant and similar in proportion to the difference evident in the UKMML's results. In contrast, the UKMMC registered only slight improvement when perfect forecasts were included in the assessment. Both the PFM and persistence showed a decrease in rainfall coverage with increasing lead-time though the PFM to a lesser extent, such that by a lead-time of six hours the two estimates were comparable. Nowcasting, particularly at lead-times of three and four hours, had significantly better rainfall coverage statistics but beyond a two hour lead-time showed a steadily decreasing ability to locate the rain field accurately, its CSI and correlations slipping from being the best at the two hour lead-time to being below all other methods thereafter.

The PFM managed to maintain the highest average rainfall rate until a lead-time of six hours when it was surpassed by persistence, the reason for which was its "no rain" prediction for the one forecast possible at the six hour lead-time for the 1st August event. In general the PFM struggled to better persistence, managing to have the better RMSE at all lead-times and the better CSI, POD and FAR at lead-times of four and five hours, but in all cases only through use of perfect data. A similar situation existed with respect to the correlations, with only use of perfect data enabling the PFM to better persistence at spatial averages over the 10km scale and in nearest neighbour correlations across all lead-times. The comparatively good performance of persistence at longer lead-times can be attributed to longevity in the conditions that provided uplift in areas of convective instability, which facilitated sustained regeneration of convective cells and ensured consistency in their pathway. The pattern of wind flow was conducive to the regeneration of rain cells, with upper-level winds allowing rainfall to fall away from the primary updrafts, whilst low-level winds were able to feed moist air into the system. An example of the wind field on the 1st August is shown in Figure 4.20. On the occasion shown in the image, the rain began to dissipate when the rain field moved into an area of almost static low-level wind flow.

		%cov_for	%cov_act	RMSE	CSI	POD	FAR	cc5km	cc10km	cc15km	cc20km	cc25km	ccNN	rate_for	rate_act
2 hour															
Perfect															
	PFM	13.956	17.945	4.554	0.186	0.291	0.613	0.023	0.038	0.050	0.063	0.079	0.141	4.375	4.171
	UKMML	11.858	17.945	3.585	0.178	0.274	0.720	0.026	0.039	0.050	0.060	0.070	0.047	0.513	4.171
	UKMMC	19.717	17.945	3.568	0.132	0.255	0.755	0.014	0.023	0.032	0.045	0.057	0.045	0.491	4.171
	nowcast	14.512	17.945	4.112	0.189	0.288	0.634	0.038	0.050	0.062	0.076	0.094	0.160	3.018	4.171
	persistence	14.746	17.945	4.845	0.199	0.303	0.596	0.035	0.043	0.048	0.054	0.064	0.131	3.781	4.171
Real-time															
	PFM	13.078	17.945	4.616	0.169	0.264	0.633	0.016	0.025	0.033	0.042	0.054	0.110	4.061	4.171
	UKMML	13.540	17.945	3.593	0.152	0.260	0.763	0.022	0.032	0.042	0.051	0.060	0.041	0.502	4.171
	UKMMC	18.364	17.945	3.574	0.125	0.238	0.766	0.015	0.023	0.033	0.043	0.052	0.038	0.458	4.171
	nowcast	14.512	17.945	4.112	0.189	0.288	0.634	0.038	0.050	0.062	0.076	0.094	0.160	3.018	4.171
	persistence	14.746	17.945	4.845	0.199	0.303	0.596	0.035	0.043	0.048	0.054	0.064	0.131	3.781	4.171
3 hour															
Perfect															
	PFM	12.836	19.201	4.009	0.170	0.265	0.580	0.021	0.035	0.048	0.061	0.075	0.140	3.499	4.035
	UKMML	12.431	19.201	3.780	0.187	0.287	0.706	0.028	0.041	0.053	0.063	0.074	0.049	0.536	4.035
	UKMMC	19.401	19.201	3.763	0.135	0.238	0.743	0.015	0.023	0.032	0.042	0.053	0.043	0.496	4.035
	nowcast	17.510	19.201	4.420	0.143	0.261	0.702	0.003	0.007	0.013	0.020	0.028	0.045	2.842	4.035
	persistence	13.964	19.201	4.470	0.176	0.268	0.559	0.025	0.030	0.037	0.045	0.057	0.127	3.175	4.035
Real-time															
	PFM	11.734	19.201	4.120	0.144	0.223	0.588	0.012	0.019	0.026	0.035	0.047	0.094	3.470	4.035
	UKMML	14.200	19.201	3.782	0.159	0.272	0.752	0.023	0.034	0.044	0.053	0.063	0.043	0.524	4.035
	UKMMC	18.613	19.201	3.770	0.122	0.215	0.761	0.013	0.020	0.027	0.035	0.043	0.032	0.474	4.035
	nowcast	17.510	19.201	4.420	0.143	0.261	0.702	0.003	0.007	0.013	0.020	0.028	0.045	2.842	4.035
	persistence	13.964	19.201	4.470	0.176	0.268	0.559	0.025	0.030	0.037	0.045	0.057	0.127	3.175	4.035
4 hour															
Perfect															
	PFM	12.790	19.947	4.538	0.154	0.241	0.642	0.016	0.023	0.034	0.046	0.059	0.102	3.970	4.204
	UKMML	12.949	19.947	4.143	0.190	0.295	0.704	0.029	0.043	0.055	0.066	0.077	0.051	0.545	4.204
	UKMMC	18.741	19.947	4.126	0.136	0.229	0.734	0.015	0.022	0.031	0.040	0.050	0.044	0.497	4.204
	nowcast	16.059	19.947	4.788	0.109	0.197	0.760	0.002	0.005	0.008	0.013	0.017	0.026	2.704	4.204
	persistence	12.978	19.947	4.937	0.146	0.228	0.650	0.024	0.027	0.034	0.043	0.053	0.101	3.159	4.204
Real-time															
	PFM	11.823	19.947	4.902	0.136	0.210	0.646	0.012	0.016	0.022	0.031	0.042	0.095	5.044	4.204
	UKMML	14.927	19.947	4.152	0.167	0.286	0.739	0.024	0.035	0.046	0.056	0.067	0.045	0.549	4.204
	UKMMC	18.014	19.947	4.133	0.123	0.205	0.752	0.013	0.019	0.026	0.033	0.040	0.032	0.480	4.204
	nowcast	16.059	19.947	4.788	0.109	0.197	0.760	0.002	0.005	0.008	0.013	0.017	0.026	2.704	4.204
	persistence	12.978	19.947	4.937	0.146	0.228	0.650	0.024	0.027	0.034	0.043	0.053	0.101	3.159	4.204
5 hour															
Perfect															
	PFM	12.559	20.305	3.583	0.138	0.225	0.614	0.009	0.015	0.023	0.031	0.039	0.075	2.832	3.148
	UKMML	13.315	20.305	3.242	0.189	0.298	0.706	0.030	0.044	0.056	0.067	0.078	0.052	0.542	3.148
	UKMMC	18.194	20.305	3.221	0.141	0.238	0.717	0.011	0.018	0.024	0.032	0.039	0.045	0.504	3.148
	nowcast	13.726	20.305	3.600	0.091	0.168	0.754	0.003	0.005	0.008	0.013	0.018	0.041	1.773	3.148
	persistence	12.234	20.305	3.814	0.122	0.201	0.662	0.015	0.015	0.022	0.028	0.035	0.081	2.412	3.148
Real-time															
	PFM	11.642	20.305	3.657	0.120	0.200	0.597	0.008	0.014	0.020	0.026	0.033	0.077	3.302	3.148
	UKMML	15.690	20.305	3.248	0.176	0.301	0.726	0.025	0.037	0.048	0.059	0.070	0.047	0.575	3.148
	UKMMC	17.526	20.305	3.230	0.127	0.213	0.735	0.010	0.014	0.019	0.023	0.028	0.032	0.489	3.148
	nowcast	13.726	20.305	3.600	0.091	0.168	0.754	0.003	0.005	0.008	0.013	0.018	0.041	1.773	3.148
	persistence	12.234	20.305	3.814	0.122	0.201	0.662	0.015	0.015	0.022	0.028	0.035	0.081	2.412	3.148
6 hour															
Perfect															
	PFM	11.713	20.345	2.095	0.114	0.187	0.769	0.008	0.013	0.018	0.023	0.028	0.061	1.299	2.145
	UKMML	13.494	20.345	1.763	0.188	0.298	0.702	0.027	0.041	0.052	0.063	0.073	0.048	0.459	2.145
	UKMMC	17.235	20.345	1.744	0.143	0.237	0.701	0.006	0.011	0.016	0.023	0.029	0.048	0.543	2.145
	nowcast	11.469	20.345	2.036	0.067	0.128	0.852	0.002	0.004	0.007	0.010	0.014	0.023	1.143	2.145
	persistence	11.455	20.345	2.335	0.115	0.191	0.590	0.012	0.014	0.017	0.022	0.028	0.057	2.037	2.145
Real-time															
	PFM	11.309	20.345	2.093	0.105	0.174	0.770	0.007	0.011	0.017	0.023	0.029	0.054	1.295	2.145
	UKMML	16.011	20.345	1.773	0.174	0.301	0.723	0.023	0.033	0.044	0.054	0.064	0.042	0.491	2.145
	UKMMC	16.537	20.345	1.757	0.129	0.211	0.720	0.004	0.007	0.011	0.014	0.018	0.035	0.528	2.145
	nowcast	11.469	20.345	2.036	0.067	0.128	0.852	0.002	0.004	0.007	0.010	0.014	0.023	1.143	2.145
	persistence	11.455	20.345	2.335	0.115	0.191	0.590	0.012	0.014	0.017	0.022	0.028	0.057	2.037	2.145

Table 4.6: *Summary of the average performance statistics for the August 1999 event for both the perfect and real-time runs and from two to six hours lead-time (with respect to nowcasts, persistence and the PFM). The best performance for each particular statistic is highlighted in green.*

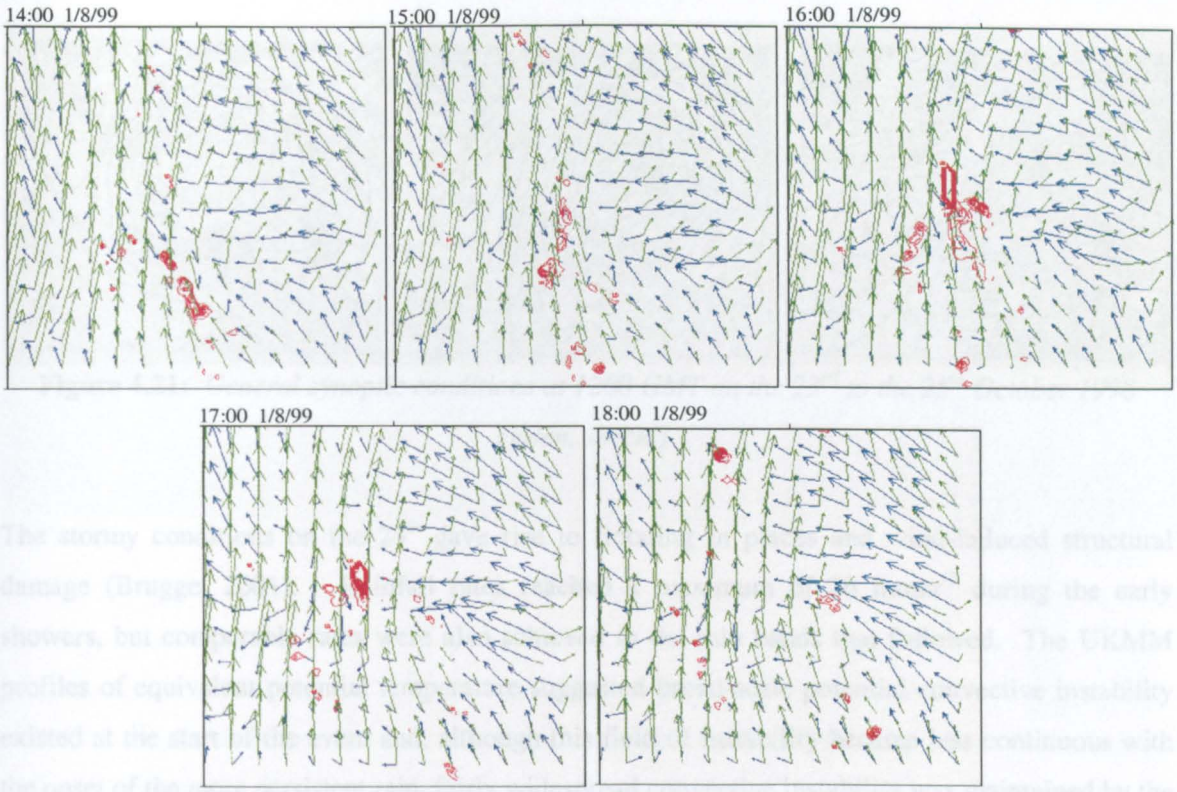

Figure 4.20: *Representation of the wind fields (direction and relative magnitude) at 700mb (green) and 1000mb (blue) between the hours of 1400 and 1800 GMT on 1st August. The rain is shown as red contours (increments of 10 mmhr^{-1}).*

4.3.4 October 1999

The last event involves a period of rainfall that occurred in late October 1999 and which exhibited both convective elements and widespread rain during the 27 hours of its duration. October had been reasonably dry that year but autumnal, showery, windy weather became prevalent from the 21st October onward, associated with a very slow moving low pressure system (Hulme, 2001). By the 23rd October this system was centred just west of the UK (Figure 4.21) and it migrated and intensified over central and eastern England during the course of the next two days. The more consistent rain and strongest winds occurred during the 24th October, having been preceded by thundery showers that had arisen in the mild conditions of the previous afternoon and evening. Some of these showers, from 2100 GMT on the 23rd to approximately 0200 GMT on the 24th, constituted the initial hours of the event which otherwise comprised the more widespread rain that followed and persisted until midnight.

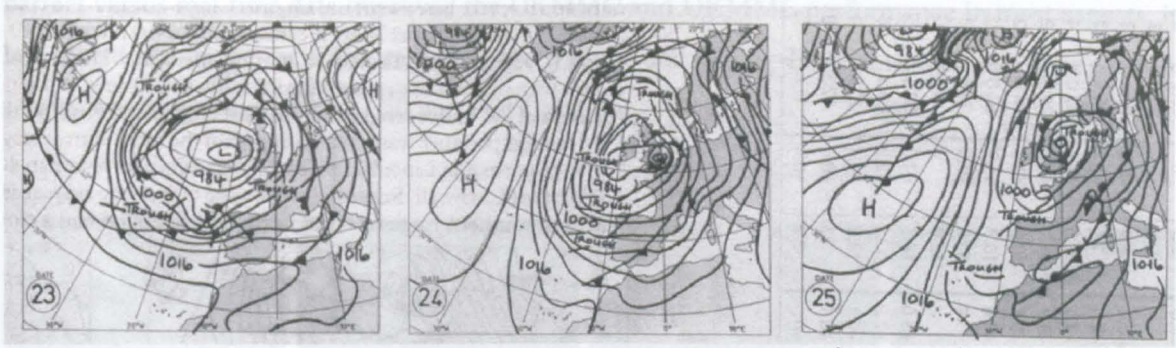

Figure 4.21: *General synoptic conditions at 1200 GMT on the 23rd to the 25th October 1998 (Eden, 1999d)*

The stormy conditions on the 24th gave rise to flooding in places and wind-induced structural damage (Brugge, 2001). Rainfall rates reached a maximum of 26 $mmhr^{-1}$ during the early showers, but comparable rates were also achieved in the rain bands that followed. The UKMM profiles of equivalent potential temperature suggested broad-scale potential convective instability existed at the start of the event and, although this field of instability became less continuous with the onset of the more persistent rain, fairly widespread convective instability was maintained by the UKMM throughout the entire event. The UKMM exhibited very little frontal development within the deepening depression, the centre of which tracked slowly northward as the event progressed and the most prominent feature of the associated rain field was its marked cyclonic rotation, as can be detected in Figure 4.22. This was equally evident in the wind field, surface winds that initially came from a southeasterly direction gradually adopted a cyclonic curvature across the whole domain. Upper-level winds began the event as southwesterlies but similarly settled into a cyclonic flow that was offset to the right of surface winds.

4.3.4.1 One hour lead-time

The event averaged performance statistics for a lead-time of one hour are presented in Table 4.7 and it can be seen from these that the PFM produced poor results in comparison to the other four forecasting methods. With use of perfect data the PFM obtained the best estimate of rainfall coverage and average rainfall rate but could not maintain that status in the real-time run, falling second to nowcasts and persistence respectively. Both nowcasts and persistence scored the equal highest CSI, persistence achieved the best FAR, and nowcasts had the best POD despite the UKMML reprising its tendency to over-predict rainfall coverage. Persistence produced the best correlations, with the PFM the next best. The PFM had the best result for RMSE out of the methods with comparable rainfall coverage and rainfall rates and was bettered only by the UKMML. The UKMMC and UKMML had similar correlation values but these were considerably worse than all other methods and their average rainfall rates were very low. Whereas the use of

perfect versus real-time data improved the UKMMC and UKMML performance in most aspects, it had mixed results for the PFM, reducing correlations and raising FAR but otherwise giving better rainfall coverage, rainfall rate, CSI and POD.

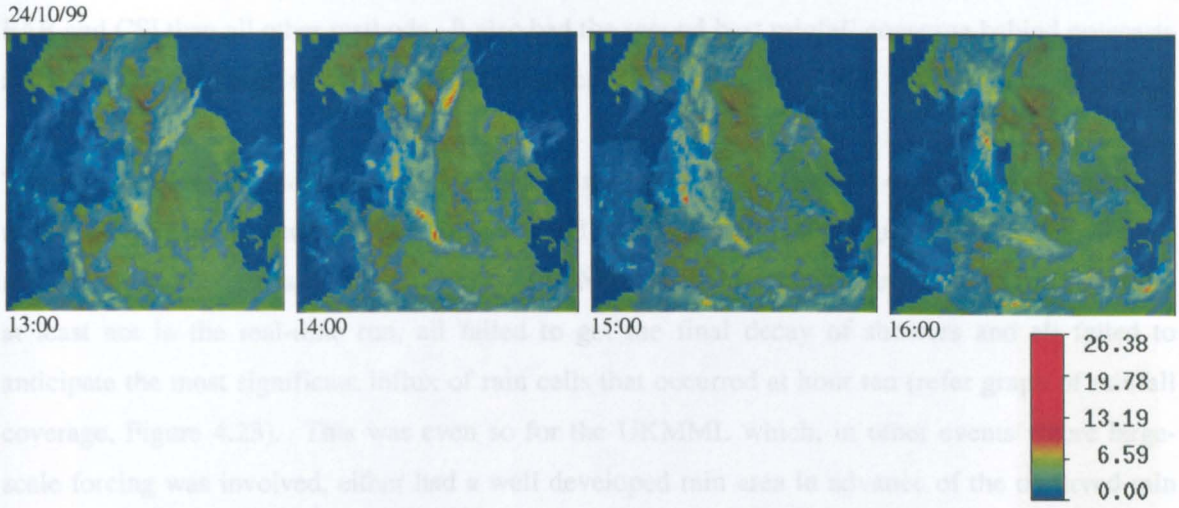

Figure 4.22: *Four consecutive hourly images of rainfall on the 24th October 1999. At the bottom left of each image is the time to which it corresponds. The legend below the set of images shows the rainfall rate in mmhr^{-1}.*

		%cov_for	%cov_act	RMSE	CSI	POD	FAR	cc5km	cc10km	cc15km	cc20km	cc25km	ccNN	rate_for	rate_act
1 hour															
Perfect															
	PFM	33.241	33.579	0.843	0.380	0.516	0.488	0.119	0.157	0.197	0.231	0.263	0.408	1.104	1.104
	UKMML	52.125	33.579	0.787	0.347	0.590	0.623	0.019	0.025	0.030	0.036	0.042	0.075	0.391	1.104
	UKMMC	16.188	33.579	0.848	0.109	0.148	0.677	0.013	0.020	0.027	0.036	0.045	0.027	0.289	1.104
	nowcast	33.923	33.579	0.929	0.384	0.546	0.487	0.074	0.111	0.150	0.193	0.235	0.350	1.176	1.104
	persistence	32.527	33.579	0.860	0.384	0.519	0.451	0.154	0.179	0.208	0.234	0.267	0.447	1.112	1.104
Real-time															
	PFM	32.972	33.579	0.843	0.378	0.513	0.477	0.120	0.159	0.199	0.234	0.266	0.408	1.093	1.104
	UKMML	49.072	33.579	0.801	0.308	0.537	0.653	0.017	0.022	0.028	0.034	0.040	0.066	0.433	1.104
	UKMMC	14.456	33.579	0.845	0.107	0.154	0.696	0.007	0.013	0.020	0.030	0.037	0.021	0.255	1.104
	nowcast	33.923	33.579	0.929	0.384	0.546	0.487	0.074	0.111	0.150	0.193	0.235	0.350	1.176	1.104
	persistence	32.527	33.579	0.860	0.384	0.519	0.451	0.154	0.179	0.208	0.234	0.267	0.447	1.112	1.104
1 hour adjusted															
Perfect															
	PFM	38.921	39.042	0.971	0.443	0.602	0.416	0.122	0.174	0.222	0.263	0.298	0.458	1.168	1.207
	UKMML	61.146	39.042	0.907	0.408	0.693	0.557	0.023	0.029	0.035	0.042	0.049	0.088	0.453	1.207
	UKMMC	18.008	39.042	0.976	0.124	0.159	0.625	0.016	0.023	0.032	0.042	0.052	0.032	0.324	1.207
	nowcast	39.286	39.042	1.067	0.439	0.615	0.413	0.086	0.128	0.172	0.221	0.269	0.409	1.246	1.207
	persistence	38.093	39.042	0.993	0.424	0.560	0.416	0.120	0.161	0.201	0.236	0.267	0.438	1.175	1.207
Real-time															
	PFM	38.605	39.042	0.971	0.440	0.598	0.403	0.124	0.177	0.226	0.267	0.302	0.460	1.159	1.207
	UKMML	57.606	39.042	0.923	0.362	0.630	0.593	0.020	0.026	0.033	0.040	0.047	0.078	0.508	1.207
	UKMMC	16.970	39.042	0.975	0.126	0.181	0.643	0.008	0.015	0.024	0.035	0.044	0.025	0.299	1.207
	nowcast	39.286	39.042	1.067	0.439	0.615	0.413	0.086	0.128	0.172	0.221	0.269	0.409	1.246	1.207
	persistence	38.093	39.042	0.993	0.424	0.560	0.416	0.120	0.161	0.201	0.236	0.267	0.438	1.175	1.207

Table 4.7: *Summary of performance statistics for the five forecasting techniques in both the perfect and real-time runs of the October 1999 event. Included are the performance statistics with and without (top and bottom respectively) the four hours during which anomalous propagation of the radar beam was thought to be occurring and influencing results.*

In trying to determine reasons for the PFM's poor performance with respect to nowcasts and persistence, it was discovered that the results were influenced by the presence of what appeared to be anomalous propagation of the radar beam during the period between convective showers and widespread rain. The effect of this is evident in the graphs of correlation and CSI (Figure 4.23),

particularly at hour seven, for which unusually high values of these performance measures were achieved by persistence. The anomalous propagation persisted for four hours and removal of the forecasts that were most affected by its presence, namely hours six, seven, eight and nine, resulted in performance statistics that for the real-time run gave the PFM better correlation coefficients, FAR and CSI than all other methods. It also had the second best rainfall coverage behind nowcasts and a better RMSE than nowcasts and persistence.

The main purpose for including in this event the remnants of the showers on the 23rd October, and the quiescent interim period before more general rain appeared, was to gauge whether any of the models handled the transition particularly well. None of them exhibited any skill on this occasion, at least not in the real-time run, all failed to get the final decay of showers and all failed to anticipate the most significant influx of rain cells that occurred at hour ten (refer graph of rainfall coverage, Figure 4.23). This was even so for the UKMML which, in other events where large-scale forcing was involved, either had a well developed rain area in advance of the observed rain field or predicted the timing of it reasonably well. The failure of the UKMML in itself probably did not bode well for the PFM's chances of correctly forecasting the initial increase in rainfall area in this event. However, looking at the graphs of rainfall coverage for the perfect run (Figure 4.24), the UKMML had the timing of storm growth correct and came close to the correct magnitude. The PFM also managed to capture some of the increase and no doubt would have done better if the UKMM's upper-level 90% relative humidity field had not trailed the leading edge of the rain band. The difference between the 600mb humidity fields of the real-time and perfect data at hour ten is shown in Figure 4.25, as is the difference between the PFM forecasts for that hour. When assessing the perfect run results it must be remembered that hour ten represents a time of 0700 GMT, which falls within the 90 minute assimilation bracket of the UKMM's 0600 analysis and so is essentially "observed" rather than forecast data, and as such its use in this manner would not be feasible in a real-time environment.

4.3.4.2 Two to six hour lead-time

The performance statistics for all five forecasting techniques with respect to a lead-time of two to six hours are given in Table 4.8. These results do not include any adjustment to account for the influence of anomalous propagation. Unlike in previous events, the average rainfall rate produced by the PFM did not decrease with increasing lead-time and was consistently the best estimate of all forecasting methods. However this, in addition to a RMSE that was typically better than nowcasts and persistence, was one of few redeeming features.

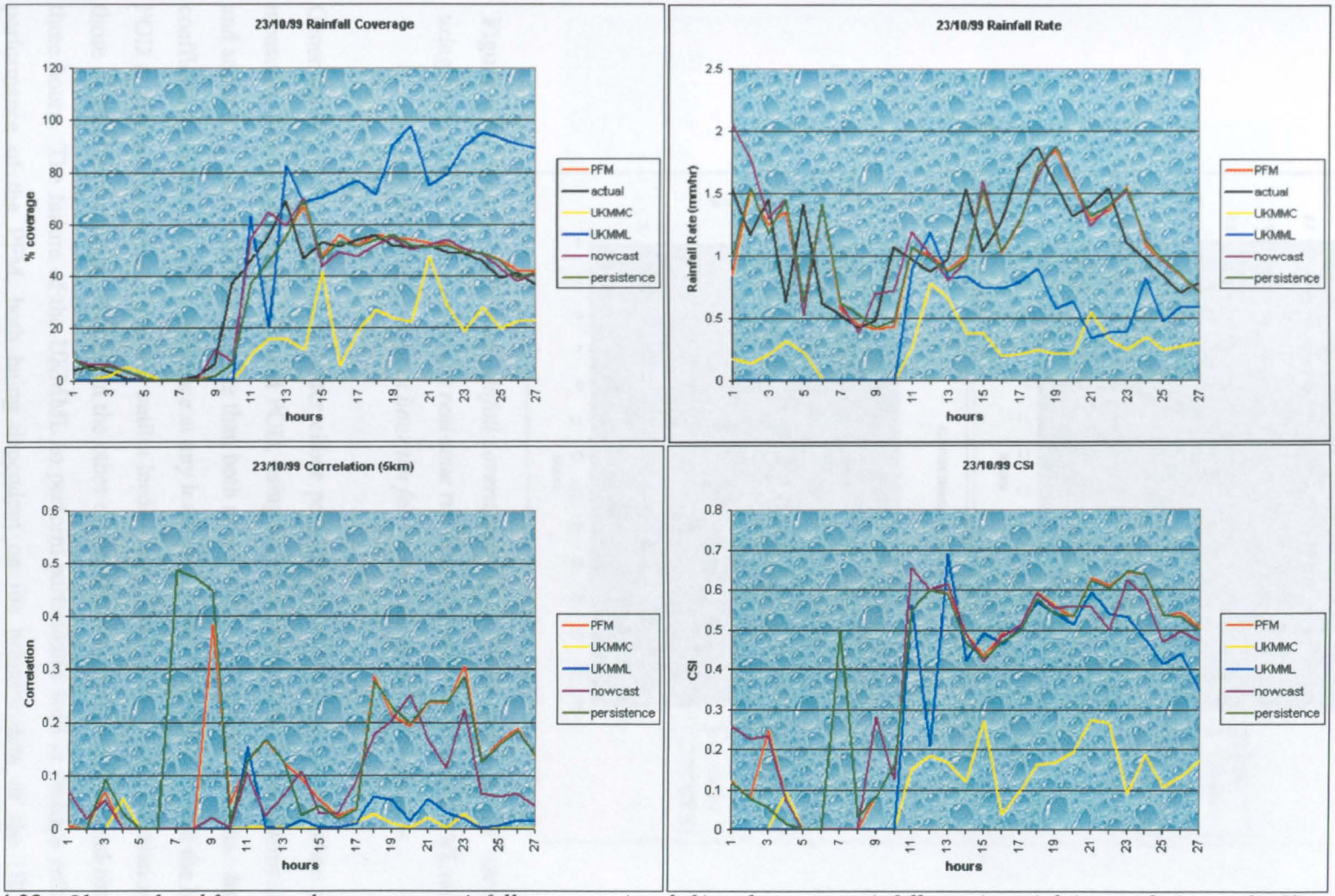

Figure 4.23: *Observed and forecasted percentage rainfall coverage (top left) and average rainfall rate (top right), correlation at the 5km scale (bottom left) and CSI (bottom right) for the rainfall event that commenced on the 23rd October 1999. The results shown are for the real-time run and to a lead-time of one hour, with hours on the horizontal axis referring to the number of hours (or the number of the forecast) since the event began.*

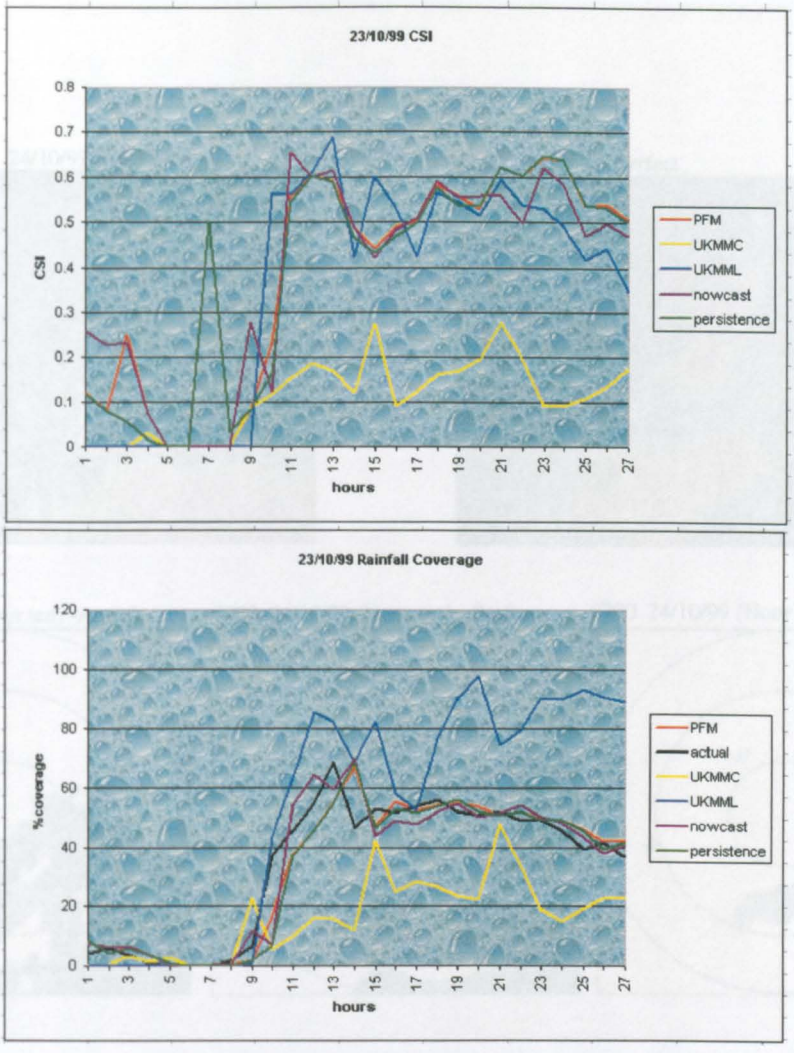

Figure 4.24: *Graphs of CSI and rainfall coverage for the event commencing 23rd October 1999, using perfect data. Compared to the real-time run (Figure 4.20), both the UKMML and the PFM show improvement at hour ten for the two performance measures.*

Generally the PFM struggled to better either persistence or nowcasts in the other performance measures, managing a better CSI and POD, using real-time data, only at a lead-time of six hours, and attaining a better rainfall coverage than both at lead-times of two and six hours. Its correlation coefficients could not better persistence at any lead-time. The UKMML achieved the best CSI and POD at all lead-times but it was not until a lead-time of five hours that its correlations exceeded those of all other methods, whereas in the other events this was achieved by a lead-time of two or three hours. The failure of the UKMML to perform particularly well is perhaps reflected in the performance of the PFM, both being dependent on the primary data of the UKMM. The performance of persistence is not unsurprising given the sequence of images in Figure 4.22, and it is easy to visualise the good match in the spatial distribution of rainfall that would result if these were to be overlaid.

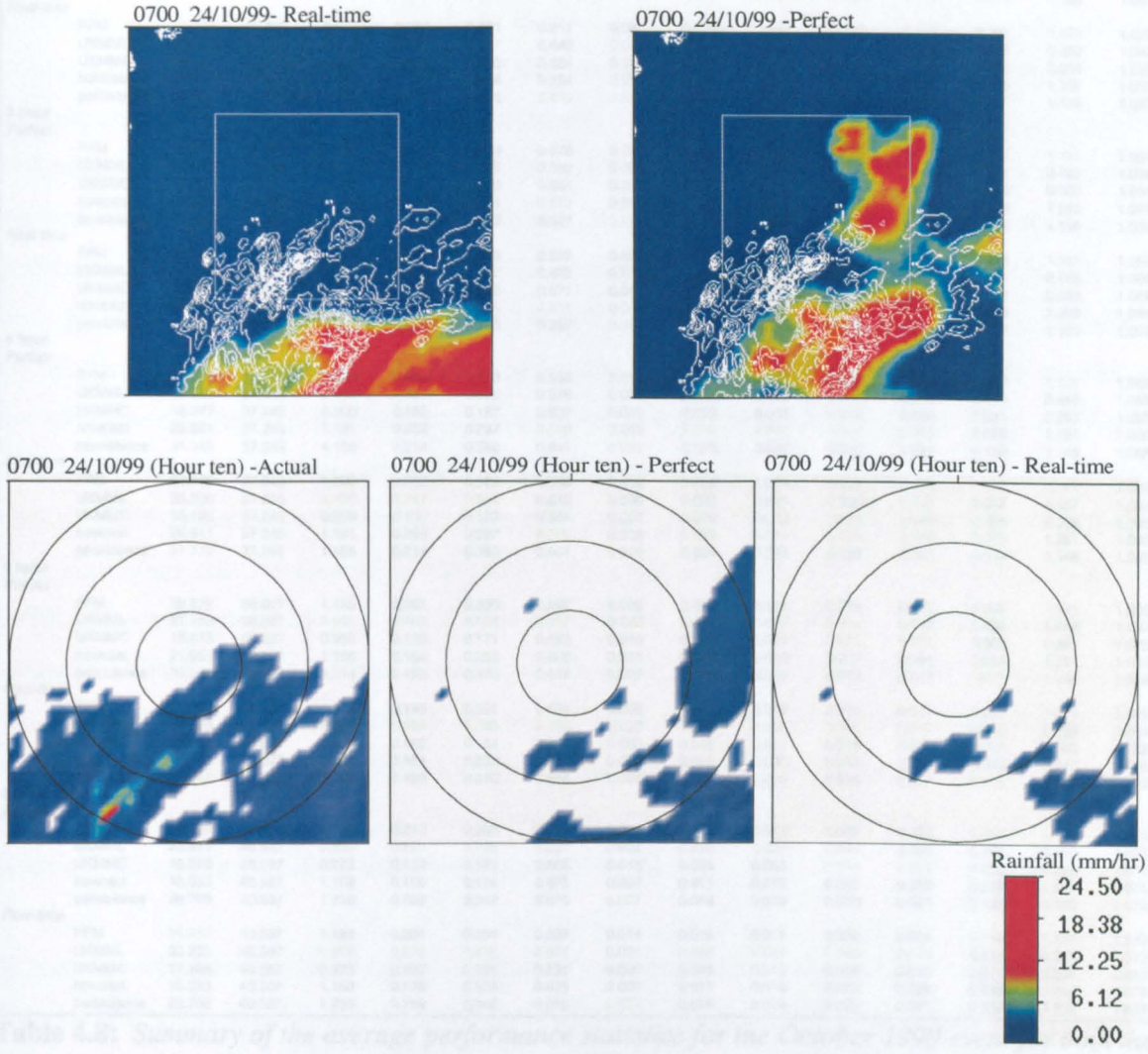

Figure 4.25: *Relative humidity fields and observed and forecasted rain fields for 24th October 1999. The top two images show areas where the UKMM 600mb relative humidity field exceeds 90% (bright colours) using real-time and perfect data (left and right respectively) for a time of 0700 GMT. The observed rain field (white contours in increments of 0.5 mmhr^{-1}) is also shown in each image and the central white box indicates the inner assessment grid of the domain. The three images below cover the area of the assessment domain and show, for the same date and time, the observed rain field (left), the PFM forecast from the perfect run (centre) and the PFM forecast from the real-time run (right). The humidity field in the perfect run assisted the PFM to capture some of the rain field development at the bottom left of the assessment area but it also caused it to create the spurious rain centre-right.*

		%cov_for	%cov_act	RMSE	CSI	POD	FAR	cc5km	cc10km	cc15km	cc20km	cc25km	ccNN	rate_for	rate_act
2 hour															
Perfect															
	PFM	32.337	34.720	0.982	0.285	0.398	0.532	0.066	0.071	0.079	0.087	0.100	0.285	1.100	1.087
	UKMML	54.130	34.720	0.801	0.361	0.613	0.608	0.020	0.025	0.031	0.037	0.043	0.078	0.406	1.087
	UKMMC	16.806	34.720	0.864	0.113	0.154	0.665	0.014	0.020	0.028	0.037	0.046	0.028	0.293	1.087
	nowcast	37.142	34.720	1.150	0.269	0.414	0.594	0.011	0.016	0.021	0.027	0.035	0.106	1.159	1.087
	persistence	32.184	34.720	1.008	0.289	0.415	0.510	0.079	0.084	0.095	0.103	0.116	0.317	1.128	1.087
Real-time															
	PFM	31.306	34.720	0.974	0.283	0.391	0.511	0.067	0.074	0.085	0.095	0.110	0.303	1.079	1.087
	UKMML	50.959	34.720	0.815	0.320	0.557	0.640	0.018	0.023	0.029	0.035	0.042	0.069	0.450	1.087
	UKMMC	15.007	34.720	0.862	0.111	0.160	0.684	0.007	0.013	0.021	0.031	0.039	0.022	0.258	1.087
	nowcast	37.142	34.720	1.150	0.269	0.414	0.594	0.011	0.016	0.021	0.027	0.035	0.106	1.159	1.087
	persistence	32.184	34.720	1.008	0.289	0.415	0.510	0.079	0.084	0.095	0.103	0.116	0.317	1.128	1.087
3 hour															
Perfect															
	PFM	31.678	35.889	1.062	0.247	0.376	0.578	0.022	0.025	0.029	0.033	0.038	0.163	1.121	1.084
	UKMML	56.295	35.889	0.815	0.375	0.638	0.593	0.021	0.027	0.032	0.039	0.045	0.081	0.422	1.084
	UKMMC	17.469	35.889	0.880	0.117	0.160	0.651	0.014	0.021	0.029	0.039	0.048	0.030	0.300	1.084
	nowcast	36.605	35.889	1.155	0.274	0.426	0.572	0.014	0.022	0.032	0.045	0.057	0.158	1.240	1.084
	persistence	31.896	35.889	1.085	0.250	0.400	0.587	0.039	0.040	0.043	0.046	0.051	0.229	1.139	1.084
Real-time															
	PFM	30.859	35.889	1.056	0.241	0.368	0.592	0.024	0.027	0.032	0.036	0.042	0.204	1.101	1.084
	UKMML	52.998	35.889	0.830	0.333	0.580	0.625	0.019	0.024	0.030	0.037	0.043	0.071	0.468	1.084
	UKMMC	15.599	35.889	0.878	0.115	0.166	0.671	0.007	0.014	0.022	0.032	0.040	0.023	0.263	1.084
	nowcast	36.605	35.889	1.155	0.274	0.426	0.572	0.014	0.022	0.032	0.045	0.057	0.158	1.240	1.084
	persistence	31.896	35.889	1.085	0.250	0.400	0.587	0.039	0.040	0.043	0.046	0.051	0.229	1.139	1.084
4 hour															
Perfect															
	PFM	29.925	37.245	1.098	0.208	0.343	0.596	0.017	0.019	0.024	0.032	0.040	0.127	1.126	1.068
	UKMML	58.640	37.245	0.833	0.391	0.664	0.576	0.022	0.028	0.034	0.040	0.047	0.084	0.440	1.068
	UKMMC	18.077	37.245	0.900	0.122	0.167	0.637	0.015	0.022	0.031	0.040	0.050	0.031	0.293	1.068
	nowcast	29.941	37.245	1.191	0.209	0.297	0.590	0.018	0.029	0.041	0.055	0.068	0.079	1.251	1.068
	persistence	31.319	37.245	1.156	0.214	0.388	0.641	0.030	0.025	0.027	0.033	0.041	0.130	1.146	1.068
Real-time															
	PFM	29.476	37.245	1.099	0.202	0.336	0.639	0.018	0.019	0.024	0.032	0.040	0.138	1.077	1.068
	UKMML	55.206	37.245	0.848	0.347	0.604	0.610	0.020	0.025	0.031	0.038	0.045	0.074	0.487	1.068
	UKMMC	16.180	37.245	0.898	0.120	0.173	0.657	0.007	0.014	0.023	0.033	0.042	0.024	0.265	1.068
	nowcast	29.941	37.245	1.191	0.209	0.297	0.590	0.018	0.029	0.041	0.055	0.068	0.079	1.251	1.068
	persistence	31.319	37.245	1.156	0.214	0.388	0.641	0.030	0.025	0.027	0.033	0.041	0.130	1.146	1.068
5 hour															
Perfect															
	PFM	29.572	38.827	1.156	0.205	0.330	0.569	0.009	0.010	0.014	0.019	0.025	0.087	1.101	1.088
	UKMML	61.190	38.827	0.866	0.408	0.693	0.557	0.023	0.029	0.035	0.042	0.049	0.088	0.459	1.088
	UKMMC	18.813	38.827	0.936	0.126	0.171	0.623	0.016	0.023	0.031	0.042	0.051	0.029	0.291	1.088
	nowcast	21.951	38.827	1.190	0.164	0.253	0.600	0.015	0.022	0.030	0.037	0.045	0.049	1.241	1.088
	persistence	30.551	38.827	1.214	0.198	0.370	0.614	0.027	0.017	0.015	0.015	0.017	0.115	1.148	1.088
Real-time															
	PFM	29.427	38.827	1.164	0.195	0.321	0.624	0.009	0.009	0.012	0.015	0.017	0.099	1.076	1.088
	UKMML	57.606	38.827	0.882	0.362	0.630	0.593	0.020	0.026	0.033	0.040	0.047	0.078	0.508	1.088
	UKMMC	16.659	38.827	0.934	0.122	0.154	0.647	0.005	0.008	0.011	0.015	0.019	0.017	0.262	1.088
	nowcast	21.951	38.827	1.190	0.164	0.253	0.600	0.015	0.022	0.030	0.037	0.045	0.049	1.241	1.088
	persistence	30.551	38.827	1.214	0.198	0.370	0.614	0.027	0.017	0.015	0.015	0.017	0.115	1.148	1.088
6 hour															
Perfect															
	PFM	30.909	40.587	1.196	0.210	0.365	0.554	0.014	0.015	0.018	0.022	0.025	0.140	1.177	1.073
	UKMML	63.971	40.587	0.903	0.426	0.725	0.537	0.024	0.030	0.037	0.044	0.051	0.092	0.480	1.073
	UKMMC	19.550	40.587	0.976	0.132	0.179	0.606	0.016	0.024	0.033	0.044	0.054	0.030	0.294	1.073
	nowcast	15.033	40.587	1.188	0.106	0.154	0.675	0.007	0.011	0.016	0.022	0.028	0.039	1.242	1.073
	persistence	29.708	40.587	1.230	0.189	0.342	0.616	0.027	0.019	0.019	0.020	0.021	0.128	1.130	1.073
Real-time															
	PFM	30.352	40.587	1.190	0.201	0.354	0.633	0.014	0.015	0.019	0.022	0.025	0.140	1.100	1.073
	UKMML	60.225	40.587	0.919	0.378	0.659	0.574	0.021	0.028	0.034	0.042	0.049	0.081	0.531	1.073
	UKMMC	17.298	40.587	0.973	0.127	0.161	0.631	0.006	0.008	0.012	0.015	0.019	0.017	0.264	1.073
	nowcast	15.033	40.587	1.188	0.106	0.154	0.675	0.007	0.011	0.016	0.022	0.028	0.039	1.242	1.073
	persistence	29.708	40.587	1.230	0.189	0.342	0.616	0.027	0.019	0.019	0.020	0.021	0.128	1.130	1.073

Table 4.8: *Summary of the average performance statistics for the October 1999 event for both the perfect and real-time runs and from two to six hours lead-time (with respect to nowcasts, persistence and the PFM). The best performance for each particular statistic is highlighted in green.*

4.4 Summary and discussion

Brooks *et al* (1996), when outlining their ingredients-based approach to flood forecasting, made the revelation that floods often arise from heavy precipitation and that "the heaviest precipitation occurs where the rainfall rate is the highest for the longest time". Most of the events examined in the case study consisted of a period of rainfall of sufficient intensity and duration to lead to flooding. This in itself indicated that the persistence method of forecasting, particularly at a lead-time of one hour, was likely to perform reasonably well in the case study. It might also seem to justify reliance on the persistence approach as an expedient rainfall forecast for use in flood

prediction, however it would be at risk of regularly creating floods out of mobile, transitory storm systems.

One of the aims in producing the PFM was to achieve an adapted form of the F&K model that was conceptually more acceptable, and that was also competent, to use across the mixed array of storms experienced in the UK, a good many of which are associated with eastward moving fronts embedded in low pressure systems. Although the PFM exhibited daily variability in its standard of performance under similar synoptic conditions, in which it was not alone, its event-averaged performance with respect to a lead-time of one hour was, for the frontal events, always competitive with the other forecasting techniques against which it was compared, and often better, especially in correlations, RMSE (against nowcasts and persistence) and CSI. Notably the UKMML proved, on occasions, quite adept at predicting the timing of the frontal storms and also the relative distribution of rainfall rate within them, and this reflected the reasonable skill of the UKMM under these conditions in emulating the dynamics of the mesoscale atmospheric environment for a period of at least nine hours into the future. It was clear the signifiers chosen from the UKMM to locate the PFM's forecasted rain field, i.e. the criteria established in the preceding chapter, were key to its success in identifying the increases and decreases in rain field size that were not related simply to rain field advection. The chapter to follow will take a closer look at the contribution of other components of the PFM algorithm, specifically the implementation of orographic uplift and the mode of forcing adopted, to its rainfall production and its spatial distribution of rainfall rate, the latter as reflected in the correlation coefficients achieved.

In the convective events the PFM's performance was again mixed with respect to individual days. But overall, and if considering the last event within which convection was actively coupled with the broad-scale lifting induced by the deepening depression, the results were, like the frontal events, good in comparison to other methods despite a very poor showing on the first day of the August event (and after adjustment for occurrences of anomalous propagation). The performances of the UKMML and the UKMMC forecasts were also mixed in the convective events, drawing attention to the nature of the UKMM data the PFM was working with and exposing drawbacks in relying on this data in conditions that create forecasting difficulties for most operational NWP models.

It was evident that some aspects of the PFM's operation were problematic. The estimation of the average rainfall rate in the PFM was one of them, the results being a product of the rudimentary way cloud column liquid water was apportioned to cloud base liquid water. The methodology adopted rather purposefully took away any emphasis on the initial values of the primary input data by effectively normalising the rate of moisture production attributed to initial conditions with the

corresponding rainfall rate. Therefore the PFM's representation of rain field dynamics, in terms of rainfall intensity changes and also decay of the existing rain field, depended on changes in the primary input variables over the forecast lead-time. Little change in these variables, namely temperature, pressure, mixing ratio and cloud top temperature, meant little difference between nowcasts, persistence and the PFM's forecasts, other than those resulting from the choice of advection scheme and changes in the instability field. Although the factor employed to determine CBLWC from cloud column condensation attempts to implicitly account for phase changes and how those might influence the rate of precipitation development, the failure of the PFM to explicitly determine the type of precipitation ultimately occurring and the effect of precipitation type on radar reflectivity measurements were together likely to have contributed to the difficulty the PFM had in correctly forecasting the precipitation rate.

Selection of the appropriate advection scheme was another troublesome area of the PFM's operation. The most favoured scheme appeared to be persistence followed by the nowcast method, with instances of either the UKMM 700mb or 850mb wind field providing the velocity vector. The difficulty in appropriate selection arose for two reasons: firstly the nature of storms in the UK, whereby many, if not most, approach over sea areas and change the nature of their momentum over land; secondly there was often a trade-off between different approaches, persistence typically gave better correlations but resulted in a failure to track the progression of rain fields into and out of the domain.

When the one-hour lead-time statistics were averaged over all four events (Table 4.9) the PFM showed itself to be superior to the other methods in both its spatial distribution of the rain field and relative spatial distribution of rainfall intensity, attaining the best CSI as a measure of the former and the best correlation coefficients across all scales, and also nearest neighbour, as a measure of the latter. The PFM's estimates of rainfall coverage and average rainfall rate were comparable to nowcasts and persistence and most importantly to that observed. The PFM's rainfall coverage was approximately 1% short of the observed value (equivalent to 18 grid cells) and within 0.1 $mmhr^{-1}$ of the actual average rainfall rate.

At lead-times greater than one hour the UKMML was the most successful in many of the performance measures, even at a two-hour lead-time when most of the UKMML forecasts had a lead-time in excess of three hours (three hours that is from the time of the analysis but with the benefit of the 90 minute assimilation period after that time). Its CSI, POD and correlations at all scales (except nearest neighbour) were better than all other methods. Nimrod forecasts were unavailable for inclusion in this assessment but, judging from these results, its method of merging UKMM predicted rainfall with nowcasts appears to be founded on a good proposition. The main

problem with the UKMML as a stand-alone option is its resolution, which gives rise to excessive rainfall coverage and a lowly average rainfall rate, the latter perhaps in danger of not signalling the flooding potential of a storm.

		%cov_for	%cov_act	RMSE	CSI	POD	FAR	cc5km	cc10km	cc15km	cc20km	cc25km	ccNN	rate_for	rate_act
1 hour															
	PFM	24.61229	25.68365	*2.116313*	0.296989	0.441384	0.503715	0.093029	0.117062	0.138648	0.160216	0.185542	0.29768	2.290928	2.23268
	UKMML	41.17125	25.68365	1.903648	0.26545	0.552091	0.67791	0.046928	0.060799	0.073446	0.08627	0.098476	0.088244	0.690501	2.23268
	UKMMC	12.90302	25.68365	1.755342	0.090233	0.159117	0.750978	0.011928	0.017907	0.024859	0.033124	0.041582	0.029869	0.262436	2.23268
	nrad	25.56959	25.68365	2.490422	0.271683	0.40866	0.579302	0.042345	0.065126	0.087581	0.109387	0.130718	0.197827	2.125041	2.23268
	persist	24.75426	25.68365	2.304137	0.292891	0.449648	0.496804	0.092156	0.109839	0.129168	0.148116	0.172258	0.286088	2.174451	2.23268
2 hour															
	PFM	23.49341	27.62733	2.54686	*0.205951*	0.334685	0.575475	0.027632	*0.037088*	*0.047432*	*0.059029*	*0.072837*	0.157712	2.186293	2.308488
	UKMML	43.40652	27.62733	2.07261	0.282261	0.572436	0.657283	0.04593	0.060666	0.074207	0.088187	0.101532	0.0888	0.722502	2.308488
	UKMMC	13.56633	27.62733	1.975835	0.105473	0.204274	0.723872	0.012915	0.019378	0.026861	0.035733	0.044793	0.030865	0.270706	2.308488
	nrad	23.60768	27.62733	2.481563	0.194578	0.302111	0.626426	0.022129	0.030034	0.037236	0.045225	0.055152	0.113747	1.843304	2.308488
	persist	24.99747	27.62733	2.754288	0.196696	0.348608	0.565068	0.030066	0.035743	0.042769	0.050656	0.061078	0.148045	2.155739	2.308488
3 hour															
	PFM	24.99831	29.13177	*2.485137*	*0.178902*	*0.327714*	*0.580238*	*0.021296*	*0.031735*	*0.042826*	*0.055987*	*0.070503*	0.123085	1.976851	2.287351
	UKMML	45.03628	29.13177	2.175973	0.292779	0.580277	0.646785	0.045223	0.060841	0.075221	0.090013	0.103977	0.090052	0.738242	2.287351
	UKMMC	14.00003	29.13177	2.081645	0.110207	0.198292	0.704141	0.013114	0.019264	0.026328	0.034799	0.043732	0.029084	0.279923	2.287351
	nrad	21.97504	29.13177	2.612463	0.146001	0.259373	0.685713	0.005272	0.009061	0.013789	0.019628	0.025896	0.051416	1.688938	2.287351
	persist	24.71524	29.13177	2.743061	0.150445	0.309456	0.600117	0.02084	0.02729	0.035457	0.044877	0.055922	0.113051	1.960195	2.287351
4 hour															
	PFM	24.08936	29.09867	2.766793	*0.15148*	*0.301642*	0.624236	*0.018973*	*0.0257*	*0.034038*	*0.043986*	*0.055215*	0.096904	2.496123	2.330813
	UKMML	45.30169	29.09867	2.292902	0.289084	0.57751	0.648601	0.042864	0.058806	0.073446	0.088632	0.102848	0.086006	0.744282	2.330813
	UKMMC	14.26569	29.09867	2.183852	0.113249	0.204235	0.700719	0.011947	0.017549	0.024043	0.031823	0.039913	0.026705	0.282854	2.330813
	nrad	17.38463	29.09867	2.673355	0.104159	0.187467	0.725372	0.006466	0.010513	0.015109	0.020465	0.026624	0.034004	1.556103	2.330813
	persist	23.65237	29.09867	2.874347	0.12194	0.289752	0.63594	0.017957	0.020391	0.025586	0.03182	0.039305	0.07999	1.92798	2.330813
5 hour															
	PFM	21.35007	27.95557	2.334345	*0.132588*	*0.263408*	0.607426	0.009021	*0.013257*	*0.018396*	*0.024244*	*0.030181*	*0.075869*	1.885178	1.984486
	UKMML	44.69979	27.95557	1.997705	0.280821	0.580575	0.654967	0.041273	0.057531	0.072337	0.087648	0.101771	0.083971	0.734829	1.984486
	UKMMC	14.57404	27.95557	1.872871	0.114838	0.214718	0.714084	0.009304	0.013538	0.018352	0.023972	0.030195	0.023186	0.286433	1.984486
	nrad	13.5908	27.95557	2.234382	0.072192	0.142669	0.799349	0.003361	0.005635	0.008293	0.011654	0.015645	0.024115	1.109393	1.984486
	persist	21.48122	27.95557	2.467626	0.110569	0.257311	0.620625	0.011868	0.012442	0.016274	0.021027	0.026398	0.069728	1.627979	1.984486
6 hour															
	PFM	18.25672	25.95554	1.700785	*0.120437*	*0.228763*	0.690315	*0.011986*	*0.017668*	*0.024478*	*0.032612*	*0.041601*	0.078582	1.169845	1.602158
	UKMML	42.99819	25.95554	1.455935	0.256767	0.565461	0.679525	0.033348	0.048737	0.062979	0.07802	0.092052	0.069494	0.678549	1.602158
	UKMMC	13.87969	25.95554	1.293603	0.11388	0.224372	0.725118	0.006481	0.00972	0.013182	0.016843	0.020711	0.022111	0.296636	1.602158
	nrad	9.612477	25.95554	1.608495	0.044213	0.100147	0.862706	0.001706	0.003159	0.004959	0.007182	0.009796	0.016101	0.761914	1.602158
	persist	18.24795	25.95554	1.85962	0.105505	0.22421	0.597006	0.011843	0.012871	0.016125	0.02079	0.026733	0.057931	1.474984	1.602158

Table 4.9: *The performance statistics for lead-times of one to six hours averaged over all four storm events of the UK case study. The results for real-time runs only are shown. The values presented were calculated by taking the mean of original daily performance averages calculated to six decimal places (therefore they do not include any adjustment for anomalous propagation of the radar beam during the October event). The best performance is highlighted in green and where the PFM is better than both nowcasts and persistence, the result is in italics.*

With increasing lead-time the PFM generally maintained its standard of performance relative to nowcasts and persistence. Apart from coming second to persistence in correlations at the 5km scale at the two and five hour lead-times, the PFM produced the best correlation coefficients over the range of scales at all lead-times. Additionally, it had the best nearest neighbour correlation coefficient of all five forecasting methods at all lead-times except five hours, beaten by the UKMML in that instance. The PFM had the better CSI than nowcasts and persistence at all lead-times and beyond two hours had the better POD and FAR, the latter being the best of all methods except at a lead-time of six hours. Its RMSE was consistently lower than persistence, the only other forecast method with similar rainfall coverage and rainfall rate to the PFM as lead-time increased. From lead-times of two to five hours the PFM had the best average rainfall rate and for lead-times of three, four and six hours, the best rainfall coverage.

These results seem to suggest that use of NWP forecast data, specifically being UKMM data in this research, and an attempt to employ some representation of storm dynamics do add value to simpler forms of forecasting and enable better attainment of some of the spatial characteristics of the observed rain field at longer lead-times. The PFM's level of success was clearly dependent on the NWP forecasts that served as inputs to the algorithm and a closer look at the appropriateness of the chosen signifiers would be useful upon availability of more data. An example of one possible alteration would be lowering the relative humidity threshold to 85%, the figure used in MOPS for cloud formation, which would expand the rain area. This may have the effect of increasing POD but it may not necessarily produce commensurate gains in CSI due to incorrect assignment of rainfall to cells in which none is observed, similarly if the humidity signifier is replaced with the UKMML rainfall area itself. Additional UKMM fields might be of use in the PFM algorithm such as cloud top pressure which, mainly at longer lead-times, could replace advected satellite cloud top temperatures in areas outside the existing rain field. However, not all NWP models routinely produce this information, a factor that has to be considered if intending to apply the model outside the range of the UKMM. It remains to be seen how well the PFM performs in different settings using NWP data from other models and whether the signifiers chosen prove suitable in alternative conditions. This will be looked at in the penultimate chapter, which presents a case study centred on the Mediterranean coast of France using NWP data from the ALADIN model. Irrespective of the primary source data, there is obvious room for improvement in the PFM's operation, namely determination of CBLWC from the time evolution of liquid within the cloud column, for which the use of full scan radar would probably prove beneficial. Ideally though it would be useful to have a methodology that circumvented the need to have existing rain in the domain before effective forecasts are possible. Advection scheme implementation needs closer consideration and ideally one developed that allows differential advection over sea and over land. As mentioned previously, the following chapter investigates whether the attempts to incorporate orographic influences in the PFM algorithm offered any improvement in results and likewise attempts to differentiate between modes of uplift.

Although the PFM's results varied with use of the most current data versus extended forecasts, the latter was not necessarily detrimental to the PFM's performance. At times the PFM's performance statistics were better using the real-time rather than perfect UKMM inputs and this appeared to be simply dependent upon the nature of the UKMM forecasts. Figure 4.25 provides an example of when the UKMM's perfect forecast of 600mb relative humidity appeared more accurate than the real-time forecast and although this led the perfect PFM forecast to have a superior CSI, it also led to a higher FAR and lower correlation coefficients because the PFM consequently predicted rainfall in the central eastern area of the domain where it was not observed. Overall the results

appeared to suggest that the three to nine hour separation of forecasts from their respective analysis, which would have to be endured in an operational environment, would not severely compromise success in flood forecasting. At longer lead-times the UKMM rainfall forecasts themselves provided better performance statistics than other methods but the forecasts of the PFM still retained value through their closer approximation to rain field size and rainfall rate and their greater nearest neighbour correlation.

It should be noted that the forecasts made in the four storm events were based on radar estimates of rainfall that had not undergone extensive correction procedures and the forecasts were not of rainfall per se but of a radar estimate of rainfall, the recorded values of the latter being against which all forecasts were evaluated. A flood forecasting system would need to incorporate comprehensive quality control and correction of the weather radar data, such as undertaken in the Nimrod system and which, in addition to the on-site processing mentioned in the previous chapter, includes identification and removal of corrupt radar images, identification and removal of anomalous propagation, accounting for variations in the vertical profile of reflectivity (corrections for bright band and orographic enhancement beneath the radar beam) and adjustment for calibration errors by use of data from rain gauges (Driscoll *et al*, 2000).

CHAPTER FIVE

THE ROLE OF FORCING MECHANISMS IN THE PFM

5.1 Introduction

A conclusion stated in the previous chapter, with respect to the PFM's performance at a lead-time of one hour, was that the correlation coefficients achieved at the $5km^2$ scale, as averaged over the nine separate occasions of rainfall in the four storm events included in the UK case study, were better than any other method. The reason for this might simply be success in juggling advection schemes or it might be indebted to high quality UKMM moisture and temperature fields. Alternatively or additionally there may have been contributions from the different facets of the algorithm that govern the rate of uplift attributed to each grid cell. This last supposition will be given attention in this chapter, the key questions being whether inclusion of the orographic component of the PFM actually improved its performance and whether the effort of identifying the predominant mode of forcing behind grid-scale vertical motion (free convection or mainly forced uplift) was to some extent rewarded and therefore justified, not only in theory but also in practice. The limited amount of data available to undertake this assessment, being exactly the data used in the previous case study, means that the results of this investigation cannot be taken as definitive, likewise the results detailed in the preceding chapter, but they provide a starting point for commenting on the significance of various components of the PFM.

5.2 Orographic influences on precipitation and rain field development

The array of network radar images of rainfall displayed in Figures 4.1, 4.10, 4.16 and 4.22 are alone sufficient to gauge that orographic enhancement of rainfall was occurring over the Pennines and Cambrian Mountains in most of the rainfall periods constituting the four storm events. More than that, it seemed that these and other areas of elevated terrain served to modify storm movement, particularly during the wintertime frontal events when the outcome of the interaction was often a protracted passage of the storm system over the aforementioned areas and a change in the organisation and intensity of rain cells to the lee of hills. Explanations for this can be sourced from Barry (1981), who noted how the presence of topographic barriers can modify frontal

characteristics through both thermodynamic and dynamic mechanisms: the thermal structure of fronts can be altered when they pass over cold air lying in inter-montane basins, with the horizontal temperature gradient in the vicinity of warm and cold fronts intensified and weakened respectively; the temperature profile within the front can be altered through the expansion and cooling of air as it rises over elevated terrain; orographic lifting of frontal air may produce condensation and precipitation, with the resultant changes in humidity and also the drying of air as the front moves to leeward causing changes in its thermodynamic properties, these processes often serving to weaken its intensity; the gradient of mountain barriers can cause advancing frontal air to be trapped at low levels thereby slowing progress of the front and as a consequence prolonging rainfall on upwind slopes, with the additional possibility that free-moving upper fronts may separate from surface fronts and later regenerate downwind of the barrier. The potential of hills to retard a frontal system's momentum is generally considered greater with respect to warm fronts, which often have a gentler slope than mountain ranges (eg. 1:100 versus 1:20 respectively), than for cold fronts (typical slopes of 1:20), but the same effect can occur with both. The occurrence and magnitude of all the effects described are dependent on the speed and intensity of the system and are most notable when the front's line of approach lies normal to the alignment of the relief.

Orographic enhancement of rainfall, according to Smith (1982), chiefly occurs under three conditions: in association with existing stratiform rain within which rainfall rates are enhanced by Bergeron's seeder-feeder mechanism; through release of instability by forced uplift over elevated terrain to give deep convection or convection embedded in stratiform rain; and through blocking of surface fronts, as mentioned above, leading to differential advection aloft and again a situation of instability which is subsequently released. Once initiated the enhancement may persist and appear anchored to a topographic feature while the conditions producing the enhancement remain in place (Sumner, 1988). Orographic enhancement of rainfall can be seen to occur over hills as low as 50 metres in height (Brown and Kitchen, 1992) and terrain differences alone can influence the distribution of precipitation and intensity of rainfall, with surface frictional and/or temperature differences in areas such as the sea-land interface of coasts causing local boundary layer convergence and uplift (Browning, 1980). Most rainfall enhancement is thought to occur within 1500 metres of the surface (Bader *et al*, 1981), a phenomenon that creates problems for the UK weather radar network which, at times, because of beam overshooting, misses some of the orographic enhancement that occurs. Corrections are routinely applied within the UKMO's Nimrod system to account for this, a correction scheme based on the values of relative humidity at low levels and the speed and direction of winds 800m above the ground (Driscoll *et al*, 2000), all of which are seen as key factors governing the extent of the orographic enhancement that occurs in the British Isles (Bader *et al*, 1981). In the UK, enhanced rainfall intensities over hill slopes are most associated with winds coming from the sector between the south and west because they are often

strong and carry moist maritime air (Hill, 1983). Western areas, therefore, generally have the heaviest rainfalls, which Browning (1980) attributed not only to moisture-laden winds from the southwest quarter but also to the uplift induced by the hills in those areas and also the near-neutral or weak potential instability commonly present in the approaching air. The role of instability in orographic enhancement was seen as quite crucial by Elliot and Shaffer (1962), who, in their study of rainfall over the San Gabriel Ranges north of Los Angeles, found, contrary to what was expected, that the coastal plains upwind of the mountains with respect to the predominant wind direction sometimes received noticeably more rainfall than the mountains themselves. They identified atmospheric stability as the key determinant of whether the coastal plains or the hills received the heaviest rainfall, stable air masses giving greater rainfall at the coasts and unstable air giving greater rainfall over hills.

The importance of wind speed in the orographic enhancement of rainfall, and more specifically the strength of the uplift it creates by flowing over elevated terrain, was highlighted by Bader *et al* (1981) who discovered rates of enhancement to be dictated more by surface wind speed than the background rainfall rate, provided the background rainfall rate exceeded 0.5 $mmhr^{-1}$. This was an observation supported to some extent by the conclusions of Browning *et al* (1975) in their study of orographic effects within frontal rainfall, finding that the presumption of ana cold fronts producing higher intensity rainfall than kata fronts, while valid over low land, did not hold over hills, where it seemed orographic enhancement could be of equal intensity for both types of front. The orographic component of the PFM concentrates on this aspect of rainfall enhancement, principally that the intensity of orographic precipitation at any point has a strong dependency on the speed and direction of surface winds because of the uplift they can induce. As such, the rate of orographic uplift is determined in the PFM through term 2 of equation (2.45), isolated below for ease of reference.

$$w_T = \bar{v}_0 \nabla \bar{z}_0 \tag{5.1}$$

where w_T is the vertical wind component relative to the slope of the topography (ms^{-1}) (Barry, 1981). Obviously, equation (5.1) is not a sophisticated determination of the profile of vertical motion produced by winds flowing over a topographic barrier, rather it is a simple formulation aimed towards differentiating the relative strength of the forcing across the domain, to identify where orographic uplift may be augmenting upward vertical motion, where it may be contributing to the release of instability or alternatively where orographic downflows are serving to extinguish the potential for rainfall production. Reliance on such a simple representation of orographic forcing in the PFM appeared justified in light of Banta's (1990) judgement on how this mechanism is implicated in the enhancement of rainfall, describing it as "effectively simple dynamics", "an

unsubtle effect" and adding that "a model forced simply by continuity of air flowing over a barrier can capture the dominant lifting of the moisture rich air".

Equation (5.1) was essentially the means by which Bell (1978) and Collier (1975) calculated orographically induced velocity motion in their respective rainfall forecasting models. Collier incorporated this term in a detailed parameterisation of the vertical velocity at the top of the boundary layer, which included terms for frictionally induced convergence and variability in boundary layer depth, but he noted how the orographic term tended to dominate. In Bell's layered model, the term was applied to each layer but its influence was regulated by a factor that decreased linearly with height, in contrast to others who have suggested the decrease takes a parabolic form (Barry, 1981). Andrieu *et al* (1996) modified the product of equation (5.1) with a parameter that required local calibration, intending the velocity obtained to be representative of the column-averaged rate of uplift. Wild (1996), in testing his version of the F&K model, chose to use equation (5.1) without modification or the addition of further parameters and argued against the need for their inclusion by presenting two-dimensional Regional Atmospheric Model System (RAMS) simulations of surface winds flowing over topography. The results showed that, in the RAMS simulations at least, the modification of the wind field with height was very much dependent on the height-to-width ratio of the topographic feature. Wild cited the typical dimensions of hills in the area covered by his model's domain (the same as that of the PFM) as being 500m(height):20000m(width) and in the simulations he found this shape to be associated with barely discernible variation in the vertical component of wind velocity with increasing height in the vicinity of the topographic feature. In presenting these results Wild acknowledged that the simulations were undertaken using unrealistic conditions that included a vertical profile of uniform horizontal wind speed and topography of smooth parabolic form.

Lacking surface wind data, Wild relied on the vector of storm velocity to represent the horizontal wind field of equation (5.1), whereas both Collier and Bell had surface wind data at their disposal. For the case study presented in the previous chapter, the UKMM wind field at the 1000mb level took the role of surface winds in generating positive orographic updraft on windward slopes and downdrafts to the lee of hills (and for the rest of this chapter any use of the term "surface winds" should be understood to be a reference to the 1000mb wind field). The gradients at each computational point, in both the x and y directions, were calculated over a distance of 10 000 metres, in the same manner as Wild (1996), and undertaken this way with the assurance that airflow does not follow every detail of local topography especially when hills are clustered together (Browning, 1980).

In order to gauge whether the orographic component of the model contributed positively to the PFM's forecasting in the four storm events of the UK case study, in terms of improving its performance statistics, the same data sets were utilised again to run the PFM a number of additional times and in each run different adjustments were made to either the way the orographic updraft was determined or to the precedence given to orographic forcing in the PFM algorithm. Specifically, three variations were explored:

1. to increase the time-step of the PFM to be commensurate with the forecast lead-time so that only one time-step was necessary to make a forecast
2. to experiment with using different wind fields, namely the UKMM wind field at a higher level and the vector of storm velocity, the latter as determined in the "nowcasting" method referred to in the previous chapter and in essence being those produced from maximising the cross correlation between consecutive network radar images.
3. to completely remove the orographic component of the PFM by setting the orographic updraft to zero in all cells of the PFM domain.

It should be remembered that the PFM in its original form used positive orographic updrafts not only to increase the strength of uplift within a grid cell but also, in the presence of atmospheric instability, to trigger the convective parameterisation for quantification of the updraft velocity. All nine days of rainfall making up the four storm events of the previous chapter were included in this exercise but only the real-time data set was used and only a lead-time of one hour assessed.

5.2.1. One versus multiple time steps

The purpose of employing multiple time-steps to produce one forecast was to allow the rain field to be modified by its traverse over the irregular topography of the domain during the period of the forecast lead-time. The 300 seconds (5 minutes) duration chosen for each time-step was a compromise between trying to avoid movement of rain cells over more than one computational point within a time-step and allowing a period of time during which rainfall could feasibly be produced from the processes acting within the grid cell. The alternative, which was the methodology of F&K and Wild, was to employ one time-step equivalent to the forecast lead-time. The computational efficiency of that approach is highly desirable and thus provided motivation for a comparison between implementing one versus twelve time-steps, the single time-step being of 60 minutes length. It was noted in Chapter Two that F&K kept the units of their forecast time-steps in minutes rather than seconds, despite units of seconds being more consistent with the units used to express the time evolution of VIL ($kgm^{-2}s^{-1}$), and the same approach was retained for this particular run of the PFM. It was found that the effect of using seconds, 3600 seconds for a forecast lead-

time of one hour, had considerable potential to deplete existing rain cells of water if the rate of liquid water removal exceeded its production, to a greater extent than appeared to be actually occurring particularly to the lee of hills where orographic downdrafts were enforced by the PFM. This drew attention to the similar, although not so severe, implications of multiplying the net rate of change in cloud liquid water by 300 (seconds), when implementing the PFM's five minute time-step, compared to that of 60 (minutes), the former being an order of ten greater than the latter. The effects were not limited to grid cells with pre-existing rain in areas of orographic downflow, but were found to extend across all time-steps and to all cells of the domain. This was because the greater extremes in CBLWC estimates attained in the preliminary 300-second time-step, influenced the calculation of the linear regression coefficients that subsequently governed the distribution of cloud column liquid water to the cloud base in cells lacking pre-existing rain.

The results of running the PFM with multiple and single time-steps are presented in Table 5.1, which features all the performance statistics used to assess the PFM's forecasts in the previous case study. The values of the statistics shown for each of the nine separate periods of rainfall are the average of that day's hourly statistics. The overall performance has been taken as the average of the daily statistics. Of particular interest is the correlation coefficient at the 5km ($25km^2$) scale for which the run with multiple time-steps provided the better statistic. Its RMSE was also better but it was noticeable that in most other respects the single time-step proved more able. CSI, POD, FAR, rainfall coverage and correlation coefficients over spatial averages of $225km^2$ (15km scale) and greater, as well as nearest neighbour correlations, all improved when only one time-step was implemented. The better spatially averaged correlations generally coincided with better CSI results while the higher nearest neighbour correlations coincided with better estimation of the rainfall rate and, although not discernible in the results displayed, the single time-step was often more capable than multiple time-steps at maintaining the peaks in observed rainfall intensities. In light of the discussion above, regarding inconsistencies in the units of time-step used in the two runs, it is difficult to distinguish between the influence the units of time had from that of the attempt to allow the storm pathway to be more intimately involved in the time evolution of the cloud column liquid water. Out of interest, the PFM was run again using the nine events, but on this occasion using multiple time-steps that had units of minutes rather than seconds, such that the value of 5 replaced 300. The results of this are not displayed but apart from giving small increases in rainfall coverage and associated increases in POD and CSI, the rest of the performance measures deteriorated in value. It might be that a forecast produced from sixty 60-second time-steps would provide the best result of all but the computational requirements of this are a little discouraging and thus it has not been further investigated.

	%cov_for	%cov_act	RMSE	CSI	POD	FAR	cc5km	cc10km	cc15km	cc20km	cc25km	ccnneigh	rate_for	rate_act
23/10/99 PFM	32.972	33.579	0.843	0.378	0.513	0.477	0.120	0.159	0.199	0.234	0.266	0.408	1.093	1.104
1/8/99 PFM	7.644	15.665	7.835	0.126	0.165	0.525	0.094	0.110	0.116	0.116	0.123	0.202	9.582	7.577
2/8/99 PFM	15.514	15.363	1.941	0.306	0.479	0.538	0.110	0.138	0.165	0.193	0.231	0.310	2.030	2.370
4/8/99 PFM	19.203	19.256	1.590	0.319	0.456	0.515	0.061	0.095	0.124	0.152	0.182	0.253	1.569	1.935
14/01/99 PFM	31.897	29.579	1.163	0.403	0.579	0.401	0.061	0.087	0.111	0.144	0.182	0.314	1.085	1.388
15/01/99 PFM	43.204	40.096	2.005	0.421	0.597	0.426	0.091	0.114	0.134	0.156	0.178	0.349	1.634	1.904
24/12/98 PFM	24.616	28.326	1.239	0.266	0.463	0.503	0.188	0.211	0.243	0.271	0.317	0.411	1.273	1.146
25/12/98 PFM	20.326	23.520	1.831	0.249	0.398	0.570	0.040	0.045	0.051	0.058	0.065	0.183	1.566	1.930
26/12/98 PFM	26.134	25.699	0.599	0.205	0.322	0.577	0.073	0.094	0.105	0.117	0.127	0.248	0.786	0.740
PFM	24.612	25.676	2.116	0.297	0.441	0.504	0.093	0.117	0.139	0.160	0.186	0.298	2.291	2.233
23/10/99 one t-s	32.380	33.579	0.879	0.401	0.555	0.454	0.123	0.188	0.240	0.284	0.320	0.482	1.171	1.104
1/8/99 one t-s	10.875	15.665	9.414	0.189	0.257	0.531	0.005	0.014	0.034	0.076	0.130	0.132	8.081	7.577
2/8/99 one t-s	14.653	15.363	2.155	0.318	0.478	0.513	0.113	0.155	0.196	0.234	0.281	0.323	2.300	2.370
4/8/99 one t-s	17.375	19.256	1.781	0.324	0.447	0.501	0.046	0.093	0.142	0.189	0.232	0.300	1.785	1.935
14/01/99 one t-s	29.346	29.579	1.301	0.367	0.534	0.405	0.040	0.064	0.088	0.122	0.162	0.300	1.075	1.388
15/01/99 one t-s	42.505	40.096	2.259	0.416	0.604	0.441	0.075	0.095	0.113	0.132	0.151	0.315	1.620	1.904
24/12/98 one t-s	28.294	28.326	1.363	0.284	0.531	0.511	0.171	0.200	0.236	0.267	0.312	0.423	1.184	1.146
25/12/98 one t-s	20.950	23.520	1.834	0.285	0.439	0.538	0.068	0.098	0.117	0.135	0.147	0.273	1.763	1.930
26/12/98 one t-s	26.121	25.699	0.568	0.208	0.338	0.589	0.089	0.109	0.127	0.149	0.154	0.229	0.658	0.740
one t-s	24.722	25.676	2.395	0.310	0.465	0.498	0.081	0.113	0.144	0.176	0.210	0.309	2.182	2.233

Table 5.1: *Summary of the average performance statistics of the PFM when varying the length of time-step. The results are averaged over the nine separate days of rainfall and relate to a lead-time of one hour. Results labelled "PFM" are the original PFM formulation, which utilises twelve 300 second time-steps to generate one forecast. Results labelled "one t-s" refer to a PFM run that achieves the forecast in one 60 minute time-step. The best performance for each particular overall statistic is highlighted in green.*

5.2.2 Wind fields versus storm velocity

It has already been noted that Wild (1996) had to rely on the vector of storm velocity to generate orographically-induced vertical motion, and it is uncertain whether this might have compromised his results or led to an equivalent or better performance. Table 5.2 provides the performance statistics of the PFM forecasts, for each of the nine rainfall periods, when using the vector of storm velocity as the horizontal wind field and when using the UKMM 1000mb wind field. Again the full range of performance statistics used in previous assessments were calculated and averaged in the same manner as in Table 5.1. The differences in performance statistics between 1000mb winds and storm velocity vectors were, obviously, related to differences in the strengths and directions of the wind vectors applied.

The correlation statistics are not the only ones of interest here as the differences between the wind vectors not only created within-storm variations in rainfall intensity but were sufficiently different to enforce changes in the shape and size of the rain field. In all cases the storm velocity vector produced a decrease in rainfall coverage and, in all but two (one of which was very marginal), an increase in rainfall rate. An example of the nature of these differences can be viewed in Figure 5.1, which shows the forecasted rain fields of both PFM runs for 1400 GMT on the 14th January 1999. The surface winds in this case were oriented from a west-southwest direction while storm movement was mainly from a west-northwest direction. Both wind fields were of ample strength to create gaps in the rain field to the lee of hills but with the storm velocity tending to do so more

than surface winds. Additionally, use of the latter eliminated some of the rainfall to the north and centre south but broadened and strengthened the enhancement of rainfall over the Welsh hills and Pennines. In this example, and also more generally, the decrease in rainfall coverage was at the expense of correctly identified rain cells, more so than the removal of superfluous ones. As a result, the CSI of the PFM using storm velocity suffered in every event except on 1st August 1999 when the reduction of rain cells proved more judicious. Also contributing to the better CSI on the 1st August was the movement of rainfall from a south-easterly direction which caused the PFM using storm velocity to produce more precipitation on the Welsh Hills at 1700 GMT than was achieved using surface winds, and this pattern of rainfall concurred with observations at that time (refer Figure 4.16) despite surface winds being extremely light and variable as depicted in Figure 4.20.

	%cov_for	%cov_act	RMSE	CSI	POD	FAR	cc5km	cc10km	cc15km	cc20km	cc25km	ccnneigh	rate_for	rate_act
23/10/99 PFM	32.972	33.579	0.843	0.378	0.513	0.477	0.120	0.159	0.199	0.234	0.266	0.408	1.093	1.104
1/8/99 PFM	7.644	15.665	7.835	0.126	0.165	0.525	0.094	0.110	0.116	0.116	0.123	0.202	9.582	7.577
2/8/99 PFM	15.514	15.363	1.941	0.306	0.479	0.538	0.110	0.138	0.165	0.193	0.231	0.310	2.030	2.370
4/8/99 PFM	19.203	19.256	1.590	0.319	0.456	0.515	0.061	0.095	0.124	0.152	0.182	0.253	1.569	1.935
14/01/99 PFM	31.897	29.579	1.163	0.403	0.579	0.401	0.061	0.087	0.111	0.144	0.182	0.314	1.085	1.388
15/01/99 PFM	43.204	40.096	2.005	0.421	0.597	0.426	0.091	0.114	0.134	0.156	0.178	0.349	1.634	1.904
24/12/98 PFM	24.616	28.326	1.239	0.266	0.463	0.503	0.188	0.211	0.243	0.271	0.317	0.411	1.273	1.146
25/12/98 PFM	20.326	23.520	1.831	0.249	0.398	0.570	0.040	0.045	0.051	0.058	0.065	0.183	1.566	1.930
26/12/98 PFM	26.134	25.699	0.599	0.205	0.322	0.577	0.073	0.094	0.105	0.117	0.127	0.248	0.786	0.740
PFM	24.612	25.676	2.116	0.297	0.441	0.504	0.093	0.117	0.139	0.160	0.186	0.298	2.291	2.233
23/10/99 storm_vel	32.389	33.579	0.844	0.374	0.503	0.476	0.117	0.155	0.193	0.228	0.259	0.403	1.096	1.104
1/8/99 storm_vel	7.577	15.665	7.763	0.127	0.166	0.511	0.094	0.113	0.120	0.122	0.130	0.205	8.372	7.577
2/8/99 storm_vel	15.155	15.363	2.158	0.301	0.465	0.539	0.098	0.121	0.148	0.178	0.217	0.293	2.193	2.370
4/8/99 storm_vel	18.854	19.256	1.592	0.312	0.445	0.517	0.060	0.095	0.124	0.151	0.182	0.255	1.595	1.935
14/01/99 storm_vel	26.153	29.579	1.176	0.359	0.495	0.389	0.063	0.096	0.127	0.164	0.203	0.335	1.109	1.388
15/01/99 storm_vel	39.102	40.096	2.057	0.402	0.551	0.415	0.088	0.114	0.137	0.160	0.184	0.359	1.684	1.904
24/12/98 storm_vel	23.274	28.326	1.716	0.258	0.430	0.501	0.146	0.168	0.198	0.225	0.269	0.424	1.348	1.146
25/12/98 storm_vel	17.800	23.520	1.614	0.239	0.351	0.547	0.048	0.060	0.067	0.075	0.079	0.212	1.565	1.930
26/12/98 storm_vel	22.046	25.699	0.583	0.181	0.272	0.579	0.050	0.071	0.083	0.098	0.112	0.212	0.825	0.740
storm_vel	22.483	25.676	2.167	0.284	0.409	0.497	0.085	0.110	0.133	0.156	0.182	0.300	2.199	2.233
23/10/99 900mb	32.932	33.579	0.842	0.377	0.510	0.478	0.119	0.159	0.199	0.234	0.266	0.411	1.091	1.104
1/8/99 900mb	7.644	15.665	7.835	0.126	0.165	0.525	0.094	0.110	0.116	0.116	0.123	0.202	9.582	7.577
2/8/99 900mb	15.514	15.363	1.941	0.306	0.479	0.538	0.110	0.138	0.165	0.193	0.231	0.310	2.031	2.370
4/8/99 900mb	19.201	19.256	1.590	0.319	0.456	0.515	0.061	0.095	0.124	0.152	0.182	0.253	1.571	1.935
14/01/99 900mb	31.878	29.579	1.163	0.402	0.569	0.396	0.061	0.087	0.111	0.142	0.178	0.313	1.097	1.388
15/01/99 900mb	43.202	40.096	2.005	0.420	0.596	0.427	0.091	0.114	0.134	0.156	0.178	0.350	1.635	1.904
24/12/98 900mb	24.578	28.326	1.238	0.271	0.463	0.497	0.195	0.223	0.254	0.281	0.326	0.411	1.278	1.146
25/12/98 900mb	20.320	23.520	1.831	0.249	0.398	0.570	0.040	0.045	0.051	0.058	0.065	0.183	1.562	1.930
26/12/98 900mb	26.115	25.699	0.599	0.203	0.320	0.581	0.069	0.092	0.103	0.116	0.126	0.244	0.785	0.740
900mb	24.598	25.676	2.116	0.297	0.440	0.503	0.093	0.118	0.140	0.161	0.186	0.298	2.292	2.233

Table 5.2: *Summary of the average performance statistics of the PFM when using different wind fields to generate the orographic updraft. The results are averaged over the nine separate days of rainfall and relate to a lead-time of one hour. Results labelled "PFM" are the original PFM formulation using UKMM surface winds. Results labelled "storm_vel" refer to a PFM run using the vector of storm velocity and results labelled "900mb" are from the PFM run using the UKMM wind field at 900mb. The best performance for each particular overall statistic is highlighted in green.*

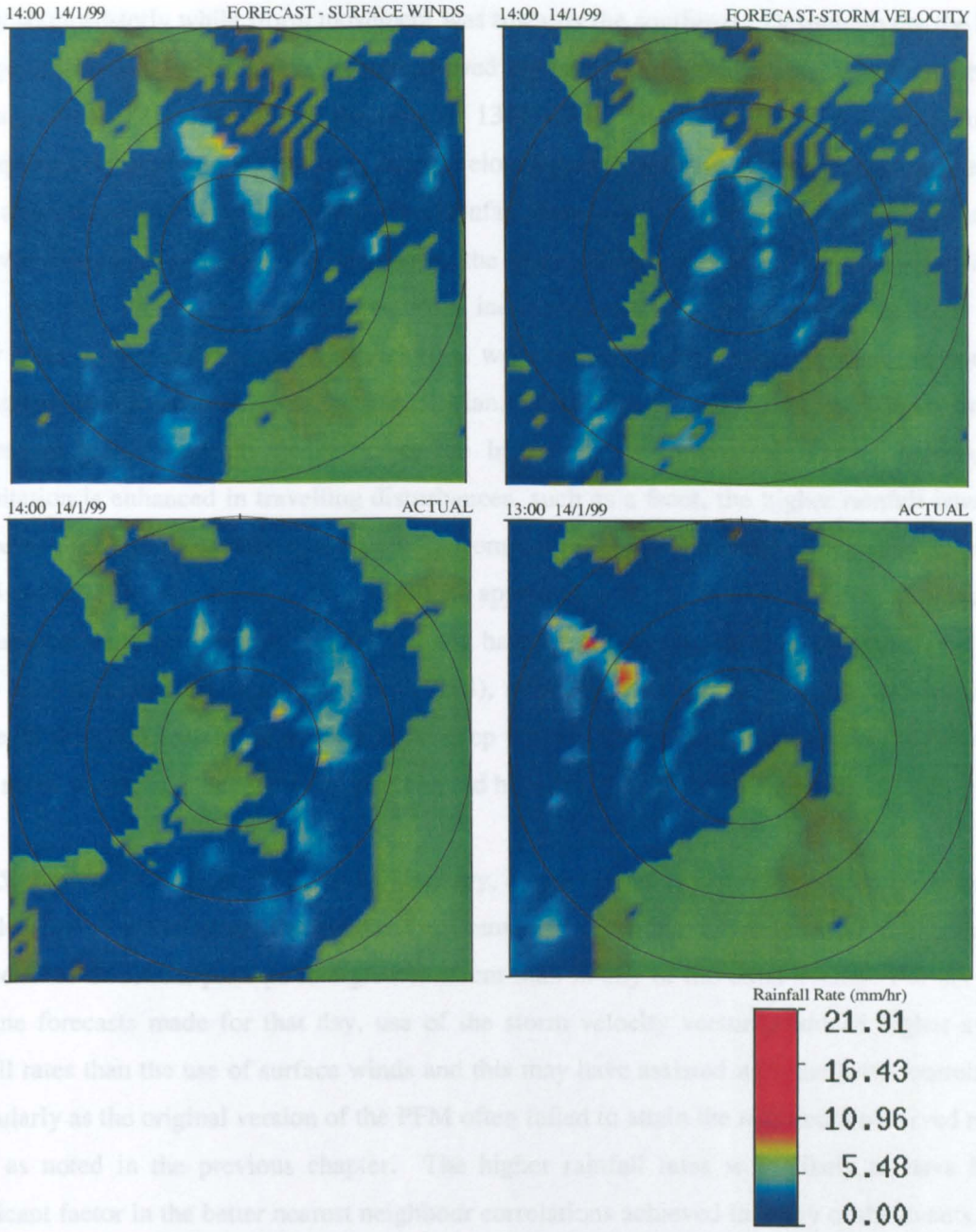

Figure 5.1: *Forecasted rainfields (one hour lead-time) produced by the PFM using surface winds (above left) and the vector of storm velocity (above right) for a time of 1400 GMT on 14/1/99. The observed rain field is shown bottom left and the actual rain field of the preceding hour features bottom right. Use of the storm velocity vector tended to result in the removal of more rain cells to the lee of hills and sometimes gave broader and more intense regions of enhanced precipitation, such as in the southwest corner and in the centre of the picture.*

It can be seen in Table 5.2 that the correlation coefficients at scales from 5 to 25km inclusive were better using surface winds than the vector of storm velocity, this was so when averaged overall and in all individual cases except for the 25th December 1998 and the 14th January 1999. With respect to the latter, surface winds and storm movement were not similarly directed, surface winds being

mainly southwesterly while storm movement was towards the southeast. Despite giving the higher average correlation, use of storm velocity proved superior in less than half the forecasts but the most significant of these was for the time of 1300 GMT, shown in Figure 5.2. The stronger orographic downdrafts produced using storm velocity largely eliminated the rainfall to the north while stronger updrafts marginally increased rainfall rates in areas of enhanced rainfall towards the northwest corner of the domain. Additionally, the correlations achieved by the PFM using surface winds were not helped by the southwesterlies inducing areas of enhanced rainfall closer to the higher ground of Cumbria, which at that time were not observed. Missing from the domain's representation of topography was the Isle of Man, which may have been responsible for creating the area of higher intensity rainfall over the Irish Sea. As noted by Sumner (1998), once precipitation is enhanced in travelling disturbances, such as a front, the higher rainfall intensities may persist for a considerable distance away from the relief that created it and particularly when there is instability present (Browning, 1975), as appeared to be the case on this day. Alternatively the cluster of cells with enhanced rainfall might have been a Mesoscale Precipitation Area (MPA) of the kind discussed by Browning *et al* (1974), although the UKMM forecasts did not show a profile of potential instability suggestive of deep convection but rather a thin layer of low level moist static instability, the release of which could have been triggered by high terrain.

The 25th December differed from the 14th January, in that use of storm velocity almost consistently provided higher correlations throughout the event and storm movement was more aligned with surface wind direction, perhaps to a greater extent than in any of the other events. For six out of the nine forecasts made for that day, use of the storm velocity vector produced higher average rainfall rates than the use of surface winds and this may have assisted with the better correlations, particularly as the original version of the PFM often failed to attain the maximum observed rainfall rates, as noted in the previous chapter. The higher rainfall rates were likely to have been a significant factor in the better nearest neighbour correlations achieved in many of the events by the PFM using storm velocity, with the exception of 26th December 1998, 2nd August 1998 and 23rd October 1999. The first and last of these events were occasions when the UKMM showed surface winds to be at their strongest, enabling production of rainfall maximums closer to the actual. The association between higher nearest neighbour correlations and closer approximation to observed rainfall rates was also evident in the 2nd August 1998 event, the initial six hours of which the PFM using surface winds produced low rainfall rates and lower nearest neighbour correlations than those achieved using storm velocity, but thereafter managed to give average rainfall rates that largely mirrored observed rates and correlations that exceeded its counterpart. Its improvement in nearest neighbour correlations was also helped by rainfall in the final hours being located mainly over sea areas and northern parts of Wales. In those areas it appeared to lack an orographic signature, so that the PFM run with light surface winds correctly featured little orographic influences in its

forecasting, whereas the magnitude of the storm velocity was sufficient to either induce enhancement or, more commonly, induce a downdraft that reduced the rain field.

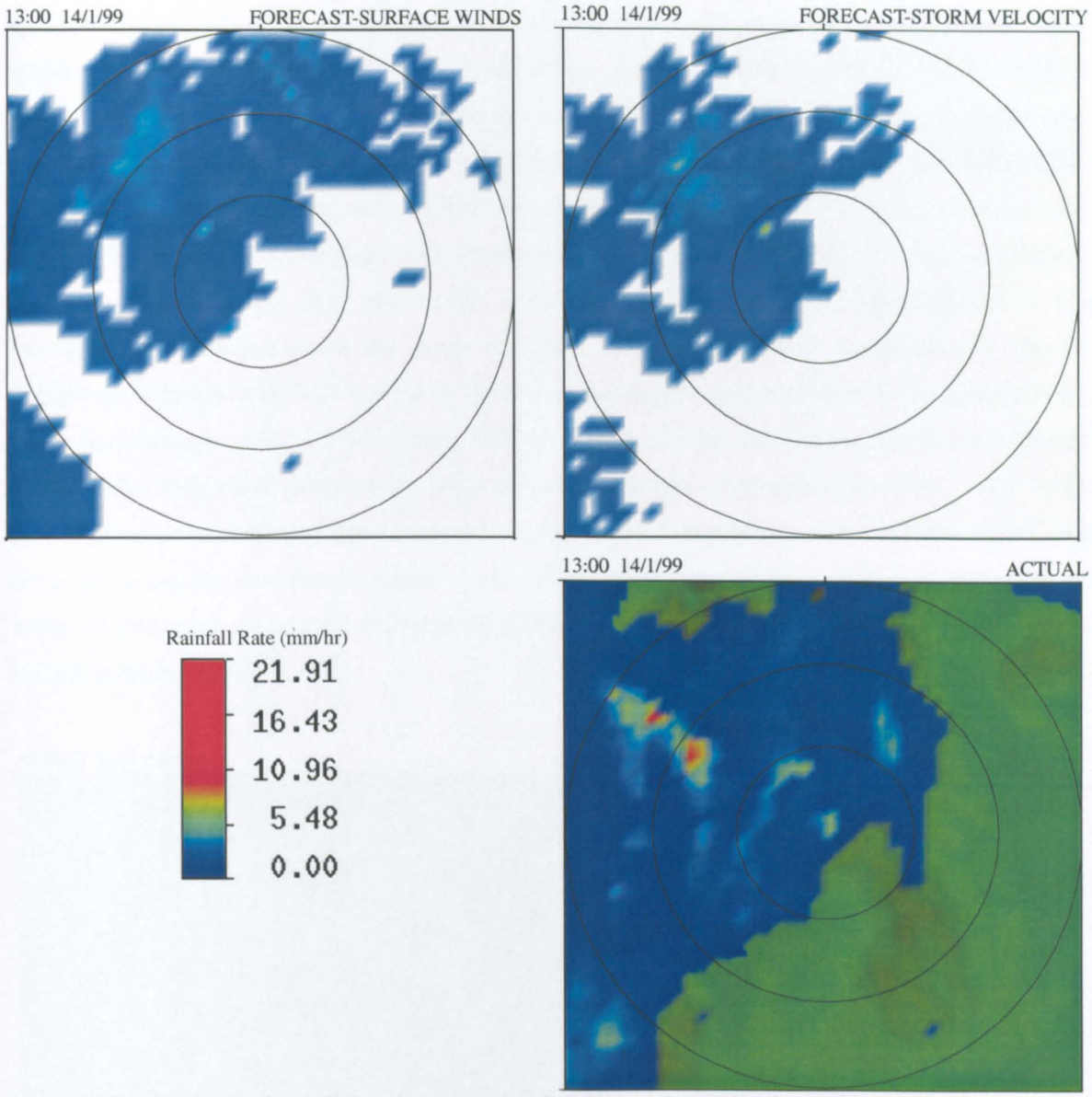

Figure 5.2: *Forecasted rainfields (one hour lead-time) produced by the PFM using surface winds (above left) and the vector of storm velocity (above right) for a time of 1300 GMT on 14/1/99. The topography is not shown in either image for clarity. The observed rain field is shown bottom left (with topography included). Use of storm velocity resulted in a greatly diminished rain field, particularly in the southwest and northeast sectors, but the line of enhanced rainfall in the northwest had slightly better placement, orientation and intensity than produced through the use of surface winds.*

The greater ability of the PFM using storm velocity to match the peaks in observed rainfall rate raised the question of whether a wind field at a higher level might offer a more successful combination of appropriate wind speed and direction than provided by 1000mb winds. Bader *et al*,

Hill (1983) and Browning *et al* (1975) focussed on wind fields above the boundary friction layer in their studies of orographic enhancement and it should be noted that frictional effects are not neglected in the UKMM. Figure 5.3 provides an example of the UKMM's north-south component of the horizontal wind field at 1000mb, in which the UK outline is discernible by slower winds speeds over land compared to those over sea areas. An alternative to 1000mb winds could be winds at 900mb, a level consistent with the aforementioned studies and given that Browning *et al* (1975) found a correspondence between high-speed (in excess of 20-25ms^{-1}), low-level (800-900mb) jets in frontal storms with significant orographic enhancement. A PFM run using the 900mb wind field was undertaken with the results also presented in Table 5.2. At first glance it seems the 900mb wind field proves the best option given the overall improvement in the correlation coefficients across the range of scales, nearest neighbours excepted, and also an improvement in CSI and POD and FAR. However the overall improvement is only achieved by a better performance on the 24th December 1998 whilst for all other rainfall periods the performance is the either the same (particularly the convective events) or marginally worse. The better performance on the 24th was itself managed through just one out of the nine forecasts constituting the event, being the very first forecast for which the smaller rainfall area attained by using 900mb winds proved more appropriate than that of 1000mb winds. Therefore the merit of using winds at 900mb remains unclear.

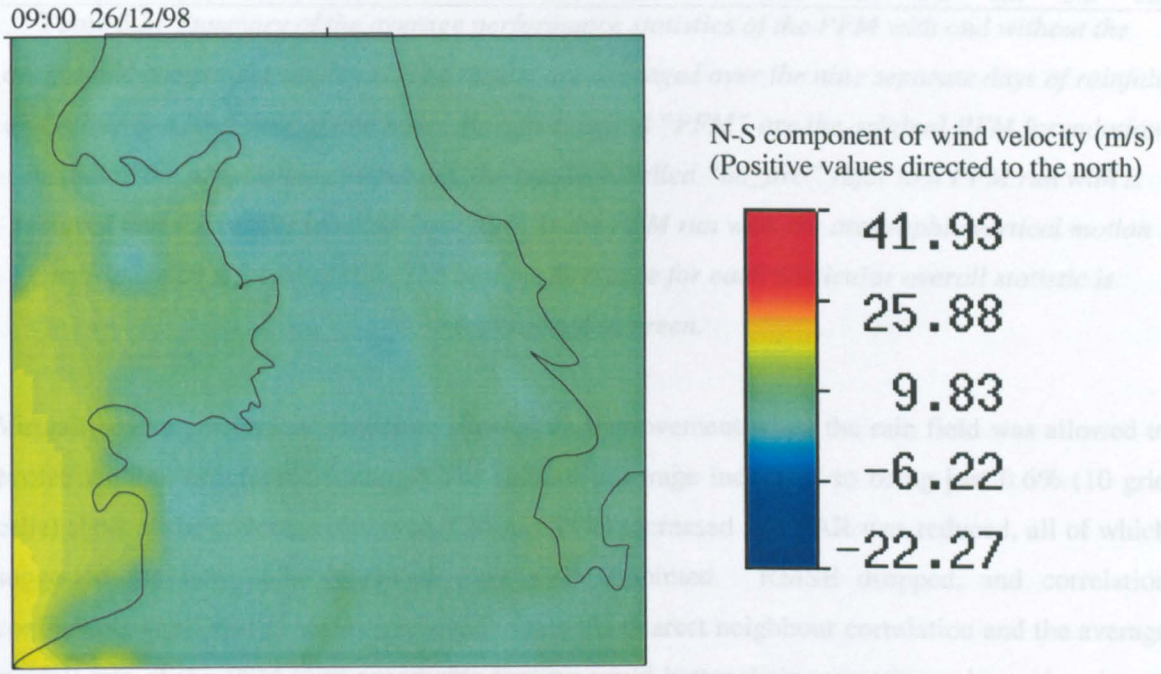

Figure 5.3: *The north to south component of the UKMM forecasted 1000mb wind field for 0900 GMT on 26/12/98. The winds tend to be stronger over sea areas than over the land within the UK outline.*

5.2.3 No orographic forcing

Reasons why some of the foregoing results occurred became more apparent when the orographic updraft component of the PFM was effectively "turned off". The performance of the PFM in that mode is given in Table 5.3.

	%cov_for	%cov_act	RMSE	CSI	POD	FAR	cc5km	cc10km	cc15km	cc20km	cc25km	ccnneigh	rate_for	rate_act
23/10/99 PFM	32.972	33.579	0.843	0.378	0.513	0.477	0.120	0.159	0.199	0.234	0.266	0.408	1.093	1.104
1/8/99 PFM	7.644	15.665	7.835	0.126	0.165	0.525	0.094	0.110	0.116	0.116	0.123	0.202	9.582	7.577
2/8/99 PFM	15.514	15.363	1.941	0.306	0.479	0.538	0.110	0.138	0.165	0.193	0.231	0.310	2.030	2.370
4/8/99 PFM	19.203	19.256	1.590	0.319	0.456	0.515	0.061	0.095	0.124	0.152	0.182	0.253	1.569	1.935
14/01/99 PFM	31.897	29.579	1.163	0.403	0.579	0.401	0.061	0.087	0.111	0.144	0.182	0.314	1.085	1.388
15/01/99 PFM	43.204	40.096	2.005	0.421	0.597	0.426	0.091	0.114	0.134	0.156	0.178	0.349	1.634	1.904
24/12/98 PFM	24.616	28.326	1.239	0.266	0.463	0.503	0.188	0.211	0.243	0.271	0.317	0.411	1.273	1.146
25/12/98 PFM	20.326	23.520	1.831	0.249	0.398	0.570	0.040	0.045	0.051	0.058	0.065	0.183	1.566	1.930
26/12/98 PFM	26.134	25.699	0.599	0.205	0.322	0.577	0.073	0.094	0.105	0.117	0.127	0.248	0.786	0.740
PFM	24.612	25.676	2.116	0.297	0.441	0.504	0.093	0.117	0.139	0.160	0.186	0.298	2.291	2.233
23/10/99 no_oro	33.123	33.579	0.844	0.377	0.514	0.479	0.120	0.159	0.199	0.234	0.266	0.406	1.089	1.104
1/8/99 no_oro	7.558	15.665	7.718	0.125	0.164	0.515	0.095	0.112	0.119	0.121	0.127	0.192	8.477	7.577
2/8/99 no_oro	15.514	15.363	1.928	0.306	0.479	0.538	0.111	0.138	0.165	0.193	0.230	0.311	2.005	2.370
4/8/99 no_oro	19.319	19.256	1.591	0.319	0.458	0.520	0.060	0.095	0.123	0.151	0.182	0.253	1.564	1.935
14/01/99 no_oro	33.182	29.579	1.164	0.410	0.594	0.400	0.065	0.090	0.112	0.143	0.179	0.311	1.086	1.388
15/01/99 no_oro	44.244	40.096	1.970	0.428	0.611	0.426	0.096	0.117	0.138	0.160	0.182	0.335	1.592	1.904
24/12/98 no_oro	24.754	28.326	1.218	0.273	0.490	0.498	0.183	0.208	0.241	0.271	0.317	0.405	1.231	1.146
25/12/98 no_oro	21.088	23.520	1.636	0.257	0.416	0.570	0.039	0.045	0.050	0.058	0.064	0.204	1.506	1.930
26/12/98 no_oro	26.972	25.699	0.600	0.209	0.343	0.571	0.075	0.095	0.106	0.120	0.131	0.240	0.739	0.740
no_oro	25.084	25.676	2.074	0.301	0.452	0.502	0.094	0.118	0.139	0.161	0.187	0.295	2.143	2.233
23/10/99 oro_0.1	33.119	33.579	0.844	0.377	0.514	0.479	0.120	0.159	0.199	0.234	0.266	0.406	1.089	1.104
1/8/99 oro_0.1	7.558	15.665	7.715	0.125	0.164	0.515	0.096	0.113	0.119	0.121	0.128	0.192	8.469	7.577
2/8/99 oro_0.1	15.514	15.363	1.928	0.306	0.479	0.538	0.110	0.138	0.165	0.193	0.230	0.310	2.003	2.370
4/8/99 oro_0.1	19.329	19.256	1.591	0.319	0.459	0.519	0.060	0.095	0.124	0.151	0.182	0.253	1.563	1.935
14/01/99 oro_0.1	33.195	29.579	1.162	0.410	0.594	0.400	0.065	0.090	0.113	0.144	0.180	0.311	1.085	1.388
15/01/99 oro_0.1	44.204	40.096	1.969	0.428	0.611	0.426	0.096	0.117	0.138	0.160	0.182	0.337	1.594	1.904
24/12/98 oro_0.1	24.704	28.326	1.256	0.273	0.488	0.499	0.183	0.206	0.239	0.268	0.313	0.401	1.305	1.146
25/12/98 oro_0.1	21.006	23.520	1.635	0.257	0.415	0.569	0.039	0.045	0.050	0.058	0.064	0.204	1.509	1.930
26/12/98 oro_0.1	26.959	25.699	0.600	0.209	0.343	0.576	0.074	0.094	0.105	0.118	0.129	0.241	0.741	0.740
oro_0.1	25.065	25.676	2.078	0.301	0.452	0.502	0.094	0.117	0.139	0.161	0.186	0.295	2.151	2.233

Table 5.3: *Summary of the average performance statistics of the PFM with and without the orographic component employed. The results are averaged over the nine separate days of rainfall and relate to a lead-time of one hour. Results labelled "PFM" are the original PFM formulation including the orographic component, the results labelled "no_oro" refer to a PFM run with it removed and the results labelled "oro_0.1" is the PFM run with the orographic vertical motion multiplied by a factor of 0.1. The best performance for each particular overall statistic is highlighted in green.*

Virtually every performance measure showed an improvement when the rain field was allowed to evolve without orographic forcing. The rainfall coverage increased to being just 0.6% (10 grid cells) short of the coverage observed, CSI and POD increased and FAR was reduced, all of which suggested the new cells generated were well appointed. RMSE dropped, and correlation coefficients at all spatial scales improved. Only the nearest neighbour correlation and the average rainfall rate of the PFM with orographic forcing could better their respective values when it was removed. These results confirmed a suspicion raised by the visual appearance and statistical performance of the PFM's forecasts when changing the number of time steps or horizontal wind field, and specifically being that the down flows induced through use of equation (5.1) were to the detriment of the PFM's performance and appeared to be drying out cells within the time frame of

the forecast lead-time, to an extent that was not being observed. The previous studies of Sections 5.2.1 and 5.2.2 indicated that the extent of drying depended on the length of the time-step and that it could be regulated to some degree by manipulating the units of the time-step, although in doing so the correlations at the 5km scale were degraded. It was notable that this degradation in correlation did not similarly occur with complete removal of orographically-induced vertical motion. In an attempt to steer the results of the PFM with orographic forcing towards those attained without it, rather than adjust the units of the time-step to achieve smaller net changes in cloud liquid water, the orographic vertical motion was modulated by a factor of 0.1 in the hope of reducing its strength whilst still retaining some of its signature. This served to improve all statistics apart from the nearest neighbour correlation and average rainfall rate, as can be seen in Table 5.3, but not to the extent that they exceeded the values gained by eliminating the orographic component of the PFM altogether, except for a marginally better CSI.

In order to understand these results it is necessary to look more closely at the atmospheric conditions during the nine events to gain an impression of whether, and if so how, an orographic component of rainfall was being manifest. As mentioned previously, some of the main factors influencing orographic enhancement of pre-existing rain, apart from the form of the topography itself, are a high moisture content in air at low levels, relatively strong low-level winds and instability. Strong winds combined with high low-level moisture can often give rise to an orographic cloud that pre-existing rain can then seed, giving rise to heavier rainfalls. The lifting of parcels or layers of air by strong winds flowing over topographic barriers provides the forcing required to both realise and release instability in conditionally or potentially unstable air, so that the resultant convection accelerates the rate of condensation and precipitation formation (Barros and Lettenmaier, 1994). When reviewing the conditions in each of the nine days of rainfall in this context most of them featured an environment conducive to orographic enhancement of rainfall, all of them except the three periods of convective rainfall in early August 1999.

From the 1st to the 5th August 1999 surface winds were both light and variable, potential convective instability was extensive throughout the vertical profiles of grid cells across the domain and convection was readily occurring and focussed along the line of uplift associated with the trough of low pressure. The UKMM forecasted fields of relative humidity lacked low-level moisture on the 1st August 1999 and gave patchy areas of greater than 80% relative humidity on the remaining days. In contrast, the UKMM forecasted moisture fields during the three December 1998 wintertime periods of rainfall featured broadly distributed high relative humidity (in excess of 80%) at low levels and strong to gale force winds, the winds particularly strong on the 26th December and on all three days coming predominantly from a southwesterly direction, the direction Hill (1983) associated most with moist airstreams and orographic enhancement of

rainfall. The reasonably high moisture content of the air and the windiness were accompanied by the presence of moist static instability at low levels on the 24th and 26th and large swathes of potential instability on the 25th that appeared in conjunction with the rain that passed over the Pennines during the afternoon of that day. Winds were again up to gale force through the course of the 14th and 15th January 1999, with wind direction on those occasions ranging between southwesterly and northwesterly. Over the two days, the UKMM relative humidity at low levels usually exceeded 80% only within the immediate vicinity of rain bands and not over wide areas as in the events of the previous month. The 14th January featured thin layers of moist static instability, which grew in vertical extent towards the end of the period of rainfall, whilst the 15th January had a thin layer of moist static instability that persisted throughout the day and was partnered with potential convective instability for the latter two-thirds of the event. Potential instability and moist static instability were evident together again on the 24th October and were combined with plenty of moisture at low levels and also strong winds, the latter following a cyclonic pattern of flow and, as such, were variable in direction across the domain.

With most of the nine days exhibiting conditions likely to produce orographic enhancement of rainfall, an attempt was made to gain some idea, in a statistical sense, of how rainfall was distributed across the domain for each of those days. Towards this purpose, all cells of the domain were categorised according to the nature of the orographic forcing in the cell and were assigned to one of three possibilities: positive (upward), negative (downward) or zero orographically-induced vertical motion. Orographic forcing in a cell was determined using equation (5.1) (the product of UKMM 1000mb winds and windward facing topographic gradients), and being exactly that employed in the PFM, with the aim of assessing whether the PFM's treatment of orographic rainfall processes was consistent with observations. Event-averaged rainfall rate, event-averaged maximum rainfall rate (the average of the maximum rainfall rate recorded for each hour of the rainfall event) and absolute maximum rainfall rate in each of the three sectors for the nine rainfall periods are given in Table 5.4. Values obtained for observed rainfall were compared to those obtained using PFM rainfall forecasts made with and without the orographic component in place.

Without reference to the statistics, and given the above description of conditions in the nine rainfall events, it would be expected that orographic enhancement would be less likely to occur during the three days of convective rainfall in August 1999 than on all other occasions. However, when looking at the statistics, it was only on those days and not on any others that the areas attributed with positive orographic updraft held the highest values in all of the three aforementioned measures (average, average maximum and absolute maximum rainfall rate) with respect to observed rainfall. Next highest were cells with orographic downdrafts followed by sea areas, with this order unsurprising given that any countering effects of orographic downdrafts on convective updrafts

were likely to have been small, if they existed at all in the light winds, and additionally the line of the trough and therefore the line of convergence and uplift was located over downdraft areas.

	average			average maximum			absolute maximum		
	positive	*negative*	*no*	*positive*	*negative*	*no*	*positive*	*negative*	*no*
24/12/98									
Actual	0.801	0.889	2.092	8.315	9.130	7.957	15.984	21.000	20.419
F-surface winds	1.022	0.967	1.892	6.765	7.804	6.506	16.436	16.588	20.565
F-no updraft	0.923	0.977	1.966	6.573	7.222	7.094	16.247	18.569	22.717
25/12/98									
Actual	1.902	1.886	2.569	13.031	10.347	9.674	37.795	25.388	28.867
F-surface winds	1.506	1.476	1.433	6.112	6.276	3.881	9.584	11.592	8.580
F-no updraft	1.483	1.511	1.371	6.202	6.021	3.887	9.412	9.412	8.602
26/12/98									
Actual	0.769	0.704	0.689	3.602	4.450	2.038	6.810	10.957	3.995
F-surface winds	0.793	0.728	0.449	2.960	4.031	1.182	4.918	8.241	3.541
F-no updraft	0.695	0.752	0.486	2.796	4.277	1.205	4.594	8.933	3.535
14/1/99									
Actual	1.247	1.316	1.246	8.205	10.878	4.978	15.354	20.500	7.946
F-surface winds	1.051	1.081	1.032	5.378	4.526	3.398	12.117	8.348	5.295
F-no updraft	1.008	1.102	0.981	3.959	4.083	3.369	6.252	6.452	5.274
15/1/99									
Actual	1.778	1.832	1.811	16.912	15.438	9.903	50.000	37.598	41.395
F-surface winds	1.606	1.702	1.379	8.791	8.763	5.718	37.901	28.351	24.024
F-no updraft	1.558	1.617	1.313	6.765	6.739	4.946	10.347	10.470	10.636
1/8/99									
Actual	9.188	6.479	4.518	81.223	71.226	32.716	126.000	126.000	111.118
F-surface winds	8.217	8.060	3.878	68.205	66.137	25.724	156.494	144.686	111.078
F-no updraft	8.118	7.807	3.821	67.445	66.239	25.465	156.636	145.083	111.258
2/8/99									
Actual	2.536	2.319	2.109	28.058	21.257	14.666	126.000	89.646	83.999
F-surface winds	2.021	1.941	1.717	13.107	11.934	7.918	41.513	30.889	25.557
F-no updraft	1.984	1.946	1.699	12.631	11.706	7.920	41.771	31.011	23.415
4/8/99									
Actual	1.994	1.936	1.751	20.832	17.340	10.563	58.000	55.717	41.866
F-surface winds	1.617	1.466	1.596	10.433	9.481	6.731	17.760	17.620	17.199
F-no updraft	1.586	1.477	1.590	10.338	9.586	6.738	17.679	17.642	17.199
23/10/99									
Actual	0.982	1.107	0.950	5.945	7.295	3.509	11.953	24.500	9.927
F-surface winds	1.092	1.071	0.967	5.814	5.816	3.484	12.142	10.521	9.792
F-no updraft	1.053	1.068	0.973	5.521	6.081	3.481	10.097	10.368	9.792

Table 5.4: *Values of average rainfall rate, average maximum rainfall rate and absolute maximum rainfall rate. Values for each are shown for the nine days of rainfall and separated into areas designated as having an orographic updraft (positive), an orographic downdraft(negative) or no orographic (no) influence on vertical velocity. These areas were determined according to the direction of UKMM surface winds and windward facing topographic slopes. Results are shown for observed rainfall ("actual"), PFM forecasts including the orographic component using surface winds ("F-surface winds") and PFM forecasts without the orographic component implemented ("F-no updraft"). The maximum in each category are highlighted in green.*

Banta (1990) discussed the role of mountains in localising rainfall in situations of deep moist convection, establishing that while synoptic and mesoscale conditions provide the moist unstable environment for convective precipitation to occur, mountains can initiate convection in a number of ways. These Banta divided into three categories: the uplift associated with air flowing over topographic barriers raising air to its lifting condensation level and level of free convection; similarly the uplift associated with airflow being blocked or with the creation of mountain waves that have upward motion on their rising limbs; and lastly, an important factor in daytime convection, is the convergence of upslope and up-valley flows towards, up and over peaks as a result of the heating of mountain surfaces. Therefore, even in seemingly light winds, there may be a tendency for convective cells to be aligned with areas of elevated terrain. Despite the statistical, and to some extent visual, association of high ground with higher intensity rainfall on 1st, 2nd and 4th August 1999 it was evident from Table 5.3 that the PFM performed better without its orographic component than with it on the first two days. This was not the case on the 4th, and it can be seen from Table 5.4 that the PFM without orographic forcing placed the highest average rainfall rates out to sea on that day rather than over windward slopes as observed. In describing the influence of mountains on convective processes, Banta (1990) also drew attention to how convective rain, almost by definition, is turbulent and stochastic and commented that once deep convection becomes established at one site it can suppress its occurrence nearby. Therefore, trying to extract a simplistic topographic signature from a field of convective rain cells is unlikely to be very successful. Notably the 4th August, for which it was more favourable to include the orographic component in terms of the better 5km scale correlations achieved, had more uniform rain, was driven mainly by a frontal system and lacked some of the randomness exhibited in the previous two days.

Despite conditions appearing to be conducive to orographic enhancement on the other six days examined, a characteristic they all shared was the tendency for higher rainfall rates to be distanced from regions of positive orographic updraft. The greater average rainfall rate over sea areas on the 24th was not unexpected given the event's sample of images displayed in Figure 4.1, which clearly shows a preponderance of heavy rain cells off the coast of northwest England. The PFM in both orographic and non-orographic modes replicated this pattern and also correctly placed the average maximum rainfall rates in areas of orographic downdrafts but misplaced the location of the absolute maximum rainfall rate. The 25th saw a repeat of higher average rainfall intensities over sea areas but with maximum rainfall rates instead tending to occur in areas of orographic updrafts, perhaps the greater potential instability on that day requiring little lifting for its release so that convection occurred well in advance of topographic peaks. Notably both modes of the PFM struggled to match the distribution of rainfall rates observed on the 25th. On the 26th the average rainfall rates were highest over upwind slopes but downwind sides seemed to harbour the

maximum rainfall rates. The penchant for maximum rates to occur on the lee side of hills was retained reasonably well by both modes of the PFM but with higher rainfall rates achieved by the PFM without topographic forcing, which may have contributed to its better 5km scale correlations for that day.

Areas of orographic downdrafts provided the location for the heaviest rainfall on the 14th January 1999, giving the highest average rainfall rate, the highest average maximum rainfall rate and the highest absolute maximum rainfall rate. Figure 4.10 substantiates the statistics and shows heavy showers on the eastern side of hills (UKMM 1000mb winds were southwesterly). The observations did not match the PFM's orographic forcing which attributed windward slopes with the maximum rainfall rates while the PFM without orographic forcing, although it produced considerably lower maximum values, did not have this flawed distribution and thus attained the better correlations. The average rainfall intensity on the 15th January 1999 was highest in areas of downdrafts but maximum rates appeared to occur on windward slopes. The pattern was tracked well by the PFM with the orographic component employed, more so than with it absent, so it was a little surprising that the latter produced the better average correlation coefficient at the 5km scale. The greater rainfall coverage and CSI achieved by removing the effect of topography may have given rise to that result. On the 15th January, sea areas recorded a higher average rainfall rate than areas with positive orographic updraft and had the second highest absolute maximum rate. Some of those sharp, probably convective, showers are visible over the Irish Sea in Figure 4.10 and the PFM without orographic forcing accordingly attributed sea-based cells with its absolute maximum rainfall rate. On the 23rd October 1999, the most intense rainfall was located over areas with orographic downdrafts. The PFM without orographic forcing placed it similarly but the PFM with representation of orographic effects favoured areas of positive updraft more than was observed.

The correlation coefficient at the 5km scale is a fairly strict and demanding performance measure, leaving little room for error in pinpointing actualisation of orographic influences on rainfall rates and rainfall distribution. It was apparent that in some of the above events, and particularly on the days orographic enhancement was expected, there was a mismatch between where the PFM with orographic forcing located maximum rainfall rates and where they were observed, and this was reflected in the lower 5km scale correlations achieved by the PFM in that mode. However, it is of interest that its nearest neighbour correlations exceeded those attained when the orographic component was removed. Together these raise the possibility that problems experienced with the PFM's orographic component were not entirely related to the magnitude of the vertical motion produced by equation (5.1). They may, to some extent, have been the product of enhanced rainfall drifting from its source of forcing. Additional explanations could include: the network of weather radars missed some of the evaporation that occurred beneath the beam (although the same would

have to be said for enhancement) but which is accounted for inherently in the PFM formulations by allowing the moisture source term to be negative; the topographic smoothing that was employed created negative gradients across cells in which the topography actually peaks and although smoothing can often satisfactorily retain gross features of a system's response to orography it can fail to get local maxima and minima (Barros & Lettenmaier, 1994); the very simplistic treatment of the flow over topography in equation (5.1), such that updrafts occur on windward slopes and downdrafts on lee slopes, grossly belies the behaviour of wind in the vicinity of the terrain found within the PFM's domain. With respect to the last of these, Browning *et al* (1974) presented a case where extensive middle level convection was triggered by air being lifted over hills but with both the lifting and the triggered convection beginning well upwind of the hills to the extent they occurred over the sea, and found this phenomenon in keeping with theoretical studies of mountain waves. Mountain waves have been observed in Wales and, as noted by Banta *et al* (1990), these waves in stable conditions can provide stronger updrafts than would be predicted by simple orographic models, resulting in greater condensation and slower horizontal flow over the upwind slope. Alternatively, air motion may go around rather than over hills especially in conditions of high static stability (Browning, 1980) or, in situations of high stability and relatively light winds, a train of waves may develop and form into an oscillating pattern to the lee of mountains, with clouds and precipitation featuring in the ridges of the lee waves (Barros &Lettenmaier, 1994).

5.2.4 Precipitation drifting

Of the factors mentioned as likely to be contributing to the poor performance of the PFM's orographic component, one, namely drift, will be given further attention here. A speculative comment on the drifting of rainfall was made earlier with reference to Figure 5.1 and the possibility that the Isle of Man might have been responsible for the contained enhancement of precipitation positioned within stratiform rain that was evident over the Irish Sea. In a simple orographic model, such as the PFM, in which condensation is made to immediately precipitate, Banta *et al* (1990) points out that peak rainfall rates will occur over the location of maximum positive slope and uplift but in reality it is quite likely the highest rainfall rates will occur some distance downwind. Browning (1980) found that in light winds and heavy background rain the maximum rainfall rates occur upwind of the hill crest but in strong winds the peak rates are displaced to leeward of the point of strongest upslope motion. The distance of this displacement can be sizeable if the strong winds are combined with a vertical profile dominated by potential instability and was found by Browning *et al* (1974), in one instance when the lee-side evaporation was much less than the orographic enhancement of rainfall, to extend a length of 100km from the topographic feature. Although the PFM makes the effect of orography on wind flow uniform throughout the vertical profile, in reality the rate of ascent slopes upwind with height, the effect of which, Sinclair (1994)

suggested, was to shift precipitation upwind and to increase the possibility of convection being triggered upwind of the slope. The form of the topographic barrier is another influence on the likelihood of drift occurring. Drift is more commonly associated with hills that have a half-length less than 10km, for which the maximum rate of precipitation tends to occur at the summit or to lee. In contrast, larger hills (half length approximately 20km or greater) often have the maximum rainfall rate occurring upwind of the crest (Austin and Robichaud, 1988).

In a rudimentary attempt to gauge if the drifting of rainfall influenced the PFM's performance to some extent, another run of the PFM was undertaken, this time with the sequence of the algorithm's implementation slightly adjusted. In Figure 3.13 it was shown that, apart from the initial "calibration" time-step, producing a forecast involved following an order of advecting rain field properties and then at the destination location calculating the change in CBLWC over the period of the time-step. The order was reversed for this particular run of the PFM so that the advection occurred after the calculation of CBLWC and the performance statistics of which are presented in Table 5.5.

	%cov_for	%cov_act	RMSE	CSI	POD	FAR	cc5km	cc10km	cc15km	cc20km	cc25km	ccnneigh	rate_for	rate_act
23/10/99 PFM	32.972	33.579	0.843	0.378	0.513	0.477	0.120	0.159	0.199	0.234	0.266	0.408	1.093	1.104
1/8/99 PFM	7.644	15.665	7.835	0.126	0.165	0.525	0.094	0.110	0.116	0.116	0.123	0.202	9.582	7.577
2/8/99 PFM	15.514	15.363	1.941	0.306	0.479	0.538	0.110	0.138	0.165	0.193	0.231	0.310	2.030	2.370
4/8/99 PFM	19.203	19.256	1.590	0.319	0.456	0.515	0.061	0.095	0.124	0.152	0.182	0.253	1.569	1.935
14/01/99 PFM	31.897	29.579	1.163	0.403	0.579	0.401	0.061	0.087	0.111	0.144	0.182	0.314	1.085	1.388
15/01/99 PFM	43.204	40.096	2.005	0.421	0.597	0.426	0.091	0.114	0.134	0.156	0.178	0.349	1.634	1.904
24/12/98 PFM	24.616	28.326	1.239	0.266	0.463	0.503	0.188	0.211	0.243	0.271	0.317	0.411	1.273	1.146
25/12/98 PFM	20.326	23.520	1.831	0.249	0.398	0.570	0.040	0.045	0.051	0.058	0.065	0.183	1.566	1.930
26/12/98 PFM	26.134	25.699	0.599	0.205	0.322	0.577	0.073	0.094	0.105	0.117	0.127	0.248	0.786	0.740
PFM	24.612	25.676	2.116	0.297	0.441	0.504	0.093	0.117	0.139	0.160	0.186	0.298	2.291	2.233
23/10/99 drift	32.972	33.579	0.843	0.378	0.513	0.477	0.120	0.159	0.199	0.234	0.266	0.408	1.095	1.104
1/8/99 drift	7.644	15.665	7.835	0.126	0.165	0.525	0.094	0.110	0.116	0.116	0.123	0.202	9.582	7.577
2/8/99 drift	15.514	15.363	1.941	0.306	0.479	0.538	0.110	0.138	0.165	0.193	0.231	0.310	2.031	2.370
4/8/99 drift	19.203	19.256	1.590	0.319	0.456	0.515	0.061	0.095	0.124	0.152	0.182	0.253	1.569	1.935
14/01/99 drift	32.036	29.579	1.164	0.404	0.581	0.401	0.062	0.088	0.112	0.144	0.182	0.315	1.086	1.388
15/01/99 drift	43.188	40.096	1.970	0.420	0.596	0.426	0.091	0.114	0.134	0.156	0.178	0.351	1.602	1.904
24/12/98 drift	24.616	28.326	1.239	0.266	0.463	0.503	0.188	0.211	0.243	0.271	0.317	0.411	1.273	1.146
25/12/98 drift	20.371	23.520	1.628	0.250	0.400	0.570	0.041	0.047	0.052	0.059	0.066	0.210	1.509	1.930
26/12/98 drift	26.165	25.699	0.602	0.205	0.322	0.576	0.073	0.095	0.107	0.120	0.130	0.246	0.791	0.740
drift	24.634	25.676	2.090	0.297	0.442	0.504	0.093	0.117	0.139	0.161	0.186	0.301	2.282	2.233

Table 5.5: *Summary of the average performance statistics of the PFM, with and without an attempt to account for drift. The results are averaged over the nine separate rainfall events and relate to a lead-time of one hour. Results labelled "PFM" are the original PFM formulation for which advection of the rainfield preceded CBLWC calculations and the results labelled "drift" refer to the PFM run with this order reversed. The best performance for each particular overall statistic is highlighted in green.*

A striking feature of these results (although obscured a little by the rounding of numbers employed) is that the overall performance of the PFM improves across all statistical measures when advection follows the CBLWC calculations. Even so, they still do not match those achieved without the orographic component, succeeding to better them only in the same performance measures as the PFM in its original form, namely nearest neighbour correlation and average rainfall rate. On some

of the days, specifically the 1st, 2nd and 4th August 1999 and also the 23rd October 1999 and 24th December 1998, the attempt to account for drift made no impression at all. The principal reason for this was the predominance of persistence over the other advection options, which rendered the changes made to the timing of advection implementation ineffectual. Another possible contributor to this lack of variation, but to a far lesser extent, could have been the greater potential of convective updrafts, compared to UKMM values of vertical velocity, to very occasionally dwarf orographically induced downdrafts. These convective updrafts would have been extensive across the domain on the aforementioned days, as the PFM's trigger for release of instability and implementation of the convective parameterisation of vertical velocity requires just one of either orographic updraft, a positive UKMM vertical velocity or pre-existing rain. With respect to the remaining four days, the very simple approach taken to account for drift improved results on the 14th January 1999 and the last two days of rainfall in December 1998 but slightly degraded those of the 15th January 1999.

Alongside experimenting with the "drift" version of the PFM, greater attention was given to the nearest neighbour correlations achieved by the original PFM configuration and which were typically greater than those produced when the orographic component was removed. The positions of the nearest neighbours were identified in an attempt to see if there was any information contained in their distribution, particularly whether they exhibited bias towards a particular position that might be attributed to rainfall drift or storm system movement. Towards this purpose the grid cell of interest and its surrounding neighbours where numbered in the following way:

1	2	3
4	5	6
7	8	9

with values of 2, 8, 4 and 6 having the orientation of north, south, west and east respectively. Determination of the nearest neighbour correlation coefficient involved searching all nine cells for a forecast value of rainfall rate that best matched the actual rainfall rate in the central cell. All nearest neighbour positions were recorded except when the actual rainfall rate in the central cell or any of the forecasted rainfall rates in and around the cell had values of zero, so as to place the emphasis on the distribution of rainfall rates in clusters of rain cells (that is enhancement within

pre-existing rain) rather than have results greatly influenced by changes in storm size. In addition to noting the nearest neighbour position, a record was also made of the 1000mb wind direction in the central cell and whether positive, negative or no orographically induced vertical motion had been assigned to the cell. In this exercise 1000mb wind directions were grouped into the four broad divisions of northwesterlies, northeasterlies, southeasterlies and southwesterlies. In each of the three categories of vertical motion, a tally was kept of the number of times each position was selected to produce an "event" total for each of the nine days of rainfall.

Figure 5.4 shows graphs of the totals for the three convective days of August 1999, with bars of the graphs coloured according to how the totals were apportioned with respect to the 1000mb wind direction. On the 1st August, the rainfall rates observed over sea areas were best represented by the forecast value in the same grid cell, which perhaps indicated that storm movement in this case was replicated reasonably well. Whereas northeasterly winds predominated over sea areas, the winds were much more variable over land although most of the orographic uplift appeared to be generated by northwesterly winds. In updraft areas the actual rainfall rates again tended to match the corresponding forecasted rates better than those in adjoining cells, but with positions 7 and 9 also well represented. Although the wind direction near the surface was variable, just above the level of the terrain the winds were quite consistently southeasterly (placing position 9 upwind) and sheared to the right with height to become southwesterly by the 600mb level (placing position 7 upwind). Therefore the inclination towards those two nearest neighbour positions was perhaps suggestive of convective precipitation, which would extend to high levels, being sustained and carried downwind a little at higher levels. Alternatively surface winds were frequently from the northeast sector when position 7 was selected and a possible explanation for its association with that wind direction may be that stronger convection was being triggered upwind of the slopes rather than actually on the slopes, as probably predicted by the PFM. Positions 3 and 7 were the most often selected in areas of orographic downdrafts. A strong northeasterly wind component was associated with position 3, giving it an upwind orientation and therefore possibly indicating a drift effect. It should be noted that the lightness of the winds during the 1st August puts much of the above reasoning into question however.

Forecasts of grid cell rainfall rates on the 2nd August were largely, as on the previous day, best positioned on the grid cell to which they were meant to correspond, although a greater spread in favoured nearest neighbour positions was evident particularly over sea areas. In these areas surface winds were from the southeast, in common with the direction of storm movement, and the relatively high incidence of position 9 probably indicated a failure to adequately attain the vector of the storm's velocity, particularly as the slight prominence of positions 5 and 9 was repeated in both updraft and downdraft areas.

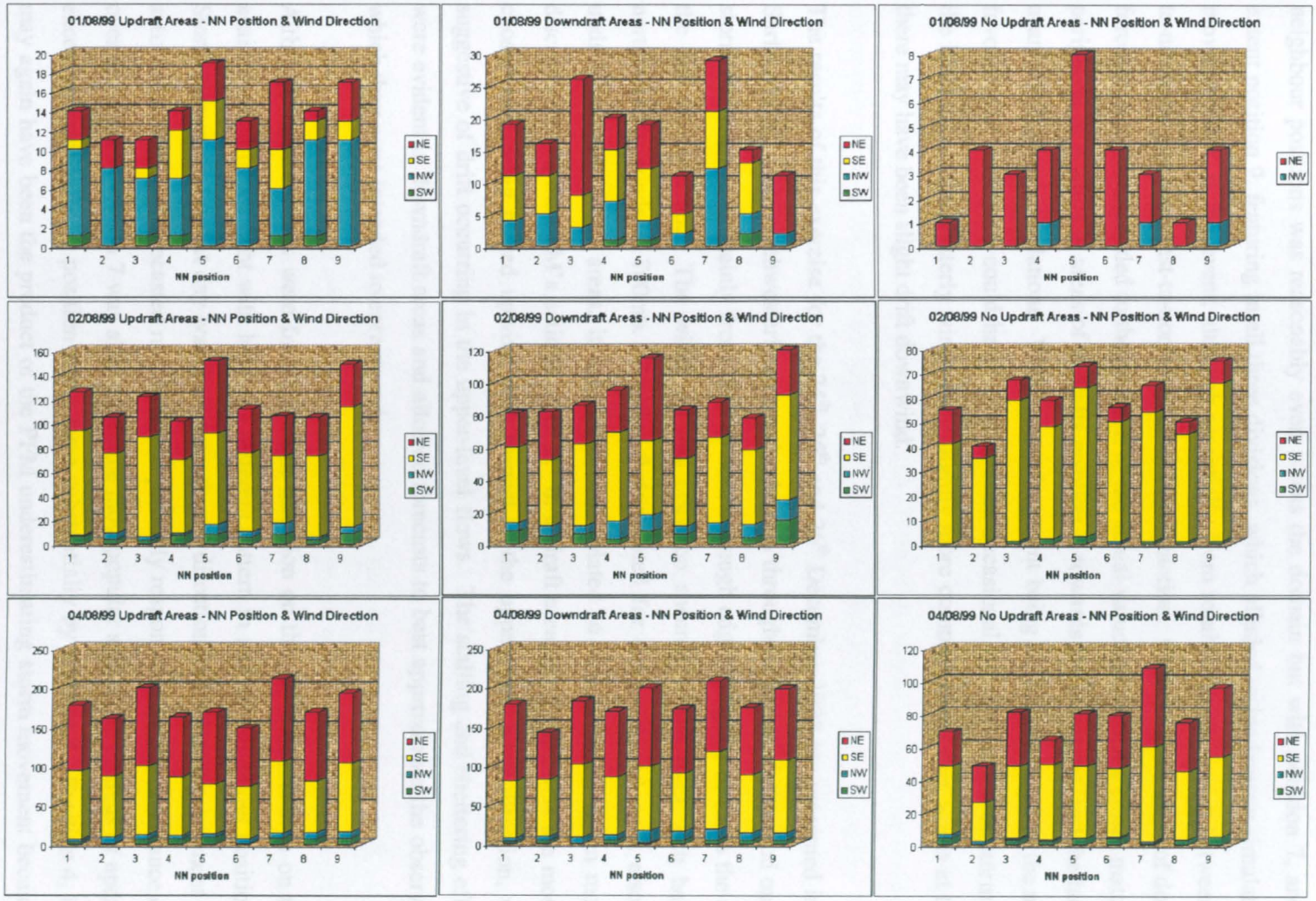

Figure 5.4: *The totals for each of the nearest neighbour positions for the 1st (top), 2nd (middle) and 4th (bottom) August 1999. The positions for each day are separated according to areas of orographic updraft (left), downdraft (centre) and no updraft (right), the latter equating to sea areas. Totals are coloured according to the 1000mb wind directions that featured when the position was selected.*

Winds on the 4th August were a mixture of mainly northeasterlies and southeasterlies, with minor contributions from northwesterlies and southwesterlies, and this time the relative proportions of the different wind directions were comparable over all areas of the domain. The spread of nearest neighbour positions was reasonably even across the domain but with position 7, and to a lesser extent position 9, featuring in all three divisions, which alluded to inadequate simulation of storm movement that, in this event, although essentially from south to north, varied between southwest-to-northeast and southeast-to-northwest lines of orientation. Otherwise, in areas of downdrafts the forecasts that corresponded to the grid cell of the actual values presented a closer match than those peripheral to it while in areas of updrafts position 3, towards the northeast, had the larger share of nearest neighbour correlations. With storm movement being at times directed to the northeast, the favouring of position 3 could have resulted from occasional overestimation of storm progress by the PFM or, as northeasterly winds were slightly more common than other winds at this position, there may have been slight drift downwind.

The results of this exercise for the 24th, 25th and 26th December 1998 are presented in Figure 5.5. Surface winds were southwesterly across the domain throughout the rainfall period on the 24th and storm movement was mainly from west to east, although edging slightly towards the southeast by the end of the event. The winds on this occasion sheared to the right with height to give northwesterly winds at 700mb. Position 9 dominated for sea areas and, as it also featured in updraft and downdraft areas, it may have been related to the nature of storm movement and discrepancies in the PFM's estimation of it. In updraft areas position 1 was the most frequently chosen and, being placed upwind with respect to the upper-level wind direction, was perhaps suggestive of drift occurring in the upper-level flows. The stalling and sheltering effects of hills were evident in downdraft areas and allowed forecasts to best approximate the observed values to which they were intended to correspond.

Although surface winds were from the same direction on the 25th December as on the 24th, and again sheared to the right with height, a different pattern in nearest neighbour positions emerged. Storm movement on that day was from a southwest direction and a lag in movement between the actual rain field and forecasted rain field was probably responsible for the dominance of position 7 over sea areas. Position 7 was also one of the most popular selections in areas of updraft, but was exceeded marginally by position 4 and more substantially by position 1. Position 4, in particular, may again have been the product of the PFM underestimating storm movement because, although rain cells tracked towards the northeast, the storm system as a whole incremented eastward. Alternatively the frequent selection of positions 1 and 4 may have been influenced by precipitation drifting at higher levels in the wind shear directed to the right of surface winds. Similar to the

previous day, the retarding and sheltering effects of hills elevated position 5 in downdraft areas and perhaps contributed to a preference for forecasts at position 9, a choice consistent with the eastward progression of the storm system, which to the lee of hills had slowed.

Position 5 featured again, and probably for the same reason given above, in downdraft areas on the 26th December, but more noticeable was the dominance of position 7 in all areas of the domain. The surface winds on the 26th were southeasterly but sheared to the right and were southwesterly at 700mb, placing position 7 upwind of the upper-level winds and also in line with the main direction of storm movement, which was east to northeast. Over sea areas, where the southeasterlies were at their strongest, positions 3 and 9 were also prominent and both likely arising from the nature of the storm movement. Position 3 in particular was, like position 7, in line with storm movement and together they perhaps indicated overestimation and underestimation of displacement along that line respectively. Over updraft areas, positions 1 and 4 featured as they had the day before and possibly for much the same reasons, the wind shear and eastward movement of the storm contributing to the occurrence of them both, with the additional possibility that, with respect to position 1, orographic influences on the southeasterly surface airflow and precipitation production were occurring further upwind than anticipated by the PFM.

A southwesterly (to westerly) surface wind direction persisted through the 14th January 1999 but upper-level winds and storm movement were mainly from the northwest. Over sea areas, there was a preference for nearest neighbours to be towards the coast at position 9, as can be seen in Figure 5.6. In this instance the bias toward position 9 may have been related to the PFM's development of rainfall slightly in advance of the rain approaching across the Irish Sea, matching the UKMM's areas of high humidity at 600mb. Land-based areas did not follow the pattern of sea areas in terms of favoured nearest neighbour positions, with both updraft and downdraft areas showing tendencies toward positions 1 and 7, although they differed in the weighting given to each. Position 7 lay upwind of surface winds and was most common in areas of updraft while position 1 lay upwind of both storm movement and upper-level winds and was most common in areas of downdraft. A possible explanation for the different emphasis placed on these positions in the two areas is that, on windward slopes (updraft areas), surface winds might be expected to exert the greater influence on the displacement of orographic rainfall from its source while upper-level winds would have the greater influence on the orographically enhanced rainfall once the air had been lifted to higher levels by the forcing of airflow over high terrain.

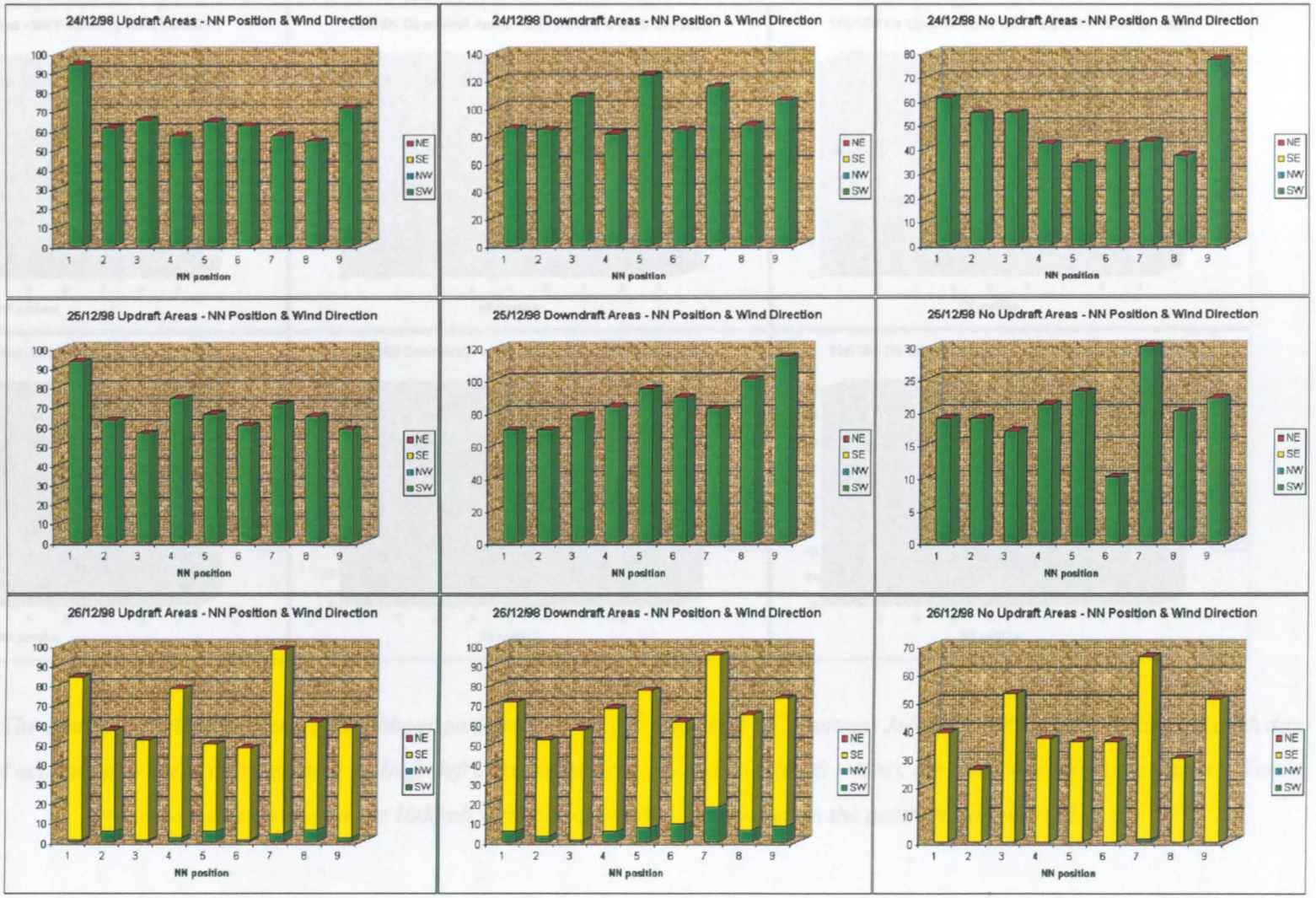

Figure 5.5: *The totals for each of the nearest neighbour positions for the 24th (top), 25th (middle) and 26th (bottom) December 1998. The positions for each day are separated according to areas of orographic updraft (left), downdraft (centre) and no updraft (right), the latter equating to sea areas. Totals are coloured according to the 1000mb wind directions that featured when the position was selected.*

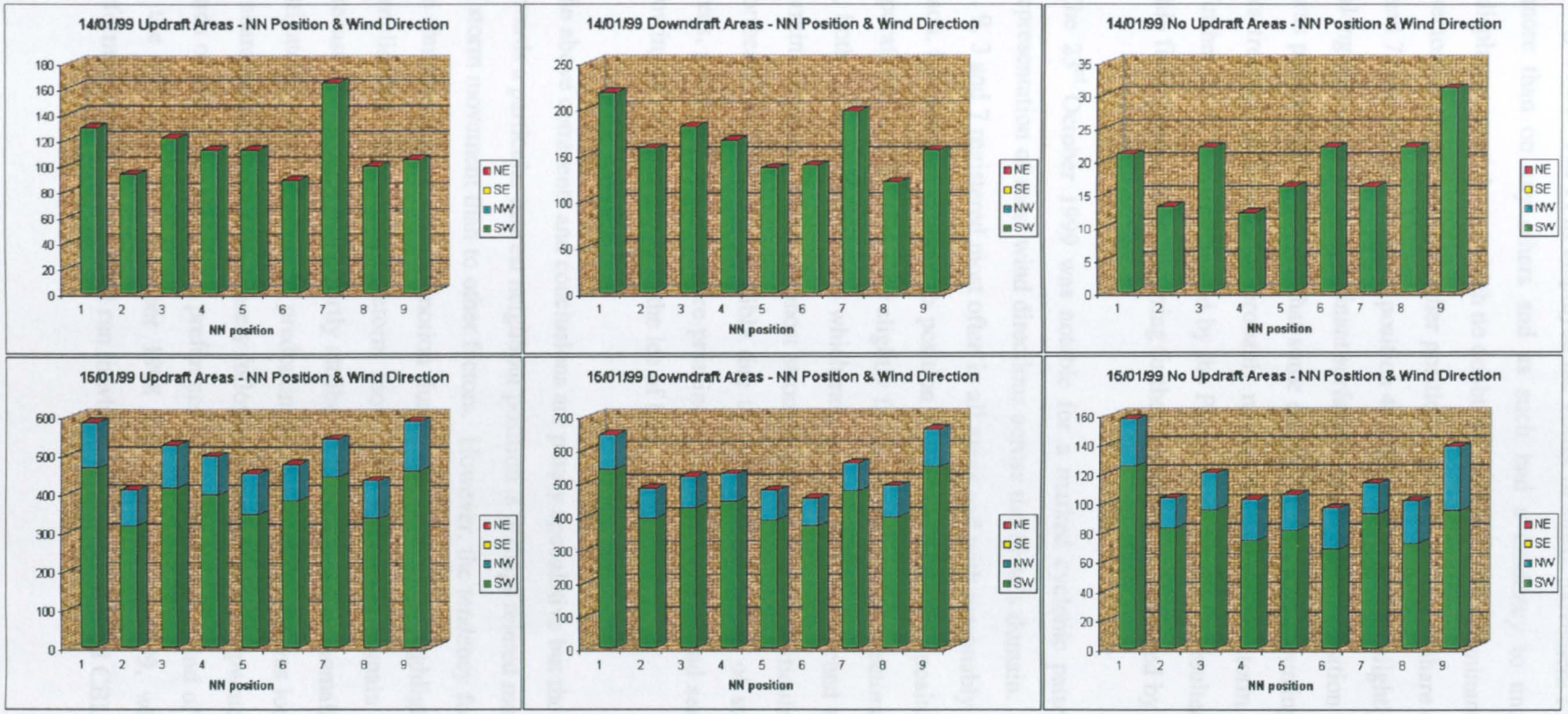

Figure 5.6: *The totals for each of the nearest neighbour positions for the 14th (top) and 15th (bottom) January 1999. The positions for each day are separated according to areas of orographic updraft (left), downdraft (centre) and no updraft (right), the latter equating to sea areas. Totals are coloured according to the 1000mb wind directions that featured when the position was selected.*

Storm movement on the 15th January 1999 was similar to the 14th, being generally towards the southeast. Surface winds comprised both northwesterlies and southwesterlies with the latter dominating. Results for the 15th are displayed in Figure 5.6 and all areas similarly had positions 1 and 9, at either end of the line of storm movement, as their most frequently selected nearest neighbours. The PFM employed the vector of storm movement to advect the rain field on this day more than on any others and as such had a tendency to underestimate or overestimate the displacement at times, which no doubt was a factor in the dominance of these positions. In all three sectors of the domain the other positions had a fairly equal share of being selected but positions 3 and 7 (and to a lesser extent position 4) tended to be chosen slightly more often. Both positions lay along the line of the predominant surface wind direction. Position 7 lay upwind and its prominence was possibly an indication that some degree of drift was occurring. Position 3 lay downwind and its frequent selection was probably related to vagaries in storm movement (which was perhaps further south than anticipated by the PFM) or alternatively resulted from orographic influences on rain field development occurring further upwind than instigated by the PFM.

The 23rd October 1999 was notable for a marked cyclonic pattern of wind flow, which led to representation of most wind directions across the PFM's domain. Figure 5.7 shows that positions 1, 9, 3 and 7 registered most often in all areas and with reasonably close allocation of frequency to each, but marginally more to position 3 over sea areas and position 9 over downdraft areas. In updraft areas, selections very slightly favoured the northern sectors represented by positions 1 and 3, both being positions from which rain moved as it approached the windward sides of elevated terrain. Position 3 featured most strongly over sea areas, particularly when winds were from the northeast, and this was possibly due to incorrect estimation of storm movement. In downdraft areas, position 5 featured more prominently than in updraft and sea areas and perhaps indicated a slowing of rain movement to the lee of hills.

The above comments and conclusions are purely speculative but the general impression is that bias towards a particular nearest neighbour position is perhaps related more to inadequate representation of storm movement than to other factors. However, the tendency for differences to be observed in the three sectors of vertical motion during the same event highlighted the influence hills had in complicating the pattern of storm movement across the domain and raised the possibility of forecast inaccuracies being partly attributed to precipitation anomalies being carried downwind or instigated upwind of where its predominant source of forcing was located. Typically the allocation of nearest neighbours most closely followed positions placed upwind of surface winds, upper level winds or storm movement. A preference for the position upwind of storm movement was evident on the 25th and 26th December 1998 and 14th January 1999, which explained the improved performance given by the PFM run in which advection followed CBLWC evolution equations.

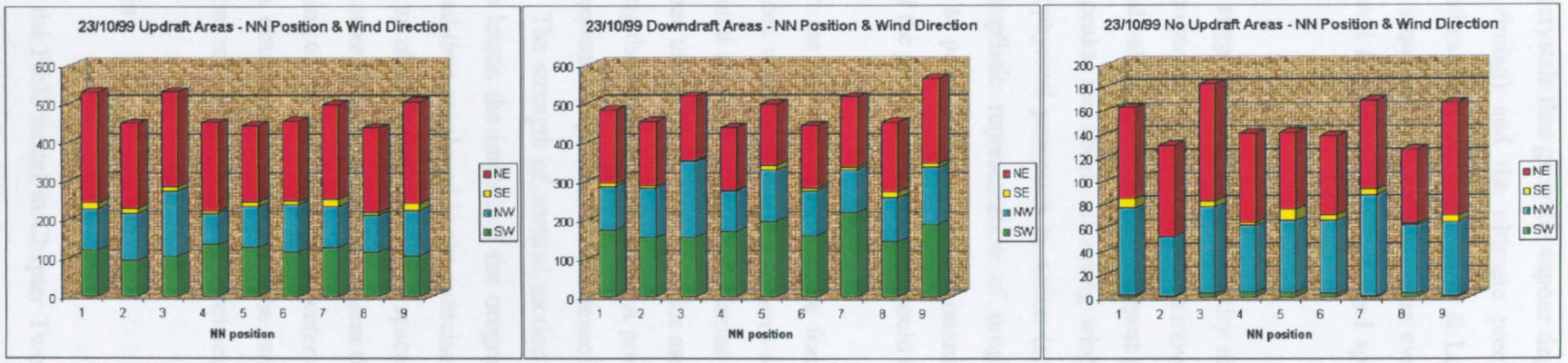

Figure 5.7: *The totals for each of the nearest neighbour positions for the rainfall commencing 23rd October 1999. The positions are separated according to areas of orographic updraft (left), downdraft (centre) and no updraft (right), the latter equating to sea areas. Totals are coloured according to the 1000mb wind directions that featured when the position was selected.*

The aforementioned December and January dates fall within the winter period of the UK and thus perhaps reinforce the need to account for the predominant phase of water in the atmosphere, the way in which ice crystals grow (crystals that grow by vapour deposition and aggregation are less dense than those obtained by riming) and the ultimate precipitation type, with all having implications for the likelihood and extent of drifting (Barros & Lettenmaier, 1994). There may be scope in the PFM to change the sequence of advection on an event basis given, for example, the presence of a certain freezing level height and level of wind speed that might be suggestive of snowdrift potential.

However, in general, the results suggested that the complexity of wind flow in areas of elevated terrain, the retarding effect of topographic barriers on system movement, the influence of triggered convection in producing enhanced values upwind of the steepest point on windward slopes and in sustaining precipitation beyond peaks, the ability of strong winds to carry rainfall considerable distances and the array of microphysical processes in action (such as feeder-seeder effects) all rendered the PFM's current simplistic representation of orographic forcing to some extent ineffectual but at least still able to provide higher rainfall intensities, and able to place a better forecast within close proximity of the point of interest, than could be achieved without it.

It could be argued that although the removal of orographic forcing altered the PFM's average performance, the actual differences were very small and were suggestive of insensitivity to its employment. This can be attributed to some extent to the input UKMM wind fields, with more significant differences evident when using the greater velocities associated with the vector of storm movement and also when adjusting the length of time-step. A possible contributor to this relative insensitivity was the PFM's frequent adoption of the convective pathway of the algorithm, discussed in more detail below. The strength of vertical motion calculated from the convective parameterisation has potential to lessen the impact of the orographically induced rate of uplift. Furthermore, the length of the lead-time employed in the exercises (one hour) combined with the nature of the events often led to an observed persistence in space and time of the orographically enhanced rainfall between consecutive forecasts. To some extent this would allow the "efficiency" factor that governs the proportioning of cloud column liquid water to the cloud base to adjust to the rates of orographic precipitation observed, regardless of the strength of forcing, provided the UKMM representation of conditions remained fairly similar between forecasts, which it often did.

5.3 Mode of uplift differentiation

One of the criticisms levelled at the F&K model in Chapter Two, or rather one of the concerns regarding its indiscriminate application, was the reliance on a convective parameterisation solely to

determine the average vertical velocity in a cloud column. Justification for the F&K approach came from observations of convective cells being embedded in stratiform rain, and it should be remembered that a number of the rainfall events presented in this and the previous chapter had potential instability and convective raincells accompanying widespread rain mainly driven by frontal activity. A desire to recognise the mode of forcing primarily responsible for precipitation production was one of the factors motivating development of the PFM and as such considerable effort went into finding ways to broadly categorise the nature of the mesoscale environment within which rainfall transpired. As a result the means to identify significant fronts, symmetric instability, potential instability and moist static instability were all included in the PFM's formulations and these increased the computational burden and complexity of an adopted framework that had simplicity as one of its key attributes. Therefore it had to be questioned whether these additions made any difference to the results, and to that end a further two runs of the PFM were undertaken, one with grid cell vertical velocity always determined through the convective parameterisation and the other with it always being the average of the UKMM vertical velocity between the pressure level at the cloud base and top. All nine separate periods of rainfall of the UK case study were included, a forecast lead-time of one hour only was considered and only real-time data used in the assessment. The same performance measures used throughout this and the preceding chapter were again employed and the results for the two runs, together with those of the original PFM run, the latter for ease of reference, are presented in Table 5.6. It should be noted that in these two latest runs of the PFM, modifications were made to the vertical velocity determination only, with everything else kept otherwise as the original, including having the orographic component in place and the original advection sequence retained.

The results in Table 5.6 show that the use of the UKMM vertical velocity produced, in terms of statistical performance, inferior forecasts to those of the original PFM, with all performance measures being worse than their counterparts. The rainfall coverage decreased noticeably and can be attributed to the UKMM placing negative vertical velocity, or negligible upward motion that was easily countered by orographic downdrafts, in areas the original PFM would have otherwise employed a convective parameterisation, the latter typically giving updrafts and associated rainfall production. The rainfall rate, perhaps unexpectedly, was very high but this was an outcome of the method chosen to determine CBLWC from the total gain in liquid water to the cloud column and principally from the general application of linearly regressed coefficients that were in this case probably high compared to the original PFM run, as the set of first-estimate forecast values used in the regression would have comprised values of CBLWC that in some cases were significantly reduced from initial values by the influence of the downdrafts. With respect to the other performance measures, RMSE was high, CSI and POD low, while FAR was high despite rainfall coverage being much lower than that estimated by the PFM in its original form. Correlation

coefficients at all scales, including nearest neighbours, were appreciably lower than those achieved using the PFM with convective updrafts enabled.

	%cov_for	%cov_act	RMSE	CSI	POD	FAR	cc5km	cc10km	cc15km	cc20km	cc25km	ccnneigh	rate_for	rate_act
23/10/99 PFM	32.972	33.579	0.843	0.378	0.513	0.477	0.120	0.159	0.199	0.234	0.266	0.408	1.093	1.104
1/8/99 PFM	7.644	15.665	7.835	0.126	0.165	0.525	0.094	0.110	0.116	0.116	0.123	0.202	9.582	7.577
2/8/99 PFM	15.514	15.363	1.941	0.306	0.479	0.538	0.110	0.138	0.165	0.193	0.231	0.310	2.030	2.370
4/8/99 PFM	19.203	19.256	1.590	0.319	0.456	0.515	0.061	0.095	0.124	0.152	0.182	0.253	1.569	1.935
14/01/99 PFM	31.897	29.579	1.163	0.403	0.579	0.401	0.061	0.087	0.111	0.144	0.182	0.314	1.085	1.388
15/01/99 PFM	43.204	40.096	2.005	0.421	0.597	0.426	0.091	0.114	0.134	0.156	0.178	0.349	1.634	1.904
24/12/98 PFM	24.616	28.326	1.239	0.266	0.463	0.503	0.188	0.211	0.243	0.271	0.317	0.411	1.273	1.146
25/12/98 PFM	20.326	23.520	1.831	0.249	0.398	0.570	0.040	0.045	0.051	0.058	0.065	0.183	1.566	1.930
26/12/98 PFM	26.134	25.699	0.599	0.205	0.322	0.577	0.073	0.094	0.105	0.117	0.127	0.248	0.786	0.740
PFM	24.612	25.676	2.116	0.297	0.441	0.504	0.093	0.117	0.139	0.160	0.186	0.298	2.291	2.233
23/10/99 UKMM	25.642	33.579	1.815	0.328	0.405	0.456	0.081	0.126	0.166	0.197	0.222	0.334	1.873	1.104
1/8/99 UKMM	9.193	15.665	7.804	0.159	0.213	0.544	0.091	0.108	0.113	0.114	0.121	0.217	7.500	7.577
2/8/99 UKMM	10.782	15.363	2.633	0.243	0.339	0.524	0.079	0.102	0.125	0.153	0.192	0.234	3.882	2.370
4/8/99 UKMM	13.641	19.256	1.785	0.249	0.321	0.504	0.041	0.073	0.101	0.130	0.163	0.207	2.492	1.935
14/01/99 UKMM	17.876	29.579	2.717	0.249	0.309	0.397	0.030	0.043	0.055	0.069	0.083	0.177	2.174	1.388
15/01/99 UKMM	28.456	40.096	5.581	0.301	0.394	0.444	0.038	0.057	0.075	0.094	0.113	0.229	4.276	1.904
24/12/98 UKMM	22.884	28.326	2.493	0.258	0.428	0.500	0.126	0.166	0.204	0.230	0.270	0.361	1.926	1.146
25/12/98 UKMM	13.259	23.520	2.104	0.185	0.267	0.545	0.019	0.027	0.032	0.037	0.039	0.143	2.480	1.930
26/12/98 UKMM	19.709	25.699	2.413	0.164	0.244	0.623	0.015	0.033	0.049	0.057	0.065	0.109	4.787	0.740
UKMM	17.938	25.676	3.260	0.237	0.324	0.504	0.058	0.082	0.102	0.120	0.141	0.224	3.488	2.233
23/10/99 convection	33.010	33.579	0.843	0.378	0.513	0.478	0.120	0.159	0.199	0.234	0.266	0.408	1.092	1.104
1/8/99 convection	7.644	15.665	7.835	0.126	0.165	0.525	0.094	0.110	0.116	0.116	0.123	0.202	9.585	7.577
2/8/99 convection	15.519	15.363	1.941	0.306	0.479	0.539	0.110	0.138	0.165	0.193	0.230	0.310	2.029	2.370
4/8/99 convection	19.203	19.256	1.590	0.319	0.456	0.515	0.061	0.095	0.124	0.152	0.183	0.253	1.569	1.935
14/01/99 convection	32.206	29.579	1.163	0.405	0.583	0.402	0.062	0.088	0.112	0.145	0.182	0.323	1.093	1.388
15/01/99 convection	44.454	40.096	2.007	0.429	0.618	0.425	0.089	0.112	0.133	0.156	0.178	0.349	1.621	1.904
24/12/98 convection	29.756	28.326	1.178	0.283	0.538	0.519	0.175	0.201	0.235	0.264	0.306	0.407	1.112	1.146
25/12/98 convection	20.339	23.520	1.830	0.249	0.398	0.571	0.040	0.046	0.051	0.059	0.065	0.183	1.567	1.930
26/12/98 convection	27.822	25.699	0.600	0.214	0.343	0.576	0.072	0.092	0.102	0.113	0.122	0.235	0.772	0.740
convection	25.550	25.676	2.110	0.301	0.455	0.505	0.091	0.116	0.138	0.159	0.184	0.297	2.271	2.233

Table 5.6: *Summary of the average performance statistics of the PFM with variations to the determination of vertical velocity: the original PFM run (labelled "PFM"), a run using the convective parameterisation to determine the grid cell vertical velocity in all cells (labelled "convection"), a run using the cloud column average of the UKMM vertical velocity (labelled "UKMM"). Results are given for each of the nine separate rainfall events and these are averaged to give an overall performance. Forecasts were made using real-time data and a lead-time of one hour. The best performance for each particular overall statistic is highlighted in green.*

In contrast to the reduction in rain area produced by UKMM vertical velocities, wholesale application of the convective parameterisation increased percentage rainfall coverage, a result not unexpected with the exchange of some of the UKMM's downdrafts, or weak updrafts, with convective updrafts. With the expansion in rain area came an increase in CSI and POD but also an increase in FAR, so not all the new cells were well targeted. Notably an increase in FAR was not observed, rather there was a decrease, in the other runs of the PFM (orographic component removed and drift versions) that similarly had produced increases in rainfall coverage, although not quite to the same extent. The implementation of widespread convection dropped the average rainfall rate closer to the actual and with it dropped RMSE. The correlations, although not appreciably different to the PFM originals, could not match the originals at any scale.

Overall, there did not appear to be substantial reward in trying to distinguish between convective and dynamically forced modes of uplift. One of the reasons for this was the UKMM's

representation of the events, whereby six of the nine days of rainfall exhibited layers of potential convective instability. The primary reason, however, is likely to be the PFM's bias towards implementing the convective parameterisation rather than taking the average UKMM vertical velocity, whereby the mere presence of moist static instability or potential instability within the pre-existing rain field was taken to signal active convection and UKMM or orographic updrafts, no matter how weak, were deemed sufficient to trigger the convective parameterisation in "dry" cells featuring unstable conditions.

Despite the seeming lack of benefit in differentiating between forcing modes, upon considering the results of this latest run of the PFM in context with the results achieved earlier when other adjustments were made to it, it became evident that a domain featuring only convective updrafts offered little more than to show that a field of mainly upward vertical motion preserved the extent of the rain field. This means there is still appeal in trying to separate out the processes providing the impetus for precipitation production and governing the dynamics of the rain field, both conceptually and for the better correlations that can be achieved. To bring out the best in such a methodology may however require a more rigorous determination of the mode of forcing, or simply adding further qualification to when the convective parameterisation is employed, and also a more microphysically-based manner of attributing cloud column condensation to CBLWC. But in implementing changes, it must be remembered that continually increasing the complexity of the PFM, for what might be diminutive gains, runs counter to the objective of maintaining simplicity and speed of computation and that the results achieved using UKMM vertical velocities solely were themselves a little discouraging.

5.4 Summary

Having established in the previous chapter that the PFM could match and better other forecast methods, that is in terms of the selected performance measures averaged over nine rainfall periods, the contribution of different facets of the PFM to the results was queried, with a focus on the components of the PFM responsible for cloud column (or grid cell) vertical motion. The roles of the parameterisations for orographic forcing and convective updrafts were given specific attention. Care has be taken not to over-generalise the results given the limited amount of data used in the work but, with respect to the case studies involved, a number of observations and conclusions were proffered:

- Use of UKMM 1000mb wind fields proved more suitable than the vector of storm system velocity for generating orographically-induced vertical motion, although there was uncertainty whether using wind fields at slightly higher levels might provide consistently better results.

- On the whole, the current form of the PFM's representation of orographic forcing appeared too simplistic to derive substantial benefit from it. Improvements were obtained by allowing advection of the rain field to follow CBLWC determination and, although improvements were not to an extent that the results excelled those achieved by removing the orographic component altogether, it was encouraging that such a simple adjustment could yield a better performance. The higher nearest neighbour correlations and rainfall rates obtained by including the orographic component, as well as the visual effects exemplified in Figure 4.8, perhaps make it worth persevering with its inclusion and further experimentation with its configuration. One of the main problems identified was the seemingly excessive depletion of water in rain cells caused by orographic downdrafts and there may be scope to use a parameter to modulate this.
- The deficiencies of the orographic component of the PFM led to mixed results when trying to compare use of one, 60 minute forecast time-step with twelve, 300 second time-steps, the latter intended to allow orographic influences to be more closely implicated in storm dynamics. Complicating interpretation of the performance statistics was an inability to separate out the effects of using different units of time. The important feature of the results was that the use of multiple time-steps produced the better correlation at the smallest scale being assessed, a grid length of 5km.
- Whilst conceptually appealing, the attempt to distinguish between predominant modes of uplift, when compared to blanket application of a convective parameterisation, did not produce results that conclusively cemented its worth but they showed enough promise to warrant pursuing its further assessment amid adjustments to both it and other parts of the PFM, as influencing the assessment outcome was the nominal difference, at times, between the two approaches due to the nature of the events being studied and the loose criteria defining when to employ the convective parameterisation.

CHAPTER SIX

URBAN APPLICATIONS - HIRE '98

6.1 The HIRE experiment

In August 1998, from the 1st September to the 30th November, the consortium of research institutions involved in the HYDROMET Project (mentioned in Section 2.6.3) undertook an European Union Environment and Climate Experiment that was given the acronym of HIRE: Hydrological Integrated Radar Experiment. Specifically, the parties involved in HYDROMET and HIRE were:

- The Water and Environment Management Research Centre, University of Bristol, United Kingdom
- Advanced Research Partnership, United Kingdom
- Dipartimento Territorio e Sistemi Agro-Forestali, Universita Degli Studi di Padova, Italy
- ARPAV, Centro Meteorologica di Teolo, Italy
- Fondazione per la Meteorologia Applicata, Italy
- Laboratoire d'Etude des Transferts en Hydrologie et Environnement (LTHE), Institut National Polytechnique de Grenoble, France
- Laboratoire Central des Ponts et Chaussees, Nantes Division, France
- Department of Water Resources, Hydraulic and Maritime, National Technical University of Athens, Greece
- Departament d'Enginyeria Hidraulica, Maritima I Ambiental, Universitat Politecnica de Catalunya, Spain
- Departament de Fisica Fonamentl, Universitat de Barcelona, Spain
- FAGG-Hidrotechnica, Univerza v Ljubljana, Slovenia
- Department of Water Resources, Wageningen Agricultural University, The Netherlands

The site chosen to conduct the experiment was the Mediterranean coastal city of Marseille, France, with the intention of observing and recording the often intense storms that occur there seasonally and which, combined with the steep surrounding landscape and urban environment, have

considerable propensity to produce flash floods. For the past two years, 1999 and 2000, south-east locales of France, including Marseille, have been sites of catastrophic flooding during autumn months (November and October respectively) with the flood waters not only destroying property but also taking lives (BBC, 1999a, 1999b, 2000a). The data collected during HIRE was intended to constitute a valuable archive of the autumnal storms characteristic of the area, a resource that could be accessed by researchers for some time to come but with more immediate use as a means to amalgamate the individual research efforts of the different groups involved in HIRE, with the cooperation involved and the outcomes attained advancing and consolidating their work together towards fulfilling shared objectives embodied in the HYDROMET Project.

The HYDROMET Project encompassed six separate and distinct work packages but all were similarly aimed at realising and exploiting weather radar's potential to enhance flood forecasting capabilities. That potential of weather radar lies in the tangible possibilities of deriving from it accurate and reliable estimation of rainfall intensities at spatial and temporal resolutions needed for effective flood forecasting and flood management in rural and urban catchments: flood forecasting using coupled hydrometeorological models and flood management through real-time control systems. Realising that potential requires establishing and ensuring accuracy and reliability both in the measurement of reflectivity from rainfall and in reflectivity-to-rainfall rate estimation techniques, each demanding specific knowledge of error sources, the nature of errors, how and to what extent errors can be eliminated and/or what corrections need to be applied (Collier, 1996). Exploiting that potential means developing models to efficiently extract and utilise the information contained in the data, particularly models that make optimal use of the level of detail provided by weather radar for the benefit of flood hazard mitigation. Thus the HYDROMET project addressed aspects of: radar hydrology, principally errors in reflectivity measurements and the uncertainties in the algorithms used to estimate rainfall from reflectivity values; hydrological models, lumped versus semi-distributed versus grid models; and rainfall forecasting models, those that base forecasts on radar rainfall estimates. HIRE was designed to provide the information needed to achieve improvements in all three areas.

The resources of the various teams involved were pooled for the experiment and the assistance of Ville de Marseille and Météo France enlisted, both providing access to weather and hydrological information routinely collected from established networks of in-situ instrumentation. Out of the resources made available by the two organisations, of prime interest to HIRE participants were rainfall estimates from one of Météo France's S-band weather radars, namely the Nîmes radar positioned 60km northwest of Marseille and operated to provide five minute data at a spatial resolution of 1km^2, as well as measurements from Ville de Marseille's system of telemetered tipping bucket rain gauges and water level gauges distributed throughout the Marseille region. The

Project partners temporarily erected their own specialised equipment to provide more intricate detail of the rainfall characteristics of each storm event. The equipment commissioned uniquely for the experiment were deployed in two locations, one at the central city office of Ville de Marseille's Water Management Headquarters (referred to as Vernet) and the other on the outskirts of the city, 11km to the north of the Vernet and at an elevation of 250m upon a hill site called Vallon Dol (Andrieu *et al*, 2000b). The instrumentation consisted of:

- A mobile X-band vertically pointing radar (VPR) located at Vernet and supplied by the University of Bristol. The VPR was capable of providing detailed vertical profiles of reflectivity at resolutions of 7.5m in the vertical and 2 seconds in time.
- An X-band radar located at Vallon Dol, provided by LTHE, able to undertake both CAPPI (Constant Altitude Plan Position Indicator) and RHI (Range Height Indicator) type scans but for the experiment operated mainly in RHI mode with the beam aligned in the direction of the VPR. The horizontal resolution achievable by the radar was 300m and it took approximately 1 minute to complete one RHI scan.
- Two automatic weather stations belonging to the University of Bristol, one located at each site and providing, amongst other variables, measurement of temperature, pressure, humidity and the direction and speed of winds. Each weather station included a tipping bucket rain gauge that had a time resolution of 2 minutes and required 0.1mm of rain to tip.
- Two drop counting rain gauges (Hydra gauges), with 15 seconds resolution, both brought to Marseille by the University of Bristol and both located at the Vernet site.
- An electromechanical disdrometer operated by the University of Auckland, New Zealand, who participated in the experiment through links with the University of Bristol.
- Two optical spectropluviometers, both supplied and operated jointly by the French and Spanish groups at the Vernet site.

Two sites were necessarily chosen and so distanced in order to have the two X-band radars sampling the same air space. This was for the purpose of determining ways the VPR scan might be used to correct the vertical profile of reflectivity represented in the RHI image. Additionally the two sites provided a means to observe differences in how events were manifest at a sheltered inner city site less than 1km from the coast and at an elevated, exposed site further inland. Volunteers participating in the experiment, of which this researcher was one, recorded details of each storm and in doing so gave attention to a range of temporal and spatial scales, such that for each event a log of the day's synoptic conditions was accompanied by observed variations in the vertical profile of reflectivity, as captured every two seconds by the VPR, as well as raindrop sizes measured on scales of less than 1mm. During the three months of HIRE, thirteen rainfall events were recorded. Some of the events, particularly those in November, featured reasonably light rain that, although visible in images from the Nîmes radar and the VPR, barely registered in the tipping buckets, hydra

gauges and network rain gauges. Many of the events were associated with moving fronts but with active convection also often apparent.

6.2 Marseille case study

HIRE provided an opportunity to construct another case study by which the performance of the PFM could again be examined, but with the context of the case study being different in terms of both environmental conditions and the hydrological application. A study set in Marseille and founded on HIRE was obviously going to differ in a number of ways from one centred on northern England, such as that presented in Chapter Four, particularly in light of the primary focus of the experiment and the nature of the data therefore collected. HIRE was not so much directed towards flood forecasting over scales of regional catchments, where rural landscapes dominate terrain characteristics and where the nature of the rainfall combined with catchment response times may allow at least some, if at times rather minimal, separation between heavy rainfall, swollen watercourses and downstream flooding, rather HIRE was devised as a means to study urban hydrology and urban flash flooding in recognition that the urban environment poses specific challenges for flood forecasting. The built environment accelerates and channels runoff, storm water drainage systems and sewers modify and supplement natural drainage while specially constructed flood alleviation schemes and storage ponds assist with the management of flood waters and the mitigation of flood hazards (Hall, 1984). The typically smoother, impermeable city surfaces and the networks of piped conduits mean that response times of urban catchments are typically much shorter than rural river basins. Furthermore, in cities there are additional benefits to be had or rather additional hazards to be avoided, in terms of safeguarding water quality, from forecasting water loading on municipal sewer and storm water discharge systems, particularly combined systems, so as to prevent discharge of sewage into natural watercourses in storm water overflows (Cowpertwait *et al*, 1998). It is in this environment Collier (1996) felt that the spatial and temporal detail of rain fields provided by weather radar could be of tremendous benefit to flood forecasting, if only accuracy in rainfall measurement could be assured.

Collier's reference to spatial and temporal detail is particularly pertinent given the ability of metropolitan areas to create their own microclimates and to influence precipitation patterns within their immediate vicinity. The different types of surfaces present in urban centres can alter the radiation balance, while water vapour, heat and particulates can be added to the atmosphere through transportation and industrial processes. The result can be a higher incidence of thunderstorm activity over densely populated cities than over surrounding rural areas. While Marseille may or may not be of sufficient size to make such effects apparent, the location of Marseille alone presents particular difficulties for flood forecasting in terms of the nature of the

rainfall events that occur not only there but along the extent of the Mediterranean coastlines of France, Italy and Spain. Studies undertaken in each country have confirmed that rainfall intensities attained in regions bordering the Mediterranean Sea typically exceed those further inland or on Atlantic coasts (Desbordes, 1991). Not only can storms bring heavy rainfall but they can also be very quick to evolve because of the rapid development of strong, rain-producing circulations from temperature contrasts that arise between cool, northern continental air and air warmed by the temperate waters of the Mediterranean Sea (Andrieu et al, 1991). Thunderous, convective storms are not uncommon in coastal regions during summer and autumn when winds bring hot, moisture-rich air from the south, with the moisture readily augmented or replenished as air passes over or near the warm Mediterranean waters. The recurring, destructive, autumnal storms have been linked to certain synoptic conditions that have a tendency to arise in that season, whereby moist, warm, southerly airstreams are blocked by large, slow-moving pressure systems to the north, while at the same time eastward-moving air ascends the surrounding mountains only to be blocked and held over the high relief (Desbordes, 1991). The sustained and reinforced vertical motion associated with these interactions invariably leads to significant rainfalls and, at times, severe flooding. However, regardless of the season, the mountainous terrain lying near to the coasts in all of the aforementioned countries influences the intensity and occurrence of the rainfall events experienced in each. The combination of warm, humid air and strong orographic uplift is a mix that can readily result in heavy downpours and flash floods.

Undertaking an assessment of the PFM's performance with respect to Mediterranean storm events and with a slant towards urban hydrological applications, necessarily meant there were going to be differences between model inputs used in this exercise and those used in the UK case study, some of the more notable being: the resolution of the radar data was considerably finer ($1km^2$ as opposed to $25km^2$) and the average rainfall intensities present in the data were typically higher; the source of mesoscale NWP data was the ALADIN model of Météo France as opposed to the UKMM and the forecast products that were supplied came as three hourly, rather than hourly, data sets; and the topography covered by the range of the Nîmes radar and also the domain of the ALADIN model included mountain peaks rising above 4000m compared to 1000m in the UK.

For the Marseille case study the PFM was kept essentially unchanged from the form implemented for the UK case study and although improvements to the algorithm were discussed in Chapter Five, it was considered prudent to retain the original model to see whether and to what extent the same problems resurfaced given the different conditions and what new weaknesses emerged that might be dealt with at the same time as trying to correct the others already identified. Out of the thirteen events recorded in HIRE, six were selected to undertake further assessment of the PFM's forecasting ability. Of the seven events not included in the case study, two were November events

during which only light and minimal rain fell. The others, one in September and the others in October, proved very short-lived and the radar images for those events featured less in the way of actual rainfall than they did the anomalous propagation and clutter problems induced by the atmospheric conditions. Further comment on the quality of the Nîmes radar data will be made in the next section.

6.2.1 Data acquisition

Despite there being a plethora of observations recorded and measurements taken by HIRE participants during the experiment, they were specific to the experiment and as such only the routine products of Météo France formed the inputs to the PFM for this case study, consistent with the intention of constructing a rainfall forecasting model suitable for use in an everyday operational environment. The supplementary data collected by the experiment team did however assist with following each event's evolution, development and spatial and temporal variability, and will be referred to in that context. The routine products required from Météo France were the Nîmes PPI radar data and NWP model output. A file containing the height of the land surface within the proposed PFM domain was also needed and, on this occasion, acquired from the internet.

6.2.1.1 Nîmes radar data

Processed Nîmes radar data extends over an area 512km by 512km, having at its centre the geographical co-ordinates of 1.37° longitude and 41.52° latitude. As can be seen in Figure 6.1, that area includes significant topographic features such as the Massif Central, the southern end of the Alps and the western edge of the Pyrenees. Weather radar sited in mountainous areas are susceptible to problems of beams being blocked and/or returns occurring from the surface of high terrain with consequent errors in rainfall estimates (Andrieu *et al*, 1991). Such problems were immediately evident upon visualising the six storm events with Vis5d, the pictures revealed severe incidences of ground clutter on the Nîmes-facing slopes of the mountain ranges and around the immediate vicinity of the radar, clutter that exhibited variability in magnitude and intensity depending upon the atmospheric conditions. The nature of this problem is clearly shown in Figure 6.1, with many of the grid cells lining the mountain ranges returning high values of reflectivity when the only rainfall to be found on the image lies approximately over Perpignan, between the Pyrenees and the coast. This suggested that the radar data received from Météo France was in a relatively raw state and the only processing that appeared to have been undertaken was the transformation of radar reflectivity from polar to Cartesian co-ordinates and determination of rainfall rates at a spatial resolution of $1km^2$.

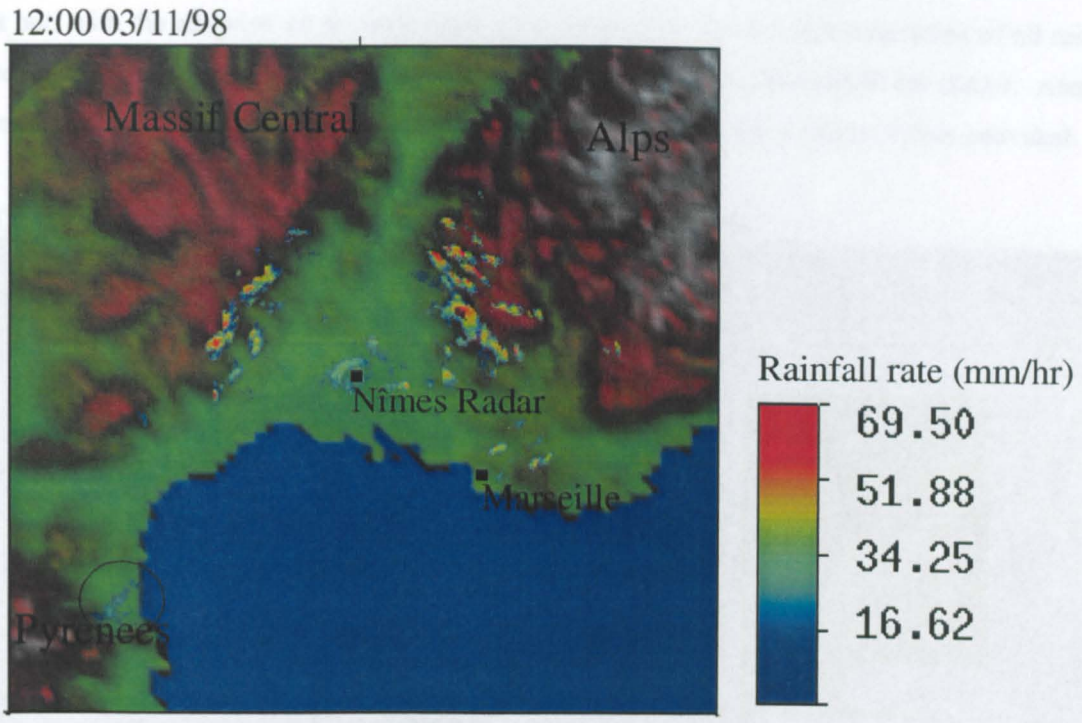

Figure 6.1: *The full coverage of the Nîmes radar. The Massif Central lies top left, the southern extension of the Alps top right and the western end of the Pyrenees bottom left. What at first appears, in this picture, to be rain cells of strong intensity are in fact returns of reflectivity from the mountainous terrain and true rain cells can be found only towards the bottom left of the image between the Pyrenees and the coast (circled).*

Not all the region displayed in Figure 6.1 constituted the PFM domain for this case study. Accompanying the files containing the Nîmes radar data was Fortran code that not only enabled the data to be read from the files but also allowed extraction of three specific areas from the footprint of the radar: the south east quarter of the radar coverage; a smaller area within this being a region around Marseille and centred on Marseille; and a smaller area again nested within the Marseille region. The second of these, the region around and including Marseille, was taken to be the PFM domain and was made so for three reasons: to match the siting of the HIRE experiment; to avoid some of the clutter problems evident in Figure 6.1; and to attain a similar number of computational points as had been included in the UK case study. With respect to achieving the latter, the resolution of the PFM ($1km^2$ to match the radar data) meant the actual physical area delineated for the domain was much smaller than that of the UK domain. The Marseille domain, shown in Figure 6.2, consisted of 100×100 grid points (compared to the 84×84 previously used), covered 100km×100km (as opposed to 420×420km) while the assessment grid centred within it measured 50km×50km (50×50 grid cells). The total number of cells included in the assessment was however reduced through efforts to eliminate any featuring permanent clutter, some of which are apparent in Figure 6.2. The removal of "contaminated" cells appeared a safer option than trying to distinguish rainfall from clutter in the grid cells affected. It resulted in exclusion not only of those particular

cells but, with the adoption of the semi-lagrangian advection scheme and translation of all rainfall values in unison across the domain, also grid cells that became the destination for clutter. Areas of permanent clutter could only be roughly determined from the limited amount of data provided.

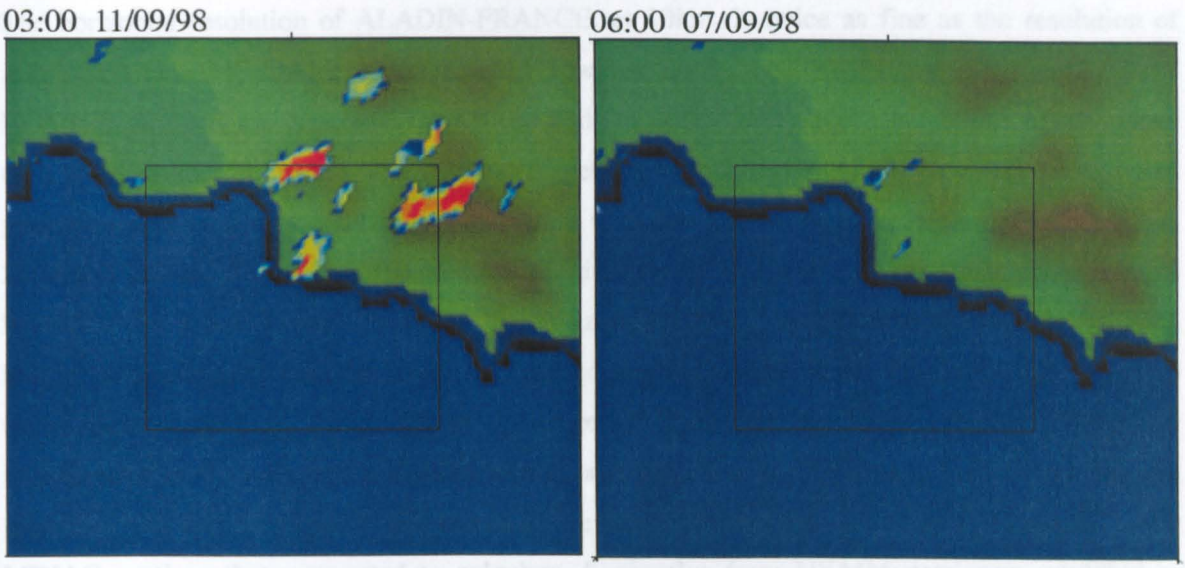

Figure 6.2: *The Marseille domain and characteristics of the Nîmes radar data. The two images (date and time of each as indicated) show the PFM's domain for the Marseille case study (the inner assessment grid indicated by the black square) and feature cells affected by problems of clutter and anomalous propagation, the extent of the problem varying between events.*

Similar to the handling of the UK network radar data, the Nîmes radar files were converted into Vis5d files. Météo France codes rainfall rates not as continuous values but employs varying increments such that only values of (in units of $mmhr^{-1}$) 0, 4, 12, 18, 23.5 and increments of 1 thereafter are used. This methodology was retained when undertaking the performance assessment, whereby forecasted rainfall rates were similarly changed to whichever one of the aforementioned values they were closest.

6.2.1.2 NWP data

The NWP data obtained to complement the Nîmes radar data came from the ALADIN-FRANCE model of Météo France. A number of ALADIN (Aire Limitée Adaptation Dynamique développement International) models exist across Europe, having evolved out of the ARPEGE (Action de Recherche Petite Grand Echelle) global model Météo France had developed in conjunction with the European Centre for Medium-Range Weather Forecasts (ECWMF). ARPEGE is notable for employing a horizontal resolution that becomes coarser with increasing distance from its centre, so that a grid length of 20km over France extends to 250km over Australasia (Météo France, 2001). The ALADIN Project, co-ordinated by Météo France, saw the

co-operation of fourteen European National Meteorological Services in producing their respective Limited Area Model (LAMs) versions of ARPEGE and for which ARPEGE now provides boundary conditions (ALADIN International Team, 1997).

The horizontal resolution of ALADIN-FRANCE, at 10km, is twice as fine as the resolution of ARPEGE and is very similar to the UKMM. However, unlike the UKMM forecasts, the ALADIN-FRANCE products are generated only twice daily at 0000Z and 1200Z, with three hourly rather than hourly forecasts made. The forecasted meteorological variables are produced on standard pressure levels ranging from 1000mb to 100mb with the size of the increments varying between 25mb and 100mb. Specifically the products acquired for the case study were: temperature, relative humidity, the x and y components of the horizontal winds, vertical velocity and geopotential height. Also supplied were the large-scale and convective rainfall rates. Unlike the UKMO, who automatically provides the complete coverage of the UKMM, Météo France allows for specification of the area required when making a request for ALADIN data, in this case the area requested was that corresponding to the coverage of the Nîmes radar as shown in Figure 6.1. The MDIAG routines that were used to calculate diagnostics from UKMM data were modified to calculate the PFM's required diagnostics from the ALADIN data and the results were processed into Vis5d files, with simple time interpolation to hourly intervals employed. The extraction of the smaller PFM domain and interpolation of the coarser resolution NWP data to the 1km grid length of the PFM were achieved using Vis5d utilities.

6.2.1.3 Satellite data

The half-hourly Meteosat infrared satellite data corresponding to the dates and times of the HIRE rainfall events were obtained from JCMM. Exactly the same type of files used in the UK case study were appropriate for this exercise because of the large footprint of the satellite, which covers all of Europe. The area of the PFM domain was delineated and the data processed into Vis5d files for merging with the ALADIN and radar data.

6.2.1.4 Elevation data

The surface elevation data for the PFM domain, needed for calculation of the orographic component of the vertical velocity, was extracted from GTOPO30, the global digital elevation model of the United States Geological Survey's (USGS) EROS Data Centre. The terrain elevation data is distributed freely via the internet and, for ease of management, the global data set is segmented into 33 tiles with all, except those covering Antarctica, extending over an area 50 degrees in latitude by 40 degrees in longitude. The tile utilised for the Marseille region is shown in

Figure 6.3. The horizontal resolution adopted by the USGS is a uniform 0.0083 degrees. This equates to approximately 1km but the geographic location of Marseille results in a slight difference in the exact metric distance covered by this resolution between north-south and east-west directions. As such the distance over which the land surface gradient was determined varied in each direction because the approach taken was simply to attribute a PFM grid point with the slope calculated from heights given at GTOPO30 grid points immediately to either side of it.

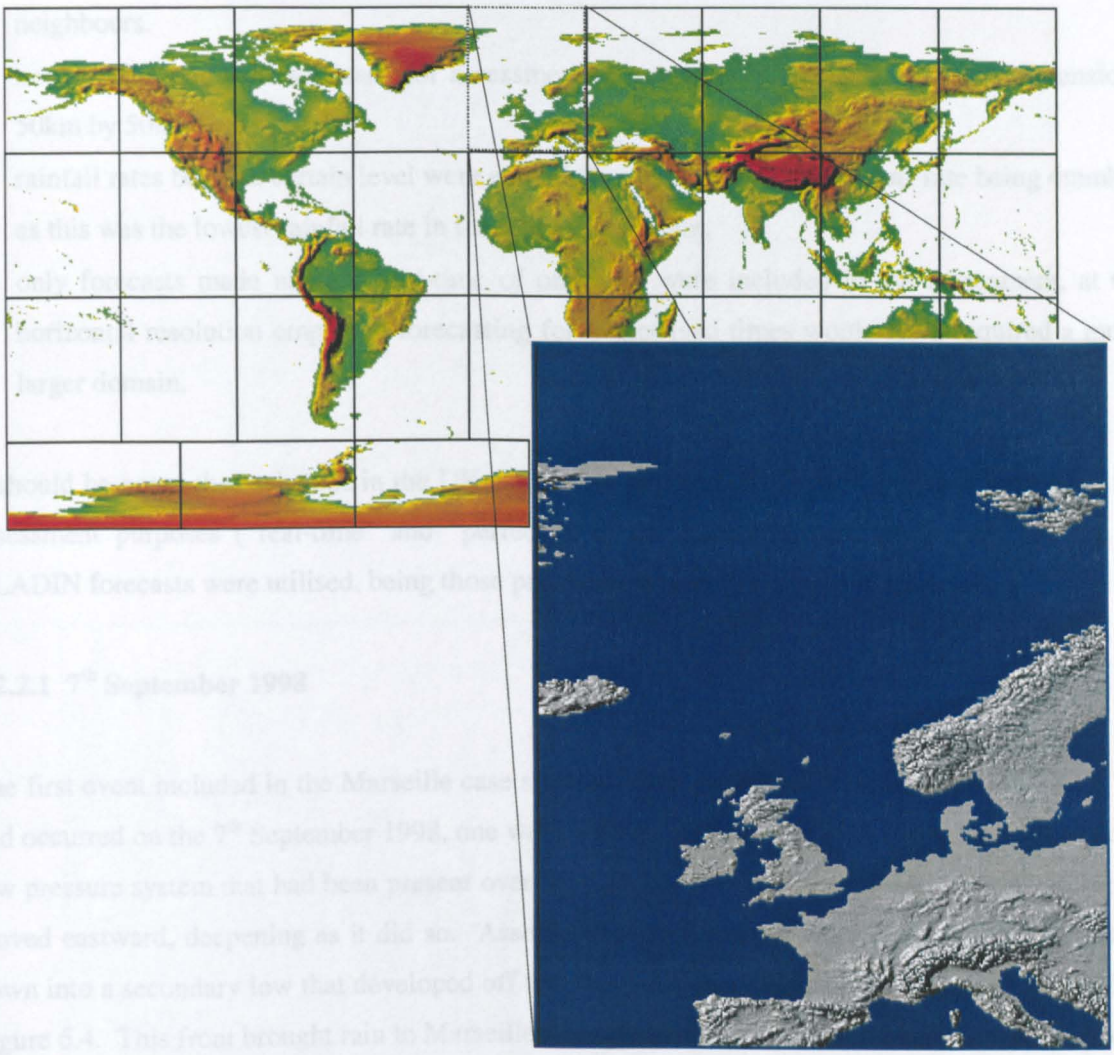

Figure 6.3: *The GTOPO30 global representation of terrain elevation (top) and the tile specific to the Marseille case study (below). The data has a horizontal resolution of 0.0833 degrees and heights are recorded to the nearest metre.*

6.2.2 The rainfall events – PFM performance

Assessment of the PFM's performance for each event was undertaken in the same way as for the UK case study:

- the PFM's results were compared with those from other forecasting methods, namely persistence, nowcasts and ALADIN's convective (ALADIN-C) and large scale (ALADIN-L) rainfall forecasts.
- instantaneous rainfall rates were the forecast product assessed.
- the same performance measures were utilised, specifically being percentage rainfall coverage, average rainfall rate, CSI, POD, FAR, RMSE and correlation coefficients at varying spatial averages which in this case were $1km^2$, $4km^2$, $9km^2$, $16km^2$ and $25km^2$ as well as nearest neighbours.
- not all of the domain was used for assessment purposes, only an inner grid with dimensions 50km by 50km.
- rainfall rates below a certain level were excluded and set to zero, the cut-off rate being $4mmhr^{-1}$ as this was the lowest rainfall rate in the Nîmes radar data.
- only forecasts made using a lead-time of one hour were included in the assessment, at the horizontal resolution employed forecasting for longer lead times would have required a much larger domain.

It should be noted that, whereas in the UK case study two sets of UKMM products were used for assessment purposes ("real-time" and "perfect"), in the Marseille case study only one set of ALADIN forecasts were utilised, being those produced closest to the time in question.

6.2.2.1 7th September 1998

The first event included in the Marseille case study was the second of those recorded in HIRE '98 and occurred on the 7th September 1998, one week into the experiment. The storm evolved out of a low pressure system that had been present over the Atlantic two days earlier and had progressively moved eastward, deepening as it did so. Associated with it was an occluded front that extended down into a secondary low that developed off the eastern coast of France and Spain, as depicted in Figure 6.4. This front brought rain to Marseille through the course of the 7th, rain that commenced mid-morning and continued into early evening as the front moved from west to east. The more persistent falls occurred in two peaks, the first of these between the hours of 1000 GMT and 1200 GMT. During that two hour period, the tipping bucket rain gauges at both the Vernet and Vallon Dol sites recorded maximum rainfall intensities in excess of $100mmhr^{-1}$, a rate with which the network system of rain gauges concurred but which was considerably higher than the rate of $60mmhr^{-1}$ recorded by the Nîmes radar. Rainfall continued after 1200 GMT but over Marseille rain cells became less organised, giving showers for a time before further more continuous rain fell later that afternoon, between 1500 GMT and 1800 GMT. The afternoon rainfall did not reach the peak intensities of the morning, the maximum rate registered by rain gauges being a little less than

90mmhr^{-1}, but by this time the speed of the storm system had slowed, the rain field was of greater extent and rainfall rates were on average higher. A rapid succession of heavy rain cells was evident in VPR imagery of the event (Figure 6.5) and both this and the high reflectivities recorded up to heights of 8km suggested that convective elements were embedded in the frontal system.

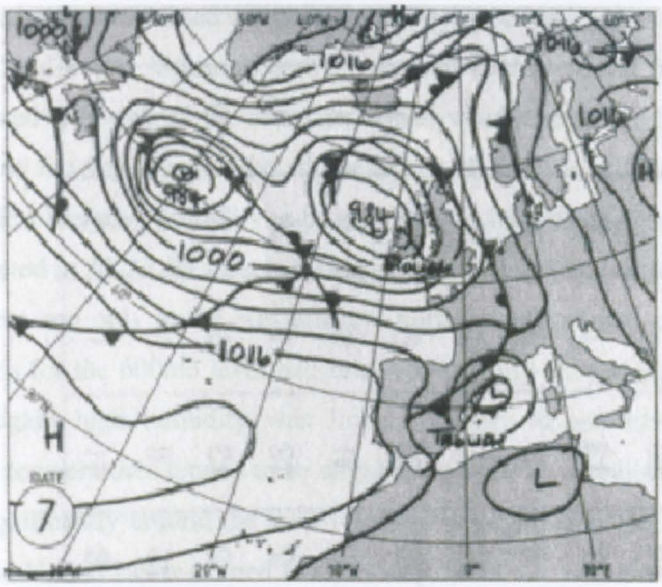

Figure 6.4: *Synoptic conditions at 1200 GMT on the 7th September 1998 (Eden, 1998a).*

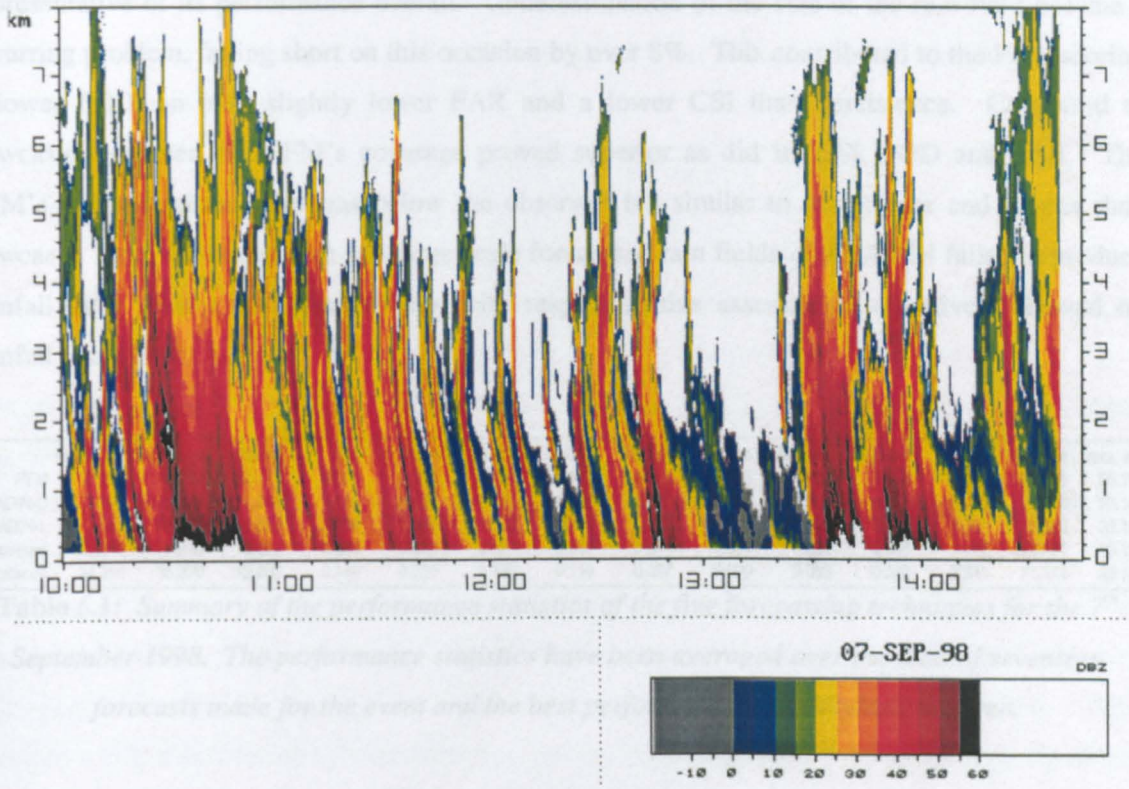

Figure 6.5: *The VPR image of radar reflectivity (dBZ) for the period between 1000 GMT and 1500 GMT (time in hours on the horizontal axis) on the 7th September 1998.*

Throughout the storm, surface winds at Vernet and Vallon Dol were, as recorded by the weather stations, northeasterlies reaching maximum speeds of $7ms^{-1}$. Comparable speeds were attained in ALADIN forecasts but the wind direction varied from that observed, southeasterlies being predicted for Marseille for much of the event though northeasterlies were expected towards the event's end. ALADIN had winds shearing to the right with height so at 600mb they were southwesterly in direction and remained that way for the entire event, and as such directly opposed surface winds in the final hours. Storm system movement, as determined from consecutive radar images, was not aligned with any of the aforementioned wind directions, the storm approaching from the northwest and moving towards the southeast. Both the Vernet and Vallon Dol weather stations showed low-level relative humidity to be consistently high throughout the event, 80-100%, but this was not reflected in ALADIN forecasts that gave 80% humidity at 1000mb only in the last few hours of the event and only at the western and northern boundaries of the PFM's domain. ALADIN's predictions for the 600mb level had relative humidity exceeding 90% only from 1300 GMT onward and again high humidity was limited mainly to western and northern areas. ALADIN's low-level temperatures tended to be slightly higher than actual measurements and were forecasted to cool significantly around the time rain finally began to clear, whereas temperatures recorded at Vernet and Vallon Dol remained fairly steady.

The PFM's performance on this day, the statistics for which are displayed in Table 6.1, was fairly representative of its performance overall. Underestimation of the size of the rain field became a recurring problem, falling short on this occasion by over 8%. This contributed to the PFM scoring a lower POD, an only slightly lower FAR and a lower CSI than persistence. Compared to nowcasts, however, the PFM's coverage proved superior as did its CSI, POD and FAR. The PFM's average rainfall rate was below the observed but similar to persistence and greater than nowcasts. Both the convective and large scale forecasted rain fields of ALADIN failed to produce rainfall rates greater than $4mmhr^{-1}$ so, with respect to this assessment, effectively showed no rainfall at all.

	%cov_for	%cov_act	RMSE	CSI	POD	FAR	cc1km	cc4km	cc9km	cc16km	cc25km	ccNN	rate_for	rate_act
PFM	27.000	35.270	12.117	0.320	0.396	0.485	0.109	0.099	0.094	0.093	0.096	0.251	21.382	23.158
ALADIN-C	0.000	35.270	14.894	0.000	0.000	1.000	0.000	0.000	0.000	0.000	0.000	0.000	0.000	23.158
ALADIN-L	0.000	35.270	14.894	0.000	0.000	1.000	0.000	0.000	0.000	0.000	0.000	0.000	0.000	23.158
nowcast	23.049	35.270	13.627	0.236	0.333	0.521	0.064	0.074	0.081	0.087	0.094	0.178	20.360	23.158
persistence	34.899	35.270	12.985	0.340	0.506	0.489	0.110	0.097	0.090	0.088	0.092	0.241	21.942	23.158

Table 6.1: *Summary of the performance statistics of the five forecasting techniques for the 7th September 1998. The performance statistics have been averaged over the total of seventeen forecasts made for the event and the best performance is highlighted in green.*

The PFM produced the lowest RMSE of all methods, though notably the PFM, persistence and particularly nowcasts gave RMSE values not considerably different to those of ALADIN's "dry"

forecasts. The RMSEs of all methods were very much higher than those produced for any of the events used in the UK case study but are associated with the greater average rainfall rates achieved and sustained during this storm compared to the UK examples.

Persistence provided the best correlation coefficient at $1km^2$ closely followed by the PFM, with the latter having the better correlations at all other spatial scales and also for nearest neighbour. Discrepancies between observed and forecasted surface wind fields could have contributed to the PFM's lack of precision compared to persistence, possibly causing the PFM to generate orographic updraft's in areas offset from where they were actually occurring (albeit probably weak). The issue of accuracy in NWP model wind fields was not, but perhaps should have been, raised in the previous chapter when discussing reasons for displacement of the PFM's orographic forcing from that observed.

ALADIN's lack of high relative humidity at 600mb in the early stages of the storm, and its later confinement mainly to western and northern fringes of the assessment grid while the storm progressed southeastward, left little possibility of the PFM anticipating storm growth. Instead the PFM appeared more adept at achieving appropriate decreases in both storm coverage and rainfall rate, such as from hours 10 through to 13 (1600-1900GMT) shown in Figure 6.6. A lot of that success can be attributed to its reasonable skill, exhibited throughout the event, at selecting the more favourable of the advection scheme options, an example of which is shown in Figure 6.7 whereby the selection of a non-zero velocity vector for hour 12 (1800 GMT) produced a better forecast than that of persistence.

6.2.2.2 11th September 1998

The duration of this event was the shortest of all those included in the case study, with most of the rainfall concentrated within a three hour period extending from 0800 to 1100 GMT. The map of synoptic conditions, valid for midday on the 11th (Figure 6.8), suggested passage of a cold front was primarily responsible for the rain that occurred. This seemed consistent with the decline in temperatures observed at the two experiment sites for a time after rainfall commenced. Consistent too was the wide spacing of the isobars on the synoptic map, suggestive of light winds, and the gentle easterlies recorded by the two weather stations during the period of rainfall. These winds reached a maximum speed of $5ms^{-1}$ before falling lighter and swinging around to become northwesterlies after the rain passed. The ALADIN wind fields similarly showed very light, variable winds over Marseille, wind directions in the initial stages varying from southerly off the coast of Marseille to southeasterly and easterly over land. The observed change to northwesterly winds, mentioned above, ALADIN predicted to occur during the time of rainfall rather than

afterwards as recorded by the weather stations. The ALADIN windfield changed again later (approximately 1300 GMT) becoming westerly and then southwesterly while the representation of winds at higher levels featured only southwesterlies for the duration of the event. Relative humidity at Vernet and Vallon Dol throughout the day was high, ranging between 90% and 100% but it was not until 1200 GMT, after the heaviest rainfall, that ALADIN's forecasts showed relative humidity of equivalent percentages at 1000mb within the PFM domain. At the 600mb level, ALADIN had 90% relative humidity existing prior to midday but restricted it mainly to eastern areas of the domain where the rain was not, for the most part, likewise located.

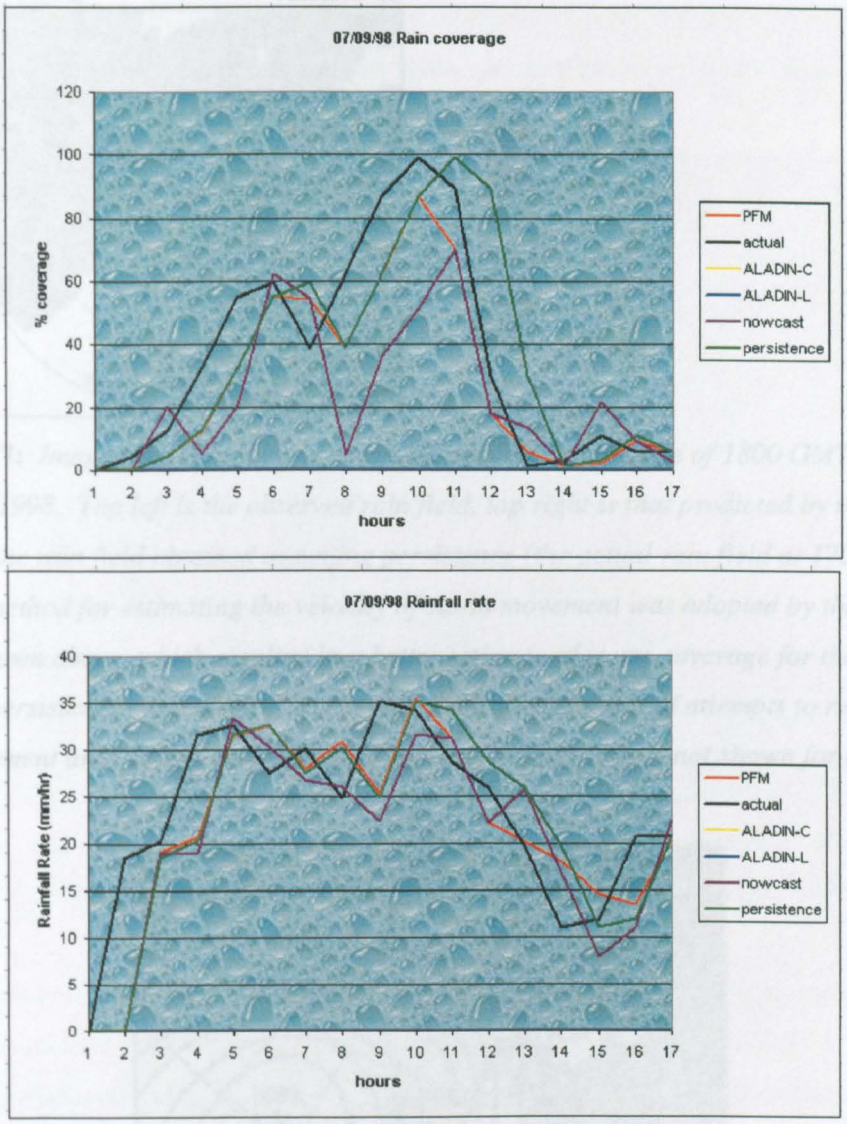

Figure 6.6: *Observed and forecasted percentage rainfall coverage (top) and average rainfall rate (bottom) for the 7th September 1998. The graphs relate to a lead-time of one hour. "Hours" on the horizontal axis refers to the number of hours (or the number of the forecast) since the event began.*

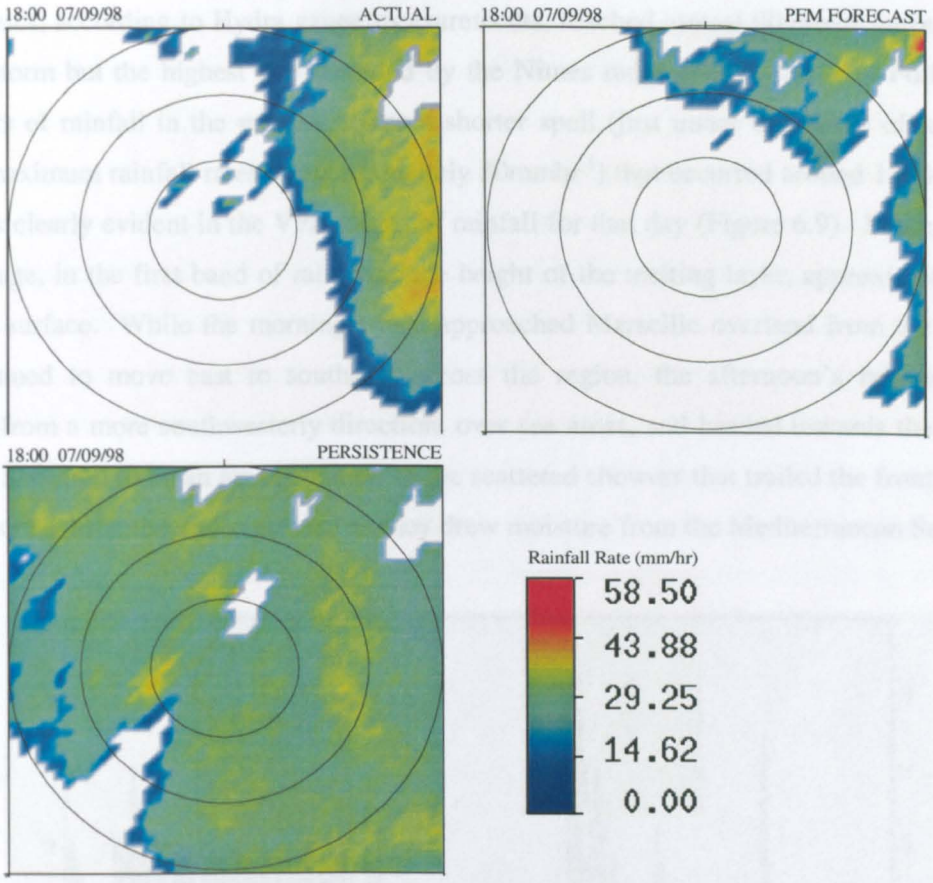

Figure 6.7: *Images of observed and predicted rainfall for the time of 1800 GMT on the 7th September 1998. Top left is the observed rain field, top right is that predicted by the PFM and below left is the rain field obtained assuming persistence (the actual rain field at 1700). The cross correlation method for estimating the velocity of storm movement was adopted by the PFM for the forecast shown above, which resulted in a better estimate of storm coverage for that hour than achieved by persistence. The "holes" in the rain field are the result of attempts to remove from the assessment area cells contaminated by clutter. Topography is not shown for clarity.*

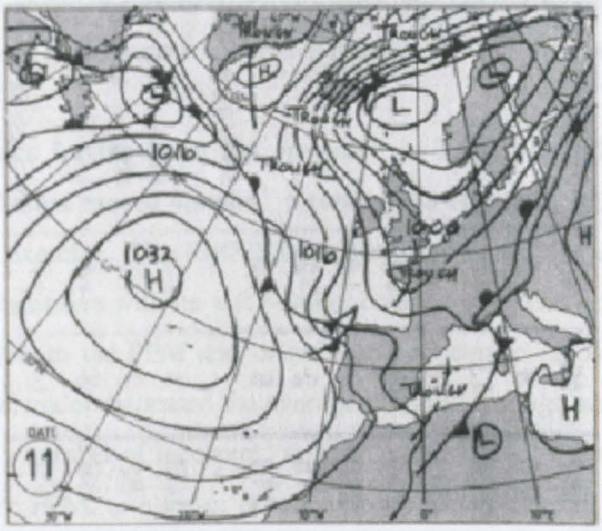

Figure 6.8: *Synoptic conditions at 1200 GMT for the 11th September 1998 (Eden, 1998a).*

Rainfall rates, according to Hydra gauge measurements, reached almost 90mm/hr during the mid-morning storm but the highest rate recorded by the Nîmes radar was 58 $mmhr^{-1}$. Following the three hours of rainfall in the morning came a shorter spell (just under one hour) of less intense rainfall (maximum rainfall rates of approximately $30mmhr^{-1}$) that occurred around 1300 GMT and which was clearly evident in the VPR image of rainfall for that day (Figure 6.9). Discernible also in that image, in the first band of rain, was the height of the melting layer, approximately 3.5km above the surface. While the morning's rain approached Marseille overland from the northwest and continued to move east to southeast across the region, the afternoon's rain approached Marseille from a more southwesterly direction, over sea areas, and headed towards the northeast. The latter appeared to be an amalgamation of the scattered showers that trailed the front but which became more substantial and organised as they drew moisture from the Mediterranean Sea.

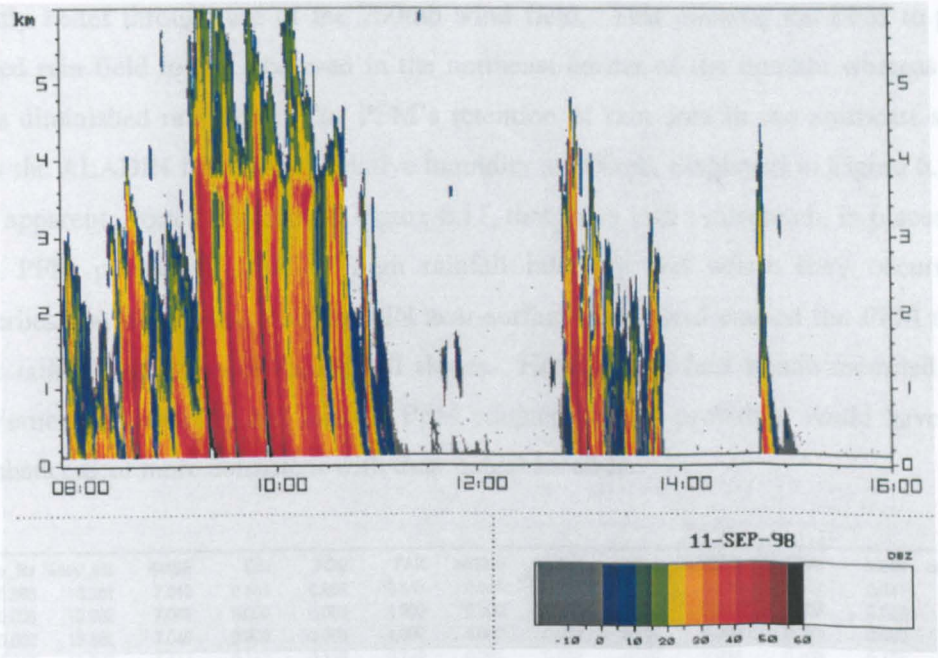

Figure 6.9: *The VPR image of radar reflectivity (dBZ) for the period between 0800 and 1600 GMT (time in hours on the horizontal axis) on the 11th September 1998.*

The performance statistics for the event are presented in Table 6.2. Once again rainfall rates predicted by ALADIN did not exceed $4mmhr^{-1}$, resulting in a failure by ALADIN to produce a rain field for the assessment exercise. The RMSE associated with predicting dry weather was, on this occasion, even more competitive with its wet weather counterparts than it had been in the previous event, proving comparable to the PFM and better than persistence. Nowcasts provided the best RMSE but, on the whole, under-estimated the average rainfall coverage and ended with an average rainfall rate lowered by a number of incorrect "no rain" predictions. The two latter characteristics were also common to the PFM, to a lesser extent with respect to rainfall rate but comparable for rainfall coverage, the latter equating to a very sizeable 50% reduction in the extent of the observed

rain field. Most of this difference accrued when the storm first appeared in the domain, with the increase in rain cells missed by all methods, as is evident in Figure 6.10. In contrast, the PFM and nowcasts fairly successfully predicted the magnitude of the storm's subsequent displacement out of the domain at hour 8, whereas the persistence method did not, causing it to over-predict rainfall for that hour. The over-prediction was sufficient to compensate for its earlier failure to match the initial increase in storm size, thereby allowing the event-averaged rainfall coverage of persistence to appear comparatively good. However, inaccuracies in the individual forecasts were reflected in the other performance statistics and resulted in the PFM, rather than persistence, producing the best CSI, FAR and correlation coefficients at all scales (including nearest neighbour) out of all the forecast methods being assessed. This was partly achieved through the PFM's judicious selection of advection options, particularly at hour 8. Figure 6.11 shows the various forecasts made for that hour and it can be seen that both nowcasts and the PFM emulated storm movement well, but the PFM slightly better through use of the 700mb wind field. This allowed the PFM to produce a similar sized rain field to that observed in the northeast corner of the domain whereas nowcasts produced a diminished rain field. The PFM's retention of rain area in the northeast sector was assisted by the ALADIN forecasts of relative humidity at 600mb, displayed in Figure 6.11, at that time. It is apparent, from the images in Figure 6.11, that there was a mismatch, in places, between where the PFM positioned areas of high rainfall intensity and where they occurred. The northwesterlies that dominated the ALADIN near-surface wind field caused the PFM to produce orographic rainfall on northwest-facing hill slopes. However, surface winds recorded at Vallon Dol and Vernet were easterly and had the PFM adopted them it probably would have produced areas of enhancement more consistent with their actual location.

	%cov_for	%cov_act	RMSE	CSI	POD	FAR	cc1km	cc4km	cc9km	cc16km	cc25km	ccNN	rate_for	rate_act
PFM	6.888	13.862	7.049	0.184	0.284	0.583	0.098	0.114	0.128	0.134	0.151	0.247	16.623	19.291
ALADIN-C	0.000	13.862	7.049	0.000	0.000	1.000	0.000	0.000	0.000	0.000	0.000	0.000	0.000	19.291
ALADIN-L	0.000	13.862	7.049	0.000	0.000	1.000	0.000	0.000	0.000	0.000	0.000	0.000	0.000	19.291
nowcast	6.359	13.862	6.444	0.113	0.136	0.742	0.062	0.082	0.087	0.096	0.109	0.152	13.443	19.291
persistence	12.736	13.862	8.817	0.159	0.371	0.622	0.059	0.074	0.088	0.096	0.113	0.195	18.332	19.291

Table 6.2: *Summary of the performance statistics of the five forecasting techniques for the 11th September 1998. The performance statistics have been averaged over the total of twelve forecasts made for the event and the best performance is highlighted in green.*

6.2.2.3 30th September 1998

The period of rainfall on the 30th of September constituted the last event for that month, being a month that had just five days of rain but the rainfall over those five days totalling an impressive 206mm, approximately 440% of the average for September (Eden, 1998a). Synoptic conditions for this particular event (Figure 6.12) were dominated by an area of low pressure that on the 29th was centred south of Ireland and west of France but by midday on the 30th had intensified and inched its

way northeast to a position over south-west England. An occluded front associated with the depression brought wet weather to Marseille, the rain beginning as a few stray showers before midnight on the 29th September, continuing as isolated showers until approximately 0200 GMT the next day but thereafter the showers becoming more frequent and closely followed by an organised band of rain moving eastward across the region. Most of the rain had cleared by 0600 GMT with only scattered showers remaining until another smaller band of rain passed over Marseille between 0900 GMT and 1200 GMT and a second between 1400 GMT and 1500 GMT. The last of these the Nîmes radar presented as a thin line of cells giving only light rain, while VPR imagery (Figure 6.13) suggested the rain never reached the ground. At the end of the event, 1800 GMT, a cluster of more intense rain cells skirted the northern periphery of the PFM's domain. The rain gauges located at Vernet and Vallon Dol recorded peak rainfall rates for the event of approximately 70mmhr^{-1} and 78mmhr^{-1} respectively while the Nîmes radar in comparison showed a maximum of 54mmhr^{-1}.

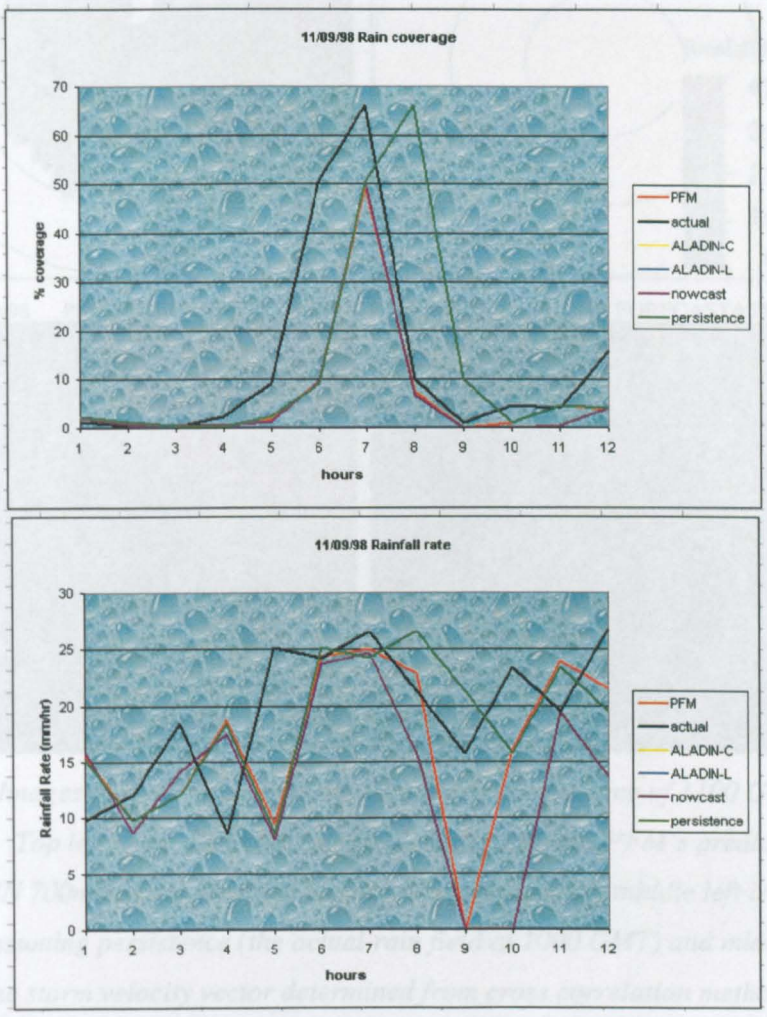

Figure 6.10: *Observed and forecasted percentage rainfall coverage (top) and average rainfall rate (bottom) for the 11th September 1998. The graphs relate to a lead-time of one hour. "Hours" on the horizontal axis refer to the number of hours (or the number of the forecast) since the event began.*

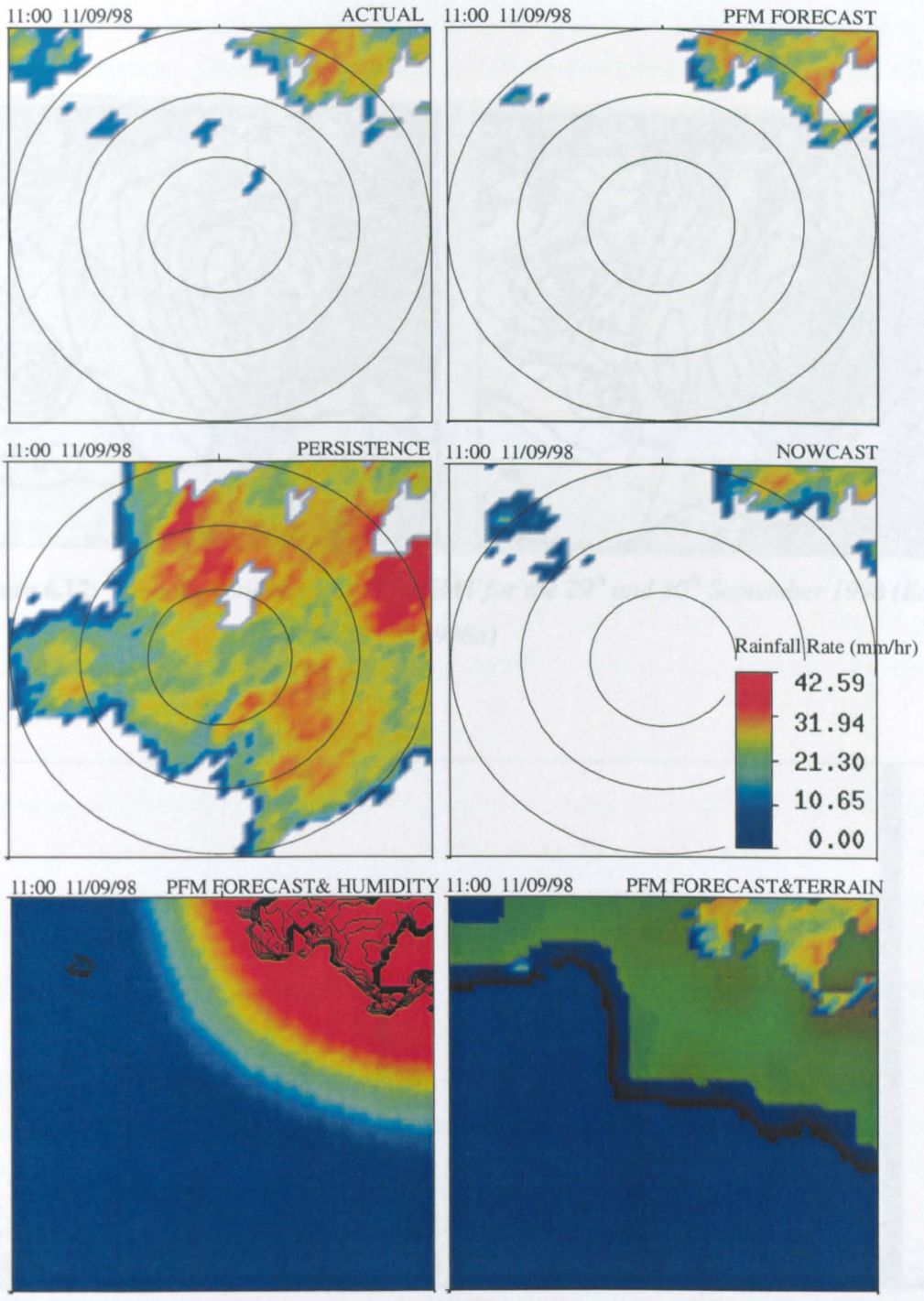

Figure 6.11: *Images of observed and predicted rainfall for the time of 1100 GMT on the 11th September 1998. Top left is the observed rain field, top right is the PFM's predicted rain field for which ALADIN 700mb winds provided the storm velocity vector, middle left is the rain field obtained by assuming persistence (the actual rain field at 1000 GMT) and middle right is the nowcast with the storm velocity vector determined from cross correlation methods. Bottom left shows the same PFM forecast as above (this time using black contours at intervals of 4mmhr^{-1}) superimposed on the 600mb relative humidity field forecasted by ALADIN, all areas with >90% humidity are coloured red. Bottom right has the PFM forecast for 1100 GMT displayed over the topography of the assessment grid, showing enhanced rainfall values on northwest-facing slopes.*

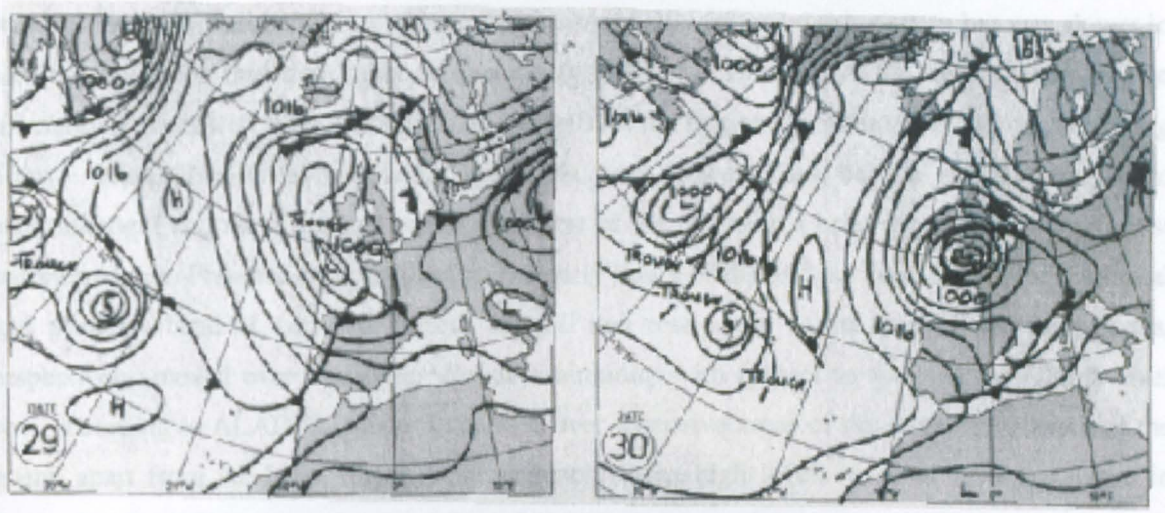

Figure 6.12: *Synoptic conditions at 1200 GMT for the 29th and 30th September 1998 (Eden, 1998a)*

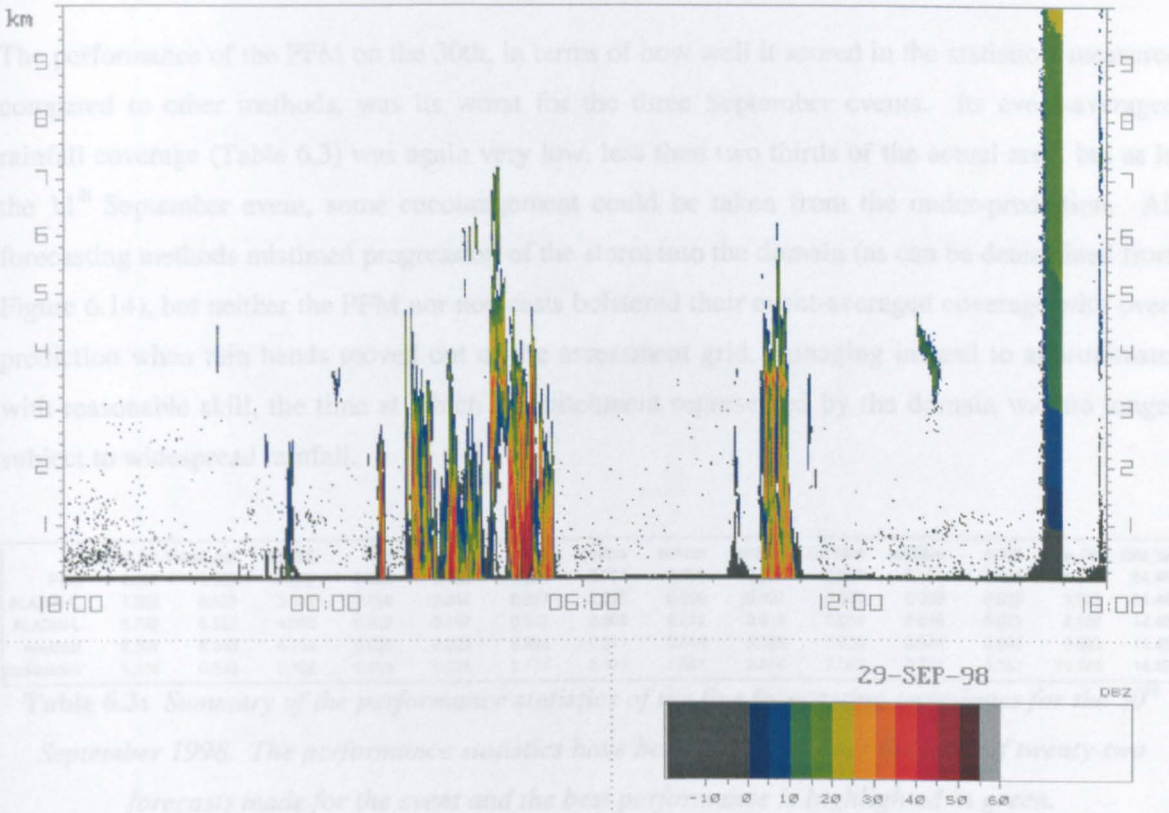

Figure 6.13: *The VPR image of radar reflectivity (dBZ) for the 24 hour period between 1800 GMT (time in hours on the horizontal axis) on the 29th September and 1800 GMT on the 30th September.*

The two weather stations and ALADIN all similarly had low-level winds initially coming from a southeasterly direction. Observations showed that these winds began turning at 0600 GMT and were by 0900 GMT directed from the northwest. ALADIN followed this pattern but was slower in settling the winds into their final northwesterly position. Both ALADIN and weather station measurements showed surface winds to be strongest at the beginning of the event but not exceeding $10ms^{-1}$. ALADIN's upper-level winds began the event as westerlies, became southwesterly soon after midnight and remained that way for the rest of the day with a brief increase in strength just before midday. Pressure dropped through the early hours of the 30th but recovered after the initial and principle band of rain had passed, but fell and rose again as the second and third bands, respectively, moved over Marseille. Relative humidity with respect to water at the 600mb level was, according to ALADIN, greater than 90% over extensive areas of the domain for much of the event, apart from the latter stages. Unfortunately these high levels were of little assistance in improving the PFM's identification of rainfall areas because the requisite high levels of relative humidity with respect to ice, needed in conjunction with water for the PFM to delineate potential rain cells, were limited to the northern areas of the PFM domain and lay outside the area of the inner assessment grid.

The performance of the PFM on the 30th, in terms of how well it scored in the statistical measures compared to other methods, was its worst for the three September events. Its event-averaged rainfall coverage (Table 6.3) was again very low, less than two thirds of the actual area, but as in the 11th September event, some encouragement could be taken from the under-prediction. All forecasting methods mistimed progression of the storm into the domain (as can be determined from Figure 6.14), but neither the PFM nor nowcasts bolstered their event-averaged coverage with over-prediction when rain bands moved out of the assessment grid, managing instead to approximate, with reasonable skill, the time at which the catchment represented by the domain was no longer subject to widespread rainfall.

	%cov_for	%cov_act	RMSE	CSI	POD	FAR	cc1km	cc4km	cc9km	cc16km	cc25km	ccNN	rate_for	rate_act
PFM	4.007	6.553	4.850	0.056	0.123	0.804	0.054	0.052	0.060	0.059	0.074	0.121	14.768	14.487
ALADIN-C	1.503	6.553	3.823	0.016	0.044	0.957	0.005	0.006	0.007	0.008	0.009	0.010	1.091	14.487
ALADIN-L	5.732	6.553	4.022	0.032	0.167	0.932	0.009	0.012	0.013	0.014	0.016	0.012	2.122	14.487
nowcast	2.301	6.553	4.154	0.025	0.029	0.895	0.011	0.016	0.021	0.030	0.044	0.042	9.883	14.487
persistence	6.324	6.553	5.402	0.089	0.228	0.771	0.065	0.068	0.074	0.067	0.071	0.163	14.264	14.487

Table 6.3: *Summary of the performance statistics of the five forecasting techniques for the 30th September 1998. The performance statistics have been averaged over the total of twenty-two forecasts made for the event and the best performance is highlighted in green.*

Unlike the two earlier September events the PFM's event-averaged rainfall rate was greater than the observed. Contributing to this was an erroneously high average rainfall rate produced by the PFM for the very first forecast, when in fact there was no rainfall at all. The rainfall predicted by

the PFM for that hour appeared to stem from anomalous propagation present in the previous hour, which the PFM appropriately reduced in size but mistakenly magnified in intensity. ALADIN, for the first time, registered in the assessment both convective and large-scale rain fields with the rainfall coverage of the latter giving a reasonable approximation to that observed. The rainfall rates predicted by both ALADIN-C and ALADIN-L for each hour were typically 4-5mmhr^{-1} (Figure 6.14) but when averaged over the twenty-two forecasts of the event the rate decreased because of the many "no rain" predictions made by both. Nowcasts produced a lower than expected event-averaged rainfall rate for the same reason.

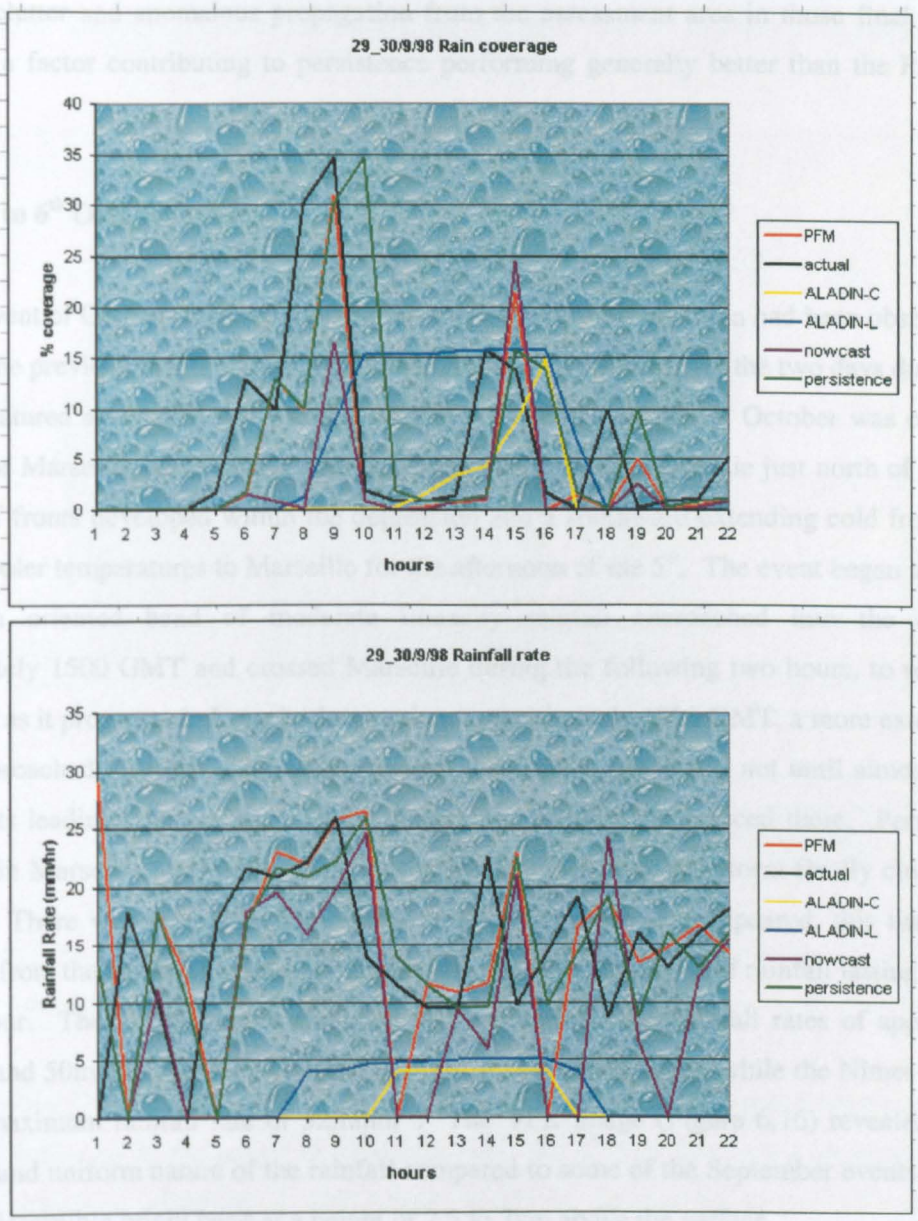

Figure 6.14: *Observed and forecasted percentage rainfall coverage (top) and average rainfall rate (bottom) for the 29th to the 30th September 1998. The graphs relate to a lead-time of one hour. "Hours" on the horizontal axis refer to the number of hours (or the number of the forecast) since the event began.*

Although the PFM achieved a lower RMSE than persistence, it exceeded the RMSE of all other forecast methods. Its CSI was second highest behind persistence, its POD fell below both persistence and ALADIN-L and even its FAR was second to persistence despite the PFM having the lower average rainfall coverage. It was unsurprising then that most of its correlation coefficients were below persistence (but higher than all other forecast methods), including nearest neighbour but excluding 25km^2 for which the PFM scored the highest overall. However, it should be noted that it was not until the final hours of the event, from hour 17 onwards, that the correlations of persistence tended to be better than those of the PFM, a period during which there were few rain cells remaining in the domain. It appeared that a failure to completely eliminate persistent clutter and anomalous propagation from the assessment area in those final hours may have been a factor contributing to persistence performing generally better than the PFM in this event.

6.2.2.4 5th to 6th October 1998

The first event of October featured more in the way of persistent rain than had been observed in the storms of the previous month. The synoptic conditions (Figure 6.15) for the two days during which rain fell featured an area of low-pressure that at 1200 GMT on the 5th October was centred just southeast of Marseille but 24 hours later had progressed northwards to lie just north of the region. A series of fronts developed within the depression and a southward-extending cold front brought rain and cooler temperatures to Marseille for the afternoon of the 5th. The event began when a thin north-south oriented band of moderate intensity rainfall encroached into the domain at approximately 1500 GMT and crossed Marseille during the following two hours, to some extent dissipating as it progressed. Later in the evening, approximately 1900 GMT, a more extensive area of rain approached from the southwest corner of the domain but it was not until almost one hour later that its leading edge lay over Marseille city and rainfall commenced there. Persistent rain continued in Marseille until 0200 GMT on the 6th, at which time the storm finally cleared to the northeast. There was a brief respite of one hour before more rain appeared, this time tracking northward from the southeast corner of the domain and with the period of rainfall lasting little more than an hour. The Hydra gauges stationed at Vernet gave peak rainfall rates of approximately 80mmhr^{-1} and 50mmhr^{-1} for the two latter periods of rain respectively, while the Nîmes radar gave an event maximum rainfall rate of 52mmhr^{-1}. The VPR image (Figure 6.16) revealed the more consistent and uniform nature of the rainfall compared to some of the September events, as well as an easily discernible bright band at a height of 2.5 to 3km above the surface.

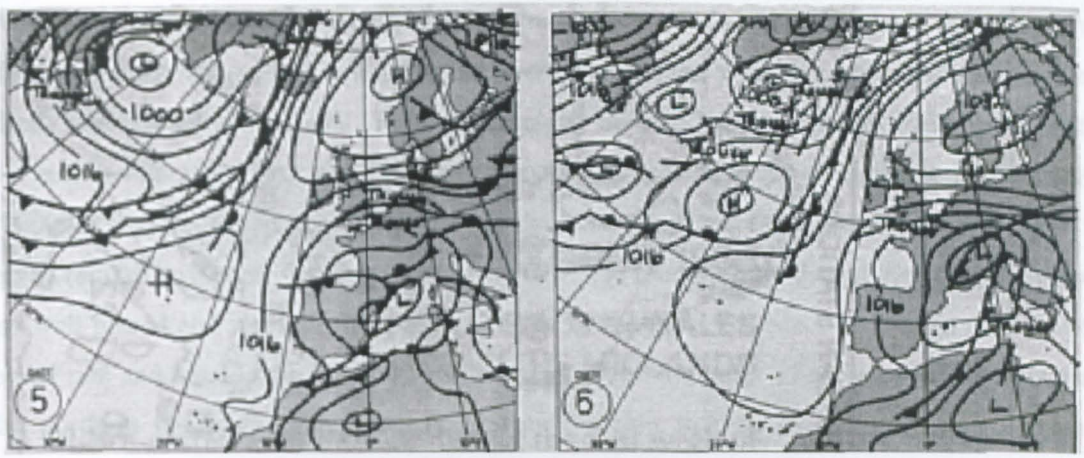

Figure 6.15: *Synoptic conditions at 1200 GMT for the 5th and 6th October 1998 (Eden, 1998b)*

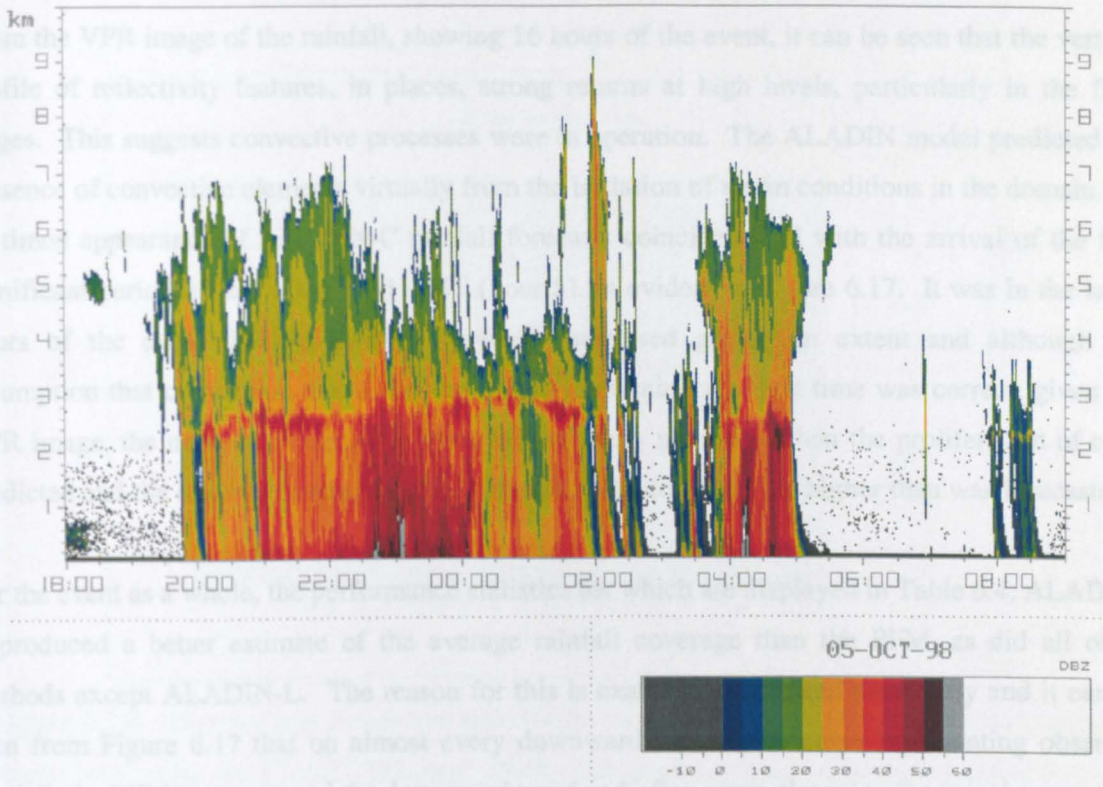

Figure 6.16: *The VPR image of radar reflectivity (dBZ) for the period between 1800 GMT (time in hours on the horizontal axis) on the 5th October 1998 to 0900 GMT on the 6th October 1998.*

Both the Vallon Dol and Vernet weather stations recorded southerly to southwesterly surface wind directions leading up to the period of persistent rain. ALADIN's forecasted 1000mb winds were similar in direction although a little more southerly to southeasterly. Weather station measurements indicated winds then changed to easterlies during the rainfall but ALADIN instead gave consistent and strong southeast winds. After the rain had passed (although at Vernet it was during the rainfall) winds became markedly variable, a characteristic predicted reasonably well by

ALADIN. In contrast to the changeability of the surface winds, ALADIN kept the 600mb wind field southwesterly for the full duration of the storm though, for a time, turned winds slightly more southerly and strengthened them. Relative humidity at both the Vernet and Vallon Dol stations varied between 85-100% and ALADIN appropriately forecasted areas of high relative humidity at the 1000mb level and had them positioned such that they corresponded reasonably well with observed rainfall coverage. Its forecasted areas of >90% relative humidity at the 600mb level were not so well placed and were, during passage of the first minor rain band, located to the east of the observed rain and outside the inner assessment grid of the domain. These areas were then pushed to the northern boundary of the domain during the rain that followed until they disappeared altogether for the last half of the event and thus provided no assistance to the PFM in terms of guiding the spatial dynamics of its forecasted rainfields.

From the VPR image of the rainfall, showing 16 hours of the event, it can be seen that the vertical profile of reflectivity features, in places, strong returns at high levels, particularly in the final stages. This suggests convective processes were in operation. The ALADIN model predicted the presence of convective elements virtually from the initiation of storm conditions in the domain and its timed appearance of ALADIN-C rainfall forecasts coincided well with the arrival of the first significant period of rain after 1900 GMT (hour 5), as evident in Figure 6.17. It was in the latter hours of the event that ALADIN-C forecasts increased greatly in extent and although the assumption that convection was to become more predominant at that time was correct, given the VPR image, the number of rain cells observed was very much less than the proliferation of cells predicted and the observed average rainfall intensity was considerably higher than was forecasted.

For the event as a whole, the performance statistics for which are displayed in Table 6.4, ALADIN-C produced a better estimate of the average rainfall coverage than the PFM, as did all other methods except ALADIN-L. The reason for this is exactly as discussed previously and it can be seen from Figure 6.17 that on almost every downward turn of the curve representing observed rainfall, the PFM best captured the downward trend and often came closest to the actual percentage coverage. The PFM's average rainfall rate was only marginally lower than the observed average rainfall rate and was only very narrowly beaten by persistence in providing the closest estimate. The PFM had the lowest RMSE of all methods and the lowest FAR but its limited rainfall coverage meant its POD was lower than both persistence and ALADIN-C (the latter having perfect scores for POD in the final hours of the storm due to a large over-prediction of rain area) and it also contributed to dragging the PFM's CSI below that of persistence. The PFM's event-averaged correlation coefficients were encouragingly superior to all other methods at all scales.

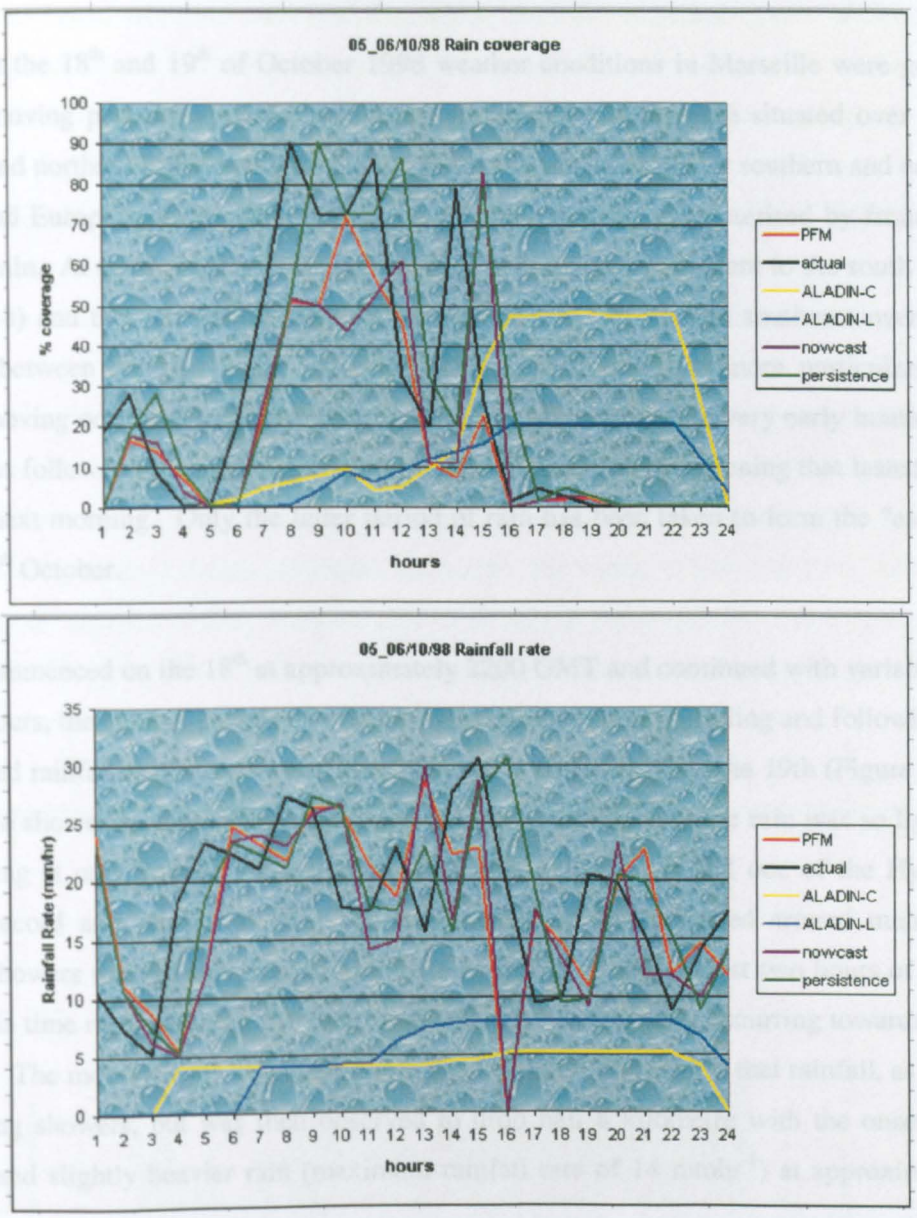

Figure 6.17: *Observed and forecasted percentage rainfall coverage (top) and average rainfall rate (bottom) for the 5th and 6th October 1998. The graphs relate to a lead-time of one hour. "Hours" on the horizontal axis refers to the number of hours (or the number of the forecast) since the event began.*

	%cov_for	%cov_act	RMSE	CSI	POD	FAR	cc1km	cc4km	cc9km	cc16km	cc25km	ccNN	rate_for	rate_act
PFM	16.083	25.858	7.910	0.225	0.299	0.546	0.087	0.129	0.142	0.159	0.121	0.240	17.555	17.845
ALADIN-C	19.153	25.858	9.168	0.072	0.373	0.744	0.043	0.047	0.048	0.049	0.051	0.046	3.690	17.845
ALADIN-L	9.663	25.858	9.287	0.055	0.130	0.742	0.026	0.029	0.031	0.033	0.034	0.031	4.776	17.845
nowcast	18.253	25.858	8.436	0.169	0.236	0.669	0.034	0.040	0.048	0.052	0.054	0.109	16.478	17.845
persistence	25.857	25.858	9.303	0.229	0.417	0.605	0.069	0.083	0.079	0.077	0.073	0.220	18.094	17.845

Table 6.4: *Summary of the performance statistics of the five forecasting techniques for the 5th and 6th October 1998. The performance statistics have been averaged over the total of twenty-four forecasts made for the event and the best performance is highlighted in green.*

6.2.2.5 18th to 19th October 1998

Throughout the 18th and 19th of October 1998 weather conditions in Marseille were governed by two slow-moving pressure systems, one being an area of low pressure situated over the United Kingdom and northern Europe and the other a high pressure system over southern and eastern parts of Spain and Europe, with the zone where their boundaries met characterised by frontal activity, cloud and rain. At midday on the 18th, a secondary depression was evident to the south of England (Figure 6.18) and through the course of a 24 hour period this tracked southeast over Marseille, squeezing between the two larger systems. These conditions, and more particularly a north-eastward moving occluded front, brought light rain to Marseille in the very early hours of the 18th and this was followed by a more significant period of rain in the late evening that lasted until 0600 GMT the next morning. Only the latter period of rain has been taken to form the "event" of the 18th and 19th October.

Rainfall commenced on the 18th at approximately 2200 GMT and continued with variable intensity for eight hours, the general pattern of which was intermittent rain preceding and following a period of prolonged rainfall that, over Vernet, briefly eased at 0130 GMT on the 19th (Figure 6.19). The first notable shower on the VPR image lasted half an hour, however the rain was so light, rainfall rates peaking at only 2mmhr^{-1}, that a number of local rain gauges and one of the Hydra gauges failed to record any rainfall at all. The next period of rain occurred around midnight when scattered showers merged and crossed Marseille en masse to give almost two hours of continuous rainfall, this time rates reaching 11mmhr^{-1} and with the heaviest falls occurring towards the end of the period. The melting layer was identifiable at a height of 3km during that rainfall, as it had been in preceding showers, but was then observed to drop half a kilometre with the onset of further extensive and slightly heavier rain (maximum rainfall rate of 14 mmhr^{-1}) at approximately 0145 GMT.

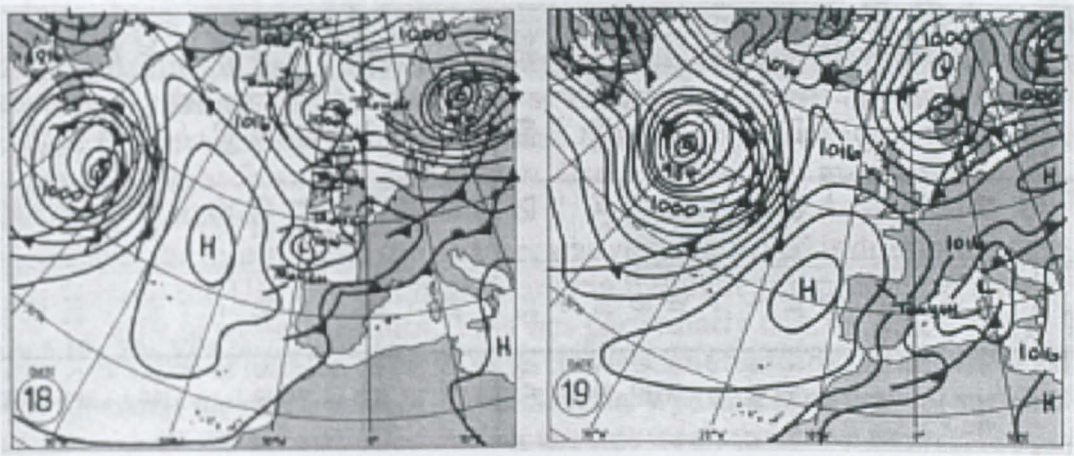

Figure 6.18: *Synoptic conditions at 1200 GMT for the 18th and 19th October 1998 (Eden, 1998b).*

Atmospheric pressure had remained fairly steady prior to the event but began dropping as the first period of rain began and then continued decreasing until the cessation of rain, a trend consistent with the movement of the secondary depression southeast over Marseille. Weather station measurements showed winds to be light and changeable leading up to the onset of rain but which, once the rain began, turned more northerly and veered between northeasterly and northwesterly directions. Wind speed increased in the initial stages of the last period of rain (0145 GMT onward) but did not rise above $3ms^{-1}$ and dropped away completely after 0430 GMT. ALADIN's wind fields for the Marseille area were similarly oriented and of comparable speed and exhibited considerable sheer with height, winds at the level of 600mb being directed from the southwest throughout the event until the final few hours when they turned westerly to northwesterly. Low-level relative humidity, as recorded by the weather stations, was high leading up to and for the duration of the event, ranging between 90 to 100%. ALADIN, in contrast, did not display high relative humidity at low levels (1000mb) until after the event, while at 600mb, >90% relative humidity (with respect to water) was confined to an area in the northwest corner of the domain up until 0300 GMT on the 19th, at which time the area grew in extent to encompass the whole domain and did not diminish in size until a few hours later.

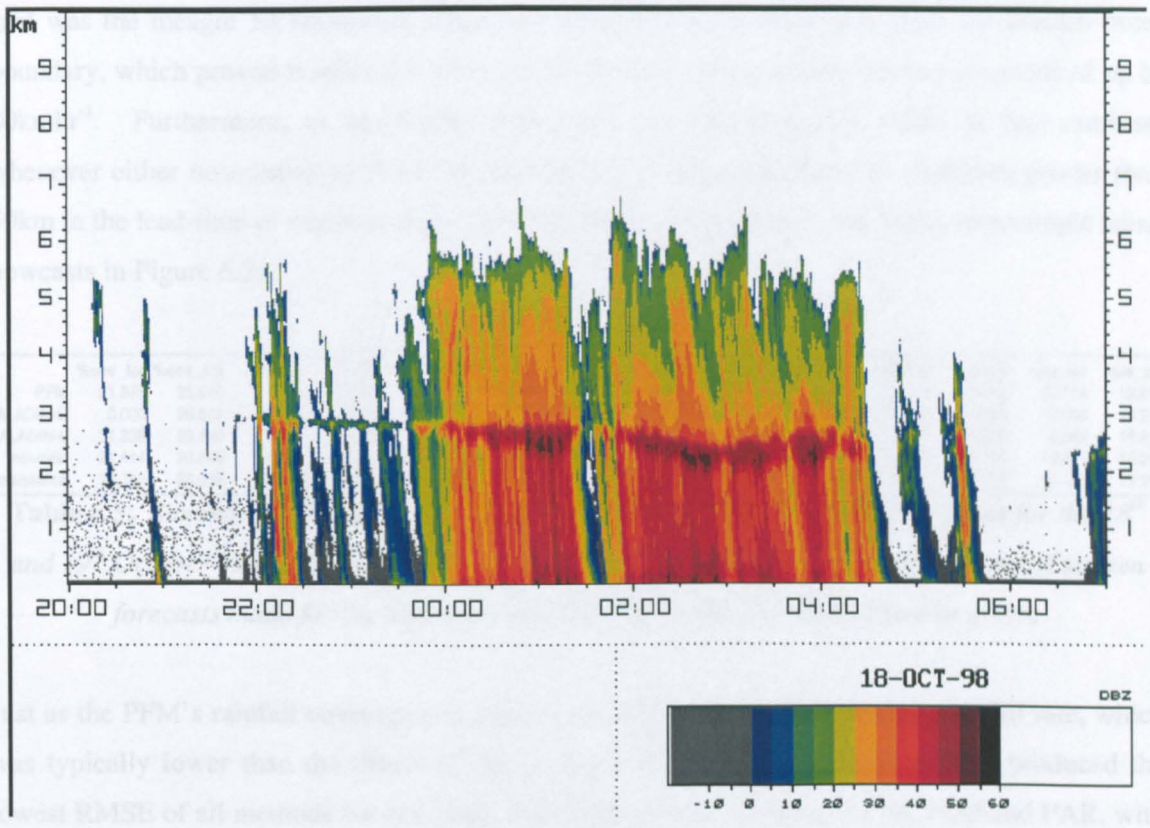

Figure 6.19: *The VPR image of radar reflectivity (dBZ) for the period between 2000 GMT (time in hours on the horizontal axis) on the 18th October 1998 and 0700 GMT on the 19th October 1998.*

The performance statistics of the PFM and other forecasting methods for the event of the 18th and 19th October 1998 are presented in Table 6.5. Both the PFM and nowcasts introduced a sizeable reduction in average rainfall coverage and once again it was for the same reasons mentioned previously. The PFM's estimate of coverage was very similar to but slightly higher than nowcasts, which elevated it to second best behind persistence. ALADIN-C did not contribute a rain field to the assessment while ALADIN-L had excess rainfall coverage which was mainly due, as can be seen in Figure 6.20, to its predictions of 100% coverage when the storm had passed and dissipated. The intervals between periods of rain, as described above in the overview of the event, are not clearly evident in the fairly smooth curve of actual rainfall coverage shown in Figure 6.20 but the curves of both nowcasts and the PFM exhibited a dip at hour 6, being the time of 0200 GMT on the 19th, close to when there was a brief lull in rain over Marseille. Notably, hour 5 (0100 GMT) corresponded to the only time in the whole Marseille case study that the PFM (in this instance using 700mb winds) and nowcasts managed to predict advection of the storm into the inner assessment grid of the domain. Displayed in Figure 6.21 are their respective forecasts, as well as the observed rain field and the persistence forecast. In hindsight the size of the PFM domain should have been larger to better accommodate fast moving storm systems. Part of the reason why the PFM and nowcasting failed to more frequently predict movement of storms into the assessment grid was the meagre 50 kilometres separating the edge of the inner grid from the domain outer boundary, which proved insufficient when storms used in the case study moved at speeds of up to 80kmhr^{-1}. Furthermore, as no attempt was made to extrapolate rain fields in this exercise, whenever either nowcasting or the PFM attempted to translate storms over distances greater than 50km in the lead-time of one hour they inevitably presented truncated rain fields, an example being nowcasts in Figure 6.21.

	%cov_for	%cov_act	RMSE	CSI	POD	FAR	cc1km	cc4km	cc9km	cc16km	cc25km	ccNN	rate_for	rate_act
PFM	21.875	26.642	7.711	0.233	0.342	0.647	0.085	0.079	0.071	0.059	0.059	0.210	18.114	19.219
ALADIN-C	0.000	26.642	9.144	0.000	0.000	1.000	0.000	0.000	0.000	0.000	0.000	0.000	0.000	19.219
ALADIN-L	31.339	26.642	11.793	0.001	0.254	0.999	0.000	0.000	0.000	0.000	0.001	0.000	2.880	19.219
nowcast	21.414	26.642	7.745	0.217	0.294	0.662	0.045	0.057	0.065	0.072	0.084	0.154	18.071	19.219
persistence	26.783	26.642	9.263	0.268	0.447	0.634	0.080	0.062	0.051	0.040	0.040	0.236	19.485	19.219

Table 6.5: *Summary of the performance statistics of the five forecasting techniques for the 18th and 19th October 1998. The performance statistics have been averaged over the total of sixteen forecasts made for the event and the best performance is highlighted in green.*

Just as the PFM's rainfall coverage was underestimated so too was its average rainfall rate, which was typically lower than the observed but second only to persistence. The PFM produced the lowest RMSE of all methods but could not match persistence in terms of CSI, POD and FAR, with its value for FAR in particular hindered by an over-prediction of rainfall at the end of the event, an over-prediction that was in the same vein but not of the same magnitude as that of ALADIN-L. The PFM's excess coverage was related to extensive areas of high relative humidity having been

predicted by ALADIN for the event's final hours combined with a vertical wind profile that exhibited predominantly upward motion. The PFM's correlation coefficients at all spatial averages exceeded all other methods but in this case excluding nearest neighbour.

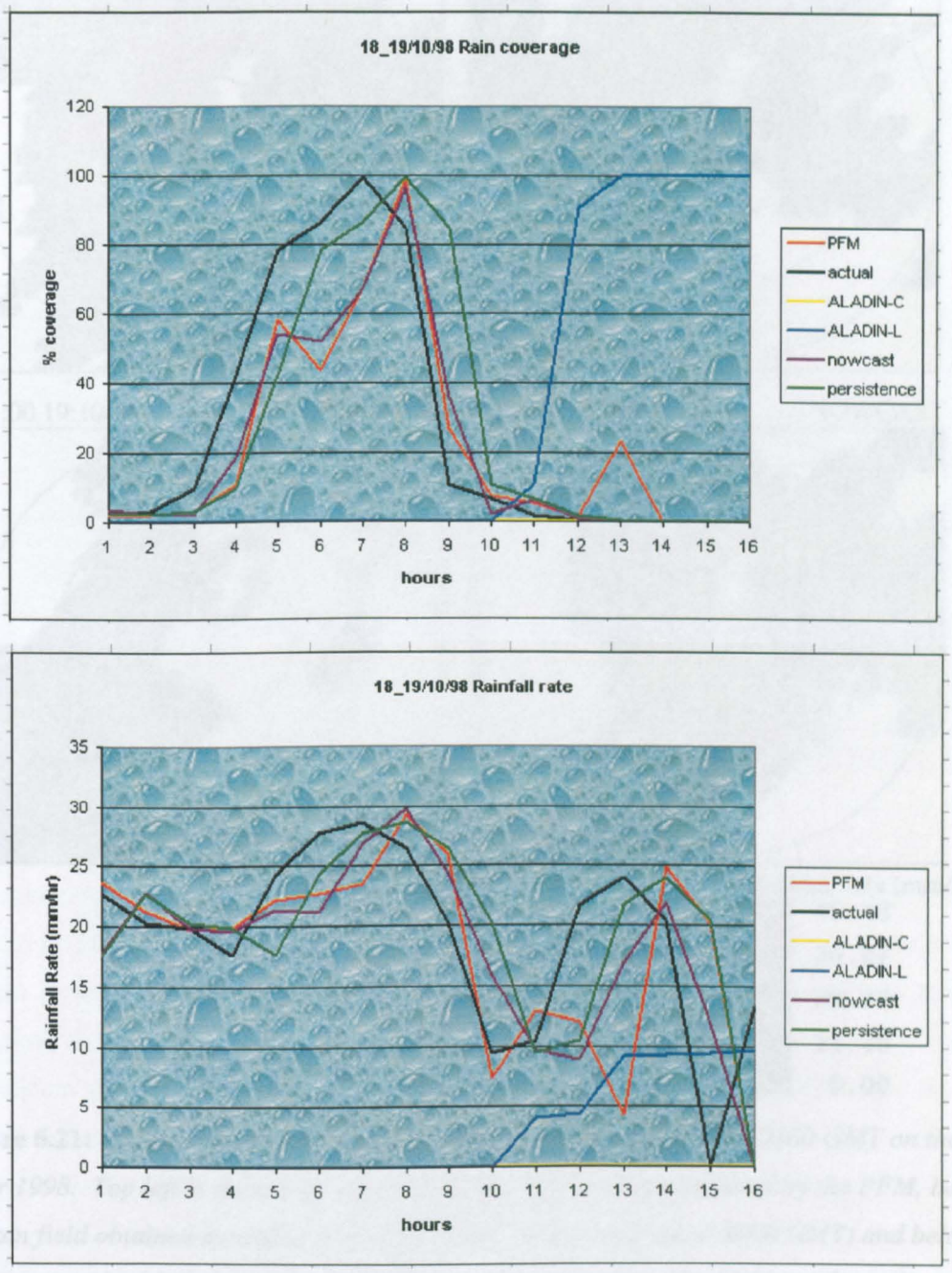

Figure 6.20: *Observed and forecasted percentage rainfall coverage (top) and average rainfall rate (bottom) for the 18th and 19th October 1998. The graphs relate to a lead-time of one hour. "Hours" on the horizontal axis refers to the number of hours (or the number of the forecast) since the event began.*

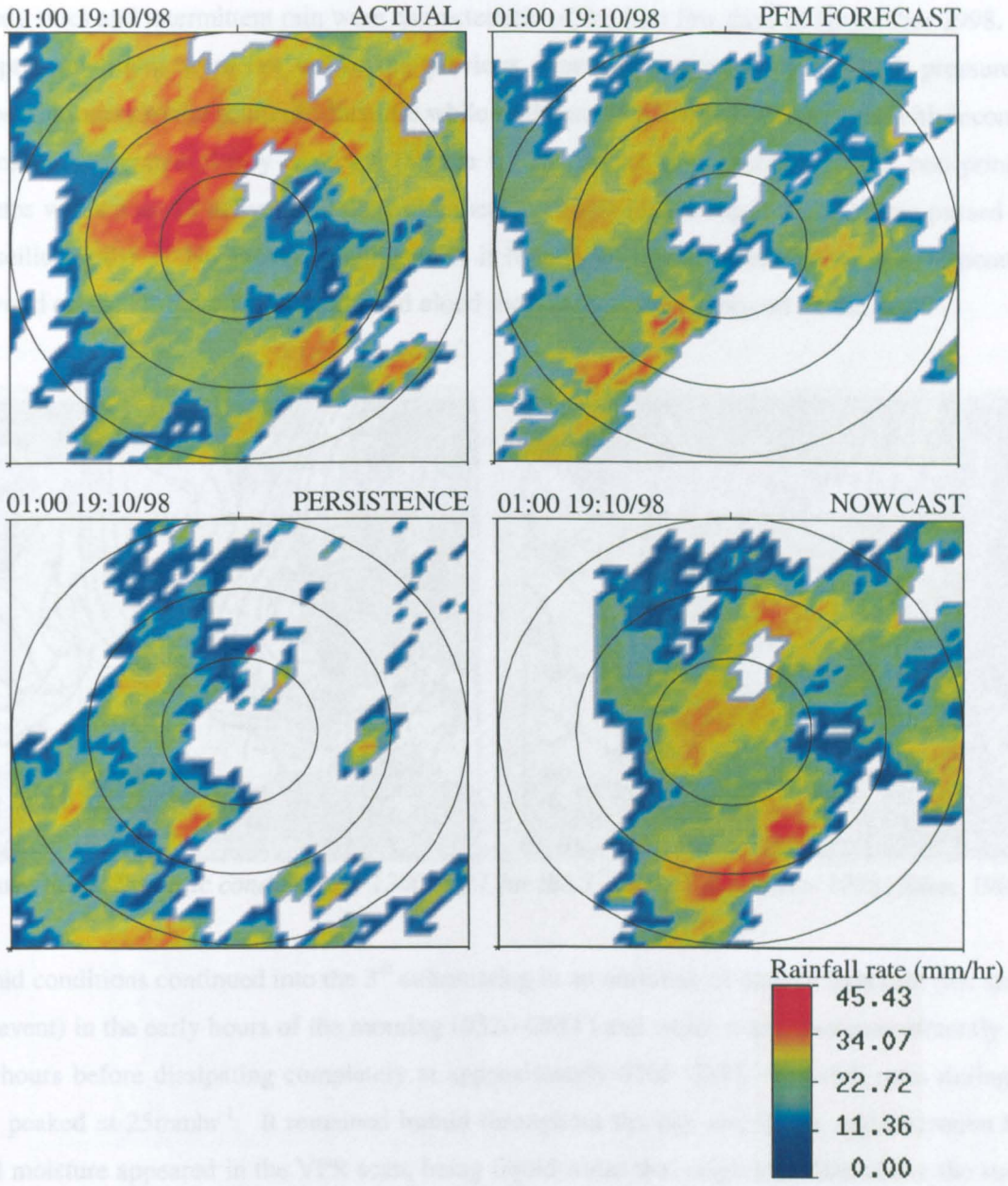

Figure 6.21: *Images of observed and predicted rainfall for the time of 0100 GMT on the 19th October 1998. Top left is the observed rain field, top right is that predicted by the PFM, below left is the rain field obtained assuming persistence (the actual rain field at 0000 GMT) and below right is the nowcast. In this instance the 700mb wind field was used by the PFM to advect the rain field while the nowcast employed the cross correlation method to determine the vector of storm velocity. Both attain reasonable approximation of storm movement but neither capture growth in the rain field in terms of both intensity and extent.*

6.2.2.6 3rd to 4th November 1998

Cloudy skies and intermittent rain were characteristic of the first few days of November 1998. The synoptic conditions were not unlike the previous event, whereby an area of high pressure lay almost stationary to the south of Marseille while to the north a low pressure system with secondary depressions migrated slowly eastward (Figure 6.22). Along the boundary of the two principal systems was a zone of active frontal development. A front emanating from that zone passed over Marseille on the 1st November bringing with it light rain. Clear skies and cooler temperatures followed on the 2nd but with humidity and cloud increasing towards the end of the day.

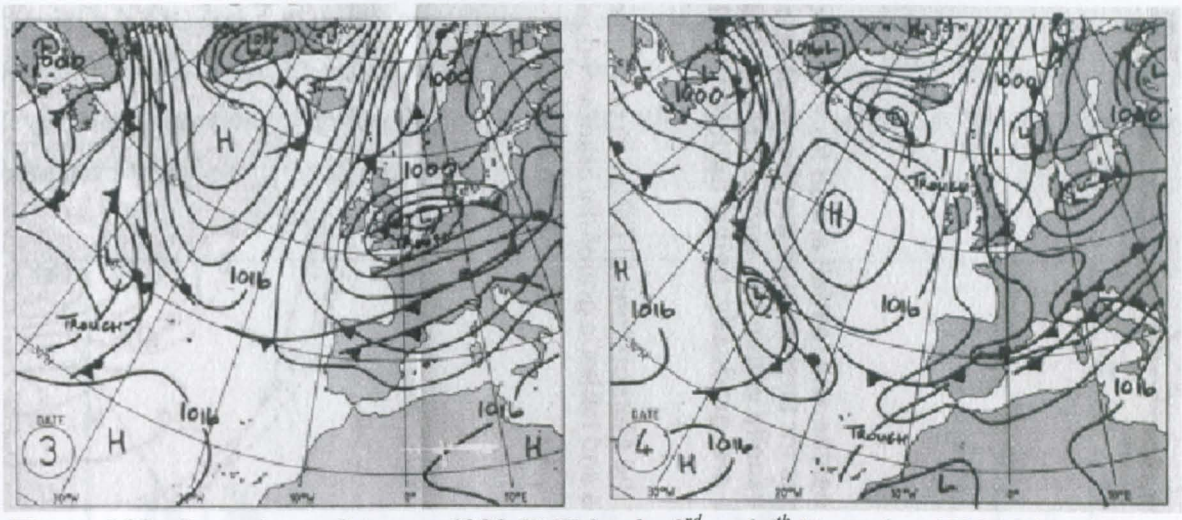

Figure 6.22: *Synoptic conditions at 1200 GMT for the 3rd and 4th November 1998 (Eden, 1998c).*

Humid conditions continued into the 3rd culminating in an outbreak of mainly light rain (the start of this event) in the early hours of the morning (0320 GMT) and which continued intermittently for a few hours before dissipating completely at approximately 0700 GMT. Rainfall rates during this time peaked at 25mmhr^{-1}. It remained humid throughout the day and in the mid-afternoon high-level moisture appeared in the VPR scan, being liquid water that originated 4km above the surface and which descended down to a level of 1.5km but did not result in surface rain (Figure 6.23). The Nîmes radar showed a band of rainfall over Marseille at the corresponding time, one that seemingly produced rainfall rates similar to those observed in the early morning rain. A period of more substantial rainfall occurred in the late evening of the 3rd, commencing just before 2300 GMT and lasting until 0240 GMT on the 4th, this time registering as surface rain in all instruments. The showers during that time were widespread over the region but at certain locales, namely Vernet, the rain was intermittent and of variable intensity. Further rain was still to come later that morning, mainly between the hours of 0600 GMT and 0700 GMT but with the odd scattered shower preceding and following the primary rain band. The Hydra gauges recorded a maximum rainfall rate of 45mmhr^{-1} for the entire event with a similar rate recorded by the Nîmes radar.

Surface winds were light throughout the 3rd and the morning of the 4th and were for the most part variable, although favouring a northeasterly direction during the very first period of rain and a northwesterly direction at the very end, the latter in contrast to ALADIN which predicted mainly southerly winds for the final hours. ALADIN's winds at 600mb began the event westerly but were quickly turned and established as southwesterlies, a direction from which most of the rain approached Marseille. The weather stations recorded high relative humidity throughout the 3rd and into the 4th, but ALADIN's forecasts restricted the times of high relative humidity at low-levels to a four hour period after the morning's rainfall on the 3rd, with the humid areas located in northern and southern sectors of the domain only, and from 0300 GMT onwards on the 4th, this time only in the northeastern corner of the domain. At the 600mb level, ALADIN forecasted >90% relative humidity (with respect to water) over almost the entire domain for the hours between 0600 GMT and 1000 GMT on the 3rd and from 2100 GMT that evening until 0700 GMT on the 4th. Upper-level relative humidity with respect to ice was also high during those periods but not over such expansive areas.

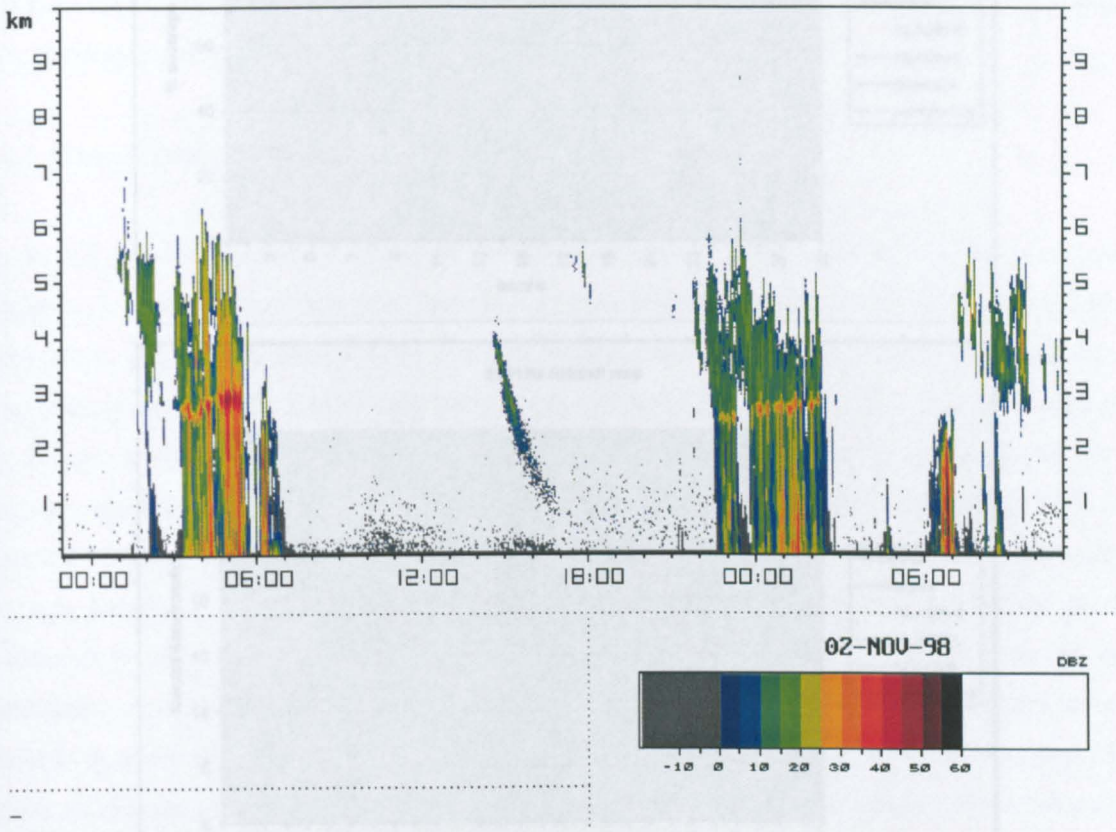

Figure 6.23: *The VPR image of radar reflectivities (dBZ) for the period between 2300 GMT (time in hours on the horizontal axis) on the 2nd November 1998 and 1100 GMT on the 4th November 1998.*

The PFM's performance on this final event of the case study was unfortunately one of its worst, the problem being two occasions of gross over-estimation of rainfall coverage (Figure 6.24), together accruing to an event-averaged rainfall coverage that exceeded the actual area by 200% (Table 6.6). The overestimation arose from a situation whereby ALADIN provided widespread high percentages of relative humidity, in terms of both ice and water, at upper-levels and combined it with positive uplift and instability in those areas. The one consolation was that during the times the PFM predicted extensive rainfall coverage in the absence of observed rain, the rainfall rate was comparable to ALADIN-L, approximately 4mmhr^{-1}, and unlikely, in an operational environment, to be interpreted as a significant flood threat warranting instigation of flood warning procedures.

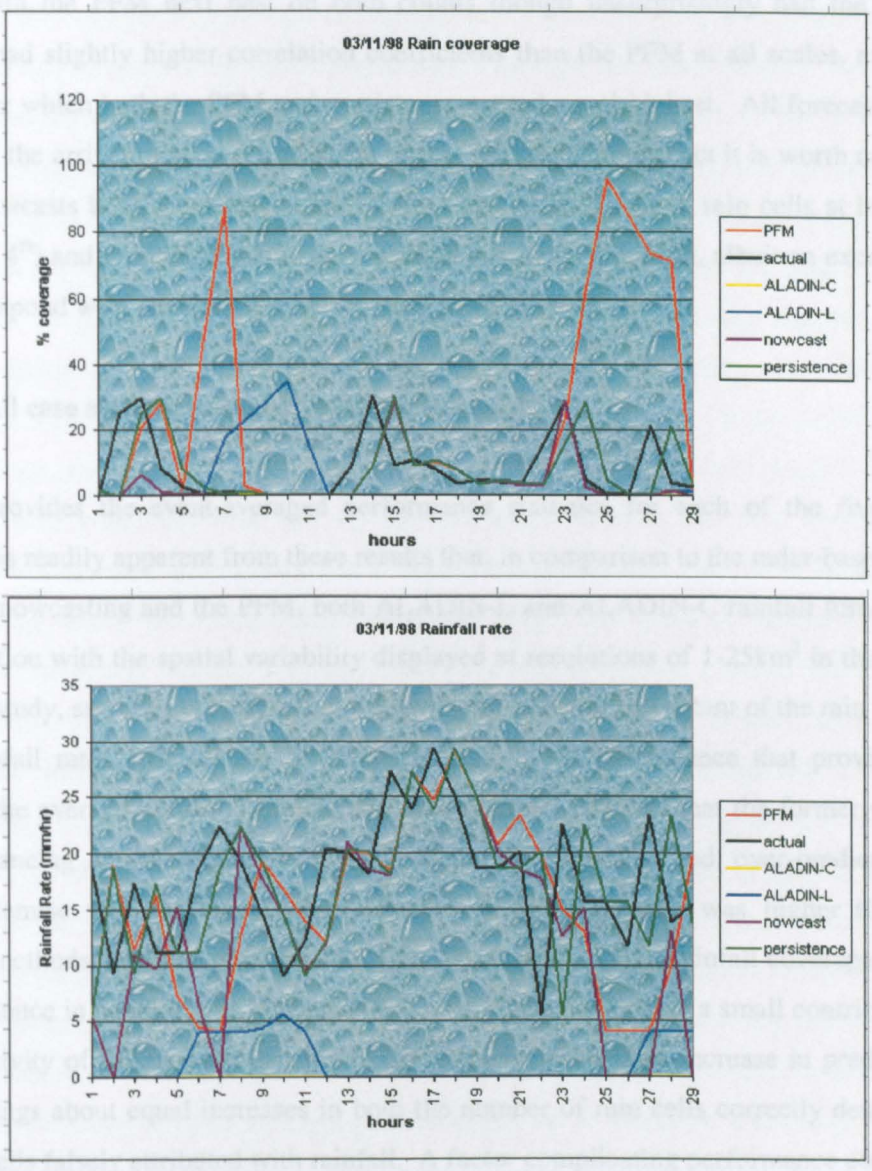

Figure 6.24: *Observed and forecasted percentage rainfall coverage (top) and average rainfall rate (bottom) for the 3rd and 4th November 1998. The graphs relate to a lead-time of one hour. "Hours" on the horizontal axis refers to the number of hours (or the number of the forecast) since the event began.*

	%cov_for	%cov_act	RMSE	CSI	POD	FAR	cc1km	cc4km	cc9km	cc16km	cc25km	ccNN	rate_for	rate_act
PFM	23.574	7.843	5.714	0.171	0.429	0.659	0.146	0.177	0.195	0.205	0.223	0.303	15.232	17.561
ALADIN-C	0.000	7.843	4.593	0.000	0.000	1.000	0.000	0.000	0.000	0.000	0.000	0.000	0.000	17.561
ALADIN-L	4.262	7.843	4.860	0.003	0.148	0.995	0.001	0.002	0.002	0.003	0.004	0.001	1.314	17.561
nowcast	4.301	7.843	4.679	0.120	0.195	0.764	0.096	0.124	0.141	0.148	0.151	0.222	13.258	17.561
persistence	7.818	7.843	5.542	0.177	0.321	0.619	0.149	0.188	0.213	0.223	0.249	0.303	17.219	17.561

Table 6.6: *Summary of the performance statistics of the five forecasting techniques for the 3rd and 4th November 1998. The performance statistics have been averaged over the total of twenty-nine forecasts made for the event and the best performance is highlighted in green.*

The PFM's average rainfall rate for the event was lower than the observed but better than all other forecast methods except persistence. The over-prediction of rainfall coverage and under-prediction of rainfall rate together conspired to give the PFM the highest RMSE. Persistence had the best CSI and FAR with the PFM next best on both counts though unsurprisingly had the better POD. Persistence had slightly higher correlation coefficients than the PFM at all scales, except nearest neighbour for which both the PFM and persistence scored equal highest. All forecasting methods often missed the arrival of showers or bands of rain into the domain, but it is worth noting that the PFM and nowcasts both accurately achieved the observed increase in rain cells at hour 23 (0100 GMT on the 4th) and the PFM was the only method to offer a rain field, albeit an excessively large one, to correspond with the observed rain at hour 27 (0500 GMT).

6.2.3 Overall case study (event-averaged) performance

Table 6.7 provides the event-averaged performance statistics for each of the five forecasting methods. It is readily apparent from these results that, in comparison to the radar-based methods of persistence, nowcasting and the PFM, both ALADIN-L and ALADIN-C rainfall forecasts showed poor correlation with the spatial variability displayed at resolutions of 1-25km^2 in the storms used for the case study, and did not correspond well with the position and extent of the rain fields nor the average rainfall rates. Of all the forecast methods, it was persistence that provided the best estimate of the average rainfall coverage and rainfall rate. The fact that the former was achieved through balancing under-prediction at each storm's instigation and over-prediction at their respective demise was to some extent reflected in a RMSE that was higher than all other forecasting methods, except that of ALADIN-L. Over-prediction of rainfall coverage did however assist persistence in attaining the highest POD and perhaps even made a small contribution to CSI, as the sensitivity of CSI is such that it can still improve even if an increase in predicted rainfall coverage brings about equal increases in both the number of rain cells correctly detected and the number of cells falsely attributed with rainfall. A factor complicating performance assessment was the difficulty in identifying and completely removing clutter and recurrent anomalous propagation from the domain and any failure to do so most likely benefited persistence more than any other forecast method. Given these circumstances, the PFM did well to provide the second best average

rainfall coverage, average rainfall rate, CSI and POD behind persistence. It was bettered (marginally) only by nowcasts with respect to RMSE and encouragingly produced the lowest FAR of all methods and the highest correlation coefficients at all scales, including nearest neighbour.

	%cov_for	%cov_act	RMSE	CSI	POD	FAR	cc1km	cc4km	cc9km	cc16km	cc25km	ccNN	rate_for	rate_act
PFM	16.571	19.338	7.559	0.198	0.312	0.621	0.096	0.108	0.115	0.118	0.121	0.229	17.279	18.594
ALADIN-C	3.443	19.338	8.112	0.015	0.070	0.950	0.008	0.009	0.009	0.010	0.010	0.009	0.797	18.594
ALADIN-L	8.499	19.338	8.651	0.015	0.117	0.945	0.006	0.007	0.008	0.008	0.009	0.007	1.849	18.594
nowcast	12.613	19.338	7.514	0.147	0.204	0.709	0.052	0.065	0.074	0.081	0.089	0.143	15.249	18.594
persistence	19.069	19.338	8.385	0.210	0.382	0.623	0.089	0.095	0.099	0.098	0.106	0.226	18.223	18.594

Table 6.7: *The performance statistics of the five forecasting techniques as averaged over the six events included in the Marseille case study. The best performance is highlighted in green.*

The tendency for the PFM to under-predict rainfall coverage for most of the events did not appear to be as related to orographic downflows as it was in the UK case study, mainly because much of the high ground in the Marseille domain lay towards the northeast corner, an area to which rain was generally heading to rather than approaching from or crossing over and also an area plagued by clutter problems so that a good portion of it was eliminated from the assessment exercise. Possibly the most crucial factor governing successful forecasting within the domain adopted for the case study, because of its overall size as well as the spatial resolution chosen and the speed of the storms, was accuracy in determining storm movement and in this respect the PFM performed comparatively well. This is a valuable attribute because as stated by Collier (1996), in terms of urban hydrology, the velocity of the storm is just as important as the total rainfall accumulation. Hall (1984) also noted the need for its consideration, pointing out that downstream storm movement could enhance peak flows and a storm velocity greater than flow velocity generally resulted in peak runoff rates being considerably less than if the storm was stationary. Berlamont and Willems (1998) advised that for large sewer systems subject to a predominant direction of storm movement, flow forecasting required spatially detailed rain fields whereas those without and of smaller size (less than 20km^2) could get away with use of a uniform rain field. The fact that the PFM often and overall attained the better average correlation coefficients, in addition to providing comparatively good estimation of storm movement, is pertinent in light of the last comment and particularly as the shape of the flood hydrograph from a catchment area is, according to Hall (1984), largely determined by the spatial and temporal distribution of rainfall intensities as well as the characteristics of the catchment. A catchment's response time is not independent of the temporal pattern of storm events, as discovered by Ball (1991), who observed how peaks in rainfall intensity near the start or towards the end of an event led to response times that were typically shorter and longer respectively than if the rainfall was uniform throughout. Furthermore, Einfalt (1991) described how spatial information contained in imprecise quantitative predictions of rainfall intensity can, provided there is some knowledge of error bounds or forecast uncertainty, have qualitative value in the real-time control of urban storm water and flood management systems,

whereby categorisation (high, low, moderate) of rainfall intensity can prove useful, and in particular may be used to assist and protect workers during inspection and maintenance routines.

The Marseille case study was undertaken using lead-times of one hour only, but it should be noted that urban drainage real-time control systems have use for forecasts with lead-times as little as five minutes (Cowpertwait *et al*, 1998), for which the PFM is ideally suited given its five minute time-step (although at such short time scales the simplicity and effectiveness of the persistence approach would typically make it the most favoured option). The key input to the PFM is weather radar data and again, as mentioned in Chapter Four, it must be remembered that the forecasts made by the PFM were adjudged according to how well they matched rainfall rates derived from network radars. It was mentioned in Section 6.1 that one of the objectives of carrying out HIRE was to obtain data to assist researchers in correcting errors made in the estimation of rainfall rates from radar reflectivity and also errors in the measurements themselves. On the basis of the Marseille case study alone this appears a worthy endeavour given the problems experienced with the quality of the Nîmes radar data and also the discrepancies that arose not only between radar and rain gauge detection of rainfall, let alone estimation of rainfall rates, but also between network radar and VPR representation of surface rainfall. Attempts to introduce dynamics into forecasting, such as orographic forcing (either upward or downward motion), may mistakenly be deemed futile if the manifestation of the forcing is imperceptible in the reference rainfall data because of how the measuring instrument is sited and operated and because of errors in both interpreting measurements and estimating rainfall rates from them.

Basing the case study around HIRE proved very useful, with the data collected during the experiment serving to illustrate the differences between NWP predictions of near-surface conditions and the isolated measurements taken directly at the surface, anomalies that through an absence of surface data could not be gauged for the UK case study. Differences in wind fields were specifically and often noted and had implications, as mentioned in reference to Figure 6.11, for the positioning of the PFM's orographic enhancement of rainfall with respect to that observed. High relative humidity at low levels was often lacking in ALADIN forecasts when it was apparent in the measurements of the two weather stations. High relative humidity with respect to both water and ice at the 600mb level was also frequently absent or not coincident with observed rain fields, and so failed to assist the PFM in predicting initiation of rain and changes in the extent of storms. This last point may simply suggest ALADIN's forecasts of humidity for the events were not particularly good but it may also indicate a need to revisit the broad-scale applicability of the signifiers chosen to delineate potential rainfall areas and it may be that for Mediterranean regions (or simply the ALADIN model) the relative humidity threshold values and/or the pressure level from which they are taken need to be lowered, the latter in particular not at odds with observed

geographical variations in the typical vertical extent of rain-producing clouds (as mentioned in Section 3.6.1) and probably appropriate given that Météo France looks to the 850mb relative humidity field when attempting to diagnose deep convection (Conway *et al*, 2001).

The finer horizontal resolution of the PFM's domain, compared to that used for the UK case study, was a contributing factor in the minimal value extracted from the NWP data by the PFM. The difference in the dimensions of grid cells between ALADIN (10km×10km) and the PFM (1km×1km) meant that forecast inaccuracies in just one grid cell of the former affected one hundred cells of the latter. While at times it seemed that ALADIN needed only to extend its >90% relative humidity field a few (of its) grid cells towards the south for it to better match the rain field, the last event provided an example of how it could give rise to extensive over-prediction of rainfall coverage by the PFM. A lack of temporal detail in ALADIN's output also constrained the benefit that could be derived from it. ALADIN's forecasts of meteorological variables were spaced at intervals of three hours, being a time period during which bands of rain were able to pass through the PFM domain and also being a time scale considerably greater than the expected life cycle of convective rain cells. The simple time interpolation employed to produce hourly data from the three hourly forecasts meant that differences in the values of meteorological variables between consecutive forecasts were averaged, and therefore smoothed, over the three hour time interval. This smoothing effect was probably unrepresentative of the speed at which the energies involved in rain production were being created and consumed, a point that has particular relevance with respect to regions along the Mediterranean coastline where the storm events can be quite intense in terms of their development, duration and severity.

6.3 Summary

The HIRE experiment provided, both in terms of its mandate and the data collected, the basis for constructing a rainfall forecasting case study centred on Marseille, France, which served to test the performance of the PFM at spatial resolutions (1km^2) relevant to urban hydrological applications and with storms of greater average and peak rainfall intensities than typically observed in the UK. It is generally accepted that information regarding the spatial and temporal variability of rainfall intensity and the speed and direction of rain field movement provides valuable assistance to urban hydrologists in the prediction and management of municipal storm water, just as knowledge of these storm characteristics is important for flood forecasting on regional scales. Of the forecasting methods included in the performance assessment comparison, the PFM often best represented the spatial variability of the rain field and did so with average rainfall rates comparable to, though with a tendency to be slightly less than, those observed. It also often provided the best representation of

storm movement and would have been more successful in timing the arrival of storms had the domain been larger.

The case study exercise raised questions regarding the usefulness of mesoscale NWP forecast data for urban applications, whereby the scale of inaccuracies can appear magnified due to the spatial and temporal resolutions involved. It was clear that the ALADIN rainfall forecasts were themselves inadequate for the purposes of urban hydrology, scoring poorly in all statistical performance measures compared to the PFM, nowcasts and persistence. Enabled by the array of data collected during the HIRE experiment, it was useful and enlightening to compare locally measured meteorological variables with the NWP predictions of those variables and also to compare network radar estimates of rainfall with other rainfall measurements. It raised awareness of the nature of the input data upon which the PFM was dependent in this exercise and exposed frailties in it.

CHAPTER SEVEN

SUMMARY, CONCLUSIONS AND RECOMMENDATIONS

"A flood only becomes a hazard when it threatens human life or property", a comment made in the introduction to this research. Irrespective of whether or not global warming is upon us, bringing with it the often mooted increase in storminess (BBC, 2000), a continually expanding human population alone increases the likelihood of flood hazards occurring in the future and does so also through its inextricable link to the alteration of flow regimes by anthropogenic modification of the physical environment. In some places the population is not so much growing but ageing (BBC, 2001) and this may increase the toll of flood hazards due to its implication for the mobility of communities as flood waters rise. Any increase in world population is most likely to manifest as the spread and densification of existing urban centres, where infrastructure is already in place and more easily extended to support new inhabitants. The location of many of those metropolitan areas will have been founded upon the availability of water resources, as undoubtedly humans require water for life and the quest to fulfil physical (and sometimes spiritual) needs has driven civilisation to locate by waterways and on the arable land of alluvial floodplains. People now gravitate to the employment opportunities provided by the local economies that have become established through the development of trade and industry, for which proximity to watercourses has been vital because of their role in transportation and manufacturing, the latter in terms of both water abstraction and as receptacles for discharges. As cities grow, demand for housing may force or make tempting the development of land which is either at considerable risk of flooding itself or the urbanisation of which modifies catchment hydrology to the detriment of downstream locations.

Alongside an anticipated increase in world population there is an expected continuation of technological development, development that affects every aspect of people's lives. Technological advances do, according to Liljas (2001), alter the way weather affects society. A desire for "bigger/leaner, better and faster" everything and most of all for the attribute of efficiency can, as those goals are incrementally attained, result in greater vulnerability to weather elements or more critical consequences if weather phenomena cause "essential" items to fail. This makes for an increasingly "weather sensitive society" that demands advanced forecasting and expects it given improvements in meteorological observing systems and computing power. In an age when

culpability is quickly assigned and risk aversion is high, technological advances have been channelled not only into averting hazards by enabling their early identification but also into improving adaptability and responsiveness to perceived hazards. This is not just with respect to events that endanger whole communities but also those that threaten the everyday operations and incomes of various agencies and organisations and the safety of their personnel. As such forecast output has, over the years, adapted to the needs of consumers. Forecasts of rainfall are sought by all manner of people for all manner of reasons and for all manner of timeframes. Heightened responsiveness and an unwillingness to take drastic or disruptive action, unless confirmed as essential, together mean that providing forecasts even at very fine scales, in terms of lead-time and pinpoint location, has both relevance and value (Liljas, 2001).

Scale has been an issue of importance throughout the research presented in the preceding chapters. References have been made to the spatial scales of weather phenomena and of forecast resolution and forecast domain size, the temporal scales of weather phenomena and of forecast lead-time, as well as scales of orography, rainfall intensity, forcing, predictability and forecast accuracy. Figure 7.1 displays a diagram showing the temporal and spatial scales of certain phenomena within the earth climate system. It can be seen from this that there is a relationship between size and longevity. So too is there a relationship between size, longevity and predictability. As lead-times grade from short to long, it is usual for the resolution of forecasting models to grade from fine to coarse (Liljas, 2001) and as both lead-time and model grid size increase only the larger, enduring features are likely to be predicted with any accuracy. Figure 7.2, taken from Liljas (2001), shows the generally accepted labelling of weather forecasting in terms of lead-times. NWP models dominate the last three of the five categories displayed whilst nowcasting has established a niche in the 0-2 hour range. Very Short Range Forecasting (VSRF) is where the line between the two methods lies very blurred, mainly because neither NWP models nor nowcasting techniques provide particularly good forecasts on the temporal and spatial scales involved. This was evident in the results attained, as detailed in Chapter Four, in an exercise undertaken to compare performances of a range of forecasting techniques that included nowcasts and NWP forecasts at lead-times of up to six hours and at spatial resolutions of $25km^2$. Even at a lead-time of two hours the NWP forecasts were better correlated with the observed rain fields and gave the better CSI, but featured over-sized rain fields of very low average rainfall rate.

Although the focus of the presented research was on fine resolution (1-$25km^2$), very short range (1-6 hours) forecasting, there is an obvious need to provide as much warning as possible of potential flood-producing rainfall. Comments to that effect were made when introducing the research and were accompanied with reference to chaos in the atmosphere and the limits it places on predictability, leading to the conclusion that effective flood forecasting needed integration of

various forecast methods to enable staged awareness of flood potential so that the response could be swift when forecast uncertainty diminished closer to initiation of the event. Flood hazard avoidance therefore not only requires skilled rainfall and flow forecasting but also a decision making process structured to produce appropriate action graduated on levels of danger and degrees of uncertainty so as to achieve the right and best possible outcomes. Just as an example, the forecasting of rainfall and weather generally for the 1996 Summer Olympic Games in Atlanta demanded interplay of numerous spatial and temporal scales of forecasting and the approach taken by the meteorological service involved exemplified effective amalgamation of forecast methods and featured the operation of a sequential warning system, the latter specifically tailored to address the needs of competitors, organisers and spectators (Eilts *et al*, 2000).

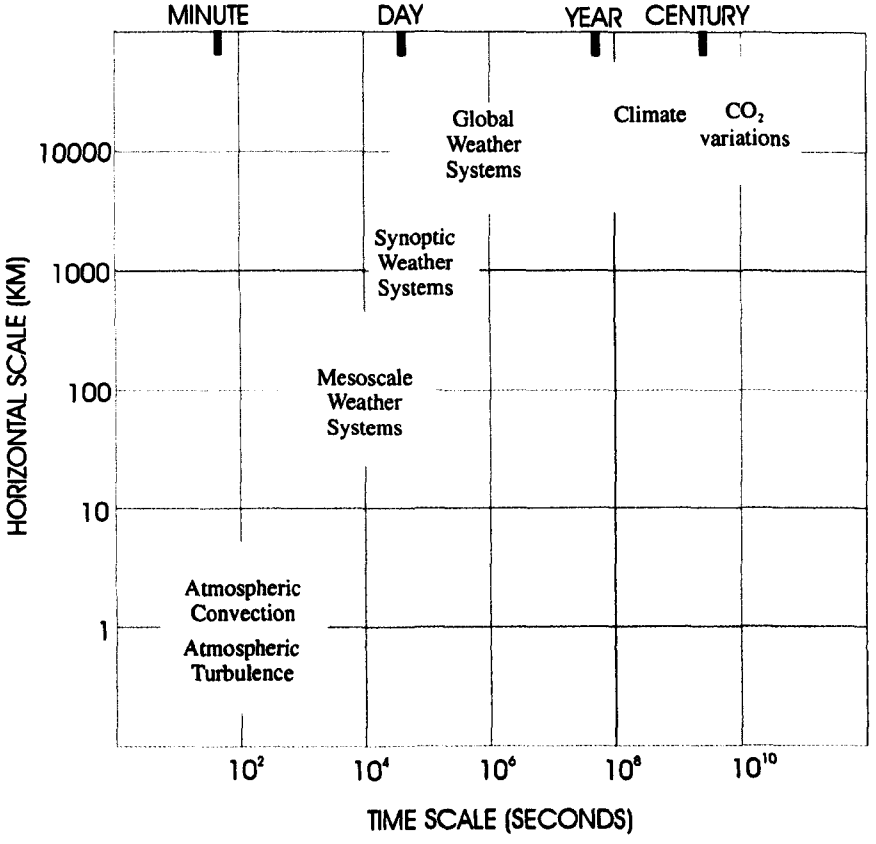

Figure 7.1: *Space and time scales of phenomena of the earth climate system (scales are logarithmic). Adapted from Daley (1991).*

Olympic venues for the various events were located not only in Atlanta but spanned the state of Georgia and also included sites in Miami, Orlando, Birmingham and Washington D.C. With respect to rainfall predictions, venue officials were less interested in specific quantities of rainfall than in the occurrence of any rainfall (or hail) and also the occurrence of rainfall above a threshold value. Three levels of forecasts were produced: watch, warning and statement. A "watch" would be issued if the 12 or 24 hour forecast suggested rainfall or hail might occur and another issued for

potential threshold exceedance. A "warning" would be issued, providing as much lead-time as possible, when it was more certain that the "watched" event would occur at a particular venue. Upon instigating a "warning", "statements" would be issued every 10-15 minutes to provide current information regarding the anticipated start time, end time and severity of the expected rainfall event. The range of forecast products used by the meteorologists graded in spatial and temporal scales from occasional storm/hurricane/tornado alerts issued at a national level, NWP forecasts from a model covering the eastern half of the USA (run twice daily producing forecasts of 3 hour increments), NWP forecasts from a model covering the state of Georgia and surrounding states with a resolution of 8km and a movable nested grid of 2km resolution (run every three hours with forecasts of one hour increments), in addition to more frequently obtained radar, satellite and ground-based sensory observations. As forecast lead-time diminished, interest moved from synoptic scale features affecting the whole country to mesoscale features affecting the more immediate region to smaller scale features affecting a localised area, with a view to how any one of those features would manifest at a specific venue, a virtual pinpoint location. NWP models were utilised to determine "watch" status and any subsequent "warnings" relied mainly on remotely sensed data and fell into two categories: the first being for existing precipitation to pass over the venue, for which nowcasting techniques were employed upon appearance of a rain field; and the second for (convective) rain to develop within the vicinity of the venue, for which both radar and satellite data were used.

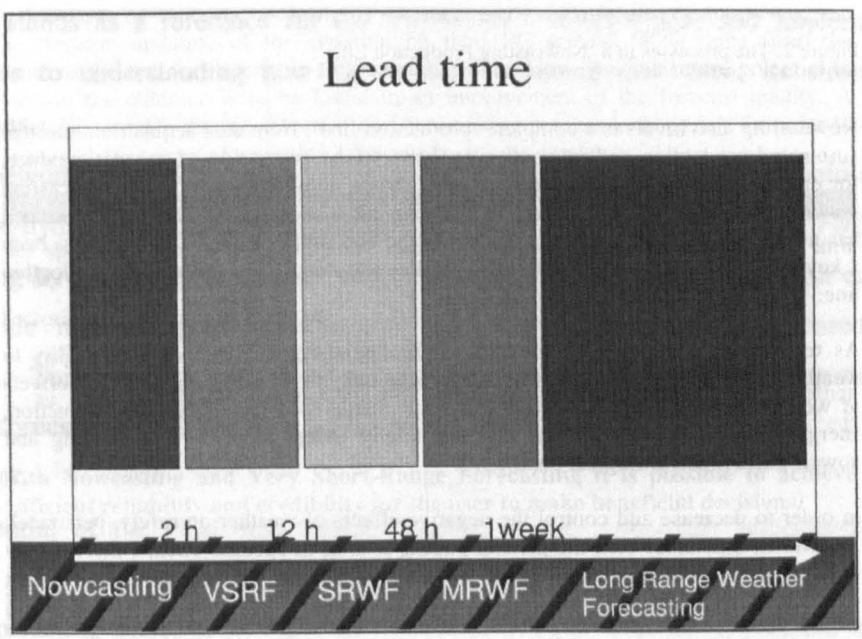

Figure 7.2: *Naming of different forecasts in relation to their lead times (VSRF – Very Short Range Forecasting, SRWF – Short Range Weather Forecasting, MRWF – Medium Range Weather Forecasting.) (Liljas, 2001).*

It is the "warning" stage, from nowcasting to VSRF, that is problematic in terms of the increased level of detail and accuracy required of the rainfall forecast (whether for flood forecasting or for activities such as described above) and in terms of the indeterminate boundaries to when the occurrence of a rainfall event, its duration and quantification of its intensity can be made with any confidence. While in the above example of the Atlanta Olympics a "watch" was flagged at either 24 or 12 hours prior to a possible event occurring (depending on the variable of concern), the stipulated lead-time that had to be provided by a "warning" was simply AMAP – as much as possible. The primary aim of undertaking the work described in the preceding chapters was to determine if improvements could be made in this grey area, mainly with respect to improving upon simple nowcasts themselves and extending their reach into VSRF by drawing into the forecast process mesoscale NWP products that have proved the mainstay of successful SRWF (Short Range Weather Forecasting) on its opposite border.

In the process of working towards that aim, a number of things were achieved:

- A simple physically-based rainfall forecasting methodology, which employs a "cloud-column as a hydrologic system" modelling approach, was selected as a tool to investigate the possibilities of using integrated mesoscale-hydrometeorological modelling for flood forecasting. It is an approach that has had extensive modelling work develop directly from its conception and those separate research efforts have been threaded together, in Chapter Two, as a cohesive, sequential, systematic progression of that particular framework. As such, the synopsis stands as a reference for the framework's development and implementation and contributes to understanding how the approach evolved over time, its strengths and its weaknesses.
- The framework adopted has been reworked, as detailed in Chapter Three, into an integrated mesoscale-hydrometeorological algorithm (referred to throughout as the PFM) for rainfall forecasting by marrying, in a novel way, mesoscale NWP forecast data with catchment and urban scale meteorological observations and the fine-scale physically-based forecasting approach. This not only constitutes an attempt at integrated mesoscale-hydrometeorological rainfall forecasting but contributes a further gradation in the timeline of the primary framework.
- The potential of the PFM was verified through a UK case study application which also provided an illustration and examination of what various forecasting techniques have to offer flood forecasting systems, as input to hydrological flow forecasting models, at progressive lead-times within the VSRF range (Chapter Four).
- A critical appraisal of components of the PFM provided some transparency to the value of its formulations and gave insight to the potential for its improvement, thus providing a springboard for future development of the approach (Chapter Five).

- A second case study revealed an element of robustness to the PFM and served as a means to illuminate some of the problems associated with incorporating NWP forecast data into finer-scale rainfall forecasting (Chapter Six).

Providing the foundation for the work was the F&K physically-based rainfall forecasting model, a model that incorporated elements of simple trend extrapolation with rainfall dynamics, the latter as encapsulated in rising parcel theory. Whereas the framework of the model was conceived upon hydrological concepts, namely treating the atmosphere as single columns each analogous to a water reservoir, its use of rising parcel theory placed it in common with other fine-scale rainfall forecasting models of its day that had developed from a meteorological perspective. Its distinction lay in the cloud-column approach and the parameterisation of vertical motion. The latter was purely convective in nature, entirely appropriate for its intended application at the time of its development. Nowcasting elements were introduced into the framework through incorporation of radar and satellite data in a semi-lagrangian frame of reference. Subsequent development of the framework by various researchers saw adaptations being made to account for the influence of orography on rainfall development, to include detailed microphysics and to broaden the model's applicability to all storm types by determining vertical motion in the cloud column not from a convective parameterisation but from how rain fields evolved over a reference area upwind of the model's domain. The experimentation with model formulations went so far as dispensing with most of them and turning the F&K framework into a simple "black box", lumped system response forecasting methodology. All of the aforementioned modifications served to confirm the adaptability of the original framework to new input data, to appended formulae, to elaboration, to reductionism and in all cases ended with a workable model that performed better than either persistence or simple advection forecasting techniques. It was therefore highly suited, and recommended as such, for the inclusion of NWP forecasts and was also amenable to a fresh perspective which positioned it as a physically-based algorithm for rainfall forecasting with NWP forecasts governing pathway decisions (the PFM). This perspective was an acknowledgement that the parameterisations and "physics" of the F&K model were perhaps based on tenuous assumptions and greatly oversimplified real atmospheric processes but, as shown by results from runs of the black box and microphysical versions, still helped in approximating the response of the system (being a cloud column of the atmosphere) to the atmospheric conditions.

The main idea behind incorporating NWP data in the PFM was to extract information from it regarding the nature of the environment in which rainfall might potentially develop, to establish the atmospheric conditions enforcing the system response. It was hoped the NWP data might provide the answer to the key question that arose from the back-to-basics, ingredients-based approach to rainfall forecasting embodied in the new algorithm - were the ingredients of rainfall, being high

moisture content combined with uplift, present or likely to become present? With this in mind a search was instigated to find NWP fields that could suitably act as indicators of the ingredients' existence, a search that culminated in the selection of a set of identifiers that were then used to assist with delineation of rainfall areas outside the existing, translated rain field itself. The primary identifiers chosen were high relative humidity with respect to water and ice at upper-levels (taken to be indicative of a cloud with large vertical extent and with potential to form rainfall) and the presence of any indication of upward motion whether in the form of convection, frontal lifting, orographic uplift or a general profile of upward movement.

Being able to differentiate between the mechanisms producing the upward motion was considered key to approximating the "response of the system" and also key to broadening the applicability of the PFM to all manner of storms. NWP data was considered the means by which that differentiation could be made. The main distinction of interest was between convective and non-convective forcing, as the former could be in the order of ten to one hundred times greater than the latter. The signifiers of convective forcing were the presence of potential instability (decreasing equivalent potential temperature with height), symmetric instability (as indicated by negative values of moist potential vorticity) and moist static instability (determined by a comparison of environmental and pseudo-adiabatic lapse rates) with only one form of parameterisation used to represent the forcing associated with the release of all three types. However, before convection could be deemed to be taking place or initiated within a model grid cell, the signifiers had to be accompanied by either a pre-existing rain field to suggest it was in operation, upward motion in the NWP profile of vertical wind as a mechanism for realisation and triggering of the instability or likewise orographic uplift within the cell. Whereas any evidence of instability led to the same convective parameterisation of vertical velocity, non-convective forcing was split into two categories, frontal and non-frontal, with the average NWP vertical velocity within the cloud column and the NWP cloud base vertical velocity taken to represent each respectively.

The parameterised orographic uplift had a dual role in the PFM. It influenced the rate of rainfall production in pre-existing rain fields and triggered convection, the possible effects of which were considered significant enough to warrant the introduction of multiple time-steps within one forecast so as to allow the rain field to develop in response to the orographic forcing associated with the terrain over which it was progressively advected. The advection scheme employed was selected from a range of options that included the vector of storm movement, as determined from consecutive radar images using cross correlation methods, as well as persistence and NWP wind fields at the 700mb and 850mb levels. Whichever scheme had provided the best estimate of storm movement for the preceding forecast was implemented for the next.

The large number of scans missing from the full volume radar data obtained to run and test the PFM, as well as the difficulties in obtaining the data, enforced adaptation of model formulations to enable use of single-level network radar data and which ensured the algorithm was developed to function with use of operationally available data only. Within the PFM the radar data had two functions, one was to track storm movement while the other and most important function was to initialise the model state. Without full volume radar data the model state could no longer be VIL, as in the F&K model, and so instead became CBLWC. Thus, estimation of how condensation within the cloud column was apportioned to CBLWC was required, to which a rudimentary approach was taken entailing a preliminary forecast time-step followed by, what was effectively, normalisation of forecasted CBLWC with observed CBLWC.

The aforementioned constituent parts of the PFM were all brought together into an algorithm for forecasting rainfall rates at fine spatial scales for any type of storm, an algorithm that through remotely sensed data and NWP forecasts sought to ensure the ingredients of precipitation production were present, attempted to determine the relative strength of forcing giving rise to condensation and to include the extent to which it was augmented or diminished by orographically induced vertical motion, and which tried to emulate storm movement and to produce an instantaneous rainfall rate from the predicted changes in cloud column liquid water. All of this whilst endeavouring to maintain simplicity and speed of computation. It was a combination and structure that appeared reasonably successful when comparing its performance, on a case study basis using UK storm events, to that of nowcasting, persistence and NWP rainfall forecasts. At a lead-time of one hour the PFM produced the highest CSI and also the best correlation at all the spatial scales considered, as well as providing comparable rainfall coverage and average rainfall rates to those observed without an apparent bias toward a particular type of event. With increasing forecast lead-time the PFM's referral to the NWP upper-level relative humidity fields for rainfall area delineation led to better spatial characterisation of rain fields than shown by nowcasting and persistence techniques and which for the most part also included better average rainfall rates and rainfall coverage.

The results suggested that the desired outcomes were largely achieved, the PFM could provide forecasts that improved upon those produced by nowcasting, and as lead-time increased the benefits of incorporating NWP data became more apparent. In considering how the PFM might be placed within a flood forecasting system, at lead-times of 0-2 hours the speed, simplicity and apparent effectiveness of a persistence approach makes it difficult to justify employing the more complex PFM methodology. However sole reliance on persistence will always carry the risk of "creating" floods out of storm systems that are transitory and cannot provide hydrologists with the speed and direction of storm movement they need to estimate the magnitude and timing of peak

flood flows. At longer lead-times, namely VSRF, the performance statistics did not clearly establish PFM forecasts as being better than NWP forecasts, with the NWP forecasts providing higher CSI scores and correlation coefficients at all spatial scales. Notable though was the very low average rainfall rates and excessive rainfall coverage presented in the NWP forecasts and which resulted mainly from their being made at a coarser resolution. In comparison the PFM achieved more realistic values for each. Also notable was the tendency for the PFM to produce the superior "nearest neighbour" correlations for similar reasons, attributable to the PFM being better able to depict spatial variability in rain fields, albeit with a lack of precision, than could be achieved by interpolating coarser resolution NWP forecasts to a finer grid. Like RMSE, for which it appeared wiser in the case study to predict no rainfall at all than to displace the rain field, correlation coefficients were generally higher when predicting uniformity of rainfall than when introducing spatial variability with inaccuracies, despite spatial variability being evident in the actual rain field. It would probably depend on the application as to which type of forecast was the more desirable. Finally, it remains to be seen how the physically-based PFM's results might compare with those of Nimrod and GANDOLF, the UKMO's operational models specifically developed to provide forecasts for lead-times of 0-6 hours. Such a comparison between the PFM and those models would need to be undertaken in a simulated operational context to account for the fact that, whereas the PFM's algorithm is adaptive to the mesoscale conditions within which it is operating, the use of either of the UKMO models is dependent upon the identification of convection. It would be of interest to see the effectiveness of the triggering mechanism that implements GANDOLF predictions and how well the UKMO system handles convective elements within frontal storms as well as convection arising from the uplift of air over orography.

Apart from contributing towards establishing the PFM as a viable forecast method, the exercise of undertaking the performance assessment for the UK case study highlighted a number of things. One was the importance of assessing model performance using a variety of measures, preferably both statistical and visual. If assessment of the forecast methods had relied solely on RMSE, then the UKMM forecasts of convective rainfall would have been adjudged the best of all techniques despite predicted rainfall coverage and rainfall rate being considerably lower than observed and despite rain fields not being particularly well positioned or correlated with actual areas of rainfall. The exercise also made clear that when using radar rainfall estimates as the reference data against which assessment is made, the quality of that data is of prime importance. It should preferably be devoid of clutter and anomalous propagation, particularly if persistence is included in the performance comparison so as to avoid giving it undue advantage. In the UK case study recurrent anomalous propagation led to difficulties in attaining the correct velocity of storm movement and, by providing persistence with high correlation, influenced the PFM's selection of advection velocity. Finally, the assessment revealed differences between PFM forecasts made with the most

current ("perfect") NWP forecasts and those made with the NWP forecasts available in real-time. This perhaps indicated the PFM was more sensitive to meteorological inputs than Bell and Moore (1998) found their version of the F&K model to be, but made so because of the greater contribution of the inputs to the evolution of the PFM's forecasted rain field. However, there was no consistent degradation in the PFM's performance with use of the real-time data, rather at times it enabled a better forecast, suggesting that the up to nine hours separation between NWP analysis and forecast was not a significant hindrance to how the PFM performed. Despite having dismissed the idea of employing the PFM in an ensemble framework in Section 3.2, the sensitivity shown by the model to the NWP inputs and also the apparent random variability of its performance under similar synoptic conditions together indicate a case exists for undertaking such an approach in order to arrive at a mean forecast that might provide a higher degree of consistency and skill. The random performance of the PFM could be attributed not only to the quality of NWP inputs (and also the chaotic nature of atmospheric processes) but also to how well storm movement was estimated by the PFM and this aspect may be improved by deriving a mean forecast from an ensemble of predictions that each adopt different advection schemes.

A number of facets of the PFM's implementation were singled out for examination and were found to be less than ideal, with the conclusion being that the PFM's overall performance would no doubt benefit if they were given further attention. The rudimentary method of attributing condensation to CBLWC was one aspect identified as needing improvement, particularly as there was often a failure by the PFM to attain the observed maximum rainfall intensities. It was suggested that this might be remedied if full volume radar data was available to determine the relationship between cloud column liquid water and CBLWC. That suggestion must be qualified by how well the particular radar in use is sited to achieve reliable cloud column liquid water measurements, that is without significant overshooting, undershooting, or beam blocking. An alternative and simplistic approach to the estimation of CBLWC from condensation may be to borrow and experiment with something analogous to the precipitation efficiencies cited in the literature by the likes of Rogers and Yau (1989). The usefulness of either of the two proposed methods is, however, entirely dependent on the model time-step chosen. It became clear in Chapter Five that the length of the time step was critical to forecasting success and that the length chosen needed to account for the fact that the rate at which the cloud liquid water content changes over a period of one hour is itself continually changing. Meteorological variables constantly respond to moisture loss or gain, so to adopt an instantaneous rate of change and assume it is sustained for the entire forecast lead-time will, as experienced, result in excessive moisture loss or excessive moisture gain. This problem was ameliorated by F&K through reverting to a forecast lead-time in units of minutes rather than seconds, and was not so apparent in forecasts of the PFM when using a 300 second (5 minute) time-step as opposed to one of 3600 seconds (one hour). It may be worth spending more time on

finding a length of time-step for the PFM that achieves an acceptable balance between computational speed and allowing sufficient time for processes involved in rainfall formation to act whilst not sustaining the same rate of moisture source and sink for too long a period.

The orographic component of the model was another facet of the PFM that was scrutinised and was unfortunately shown to be not as effective as hoped. The choice of using model winds as opposed to the vector of storm velocity appeared to be the right decision with respect to the UK case study, though the pressure level at which they should be taken was not conclusively determined. The intention behind employing twelve time-steps in a single forecast, being to allow orographic forcing greater influence in rain field development, was rewarded with better fine scale correlation coefficients and RMSE than were achieved through use of one time-step, but interpretation of the results became complicated by inconsistency in the units of time employed. That there were deficiencies in the PFM's orographic component became clear when the PFM produced improved performance statistics with it removed. One such deficiency was the tendency for the PFM to show less rainfall to the lee of hills than appeared to be actually occurring. A possible explanation was that the radar, through overshooting or beam blocking, may not have captured the full rain-shadow effect of high terrain and sampling may not have been occurring at the "cloud base" to which the PFM forecasts were purported to relate. Examples were given in Chapter Six of occasions when network radar images appeared to show rainfall despite other instrumentation confining liquid water to high levels. However, given that the leeside drying of the PFM was probably excessive, in future it would be relatively easy to modulate its extent by reducing the strength of the downdrafts by, for example, a factor of ten.

Another problem with the PFM's orographic forcing was that while orographic enhancement of rainfall could be detected in the observed rain fields, the PFM had trouble pinpointing its occurrence. A contributing factor was that the PFM's rather simplistic parameterisation of orographic updraft did not allow for the possibility of precipitation drifting, however this was remedied a little by employing an advection step following determination of CBLWC values. Perhaps helpful too would have been limiting the influence of the PFM's orographic updrafts in convective situations to the triggering of convection only rather than also augmenting the speed of vertical motion. The positioning of the PFM's orographic enhancement was highly dependent on the direction of the wind field being used. Through comparison of surface observations and NWP wind fields in the later Marseille case study the potential discrepancies between the two were highlighted and as such undetermined discrepancies could have been partly responsible for failure of the PFM's orographic forcing to register very well in the performance statistics of the UK case study. Despite the apparent inadequacies of the PFM's orographic component, its ability to produce the higher average rainfall rates and to at times "get it right or thereabouts", as reflected in

better nearest neighbour correlations and visual examples (such as Figure 4.7), together meant there was appeal in its retention.

The last aspect of the algorithm to receive specific attention was the effectiveness of employing different parameterisations for grid-scale vertical motion. The considerable effort that went into differentiating the mode of forcing leading to rainfall development (convective, frontal or otherwise) provided some benefit in terms of improved correlation coefficients with respect to those achieved using convective updrafts alone but otherwise did not make an impression on the remaining performance statistics. The indifferent results were partly attributed to nature of the events themselves, or at least the NWP representations of them in which atmospheric instability was often prevalent, but mainly to the criteria controlling implementation of the convective parameterisation, criteria that resulted in its employment at the slightest suggestion of instability being present. Numerous indices of convection exist (NWS Louisville, 2001), providing considerable scope to experiment with different ways in which convective areas are defined in the PFM, the possibilities including a combination of CAPE and convergence of surface moisture as used by Météo France with some success (Hand, 2001).

With the original version of the PFM intact, the Marseille case study illustrated how it was still able to perform well, particularly in terms of correlation coefficients, compared to other forecasting methods at a lead-time of one hour and at the finer resolutions associated with urban hydrology, despite the NWP data in use seeming to offer little assistance. The case study served to highlight the advantage of having advection scheme options, with the advection scheme of choice quite frequently being the NWP upper-level wind fields. It also highlighted the importance of estimating storm velocity correctly and having a broad enough surveillance area, if possible, to enable the speed of storms, provided the storms are long-lived, to be gauged prior to their impinging on the specific area of interest. Having flexibility in choice of advection scheme had also proved beneficial in the UK case study but the way in which storms progressed towards and over the UK domain posed certain difficulties, with the rain fields approaching quickly over sea areas, slowing over land and stalling over high ground and then changing their direction of movement beyond. For the PFM or any nowcasting technique to be successful in those circumstances requires some form of differential advection scheme able to cope with the challenges of storm behaviour of that nature. When forecasting over longer lead-times, three hours and beyond, rather than go through the exercise of determining which advection scheme to use it may be better to simply utilise NWP wind fields, as extrapolation techniques tend to be limited in usefulness to approximately two hours and, as mentioned above, at such lead-times the rain field may not have yet entered the domain in order to determine storm velocity from cross correlation techniques.

In the Marseille case study it was the input data to the PFM that perhaps drew more attention than the algorithm itself. Exposed were the potential problems with the representation of the model state upon which the PFM's forecasts were based and subsequently assessed, however it was noted that the sources of inaccuracies in the estimation of rainfall from radar reflectivity are fairly well known and are receiving ongoing attention. In addition to problems with the radar data, also exposed was the fallibility of NWP forecasts or at least the considerable differences that can occur between NWP fields and point measurements of meteorological variables, as mentioned above. The absence of high percentages of relative humidity in NWP data was a case in point but one which at the same time made questionable the appropriateness of applying the same set of rainfall signifiers universally, especially the humidity fields which in future should possibly be taken at another level when applying the PFM in Mediterranean regions. It was also evident that at the finer resolutions employed, achieving the localisation and spatial differentiation of rainfall was going to be much more problematic because of the relative coarseness of the resolution of the NWP data. In both case studies it was always going to be difficult to achieve local definition of convective cells when convective instability appeared broad-scale because the resolutions so chosen for the operation of the PFM (1-25km^2) were much finer than the resolution of the NWP data. This problem was particularly evident in the Marseille case study and more so with the use of NWP relative humidity fields to delineate rain areas, with excessively large PFM rain fields being the result.

Therein lies one of the main challenges if work on the PFM is to be carried further, as the potential shown suggests it should be and which is likewise supported by the recent interest taken by the European Commission in funding research into combining extrapolation techniques with NWP data (Conway *et al*, 2001). Various components of the PFM have already been singled out for suggested improvement, such as modulating orographic downdrafts, employing more discerning or stricter criteria for the implementation of the convective parameterisation, revisiting the manner by which condensation is attributed to CBLWC, reassessing the length of the model time-step, finding and adding a differential advection scheme to cope with different storm velocities over sea and land and having site-specific humidity signifiers. However, if work on the PFM is to progress and is to achieve reasonable success at all lead-times within the range of VSRF, then two key issues have to be addressed.

The first is, given that the NWP forecasts are "broad-scale" relative to the PFM, there needs to be some way of isolating where, within what will appear reasonably homogenous conditions to the PFM, rainfall is going to eventuate. This is probably more of an issue in situations of convection than in frontal rainfall due to the often showery nature of the former and the more organised structure of the latter. The area where those showers are likely to occur may be narrowed to some

extent by looking at NWP data over a period of time (preferably the analysis data) and identifying areas of persistent convergence (over periods of 1-4 hours) and persistent high CAPE in addition to high humidity (Ducrocq, 2001). Having a dense network of surface observations in the area of interest would also be helpful in that respect. Lightning data may also prove helpful with the identification of storms and in tracking their speed and direction of movement (Sénési, 2001). The UKMO perhaps leads the way in attempts to pinpoint rain cell location with its calculation of maximum probable sub-grid variations of temperature and moisture from mean values, determined according to land surface inhomogeneity as related to land use and type of landscape (eg. urban, inland water, woodland), which then leads to estimation of the probability of convection occurring in specific areas (Hand, 2001).

The second issue is that until such time as "nowcasting"-type methods can predict rainfall without the presence of a rain field then it will be difficult for those techniques to extend beyond a very limited lead-time. Such a development cannot be expected from methods based solely on the extrapolation of existing conditions, if existing conditions do not exhibit rainfall then it can not be extrapolated forward in time. However, more might be expected from a physically-based model such as the PFM, but which is currently still limited by its need to have a rain field present before forecasts of rainfall can be made because of the need to establish how cloud column condensation is attributed to CBLWC. The way forward may be found in taking advantage of the broader coverage of satellites and the work being undertaken towards quantitative precipitation estimation from satellite imagery (Wild, 1996). It may also have to rely on developing local climatologies and using this to train neural network classifiers, such as the cloud classifier in use in the UKMO's GANDOLF system (Pankiewicz, 2001), to assist with emulation of how storms tend to manifest in particular areas under particular conditions.

In recommending that further work be undertaken on the use of mesoscale NWP data to help improve the reliability, accuracy and lead-time provided by forecasting techniques falling within the "nowcasting" umbrella, commendation must be given (in the hope the situation remains and other countries follow suit) to the collaboration of the UKMO and University of Reading in establishing JCMM and through it enabling access to the varied data required for such a research project through one source at no charge.

REFERENCES

Acker, K., Arends, B.G, Berner, A., Beswick, K.M., Bizjak, M., Bower, K.N., Cape, J.N., Cederfelt, S-I., Choularton, T.W., Colville, R.N., David, M.M., Davies, T., Dollard, G., Engelhardt, T., Facchini, M.C., Fowler, D., Frank, G., Fuzzi, S. Gallagher, M.W., Georgii, H.W., Gieray, R., Hallberg, A., Hansson, H.-C., Hargreaves, K.J., Harrison, M., Helas, G., Jaeschke, W., Jones, B., Kos, G.P.A., Kruisz, C., Laj, P., Levsen, K., Lind, J.A., Lüttke, J., Martinsson, B., Maser, R., Mentes, B., Möller, D., Möls, J.J., Noone, K.J., Orsi, G., Orsini, D., Pahl, S., Peak, J.D., Preiss, M., Schell, D., Sedlak, D.L., Seyffer, E., Storeton-West, R.L, Sutton, M.A., Svenningsson, B., Swietlicki, E., Wells, M., Wendisch, M., Wiedensohler, A., Wieprecht, W., Wieser, P., Winkler, P., Wobrock, W., 1997: The Great Dun Fell cloud experiment 1993: an overview. Atmospheric Environment vol. 31, no.16, p2393-2405.

Ahrens, C.D., 2000: Meterology today: an introduction to weather, climate and the environment. 6th edition. Brooks/Cole Thomson Learning, Pacific Grove, USA.

ALADIN International Team, 1997: The ALADIN Project: mesoscale modeling seen as a basic tool for weather forecasting and atmospheric research. WMO Bulletin, vol.46 no.4 p317-324.

Amitai, E., Atlas, D., Black, R.A., Marks Jnr, F.D., Samsury, C.E., Ulbrich, C.W., Willis, P.T., 2000: Partitioning tropical oceanic convective and stratiform rains by draft strength. Journal of Geophysical Research, vol.105, no.D2, p2259-2267.

Andrieu, H., Austin, G.L., Baltas, E., Borga, M., Brilly, M., Cluckie, I.D., Creutin, J.-D., Delrieu, G., Deshons, P., Fattorelli, S., Griffith, R.J., Guarnieri, P., Han, D., Mimikou, M., Monai, M., Porra, J.M., Sempere Torres, D., Spagni, D.A., Uijlenhoet, R., 2000: Hydromet Integrated Radar Experiment (HIRE): Experimental setup and first results. Unpublished paper.

Andrieu, H., Creutin, J.D., Delrieu, G., 1991: Weather radar and urban hydrology in the context of mountainous Mediterranean regions. In Maksimović, Č (ed), New Technologies in Urban Drainage UDT '91, p53-61.

Andrieu, H., Creutin, J.D., Dolcine, L., French, M.N., 2000: Implementation considerations of a conceptual precipitation model. Journal of Geophysical Research, vol.105, no.D2, p2291-2297.

Andrieu, H., Creutin, J.D., Dolcine, L., Sempere-Torres, D., 2001: Flash flood forecasting with coupled precipitation model in mountainous Mediterranean basin. Journal of Hydrologic Engineering, vol. 6, no.1 p 1-10.

Andrieu, H., Creutin, J.D., Vignal, B., 1999: Identification of vertical profiles of reflectivity from volume scan radar data. Journal of Applied Meteorology, vol. 38 p1215-1228.

Andrieu, H., Dolcine, L., French, M.N., 1998: Evaluation of a conceptual rainfall forecasting model from observed and simulated rain events. Hydrology and Earth System Sciences, vol. 2(2-3), p173-182.

Andrieu, H., French, M.N. & Krajewski, W.F., 1994: A model for real-time quantitative rainfall forecasting using remote sensing; 2) case studies. Water Resources Research, volume 30, no.4, pg 1085-1097.

Andrieu, H., French, M.N., Krajewski, W.F., Thauvin, V., 1996: Adaptation and application of a quantitative rainfall forecasting model in a moutainous region. Journal of Hydrology, Volume 184 nos. 1-2, pgs 243-259.

Anthes, R.A. & Cotton, W.R., 1989: Storm and Cloud Dynamics. International Geophysics Series, Volume 44. Academic Press Inc, San Diego.

Atlas, D. and Wexler, R., 1958: Moisture supply and growth of stratiform precipitation. Journal of Meterology, vol. 15, p531-538.

Austin, G.L. & Robichaud, A.J., 1988: On the modelling of warm orographic rain by the seeder-feeder mechanism. Quarterly Journal of the Royal Meteorological Society, vol. 114, p967-988.

BADC, 2001: Hydrological Radar Experiment (HYREX). http://www.badc.rl.ac.uk/data/hyrex (last visited 16/03/2001)

Bader, M.J., Browning, K.A., Hill, F.F., 1981: Radar and raingauge observations of orographic rain over south Wales. Quarterly Journal of the Royal Meteorological Society, volume 107 pgs 643-670.

Ball, J.E., 1991: Temporal pattern influences on catchment response. In Maksimović, Č (ed), New Technologies in Urban Drainage UDT '91, p135-142.

Bannon, J.K., 1948: The estimation of large-scale vertical currents from the rate of rainfall. Quarterly Journal of the Royal Meteorological Society, vol.74, p57-66

Banta, R.M., 1990: The role of mountain flows in making clouds. In Blumen, W. (ed), Atmospheric processes over complex terrain. Meterological Monographs, vol.23 no. 45, June 1990. American Meteorological Society, Massachusetts. p229-283.

Barkmeijer, J., Buizza, R., Palmer, T.N., Richardson, D.S., 2000: Current status and future developments of the ECMWF Ensemble Prediction System. Meteorological Applications, vol. 7 no.2, p163-175.

Barron, E.J., Duffy, C., Frakes, B., Lakhtakia, M.N., Miller, D.A., Schwartz, F.W., White, R.A., Yarnal, M.N, Yu, Z., 1999: Simulating the river-basin response to atmospheric forcing by linking a mesoscale meteorological model and hydrologic model system. Journal of Hydrology, vol.218, nos 1-2, p72-91.

Barros, A.P. and Lettenmaier, D.P., 1994: Dynamic modelling of orographically induced precipitation. Reviews of Geophysics, vol.32 no.3, p265-284.

Barry, R.G. and Chorley, R.J., 1992: Atmosphere, weather and climate, 6th edition. Routledge, London.

Bartzis, J.G., Catsaros, N., Deligiannis, P., Varvayanni, M., 1997: Meteorological pre-processing over highly complex terrains. Radiation Protection Dosimetry, vol.73, nos.1-4, p253-256.

Battan, L.J., 1973: Radar Observation of the Atmosphere (revised edition). The University of Chicago Press. Chicago.

Baumann, K., Formayer, H., Langer, M., Piringer, M., Neininger, B., Stohl, A., Wotawa, M., 1997: Diagnostic downscaling of large-scale wind fields to compute local-scale trajectories. Journal of Applied Meterology, vol.36 no.7 p931-942.

BBC Radio Bristol, 2001: 2nd January, 2001in the news bulletins and in a specific report preceding 9am news.

BBC, 1999a: Death toll in French floods now 26: http://news.bbc.co.uk/hi/english/world/europe/news_id_518000/518710.stm (last visited 24/7/2001)

BBC, 1999b: French flood toll rises: http://news.bbc.co.uk/hi/english/world/europe/news_id_518000/518748.stm (last visited 24/7/2001)

BBC, 2000a: Stormy weather lashes Britain and France: http://news.bbc.co.uk/hi/english/world/europe/news_id_997000/997997.stm (last visited 24/7/2001)

BBC, 2000b: Worse floods ahead as world warms. http://news.bbc.co.uk/hi/english/world/newsid_976000/976363.stm (last visited 14/2/2001)

BBC, 2001: World numbers "may peak by 2100". BBC News Online. http://news.bbc.co.uk/hi/english/sci/tech/newsid_1467000/1467252.stm. (last visited 19/08/2001).

Bedrick, M.A., Bosart, L.F., Bracken, W.E., Dickinson, M.J., Hakim, G.J., Schultz, D.M., Tyle, K.R., 1997: The March 1993 superstorm cyclogenesis: incipient phase synoptic- and convective-scale flow interaction and model performance. Monthly Weather Review, vol.125 p3041-3072.

Bell, R.S., 1978: The forecasting of orographically enhanced rainfall accumulations using 10-level model data. Meteorological Magazine, volume 107, pgs 113-124.

Bell, V.S. and Moore, R.J., 1998: Sensitivity of a short-period radar rainfall forecasting model to weather fields derived from a mesoscale numerical weather prediction model. In Kirby and Wheater (eds), Hydrology in a changing environment, volume III. p115-125.

Bénard, P., Lafore, J.-P., Redelsperger, J.-L., 1992: Nonhydrostatic simulation of frontogenesis in a moist atmosphere. Part II: Moist potential vorticity budget and wide rainbands. Journal of the Atmospheric Sciences, vol.49 no.23, p2219-2235.

Berlamont, J. and Willems, P., 1998: Stochastic modelling of spatial rain cells. In Kirby and Wheater (eds), Hydrology in a changing environment, volume III. p307-318.

Berri, G., Dalu, G.A., Garratt, J.R., Miller, W., Nicolini, M., Paegle, J., Pielke, R.A., Vukicevic, T., 1990: Predictability of flows over complex terrain. In Blumen, Atmospheric processes over complex terrain. Meterological Monographs, vol.23 no. 45, June 1990. p285-299.

Billingsley, D., 2001: The distribution of PV. http://www.boi.noaa.gov/training/ipv/ipv2.html. (last visited, 29/4/2001).

Blanchard, D.O., 1998: Assessing the vertical distribution of convective available potential energy. Weather and Forecasting, vol. 13 no. 3 p870-877.

Blumen, W. (ed), 1990: Atmospheric processes over complex terrain. Meterological Monographs, vol.23 no. 45, June 1990. American Meteorological Society, Massachusetts.

Bolton, D., 1980: The computation of equivalent potential temperature. Monthly Weather Review, vol.108 (July) p1046-1053.

Brooks, H.E., Doswell III, C.A., Maddox, R.A., 1996: Flash flood forecasting: an ingredients-based methodology. Weather and Forecasting, vol.11, no.4, p560-581.

Brown, P.M., and Kitchen, M., 1992: Correction of radar measurements for orographic precipitation growth beneath the beam. 2nd International Symposium on Hydrological Applications of Weather Radar, University of Hannover.

Browning, K.A., 1980: Structure, mechanism and prediction of orographically enhanced rain in Britain, in Orographic Effects in Planetary Flows, Hide and White (eds). GARP Publication Series no.23.

Browning, K.A. (ed), 1982: Nowcasting. Academic Press Inc (London) Ltd, London.

Browning, K.A., Griffiths, M., Thorpe, A.J., 2000: Convective destabilization by a tropopause fold diagnosed using potential-vorticity inversion. Quarterly Journal of the Royal Meteorological Society, vol.126 no.562 Part A Jan 2000, p125-144.

Browning, K.A. and Hill, F.F., 1979: Persistence and orographic modulation of mesoscale precipitation areas in a potentially unstable warm sector. Quarterly Journal of the Royal Meteorological Society, volume 105 pgs 57-70.

Browning, K.A., Hill, F.F., Pardoe, C.W., 1974: Structure and mechanism of precipitation and the effect of orography in a wintertime warm sector. Quarterly Journal of the Royal Meteorological Society, volume 100 pgs 309-330.

Browning, K.A., Hill, F.F., Pardoe, C.W., 1975: The nature of orographic rain at wintertime cold fronts. Quarterly Journal of the Royal Meteorological Society, volume 101, no. 428 pgs 333-352.

Brugge, R., 2001: British Isles weather diary. http://www.met.rdg.ac.uk/~brugge/, (last visited 12/6/2001).

Byron-Scott, R., Gordon, A., Grace, W., Schwerdtfeger, P., 1998: Dynamic Meteorology: A Basic Course. Arnold, London.

Carlson, T.N., 1991: Mid-latitude weather systems. Harper Collins Academic, London.

Carpenter, K.M., 1982: Model forecasts for locally forced mesoscale systems, in Nowcasting, ed. by K.A. Browning, Academic Press, p223-234.

Carruthers, D.J. & Choularton, T.W., 1983: A model of the feeder-seeder mechanism of orographic rain including stratification and wind-drift effects. Quarterly Journal of the Royal Meterological Society, vol.109, p575-588.

Cluckie, I.D. and Collier, C.G., (eds) 1991: Hydrological applications of weather radar. Ellis Horwood Limited, England.

Cluckie, I.D., Griffith, R.J., Lane, A., Tilford, K.A., 2000: Radar hydrometeorology using a vertically pointing radar. Hydrology and Earth System Sciences vol. 4 no.4, p565-580

Cluckie, I.D., Griffith, R.J., Spagni, D.A., (eds) 2000: HYDROMET Project: Development of active on-line hydrological and meteorological models to minimize the impact of flooding. Summary report to the European Commission, Directorate-General, Science, Research and Development. 32pp.

Collier, C.G., 1975: A representation of the effects of topography on surface rainfall within moving baroclinic disturbances. Quarterly Journal of the Royal Meteorological Society, vol 101 no 429 p407-422.

Collier, C.G., 1989: Applications of weather radar systems: a guide to uses of radar data in meteorology and hydrology. Ellis Horwood Limited, England.

Collier, C.G., 1996: Applications of weather radar systems: a guide to uses of radar data in meteorology and hydrology, 2nd Edition, Ellis Horwood Limited, England.

Conway, B., Lagouvardos, K., Liljas, E., Sunde, J. (eds), 2001: Cost Action 78: Improvement of nowcasting techniques, final report. European Communities, Luxembourg.

Cortinas Jr, J.V. & Stensrud, D.J., 1995: The importance of understanding mesoscale model parameterisation schemes for weather forecasting. Weather and Forecasting, vol.10 no.4, p716-740.

Cowpertwait, P.S.P, Mellor, D., O'Connell, P.E., Threlfall, J.L., 1998: Rainfall modelling and forecasting for storm sewer system rehabilitation and control. In Kirby and Wheater (eds), Hydrology in a changing environment, volume III. p319-329.

Curry, J.A. & Webster, P.J., 1999: Thermodynamics of Atmopheres and Oceans. International Geophysics Series, Volume 65. Academic Press, London.

Daley, R., 1991: Atmospheric Data Analysis. Cambridge University Press, Cambridge.

Debie, F., Maas, A., Prangsma, G.J., Slikker, R., van Dorp, H., Winkler, R., Zeiner, B., Zwatz-Meise, V., 2001: Additional parameters and helpful tools for the diagnosis of cloudiness, Satrep Manual Version 3.0. http://www.knmi.nl/satrep/

Desbordes, M., 1991: Characteristics of heavy rainfalls in the European part of Mediterranean basin. ? In Maksimović, Č (ed), New Technologies in Urban Drainage UDT '91, p3-12.

Dicks, E. & Panagi, P., 1997: Met Office Unified Model data, diagnostics, graphics program and other observational data available from the JCMM through the aegis of the Universities Weather Research Network (UWERN). Internal Report 69, June, JCMM, Dept. Meterology, The University of Reading, Reading.

Dicks, E. & Panagi, P., 1997: Met Office Unified Model data, diagnostics, graphics program and other observational data available from the JCMM through the aegis of the Universities Weather

Research Network (UWERN). Internal Report 69 - Supplement, June, JCMM, Dept. Meterology, The University of Reading, Reading.

Doswell III, C.A., Schultz, D.M., Schumacher, P.N., 2000: The intricacies of instabilities, Monthly Weather Review, vol. 128, no.12, p4143-4148.

Driscoll, S.J., Harrison, D.L., Kitchen, M., 2000: Improving precipitation estimates from weather radar using quality control and correction techniques. Meteorological Applications, vol.7 no.2, p135-144.

Du, J., Mullen, S.L., Sanders, F., 1997: Short-ensemble forecasting of quantitative precipitation. Monthly Weather Review, vol.125, no.10, p2427-2459.

Ducrocq, V., 2001: Activities in Meteo-France (Part II). In Conway *et al* (eds), COST Action 78, p46-47.

Dudek, M. & Molinari, J., 1992: Parameterisation of convective precipitation in mesoscale numerical models: a critical review. Monthly Weather Review, vol.120 p326-344.

Durran, D.R. & Klemp, J.B., 1982: On the Effects of Moisture on the Brunt-Vaisala Frequency. Journal of the Atmospheric Sciences, vol.39 no.10, p2153-2158.

Eden, P., 1998a: Weather Log, September 1998 (supplement to Weather), Royal Meteorological Society.

Eden, P., 1998b: Weather Log, October 1998 (supplement to Weather), Royal Meteorological Society.

Eden, P., 1998c: Weather Log, November 1998 (supplement to Weather), Royal Meteorological Society.

Eden, P., 1999a: Weather Log, December 1998 (supplement to Weather), Royal Meteorological Society.

Eden, P., 1999b: Weather Log, January 1999 (supplement to Weather), Royal Meteorological Society.

Eden, P., 1999c: Weather Log, August 1999 (supplement to Weather), Royal Meteorological Society.

Eden, P., 1999d: Weather Log, October 1999 (supplement to Weather), Royal Meteorological Society.

Edwards, M., 1996: Written correspondence to members of the North West Weather Radar Steering Group Meeting, dated 15th October 1996 (9pp).

Eilts, M.D., Goodman, W., Johnson, J.T., Rothfusz, L., Ruth, D., 2000: Warning operations in support of the 1996 Centennial Olympic Games. Bulletin of the Meteorological Society, vol.81, no.3, p543-554.

Einfalt, T., 1991: Inaccurate rainfall forecasts: hydrologically valuable or useless? In Maksimović, Č (ed), New Technologies in Urban Drainage UDT '91, p63-70.

Elliot, R.D. & Shaffer, R.W., 1962: The development of Quantitative Relationships between Orographic Precipitation and Air-Mass Parameters for Use in Forecasting and Cloud Seeding Evaluation. Journal of Applied Meterology, vol. 1, p218-228.

Emanuel, K.A., 1997: Overview of atmospheric convection. In Smith, R.K. (ed), The Physics and Parameterization of Moist Atmospheric Convection, p1-28, Kluwer Academic Publishers, The Netherlands.

Foufoula-Georgiou, E. & Krajewski, W., 1995: Recent advances in rainfall modelling, estimation, and forecasting. Reviews of Geophysics Supplement vol.33, p1125-1137. US National Report of International Union of Geodesy and Geophysics 1191-1994.

French, M.N. and Krajewski, W.F., October 1992: Quantitative real-time rainfall forecasting using remote sensing. IIHR Limited Distribution Report Number 200, Iowa Institute of Hydraulic Research and Department of Civil and Environmental Engineering, The University of Iowa, Iowa City.

French, M.N. & Krajewski, W.F., 1994: A model for real-time quantitative rainfall forecasting using remote sensing; 1) formulation. Water Resources Research, volume 30, no.4, pg1075-1083.

Georgakakos, K.P., 2000: Covariance propagation and updating in the context of real-time radar data assimilation by quantitative precipitation forecast models. Journal of Hydrology vol. 239 p115-129.

Georgakakos, K.P. & Bras, R.L., 1984a: A hydrologically useful station precipitation model 1) formulation. Water Resources Research, vol.20, no.11 p1585-1596.

Georgakakos, K.P. & Bras, R.L., 1984b: A hydrologically useful station precipitation model 2) case studies. Water Resources Research, vol.20, no.11 p1597-1610.

Georgakakos, K.P. and Hudlow, M.D., 1984: Quantitative precipitation forecast techniques for use in hydrologic forecasting. Bulletin of the American Meteorological Society, vol. 65, no.11, p1186-1200.

Georgakakos, K.P. and Krajewski, W.F., 1991: Short-term rainfall forecasting using radar data and hydrometeorological models. In Cluckie and Collier (eds), Hydrological applications of Weather Radar, p368-378.

Georgakakos, K.P. and Lee, T.H., 1990: A two-dimensional stochastic-dynamical quantitative precipitation forecasting model. Journal of Geophysical Research, vol.95, no.D3 p 2113-2126.

Georgakakos, K.P. and Lee, T.H., 1996: Operational rainfall prediction on meso-γ scales for hydologic applications. Water Resources Research, Volume 32, no.4 pgs 987-1003.

Golding, B.W., 1998: Nimrod: a system for generating automated very short range forecasts. Meteorological Applications, vol.5, p1-16.

Gray, S., 2001: Personal Communication, (University of Reading) email: re: moist potential vorticity (5th April, 2001)

Gupta, V. and Waymire, E., 1981: The mathematical structure of rainfall representations: 1. A review of the stochastic rainfall models. Water Resources Research, vol. 17, p1261-1272 *** haven't got a copy of this, took notes at the Geo library.

Haile, M., Pedder, M.A., Thorpe, A.J., 1997: Short period forecasting of catchment-scale precipitation: Part 1: the role of Numerical Weather Prediction. Joint Centre for Mesoscale Meteorology, Internal Report 77.

Hall, M.J., 1984: Urban Hydrology. Elsevier Applied Science Publishers, London.

Han, D., 1991: Weather Radar Information Processing and Real-time Flood Forecasting. Unpublished PhD Thesis, University of Salford.

Hanaki, K., Hassan, H., Wilby, R.L., 1998: Statistical downscaling of hydrometeorological variables using general circulation model output. Journal of Hydrology, vol.205 p1-19.

Hand, W.H., 2001: Improvement of techniques for early warning of convection. In Conway *et al* (eds), COST Action 78, p41-66.

Hand, W.H., Macpherson, B., Maycock, A.J., Wright, B.J., 1995: The Meteorological Office mesoscale data assimilation scheme. UKMO Forecasting Research Scientific Paper 33 (Unpublished).

Hardaker, P.J., 2001: Personal communication (written) 4th December 2001.

Hewson, T.D., 1998: Objective Fronts. Meteorological Applications, vol 5, p37-65.

Hill, F.F., 1983: The use of average annual rainfall to derive estimates of orographic enhancement of frontal rain over England and Wales for different wind directions. Journal of Climatology, volume 3, pgs 113-129.

Holton, J.R., 1992: An Introduction to Dynamic Meteorology, Third Edition. (Volume 48 International Geophysics Series). Academic Press Inc, San Diego.

Hoskins, B.J., McIntyre, M.E., Robertson, A.W., 1985: On the use and significance of isentropic potential vorticity maps. Quarterly Journal of the Royal Meteorological Society, vol. 111 p877-946

Houghton, H.G., 1985: Physical Meteorology. The Massachusetts Institute of Technology. Cambridge, Massachusetts.

Hulme, M., 2001: The UK in August: Mike Hulme on last month's weather. http://www.cru.uea.ac.uk/~mikeh/datasets/uk/historic/aug99.html, (last visited 12/6/2001).

Ikebuchi, S., Nakakita, E., Shiiba, M., Takasao, T., 1991: Advanced use in rainfall prediction of a three-dimensionally scanning radar. In Cluckie and Collier (eds), Hydrological Applications of Weather Radar, p391-408.

Kessler, E., 1969: On the distribution and continuity of water substance in atmospheric circulation. Meteorological Monographs, 10, 86pp.

Kirby, C. and Wheater, H. (eds), 1998: Hydrology in a changing environment: proceedings of the British Hydrological Society International Conference, Exeter, July 1998, volume III. John Wiley & Sons, Chichester.

Klett, J.D. & Pruppacher, H.R., 1997: Microphysics of Clouds and Precipitation (2nd Revised and Enlarged Edition with an Introduction to Cloud Chemistry and Cloud Electricity). Atmospheric and Oceanographic Sciences Library Volume 18, Kluwer Academic Publishers, Dordrecht.

Kromp-Kolb, H., Seibert, P., Stohl, A., Wotawa, G., 1995: Interpolation errors in wind fields as a function of spatial and temporal resolution and their impact on different types of kinematic trajectories. Journal of Applied Meterology, vol.34, no.10, p2149-2165.

Laprise, R., Morneau, J., Zawadzki, I., 1994: Predictability of precipitation patterns: an operational approach. Journal of Applied Meteorology, vol. 33, no.12, p1562-1571.

Liljas, E., 2001: Introduction. In Conway *et al* (eds), Cost Action 78: Improvement of nowcasting techniques, final report. p19-35.

Lorenz, E.N., 1993: The essence of chaos. UCL Press Limited, London.

Maksimović, Č. (ed), 1991: New technologies in urban drainage, UDT '91. Elsevier Applied Science, London.

Météo France, 2001: Modele ARPEGE: La prévision numérique avec le modèle ARPEGE. http://www.meteo.fr/comprendre /modele_arpege/arpege.html (last visited 27/7/2001).

Moore, R.J., Pedder, M.A., Thorpe, A.J., 1995: HYREX PROJECT T04072: Methods for short-period precipitation and flow forecasting incorporating radar data. (Report up to March 1995).12pp

Morrison, F., 1991: The art of modeling dynamic sytems: forecasting for chaos, randomness and determinism. John Wiley and Sons Inc, New York.

Nash, J.E. and Sutcliffe, J.V.Z., 1970: River flow forecasting through conceptual models. Part I: a discussion of principles. Journal of Hydrology vol.10, p282-290.

NWS Louisville, 2001: Convective season parameters and indices. National Weather Service Louisville Science and Technology Web Pages, http://www.crh.noaa.gov/lmk/soo/docu/indices.htm (last visited 15/5/2001).

Panagi, P, 1997: Potential Vorticity, Fortran subroutine, JCMM, University of Reading.

Panagi, P., 2001: Unified model domains and example data files. http://.www.met.rdg.ac.uk/~panagi/ um/domains/, (last visited 1/6/2001).

Pankiewicz, G.S., 1997: Neural network classification of convective airmasses for a flood forecasting system. International Journal of Remote Sensing, vol.18, no.4, p887-898.

Pankiewicz, G., 2001: A neural network cloud classifier for the automatic detection of convective systems. In Conway *et al* (eds), COST Action 78, p73-76.

Peppler, R.A., 1988: A review of static stability indices and related thermodynamic parameters. Unpublished report for Illinois State Water Survey, Champaign, Illinois.

Pierce, C.E., Collier, C.G., Haggett, C.M., Hardaker, P.J., 2000: GANDOLF: a system for generating automated nowcasts of convective precipitation. Meteorological Applications, vol.7, no.4, p341-360.

Rogers, R.R. and Yau, M.K., 1989: A Short Course in Cloud Physics, Third Edition. Pergamon Press, Oxford.

Salby, M.L., 1992: The atmosphere. In Trenberth, K.C., Climate System Modelling. p53-115

Schultz, D.M. & Schumacher, P.N., 1999: Review: the use and misuse of conditional symmetric instability. Monthly Weather Review, vol. 127, p2709-2732.

Seo, D.J. & Smith, J.A., 1992: Radar-based short-term rainfall prediction. Journal of Hydrology, Volume 131 pg 341-367.

Sherwood, S.C., 2000: On moist instability. Monthly Weather Review, vol. 128 no.12, p4139-4142.

Sinclair, M.R., 1994: A diagnostic model for estimating orographic precipitation. Journal of Applied Meteorology, vol.33 no.10, p1163-1175.

Smith, R.B., 1982: A differential advection model of orographic rain. Monthly Weather Review, vol. 110, p 306-309.

Smith, R.K. (ed), 1997: The Physics and Parameterization of Moist Atmospheric Convection. NATO ASI Series, Series C: Mathematical and Physical Sciences, vol. 505. Kluwer Academic Publishers, The Netherlands.

Strangeways, I., 2001: Back to basics: the 'met. Enclosure': part 6 – wind. Weather, vol.56, no.5 p154-161.

Sugimoto, S., Ikebuchi, S., Nakakita, E., , 2001: A stochastic approach to short-term rainfall prediction using a physically based conceptual rainfall model. Journal of Hydrology, vol.242, p137-155.

Sumner, G., 1988: Precipitation: Process and Analysis. John Wiley & Sons Ltd, United Kingdom.

Trenberth, K.C. (ed)., 1992: Climate System Modelling. Cambridge University Press, United Kingdom.

UKMO, 1998a: Research and development: numerical modelling: dynamics. http://www.meto.govt.uk/sec5/NWP/NWP_dyn.html (last visited 23/12/1998)

UKMO, 1998b: Research and development: physical parameterizations: radiation. http://www.meto.govt.uk/sec5/NWP/NWP_phy_parm.html (last visited 23/12/1998)

UKMO, 2001a: Research: NWP: Numerical modelling: Operational numerical modelling: Producing forecasts for our customers. http://www.meto.gov.uk/research/nwp/numerical/operational/index.html (last visited 11/4/2001).

UKMO, 2001b: Research: NWP: Numerical modelling: Operational numerical modelling: numerical models of the atmosphere. http://www.meto.gov.uk/research/nwp/numerical/operational/ index.html (last visited 11/4/2001).

UKMO, 2001c: Data and products distribution system. http://www.meto.gov.uk/wfc/serv1.html, (last visited 1/6/2001).

University of Bristol, 2001: Zeus/ssa replacement server: isis. http://www.bris.ac.uk/is/services/computers/centralsuite/news/isis.html. (last visited, 1/6/2001).

Weismueller, J.L. and Zubrick, S.M., 1998: Evaluation and application of conditional symmetric instability, equivalent potential vorticity, and frontogenetic forcing in an operational forecast environment. Weather and Forecasting vol.13 pgs84-101.

Wild, A.D., 1996: Multi-Sensor Measurement for Quanitative Rainfall Forecasting. Unpublished PhD Thesis, University of Salford.

Winkler, R., Zeiner, B., Zwatz-Meise, V., 2001: Cold front, in Satrep Manual Version 3.0, http://www.knmi.nl/satrep/ (last visited 06/09/2001)

Yevjevich, V., 1972: Probability and statistics in hydrology. Water Resources Publications, Fort Collins, Colorado, USA.

APPENDIX I

UKMM diagnostics on standard pressure levels

Height m	Elapsed time of Forecasts (hours)
1000	0 1 2 3 4 5 6 7 8 9 10 11 12 13 14 15 16 17 18
950	0 3 6 9 12 15 18
850	0 1 2 3 4 5 6 7 8 9 10 11 12 13 14 15 16 17 18
700	0 3 6 9 12 15 18
500	0 3 6 9 12 15 18
400	0 3 6 9 12 15 18
300	0 3 6 9 12 15 18
250	0 3 6 9 12 15 18
200	0 3 6 9 12 15 18
150	0 3 6 9 12 15 18
100	0 3 6 9 12 15 18
70	0 3 6 9 12 15 18
30	0 3 6 9 12 15 18

Temperature K

1000	0 3 6 9 12 15 18
950	0 3 6 9 12 15 18
850	0 3 6 9 12 15 18
700	0 3 6 9 12 15 18
500	0 3 6 9 12 15 18
400	0 3 6 9 12 15 18
300	0 3 6 9 12 15 18
250	0 3 6 9 12 15 18
200	0 3 6 9 12 15 18
150	0 3 6 9 12 15 18
100	0 3 6 9 12 15 18
70	0 3 6 9 12 15 18
30	0 3 6 9 12 15 18

Wind U-component m/s

1000	0 3 6 9 12 15 18
950	0 3 6 9 12 15 18

850 0 1 2 3 4 5 6 7 8 9 10 11 12 13 14 15 16 17 18

700 0 1 2 3 4 5 6 7 8 9 10 11 12 13 14 15 16 17 18

500 0 3 6 9 12 15 18

400 0 3 6 9 12 15 18

300 0 3 6 9 12 15 18

250 0 3 6 9 12 15 18

200 0 3 6 9 12 15 18

150 0 3 6 9 12 15 18

100 0 3 6 9 12 15 18

70 0 3 6 9 12 15 18

30 0 3 6 9 12 15 18

Wind V-component m/s

1000 0 3 6 9 12 15 18

950 0 3 6 9 12 15 18

850 0 1 2 3 4 5 6 7 8 9 10 11 12 13 14 15 16 17 18

700 0 1 2 3 4 5 6 7 8 9 10 11 12 13 14 15 16 17 18

500 0 3 6 9 12 15 18

400 0 3 6 9 12 15 18

300 0 3 6 9 12 15 18

250 0 3 6 9 12 15 18

200 0 3 6 9 12 15 18

150 0 3 6 9 12 15 18

100 0 3 6 9 12 15 18

70 0 3 6 9 *12* *15* *18*

30 0 3 6 9 12 15 18

Relative humidity (dimensionless), or mixing ratio kg/kg

9999 0 1 2 3 4 5 6 7 8 9 10 11 12 13 14 15 16 17 18

1000 0 3 6 9 12 15 18

950 0 3 6 9 12 15 18

850 0 3 6 9 12 15 18

700 0 3 6 9 12 15 18

500 0 3 6 9 12 15 18

400 0 3 6 9 12 15 18

300 0 3 6 9 12 15 18

250 0 3 6 9 12 15 18

200 0 3 6 9 12 15 18

150 0 3 6 9 12 15 18

100 0 3 6 9 12 15 18

70 0 3 6 9 12 15 18

30 0 3 6 9 12 15 18

Fog Fraction at 1.5m

9999 0 1 2 3 4 5 6 7 8 9 10 11 12 13 14 15 16 17 18

Mean sea level (8888) or surface (9999) pressure Pa

8888 0 1 2 3 4 5 6 7 8 9 10 11 12 13 14 15 16 17 18

Specific humidity at 1.5 m dimensionless

9999 0 1 2 3 4 5 6 7 8 9 10 11 12 13 14 15 16 17 18

Boundary layer depth m?

8888 0 1 2 3 4 5 6 7 8 9 10 11 12 13 14 15 16 17 18

Surface temperature K

9999 0 1 2 3 4 5 6 7 8 9 10 11 12 13 14 15 16 17 18

Snow probability dimensionless

8888 0 1 2 3 4 5 6 7 8 9 10 11 12 13 14 15 16 17 18

Sensible heat flux W/m**2

9999L 0 1 2 3 4 5 6 7 8 9 10 11 12 13 14 15 16 17 18

Net solar radiation flux top (8888) or bottom (9999) W/m**2

9999 0 3 6 9 12 15 18

Surface wind stress - U N/m**2

9999L 0 1 2 3 4 5 6 7 8 9 10 11 12 13 14 15 16 17 18

Surface wind stress - V N/m**2

9999L 0 1 2 3 4 5 6 7 8 9 10 11 12 13 14 15 16 17 18

Freezing level ICAO height kft

8888 0 1 2 3 4 5 6 7 8 9 10 11 12 13 14 15 16 17 18

Freezing level height m

8888 0 1 2 3 4 5 6 7 8 9 10 11 12 13 14 15 16 17 18

1.5 m temperature K

9999 0 1 2 3 4 5 6 7 8 9 10 11 12 13 14 15 16 17 18

Freezing-level pressure Pa

8888 0 1 2 3 4 5 6 7 8 9 10 11 12 13 14 15 16 17 18

Accumulated dynamic rain kg/m**2

8888 0 1 2 3 4 5 6 7 8 9 10 11 12 13 14 15 16 17 18

Accumulated convective rain kg/m**2

8888 0 1 2 3 4 5 6 7 8 9 10 11 12 13 14 15 16 17 18

Rate of dynamic rain kg/m**2

8888 0 1 2 3 4 5 6 7 8 9 10 11 12 13 14 15 16 17 18

Rate of convective rain kg/m**2

8888 0 1 2 3 4 5 6 7 8 9 10 11 12 13 14 15 16 17 18

Accumulated dynamic snowfall kg/m**2

8888 0 1 2 3 4 5 6 7 8 9 10 11 12 13 14 15 16 17 18

Accumulated convective snowfall kg/m**2

8888 0 1 2 3 4 5 6 7 8 9 10 11 12 13 14 15 16 17 18

Rate of dynamic snowfall kg/m**2

8888 0 1 2 3 4 5 6 7 8 9 10 11 12 13 14 15 16 17 18

Rate of convective snowfall kg/m**2

8888 0 1 2 3 4 5 6 7 8 9 10 11 12 13 14 15 16 17 18

Topography m

9999 0

10 m wind U-component m/s

9999 0 1 2 3 4 5 6 7 8 9 10 11 12 13 14 15 16 17 18

10 m wind V-component m/s

9999 0 1 2 3 4 5 6 7 8 9 10 11 12 13 14 15 16 17 18

High cloud amount dimensionless

8888 0 1 2 3 4 5 6 7 8 9 10 11 12 13 14 15 16 17 18

Medium cloud amount dimensionless

8888 0 1 2 3 4 5 6 7 8 9 10 11 12 13 14 15 16 17 18

Low cloud amount dimensionless

8888 0 1 2 3 4 5 6 7 8 9 10 11 12 13 14 15 16 17 18

Convective cloud amount dimensionless

8888 0 1 2 3 4 5 6 7 8 9 10 11 12 13 14 15 16 17 18

Convective cloud base Pa

8888 0 1 2 3 4 5 6 7 8 9 10 11 12 13 14 15 16 17 18

Convective cloud top Pa

8888 0 1 2 3 4 5 6 7 8 9 10 11 12 13 14 15 16 17 18

Convective cloud base kft

8888 0 1 2 3 4 5 6 7 8 9 10 11 12 13 14 15 16 17 18

Convective cloud top kft

8888 0 1 2 3 4 5 6 7 8 9 10 11 12 13 14 15 16 17 18

Cloud Fraction below 1000ft ASL

9999 0 1 2 3 4 5 6 7 8 9 10 11 12 13 14 15 16 17 18

Soil moisture content Kg/m**2

9999 0 1 2 3 4 5 6 7 8 9 10 11 12 13 14 15 16 17 18

Snow depth (water equivalent) Kg/m**2

9999 0 1 2 3 4 5 6 7 8 9 10 11 12 13 14 15 16 17 18

Visibility 1.5m m

9999 0 1 2 3 4 5 6 7 8 9 10 11 12 13 14 15 16 17 18

Maximum screen temperature K

9999 6 12 18

Minimum screen temperature K

9999 6 12 18

Ht lowest cloud base > 0.1 okt kft

8888 0 1 2 3 4 5 6 7 8 9 10 11 12 13 14 15 16 17 18

Ht lowest cloud base > 2.5 okt kft

8888 0 1 2 3 4 5 6 7 8 9 10 11 12 13 14 15 16 17 18

Ht lowest cloud base > 4.5 okt kft

8888 0 1 2 3 4 5 6 7 8 9 10 11 12 13 14 15 16 17 18

Ht lowest cloud base > 6.5 okt kft

8888 0 1 2 3 4 5 6 7 8 9 10 11 12 13 14 15 16 17 18

Ht lowest cloud base > 7.9 okt kft

8888 0 1 2 3 4 5 6 7 8 9 10 11 12 13 14 15 16 17 18

Canopy water near surface Kg/m**2

8888 0 1 2 3 4 5 6 7 8 9 10 11 12 13 14 15 16 17 18

Roughness length m

9999 0 1 2 3 4 5 6 7 8 9 10 11 12 13 14 15 16 17 18

Total cloud, random overlap range 0-1

8888 0 1 2 3 4 5 6 7 8 9 10 11 12 13 14 15 16 17 18

Total cloud, max/random overlap range 0-1

8888 0 1 2 3 4 5 6 7 8 9 10 11 12 13 14 15 16 17 18

Lowest Convective Cloud amount

8888 0 1 2 3 4 5 6 7 8 9 10 11 12 13 14 15 16 17 18

Lowest Convective Cloud base PA

8888 0 1 2 3 4 5 6 7 8 9 10 11 12 13 14 15 16 17 18

Lowest Convective Cloud top PA

8888 0 1 2 3 4 5 6 7 8 9 10 11 12 13 14 15 16 17 18

Lowest Convective Cloud base KFT

8888 0 1 2 3 4 5 6 7 8 9 10 11 12 13 14 15 16 17 18

Lowest Convective Cloud top KFT

8888 0 1 2 3 4 5 6 7 8 9 10 11 12 13 14 15 16 17 18

Probability of Visibility less than 5KM 0 - 1

9999 0 1 2 3 4 5 6 7 8 9 10 11 12 13 14 15 16 17 18

APPENDIX II

MDIAG calculable diagnostics

1	Geopotential Height	m
2	Temperature	K
3	U component of Wind (wrt Model grid)	m s-1
4	V component of Wind (wrt Model grid)	m s-1
5	Relative Humidity (ice)	%
6	Potential Temperature	K
7	Equivalent Potential Temperature	K
8	Density	Kg m-3
9	Humidity Mixing Ratio	u
10	Sat Equ Pot Temp	K
11	du/dp	m s-1 Pa-1
12	dv/dp	m s-1 Pa-1
13	dTheta/dp	K Pa-1
14	dTheta_e/dp	K Pa-1
15	Div V	s-1
16	Dry PV	K Kg-1 m s-2
17	Moist PV	K Kg-1 m s-2
18	Geostrophic U Wind (wrt Model grid)	m s-1
19	Geostrophic V Wind (wrt Model grid)	m s-1
20	Wind strength	m s-1
21	Q1	u
22	Q2	u
23	Div Q	u
24	Absolute Vorticty	s-1
25	Vertical Velocity	m s-1
28	dug/dp	m s-1 Pa-1
29	dvg/dp	m s-1 Pa-1
31	Mag Geo Defmn	u
32	u cpt Gedef axis (wrt Model grid)	u
33	v cpt Gedef axis (wrt Model grid)	u
34	Mag Grad(ThW)	u

35 u cpt Grad(ThW) (wrt Model grid) u

36 v cpt Grad(ThW) (wrt Model grid) u

37 Geo Defmn wrt Theta_W u

38 Relative Vorticity s-1

39 Geostrophic Relative Vorticity s-1

40 Wind direction Degrees

41 Theta-W K

42 Ageostrophic U Wind (wrt Model grid) m s-1

43 Ageostrophic V Wind (wrt Model grid) m s-1

44 Mag Grad(Th) u

45 u cpt Grad(Th) (wrt Model grid) u

46 v cpt Grad(Th) (wrt Model grid) u

53 Relative Humidity (water) %

54 Inv diab. forcing u

55 Inv divQ & diab. u

56 Inv-lap of divQ u

57 Invlap divQ scaled u

58 800-600mb Inv divQ u

59 600-100mb Inv divQ u

60 1000-800mb Inv divQ u

61 Frontal Zones (ThW) u

62 Front -^DelSqd (ThW) u

63 Front -DelSqd (ThW) u

64 Front |grad (ThW)| u

65 ThW-Frnt Spd Km 3hr-1

66 ThW-advection u

67 Geost ThW-advn u

68 Frontal Zones (Th) u

69 Front -^DelSqd(Th) u

70 Front -DelSqd(Th) u

71 Front |grad(Th)| u

72 Th-Frnt Spd Km 3hr-1

73 Th-advection u

74 Geost Th-advn u

75 Shear Rel Vort u

76 Jet Stream "angle" u

77 Specific Humidity Kg Kg-1

78 U-Wind (U grid) (wrt Model grid) m s-1

79 V-Wind (U grid) (wrt Model grid) m s-1

80 Frontal waves u

81 F1 vector u

82 F2 vector u

83 Frontogenesis tilt u

84 Frontogenesis function u

85 u-wind WESTERLY m/s

86 v-wind SOUTHERLY m/s

87 omega Pa/s

88 dry static stability (N^2) s-2

89 moist static stability (N^2_m) s-2

90 Dry Richardson No. 0

91 Moist Richardson No. 0

92 Simple pseudo-wv mean rh 600-300mb mb

93 Schmez pseudo-wv brightness temp. K

94 Schmez pseudo-wv radiance Wm-2Sr-1

95 Schmez pseudo-wv corresponding pressure mb

96 Cloud liquid water kg/kg

97 Cloud ice kg/kg